Multiscale Modeling and Simulation of Human Heart Failure

Juan Francisco Gómez García

Supervisor: Dr Beatriz Trénor Gomis

Valencia, May 2015

Multiscale Modeling and Simulation of Human Heart Failure; Ph.D. thesis, Universitat Politècnica de València

This book was typeset using LaTeX2e and output as PDF. Cover: Multiscale Modeling and Simulation of Human Heart Failure. Calculated with ELVIRA and rendered with Paraview.

Multiscale Modeling and Simulation of Human Heart Failure

Juan Francisco Gómez García

Ph.D. thesis submitted to the Department of Electronic Engineering in fulfillment of the requirements for the degree of Doctor of Philosophy at the Universitat Politècnica de València, Valencia, Spain

UNIVERSITAT POLITÈCNICA DE VALÈNCIA

Supervisor:	Dr. Beatriz Trénor Polytechnic University of Valencia, Spain
External Evaluators:	Dr. Eleonora Grandi University of California, Davis, USA
	Dr. Stefano Severi Università di Bologna, Italy
	Dr. Laura Roa University of Seville, Spain
Reading Committee:	Dr. Javier Saiz Polytechnic University of Valencia, Spain
	Dr. Stefano Severi Università di Bologna, Italy
	Dr. Javier Chorro University of Valencia, Spain

This work was carried out in the Interuniversity Research Institute for Bioengineering and Technology Oriented Human Being (I3BH), Universitat Politècnica de València, Valencia, Spain.

A Maria del Mar...

Preface

”O me! O life!... of the questions of these recurring;
of the endless trains of the faithless
of cities filled with the foolish;
what good amid these, O me, O life?”

”That you are here,
that life exists, and identity;
that the powerful play goes on and you may contribute a verse.
That the powerful play goes on and you may contribute a verse.
What will your verse be?”

<<Walt Whitman, Dead Poets Society >>

”¡Oh mi yo, Oh vida!... de sus preguntas que vuelven;
del desfile interminable de los desleales
de las ciudades llenas de necios;
¿Qué de bueno hay en estas cosas?, ¡Oh mi yo, mi vida!”

”Que tú estás aquí,
que existe la vida, y la identidad;
que prosigue el poderoso drama y que tú puedes contribuir con un verso.
Que prosigue el poderoso drama y que tú puedes contribuir con un verso.
¿Cuál será tu verso?”

Abstract

Heart failure (HF) constitutes a major public health problem worldwide. Operationally it is defined as a clinical syndrome characterized by the marked and progressive inability of the ventricles to fill and generate adequate cardiac output to meet the demands of cellular metabolism. HF may have significant variability in its etiology and it is the final common pathway of various cardiac pathologies. Susceptibility to cardiac arrhythmias is increased in account of failing phenotype. Much attention has been paid to the understanding of the arrhythmogenic mechanisms induced by the structural, electrical, and metabolic remodeling of the failing heart. Due to the complexity of the electrophysiological changes that may occur during heart failure, the scientific literature is complex and sometimes equivocal. Nevertheless, a number of common features of failing hearts have been documented. At the cellular level, prolongation of the action potential (AP) involving ion channel remodeling and alterations in calcium handling have been established as the hallmark characteristics of myocytes isolated from failing hearts. At the tissue level, intercellular uncoupling and fibrosis are identified as major arrhythmogenic factors.

The rapid development of biophysically detailed computer models of single myocytes and cardiac tissues have contributed greatly to our understanding of processes underlying excitation and repolarization in the heart. In that sense, a model of the failing human ventricular myocyte was proposed, based on modifications to the Grandi et al. and O'Hara et al. human ventricular AP models, to study the mechanisms of HF-associated arrhythmias. Multiscale simulations to characterize the arrhythmia phenotype associated to this pathology were performed. At the single cell level, we specifically looked at the role of the late sodium current (I_{NaL}), including the formulation of this current. Experimental data from several sources were used to validate the model. Due to variability in literature a sensitivity analysis was performed to assess the influence of main ionic currents and parameters

upon most related biomarkers. The role of electrophysiological and structural heart failure remodeling in setting the stage for malignant arrhythmias was assessed through several configurations of transmural ventricular strands and the presence of controversial M cells was evaluated as well. Furthermore, the effect of fibrotic content and intercellular uncoupling on vulnerability to reentry was tested in transmural heterogeneous failing tissues.

The proposed model for the human I_{NaL} and the electrophysiological remodeling of myocytes from failing hearts accurately reproduce experimental observations. An enhanced I_{NaL} appears to be an important contributor to the electrophysiological phenotype and to the dysregulation of calcium homeostasis of failing myocytes. Our strand simulation results illustrate how the presence of M cells and heterogeneous electrophysiological remodeling in the human failing ventricle modulate the dispersion of action potential duration (APD) and repolarization time (RT). Conduction velocity (CV) and the safety factor for conduction (SF) were also reduced by the progressive structural remodeling during heart failure. In our transmural ventricular tissue simulations, no reentry was observed in normal conditions or in the presence of HF ionic remodeling. However, defined amount of fibrosis and/or cellular uncoupling were sufficient to elicit reentrant activity. Under conditions where reentry was generated, HF electrophysiological remodeling did not alter the width of the vulnerable window (VW). However, intermediate fibrosis and cellular uncoupling significantly widened the VW. In addition, biphasic behavior was observed, as very high fibrotic content or very low tissue conductivity hampered the development of reentry. Detailed phase analysis of reentry dynamics revealed an increase of phase singularities with progressive fibrotic components.

In conclusion, enhanced fibrosis in failing hearts, as well as reduced intercellular coupling, combine to increase electrophysiological gradients and reduce electrical propagation. In that sense, structural remodeling is a key factor in the genesis of vulnerability to reentry, mainly at intermediates levels of fibrosis and intercellular uncoupling. Electrophysiological remodeling promotes arrhythmogenesis and could be altered by the stage of HF.

Resumen

La insuficiencia cardíaca (IC) constituye un importante problema de salud pública en todo el mundo. A efectos prácticos se define como un síndrome clínico caracterizado por la incapacidad marcada y progresiva de los ventrículos para llenar y generar el gasto cardíaco adecuado para satisfacer las demandas del metabolismo celular. La IC puede tener una variabilidad significativa en su etiología y es la vía final común de varias patologías cardíacas. La susceptibilidad a arritmias cardíacas se incrementa debido al fenotipo de la IC. Se ha prestado mucha atención a la comprensión de los mecanismos arritmogénicos inducidos por la remodelación estructural, eléctrica, y metabólica del corazón afectado de IC. Debido a la complejidad de los cambios electrofisiológicos que pueden ocurrir durante la IC, la literatura científica es compleja y, a veces equívoca. Sin embargo, se han documentado una serie de características comunes en corazones afectados de IC. A nivel celular, se han establecido como las características distintivas de los miocitos aislados de corazones afectados de IC la prolongación del potencial de acción (PA), que implica la remodelación de los canales iónicos y las alteraciones en la dinámica del calcio. A nivel de los tejidos, el desacoplamiento intercelular y la fibrosis se identifican como los principales factores arritmogénicos.

El rápido desarrollo de modelos computacionales biofísicamente detallados de los miocitos y tejidos cardíacos, ha contribuido en gran medida a nuestra comprensión de los procesos que subyacen a la excitación y la repolarización cardíaca. En este sentido, un modelo de miocito ventricular humano afectado de insuficiencia cardíaca fue desarrollado, basado en modificaciones de los modelos de potencial de acción humano de Grandi y colaboradores y O'Hara y colaboradores , para estudiar los mecanismos arritmogénicos asociados a la insuficiencia cardíaca. Se llevaron a cabo simulaciones a distintos niveles para caracterizar esta patología. A nivel celular, resaltamos el papel de la corriente tardía de so-

dio, introduciendo la formulacíon de dicha corriente. Los datos experimentales de varias fuentes se utilizaron para validar el modelo. Debido a la variabilidad en la literatura de la temática se realizó un análisis de sensibilidad para evaluar la influencia de las principales corrientes iónicas y los parámetros sobre los biomarcadores relacionados. El papel del remodelado electrofisiológico y estructural debido a la insuficiencia cardíaca fue evaluado en el establecimiento de las arritmias a través de varias configuraciones de fibras ventriculares transmurales, así como la presencia de las controvertidas células M. Además, el efecto del contenido fibrótico y el desacoplamiento intercelular en la vulnerabilidad a las reentradas se puso a prueba en tejidos transmurales afectados de IC.

El modelo propuesto para la corriente tardía de sodio y la remodelación electrofisiológica de los miocitos de corazones afectados de IC reprodujeron con precisión las observaciones experimentales. Una I_{NaL} incrementada parece ser un importante contribuyente al fenotipo electrofisiológico y la desregulación de la homeostasis del calcio de los miocitos afectados de IC. Nuestros resultados de la simulaciones en fibra ilustran cómo la presencia de células M y el remodelado electrofisiológico heterogéneo en el ventrículo humano afectado de IC modulan la dispersión de la duración potencial de acción (DPA) y el tiempo de repolarización (TR). La velocidad de conducción (VC) y el factor de seguridad para la conducción (FS) también se redujeron en la remodelación estructural progresiva durante la insuficiencia cardíaca. En nuestras simulaciones transmurales de tejido ventricular, no se observó reentrada en condiciones normales o en presencia de la remodelación iónica de la IC. Sin embargo, determinadas cantidades de fibrosis y/o desacoplamiento celular eran suficientes para provocar la actividad reentrante. En condiciones donde se había generado la reentrada, el remodelado electrofisiológico de la IC no alteró la anchura de la ventana vulnerable (VV). Sin embargo, niveles intermedios de fibrosis y el desacoplamiento celular ampliaron significativamente la VV. Además, se observó un comportamiento bifásico, dado que un muy elevado contenido fibrótico o una muy baja conductividad del tejido obstaculizaban el desarrollo de la reentrada. Un análisis detallado del diagrama de fases de la dinámica de la reentrada reveló un aumento de singularidades de fase a medida que aumentaba el contenido fibrótico.

En conclusión, niveles elevados de fibrosis en corazones afectados de IC, así como la reducción del acoplamiento intercelular, se combinan para aumentar los gradientes electrofisiológicos y reducir la propagación eléctrica. En ese sentido, la remodelación estructural es un factor clave en la génesis de la vulnerabilidad a las reentradas, principalmente en niveles intermedios de fibrosis y desacoplamiento intercelular. El remodelado electrofisiológico promueve la arritmogénesis y puede ser alterado dependiendo de la etapa de IC.

Resum

La insuficiència cardíaca (IC) constitueix un important problema de salut pública arreu del món. A efectes pràctics, es defineix com una síndrome clínica caracteritzada per la incapacitat marcada i progressiva dels ventricles per omplir i generar el cabal cardíac adequat, per tal de satisfer les demandes del metabolisme cel·lular. La IC pot tenir una variabilitat significativa en la seua etiologia i és la via final comuna de diverses patologies cardíaques. La susceptibilitat a les arritmies cardiaques s'incrementa degut al fenotip de la IC. S'ha prestat molta atenció a la comprensió dels mecanismes aritmogènics induïts per la remodelació estructural, elèctrica, i metabòlica del cor afectat d'IC. A causa de la complexitat dels canvis electrofisiològics que poden ocórrer durant la IC, trobem que la literatura científica és complexa i, de vegades, equívoca. No obstant això, s'han documentat una sèrie de característiques comunes en cors afectats d'IC. A nivell cel·lular, com característiques distintives dels miòcits aïllats de cors afectats d'IC, s'han establert la prolongació del potencial d'acció (PA), que implica la remodelació dels canals iònics, i les alteracions en la dinàmica del calci. A nivell dels teixits, el desacoblament intercel·lular i la fibrosi s'identifiquen com els principals factors aritmogènics.

El desenvolupament veloç de models computacionals detallats biofísicament dels miòcits i els teixits cardíacs estretament relacionats, ha contribuït en gran mesura a la nostra comprensió dels processos subjacents a l'excitació i la repolarització cardíaca. Per això, per tal d'estudiar els processos aritmogènics a causa del fenotip de la IC, es va proposar un model cel·lular d'IC utilitzant una versió modificada del model de potencial d'acció ventricular humà de Grandi i els seus col·laboradors i el de O'Hara i el seus colaboradors, el qual incorpora la formulació del corrent de sodi tardà (I_{NaL}). Amb l'objectiu de validar el model es van utilitzar dades experimentals de diverses fonts. A causa de la diversitat en la literatura de la temàtica, es va realitzar una anàlisi de sensibilitat per tal d'avaluar la influència de les

principals corrents iòniques i els paràmetres sobre els biomarcadors relacionats. A més, es van dur a terme simulacions multiescala per a la caracterització d'aquesta patologia. El paper del remodelat electrofisiològic i estructural conseqüència de la IC va ser avaluat en l'establiment de les arítmies a través de diverses configuracions de fibres ventriculars transmurals, així com en presència de les controvertides cèl·lules M. A més a més, l'efecte del contingut fibròtic i el desacoblament intercel·lular en la vulnerabilitat a les reentrades es va posar a prova en teixits transmurals afectats d'IC.

El model proposat per al corrent de sodi tardà i la remodelació electrofisiològica dels miòcits de cors afectats d'IC van reproduir amb precisió les observacions experimentals. Una (I_{NaL}) incrementada sembla contribuir de manera important al fenotip electrofisiològic i a la desregulació de l'homeòstasi del calci dels miòcits afectats d'IC. Els resultats de les nostres simulacions en fibra indiquen que la presència de cèl·lules M i el remodelat electrofisiològic heterogeni en el ventricle humà afectat d'IC modulen la dispersió de la durada del potencial d'acció (DPA) i el temps de repolarització (TR). La velocitat de conducció (VC) i el factor de seguretat per a la conducció (FS) també es van reduir en la remodelació estructural progressiva durant la IC. A les nostres simulacions transmurals de teixit ventricular, no s'observà cap reentrada ni en condicions normals ni en presència de la remodelació iònica de la IC. No obstant això, amb determinades quantitats de fibrosi i/o desacoblament cel·lular sí que es provocà l'activitat reentrant. I amb les condicions que produïren la reentrada, el remodelat electrofisiològic de la IC no va alterar l'amplada de la finestra vulnerable (FV). Tanmateix, nivells intermedis de fibrosi i el desacoblament cel·lular sí que ampliaren significativament la FV. També es va observar un comportament bifàsic, atès que un contingut fibròtic molt elevat o una conductivitat del teixit molt baixa obstaculitzaven el desenvolupament de la reentrada. Una anàlisi detallada del diagrama de fases de la dinàmica de la reentrada revelà un augment de singularitats de fase a mesura que augmentava el contingut fibròtic.

En conclusió, nivells elevats de fibrosi en cors afectats d'IC, així com la reducció d'acoblament intercel·lular, es combinen per augmentar els gradients electrofisiològics i reduir la propagació elèctrica. Per tant, la remodelació estructural és un factor clau en la gènesi de la vulnerabilitat a les reentrades, principalment en nivells intermedis de fibrosi i desacoblament intercel·lular. La remodelació electrofisiològica promou aritmogènesi i pot canviar depenent de l'estat d'insuficiència cardíaca.

Contents

List of Figures

List of Tables

Acronyms

1D	One-dimensional
2D	Two-dimensional
3D	Tree-dimensional
σ_j	Density of channels of each ion 'j'
γ_j	Unitary conductance of channel 'j'
α	Channel opening rate
β	Channel closing rate
β1AR	Adrenergic receptors β1
β2AR	Adrenergic receptors β2
χ	Surface to volume ratio
λ	Proportionality constant
τ_{hL}	Inactivation time constant of the inactivation gate 'h'
τ_{Ca}	Decay time constant of the calcium transient
$[Ca^{2+}]_i$	Intracellular calcium concentration
$[Ca^{2+}]_{SR}$	Intracellular SR calcium concentration
$[Na^{+}]_i$	Intracellular sodium concentration
AF	Atrial fibrillation
AP	Action Potential
APD	Action Potential Duration
AP-Ca delay	Delay between the upstrokes of AP and Ca^{2+} transient
APD_{90}	Action Potential Duration at 90% of repolarization
APD_{50}	Action Potential Duration at 50% of repolarization
BCL	Basic Cycle Length
Ca^{2+}	Calcium ion

CAD	Coronary artery disease
CaMKII	Calcium/calmodulin-dependent protein kinase II
CaMKa	Calcium/calmodulin-dependent protein kinase active
$CaTD_{80}$	Time from the upstroke to 80% of calcium recovery
Cav3	Caveolin-3 protein
CCS	Cardiac conduction system
C_m	Cellular membrane capacity
CI	Coupling Interval
CV	Coduction Velocity
Cx43	Connexin 43 protein
E_j	Nerst Potential of ion 'j'
g_j	Conductance of ion 'j'
CRT	Cardiac Resynchronization Therapy
D	Conductivity tensor
D_M	Diffusion coefficient for myocytes
D_{LOW}	Diffusion coefficient for failing myocytes
D_{Fib}	Diffusion coefficient for myocytes-fibroblast interaction
DAD	Delayed Afterdepolarization
DHF	Diastolic heart failure
EAD	Early Afterdepolarization
EP	Electrophysiological
ERP	Efective refractory period
EC_{50SR}	SR Ca fluxes
f_j(t)	Percentage of open channels of ion 'j'
GPB	Grandi ,Pasqualini and Bers model
HF	Heart Failure
HH	Hodgkin and Huxley
HT	Hilbert transform
$h_{L,\infty}$	Steady-state inactivation gate
I_{ion}	Sum of all the ionic membrane currents
I_j	Current of ion 'j'
I_{Cab}	Calcium background current
I_{CaL}	L-type Calcium current
I_{Fib}	Total transmembrane ionic current for fibroblast
I_{K1}	Inward rectifier potassium current

I_{Kr}	Rapidly activating potassium current
I_{leak}	Sarcoplasmic reticulum calcium leak current
I_{MYO}	Total transmembrane ionic current for myocytes
I_{Na} or I_{NaT}	Fast sodium current
I_{to}	Transient outward potassium current
Na^+/Ca^{2+}	Sodium calcium exchanger
Na^+/K^+	Sodium potassium pump
I_{Nab}	Background sodium current
I_{NaL}	Late sodium current
I_{NaK}	Sodium potassium pump current
I_{NCX}	Sodium calcium exchanger current
I_{rel}	Sarcoplasmic reticulum calcium release current
I_{stm}	External stimulation current
I_{SERCA}	Sarcoplasmic reticulum calcium pump current
J_e	Extracellular current
J_i	Intracellular current
$J_{rel,NP,\infty}$	Non-phosphorylated calcium release, via RyR, from jsr to myoplasm
K^+	Potassium ion
LBBB	Left bundle branch block
LQT	Long QT-segment
LV	Left ventricle
M	M-cells (mid-myocardial cells)
M_e	Extracellular conductivity tensor
M_i	Intracellular conductivity tensor
m_L	Activation gate
MI	Myocardial infarction
NC	Normal conditions
NYHA	New York Heart Association
LV	Left ventricle
Na^+	Sodium ion
q_e	Extracellular charge
q_i	Intracellular charge
n	unitary normal vector
ORd	O'Hara and Rudy model
PKA	Protein Kinase A

PS	Phase singularity
PVT	Polymorphic ventricular tachycardia
RT	Repolarization time
RV	Right ventricle
RyR	Ryanodine receptors
SERCA	Sarcoplasmic reticulum calcium pump
SHF	Systolic heart failure
SF	Safety factor
SR	Sarcoplasmic reticulum
TdP	Torsade de Pointes
TDR	Transmural dispersion of repolarization
t_{NCXRP}	Time of the reversal potential for the NCX (forward mode - inward mode)
V_e	Extracellular potential
V_i	Intracellular potential
V_m	Cellular membrane potential
VT	Ventricular tachicardia
VW	Vulnerable window

CHAPTER 1

The Electrical Activity of the Heart

1.1 Introduction

The heart is the main organ of the circulatory system. It is essentially composed of muscle tissue (myocardium) and to a lesser extent, connective tissue (supportive tissue, valves and specialized conduction tissue). It is subdivided into four chambers, two right and two left, separated by a partition called medial septum. The two upper chambers are called atria and the two lower cavities ventricles (Figure 1.1A). The atria are separated by a wall or interatrial septum, and the ventricles by the interventricular septum. Both partitions are continuous with each other, forming a true muscular-membrane wall separating the heart chambers in two right and two left chambers. During a heart beat, the cava vein carry deoxygenated blood from the organism into the right atrium of the heart. The blood goes into the right ventricle which contracts to send blood through the pulmonary artery into the lungs to perform gas exchange. Afterwards, oxygenated blood returns to the left atrium through the four pulmonary veins and to the left ventricle by pressure difference, to be ejected through the aorta artery into the organism (Figure 1.1A). This process is possible due to the mechanical contraction ability of the four chambers.The mechanical contraction of the heart during a heart beat is generated by a bioelectrical signal, which excites cardiac cells. This electrical pulse originates in the sinoatrial node and spreads throughout the atria towards the atrioventricular node where it is reconducted through the His bundle to reach the ventricles through the Purkinje system ramification. The electrical excitation allows cellular contraction and the pumping of blood to circulatory system . Figure 1.1B shows a simplified representation of the electrical conduction system of the heart. The electrical signal generated and transmitted that governs cardiac contraction is called Action Potential (AP). The abnormal heart rhythm or any change of location in the initiation or sequence of the heart's electrical activity that deviates from normal activation are considered cardiac arrhythmias, and the consequences variate depending on the place where they are originated.

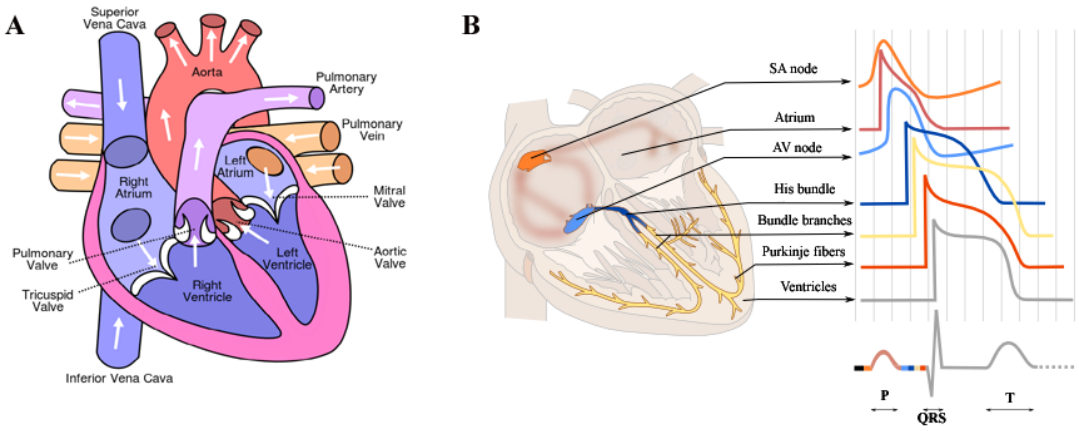

Figure 1.1: *Diagram of cardiac anatomy and circulatory function (panel A),and cardiac electrical conduction system with AP morphology depending on the area (panel B) and its relation to the body surface electrocardiogram (ECG).*

1.2 Action Potential. Genesis and propagation

In cardiomyocytes, as in other excitable cells, ionic concentrations differences between intracellular and extracellular space separated by cellular membrane generates an electrical potential. Permiability of cellular membranes allows ionic fluxes between both spaces. If the cell is dynamically balanced, the force due to the electrical potential of the intracellular space is lower than the extracellular potential so membrane potential is set to its resting value (resting potential). Ion channels, pumps and exchangers embedded into the cell membrane allow the active and passive ionic exchange between both spaces. An electrical stimulus reaching the cell favors the dynamic ion flux due to diffusive forces and the electrical field through the membrane, generating the AP.

As can be observed in Figure 1.1B, there are regional heterogeneities in AP properties and morphology. The ventricular AP is described by several stages, characterized by the activation of different ionic currents (see Figure 1.2). In the beginning, the quiescent cardiac myocyte is set to its resting membrane potential (<-80 mV). If an appropiate stimulus reaches the cell, the membrane potential grows until the trigger threshold is reached. At this membrane potential value, sodium channels open letting inward current inside the cell

and promoting an inward calcium current throuhg the L-Type calcium channels, rising up the membrane potential to positive values in about 1 ms, phase denoted as depolarization. When the membrane potential reaches positive values (10-20 mV), sodium and calcium channels begin to close and potassium channels begin to open leading to an efflux of this ion from the intracellular space, maintaining the membrane potential in positive values due to this influx-efflux electrical balance during several miliseconds, in the stage denoted as the plateau phase. As calcium channels get closed, the outward potassium currents decrease the membrane potential to its initial value in the repolarization phase. In Figure 1.2 the main ionic currents involved in the AP generation process are depicted.

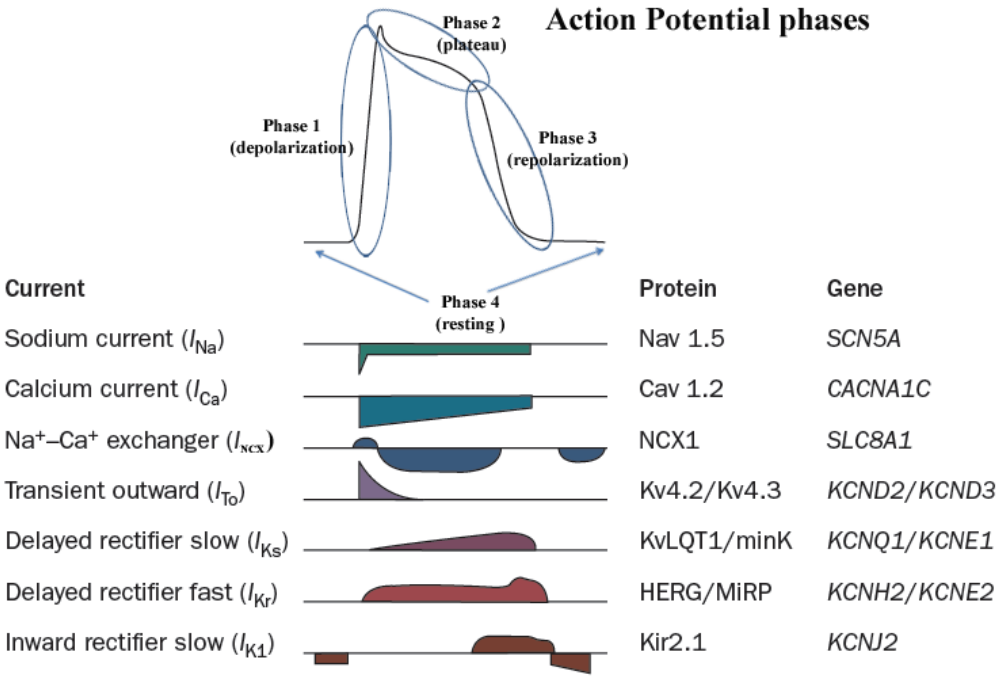

Figure 1.2: *Diagram of ion channels, ventricular action potential and major ionic currents. Reproduced from [189]*

Myocardium is formed by muscle fibers, constituted by myocytes. These fibers are interconnected longitudinally and transversally, so that any change arising in the membrane potential of a cell spreads through its neighbors. The intercalated disks, mainly located at the end of the cell and with resistivity values lower than the cellular membrane favor

ionic conduction between cells and AP propagation. Inside the intercalated disk specialized proteins called gap juntions directly connect the cytoplasm of adjacent cells. In Figure 1.3 the sequence of AP propagation is depicted. If one supra-threshold stimulus reaches the cell (1), sodium channels open and the cellular membrane depolarizes generating an AP. As a result, the voltage difference between the intracellular mediums of this cell and its neighbors generates a net current flux through the gap juntions (2) that depolarizes the next cell (3) and excitation spreads forward (4).The conduction velocity of an AP depends strongly on the propagation direction due to the structural anisotropy of the cardiac tissue, anatomic heterogeneities, cell morphology and gap junction distribution.

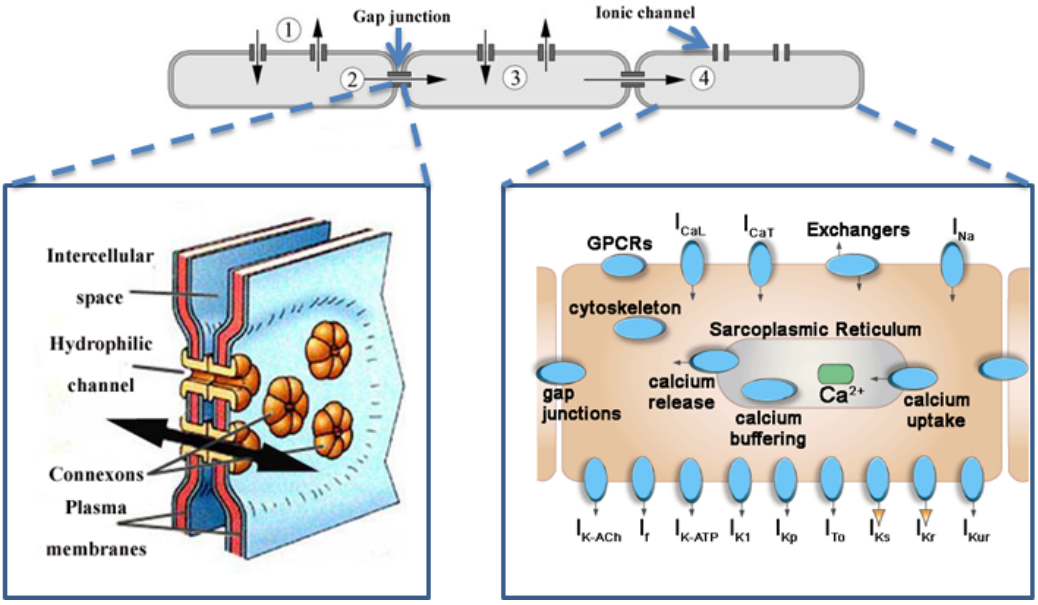

Figure 1.3: *Illustration of the propagation of electrical impulses in the myocardium.The structure of the intercellular coupling with gap junctions in myocytes is shown.*

1.3 Modeling the Electrical Activity of the Heart

1.3.1 Cellular Models

Computer modeling is a powerful tool when exploring electrophysiological phenomena. The work of Hodgkin and Huxley (HH) [91] in the 50s made possible to relate important properties of membrane ion channels to the generation of the AP. They described matematically the voltage dependent changes in excitable cells based on experimental measurements on neuronal axons. For a single cardiac cell, electrical dynamics could be expressed as in Figure 1.4, where the cellular membrane is modeled as a capacitor separating the intracellular and extracellular spaces, and ionic exchange is expressed as currents through ion channels, where g_j represents the maximal conductance of each channel and E_j represents the equilibrium potential between the diffusion and the electrical field forces (Nerst potential) of each ion. Thus, the membrane potential can be computed using circuits theory as presented in equation 1.1, which relates the tranmembrane potential (V_m) with the total transmembrane ionic current (I_{ion}).

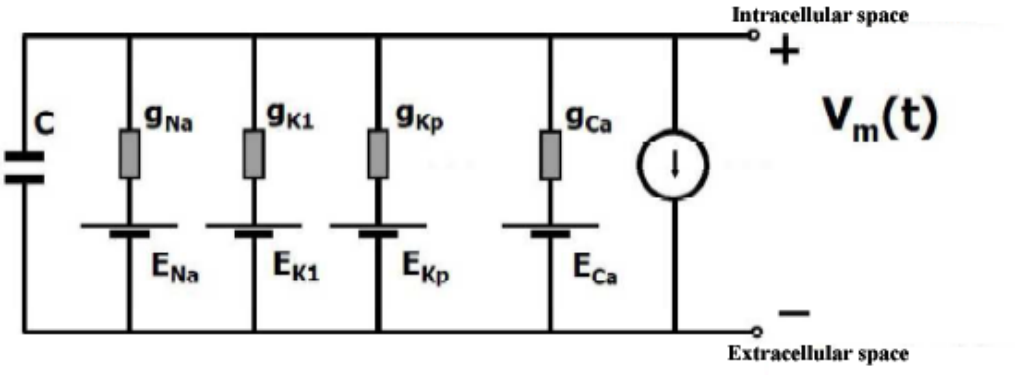

Figure 1.4: *Equivalent electrical circuit of the cell membrane.*

$$\frac{dV_m}{dt} = -\frac{I_{ion} + I_{stm}}{C_m} \tag{1.1}$$

$$I_j = g_j(V_m - E_j) \tag{1.2}$$

$$g_j(t) = \sigma_j \gamma_j f_j(t) \tag{1.3}$$

where C_m is the membrane capacitance value provided by the charge separation across the lipid bilayer and I_{stm} is the externally applied current stimulus. The ion current through each channel 'j' is solved as in equation 1.2, where 'g_j' is the variable conductance determined by the density of channels of each ion (σ_j), the unitary conductance of that channel (γ_j) and by the percentage of open channels (f_j(t)), as expressed in equation 1.3. If all currents involved in the AP are modeled as in equation 1.2 the time course of the membrane potential can be obtained by equation 1.1. This work set the basis for the electrodynamic description of cardiac cells, where a system of ordinary coupled differential equations is solved to obtain the time course of the membrane potential. The complexity and accuracy of AP models have increased thenceforth as electrophysiological techniques and computer resources have evolved.

1.3.2 Modeling of Ion Channels Activity

The measurement of ion currents can be performed with voltage-clamp and patch-clamp experiments, which allow to establish current-voltage curves. HH interpreted the dynamics of an ion channel as if it were regulated by opening or closing voltage-dependent gates which allow or block the ion current flux, as depicted in Figure 1.5. If a channel is regulated by a single gate, it stays open (O) when ions flow, or closed (C) when the flux is blocked. Thus, α and β are defined as the open and close rates respectively, so the open probability of an ion channel varies in time as in equation 1.4.

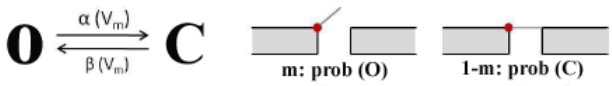

Figure 1.5: *Representation of an ionic channel regulated by one gate.*

$$\frac{dm}{dt} = \alpha(1-m) - \beta m \tag{1.4}$$

In this way, the voltage and time-dependence of gates determine the channel conductance evolution, which reaches the maximal value when all channels are open. Ion channels may have several gates depending on their response to membrane potential changes. An activation gate opens when the membrane potential increases, and an inactivation gate closes. Nowadays, it is well known that ion channels are clusters of molecules interconnected and subunits interrelated to allow the ionic flux, nevertheless HH formulation fits well in the functional electrodynamic description. In this sense, another formulation of ion channels activity is based on the description of several states of the molecules that conforms the channel (Markov formulation). Although the higher complexity and computational cost with similar results makes Markov models less efficient [63], these are useful to analyze specific pathologies, such as the effects of ion channels mutations [203]. The AP models used in this thesis contain several ion channel models, in addition to pumps and exchangers and other mechanisms based on ion diffusion across cellular compartments. Thus, a high level of complexity is developed in order to describe the electrical activity of the entire cell.

1.3.3 Human Ventricular AP Models

The first mathematical description of an AP was formulated by HH in 1952 as previously mentioned [91]. Ever since, several models have been developed as experimental data increased and measurements techniques improved. In 1994, Luo and Rudy built an AP model based on guinea pig ventricular myocytes data [127].Thenceforth several cellular AP models from different species were developed ([95, 155, 175], among others). The first attempt to develop an AP model of human ventricular myocytes was done by Priebe and Beuckelman [173]. Later, cellular human electrophysiology became more complete in other models [17, 98, 217]. In 2010, Grandi and colleagues [79] published a human ventricular AP model where the intracelular calcium handling was higly detailed, and a year later O'Hara et al.[157] formulated a new human AP model based on experimental data from more than one hundred human hearts. This last two human AP models were used in this Thesis. In Figure 1.6 a representation of the human ventricular AP model by O'Hara and colleagues is depicted. As can be observed, four intracellular compartments (bulk myoplasm (myo), junctional sarcoplasmic reticulum (JSR), network sarcoplasmic reticulum (NSR), and subspace (SS)) are described. Intracellular compartments and the relative mass balance equations for intracellular ions were first introduced in cardiac models by DiFrancesco and Noble [54]. Compartmentalization is complex due to the lack of corresponding distinct anatomical structures inside the cell. Different calcium buffers for each compartment are included as

well in the models used in this Thesis (GPB and ORd).

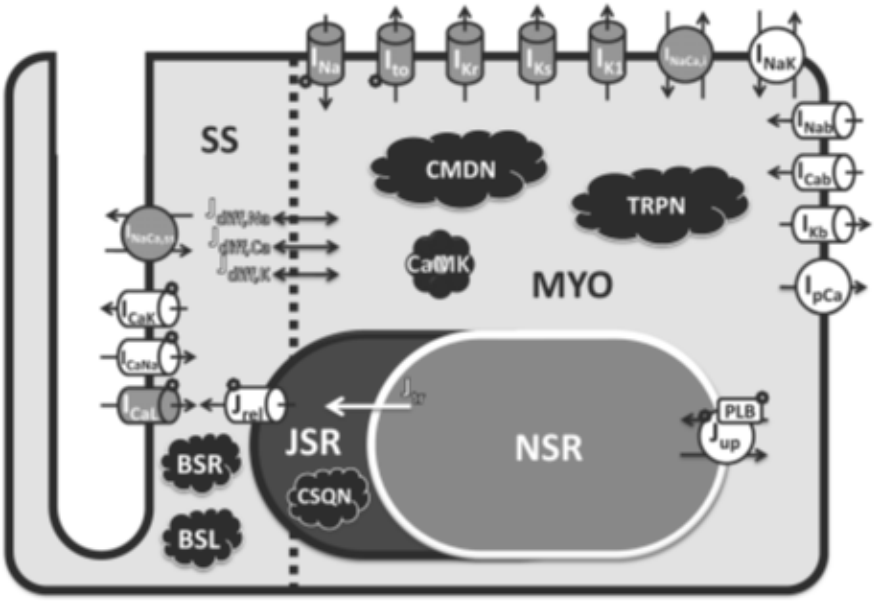

Figure 1.6: *Representation of the human ventricular AP model by O'Hara and colleagues. Model includes four compartments: 1) bulk myoplasm (myo), 2) junctional sarcoplasmic reticulum (JSR), 3) network sarcoplasmic reticulum (NSR), and 4) subspace (SS), representing the space near the T-tubules. Currents into the myoplasm: Na^+ current (I_{Na}; representing both fast and late components), transient outward K^+ current (I_{to}), rapid delayed rectifier K^+ current (I_{Kr}), slow delayed rectifier K^+ current (I_{Ks}), inward rectifier K^+ current (I_{K1}), 80% of Na^+/Ca^{2+} exchange current ($I_{INaCa,i}$), Na^+/K^+ pump current (I_{NaK}), background currents (I_{Nab}, I_{Cab} , and I_{Kb}), and sarcolemmal Ca^{2+} pump current (I_{pCa}). Currents into subspace: L-type Ca^{2+} current (I_{CaL}, with Na^+ and K^+ components I_{CaNa}, I_{CaK}), and 20% of Na^+/Ca^{2+} exchange current ($I_{NaCa,ss}$). Ionic fluxes: Ca^{2+} through ryanodine receptor (J_{rel}), NSR to JSR Ca^{2+} translocation (J_{tr}), Ca^{2+} uptake into NSR via SERCA2a/PLB (J_{up}; PLB - phospholamban), diffusion fluxes from subspace to myoplasm ($J_{diff,Na}$, $J_{diff,Ca}$, and $J_{diff,K}$). Ca^{2+} Buffers: calmodulin (CMDN), troponin (TRPN), calsequestrin (CSQN), anionic SR binding sites for Ca^{2+} (BSR), anionic sarcolemmal binding sites for Ca^{2+} (BSL). Ca^{2+}/calmodulin-dependent protein kinase II (CaMK) and its targets are labeled. Reproduced from [157].*

1.3.4 Tissue and Organ Models. The Monodomain Approach.

In addition to mathematical models that describe the human AP at the cellular level, the spread of cardiac activation in virtual multicellular tissues can be assessed, formed by a number of cells electrically interconnected as in Figure 1.7. The electrical coupling between cardiomyocytes and the spread through the tissue is modeled by mathematical equations where the cardiac tissue is assumed to be a continuous excitable medium.

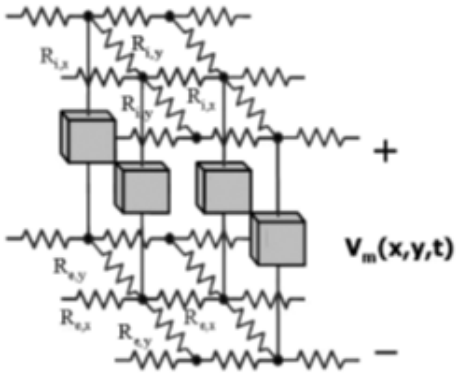

Figure 1.7: *Schematic diagram of a three dimensional node connection mesh.*

The mathematical formulation of the electrical activity of the heart has been described by the bidomain model [70, 88], in which the cardiac tissue is represented as two continuous domains (intracellular and extracellular) sharing the same space and having unequal anisotropy ratios. Since the bidomain model has a high numerical complexity and it is very demanding computationally, it is common to use a simplified tissue model known as the anisotropic monodomain model [170]. In this approach, intracellular and extracellular conductivity tensors are assumed to be proportional. The electrical current in the intracellular and extracellular domains is expressed by the Ohm's Law:

$$J_i = -M_i \nabla V_i \tag{1.5}$$

$$J_e = -M_e \nabla V_e \tag{1.6}$$

where J_i is the intracellular current, J_e is the extracellular current, M_i and M_e are the

conductivity tensors and V_i and V_e are the electrical potentials in both domains respectively. The cell membrane acts as a capacitor and due to its small thickness the electrical charge in both sides of the membrane is compensated immediately. Therefore, the accumulation of charge in any point is zero:

$$\frac{\partial(q_i + q_e)}{dt} = 0 \tag{1.7}$$

where q_i and q_e are the electrical charge in both sides of the cell membrane. The electrical current in each point is equal to the ratio of the accumulation of charge in both domains

$$-\nabla J_i = \frac{\partial(q_i)}{dt} + \chi I_{ion} \tag{1.8}$$

$$-\nabla J_e = \frac{\partial(q_e)}{dt} + \chi I_{ion} \tag{1.9}$$

where I_{ion} is the ionic current through the membrane and χ is the surface to volume ratio. The sign of the ion current is positive when it goes from the intracellular to the extracellular space. Combining 1.7,1.8 and 1.9 we obtain the current conservation equation,

$$\nabla J_i + \nabla J_e = 0 \tag{1.10}$$

that could be expressed as follows combining 1.5 and 1.6

$$\nabla(M_i \nabla V_i) + \nabla(M_e \nabla V_e) = 0 \tag{1.11}$$

where the charge in the cell membrane (q) directly depends on the membrane potential V=V_i - V_e and the membrane capacitance C_m

$$V = \frac{q}{\chi C_m} \tag{1.12}$$

$$q = \frac{q_i - q_e}{2} \tag{1.13}$$

combining and differentiating the last two equations we obtain

$$\chi C_m \frac{\partial V}{\partial t} = \frac{\partial (q_i - q_e)}{2\partial t} \tag{1.14}$$

and combining with 1.7 yields:

$$\frac{\partial q_i}{\partial t} = -\frac{\partial q_e}{\partial t} = \chi C_m \frac{\partial V}{\partial t} \tag{1.15}$$

replacing this expression in 1.11 and using $D_i = M_i$ / χ we obtain:

$$\nabla (D_i \nabla V_i) = C_m \frac{\partial V}{\partial t} + I_{ion} \tag{1.16}$$

if we replace V_i (V_i = V + V_e) in 1.11 and 1.16, and we apply the monodomain assumption $D_e = \lambda\ D_i$, and combine the two resulting equations we obtain the monodomain standard formulation

$$\nabla (D \nabla V) = C_m \frac{\partial V}{\partial t} + I_{ion} \tag{1.17}$$

where D = $\lambda\ \backslash(1+\lambda)$ is the second order symmetric and positive defined conductivity tensor. The left side of equation 1.17 is called the diffusive term and the right side the reactive term. No current is allowed out of the domain, which leads to boundary conditions

$$\overrightarrow{n} \cdot \nabla (D \nabla V_m) = 0 \tag{1.18}$$

where $\overrightarrow{n}$ is the outward pointing unit normal to the computational domain. Therefore, the monodomain approach consists of a parabolic reaction-diffusion equation describing

the dynamic of the transmembrane potential coupled to a system of ordinary differential equations describing the cellular ionic model. This equation is solved with a finite elements method based on the Operator Splitting algorithm [88].

1.4 Heart Failure

Heart failure (HF) is the inability of the heart to fill or pump blood in adequate volumes to meet the demands of cellular metabolism. HF is a syndrome resulting from disorders, either structural or functional, that interfere with cardiac function and it is characterized by a progressive deterioration of the patient's condition. HF patients are prone to develop complex ventricular tachycardias and some of them die suddenly [105]. In developed countries, about 2% of adults suffer from HF and it is the main cause of hospitalization in people over 65 years [188].

1.4.1 Classification

HF can be divided into several categories. HF patients can be subdivided into Systolic Heart Failure (SHF) and Diastolic Heart Failure (DHF). DHF refers to abnormal events occurring during heart relaxation and filling. SHF refers to abnormal events occurring during contraction and blood ejection. HF can also be classified as HF with an ischemic or with a non-ischemic origin. HF patients are classified as having an ischemic etiology based on a history of myocardial infarction (MI) or objective evidence of coronary artery disease (CAD) such as the presence of a stenosis over 75% in epicardial coronary vessels. HF patients who fail to meet these criteria are considered to have a non-ischemic etiology of HF.

In order to compare HF studies, patients are usually categorized into four classes as in the New York Heart Association (NYHA). Patients in NYHA class I have fatigue or dyspnea only with strenuous activity. Patients in NYHA class II have these symptoms during moderate activity. In Class III they show these symptoms during daily living, while NYHA class IV patients are even symptomatic at rest. However, this is a subjective approach, therefore a new classification system has been designed by the American College of Cardiology and the American Heart Association [96]. In this new system 'Stage A' patients are at high risk of developing HF, but they do not show yet any apparent structural abnormality of the heart. 'Stage B' patients have structural abnormalities of the heart but do not exhibit HF symptoms. 'Stage C' patients have structural abnormalities of the heart and have current or previous HF symptoms. 'Stage D' patients have end-stage symptoms of HF and are refractory to standard treatment.

1.4.2 Heart failure remodeling

Electrophysiological remodeling of failing hearts has been described precisely [213, 214]. AP prolongation, alterations in calcium handling and intracellular sodium accumulation among other disturbances, have been established as the hallmark characteristics of the failing heart. In addition, reduction in connexin 43 (Cx43), the gap junction protein responsible for intercellular coupling between myocytes in the ventricles [161], has been observed in HF studies [6, 57], leading to intercellular uncoupling and reduced conduction velocity [234]. In the same line, fibrosis, characterized by fibroblasts proliferation and collagen deposition is associated with arrhythmogenic processes in several cardiac pathologies. These abnormalities lead to alterations in the electrical signal propagation and as a consequence in the associated mechanical function of the heart. During HF, non-reentrant mechanisms might be initiated by either Early After Depolarizations (EADs) or Delayed After Depolarizations (DADs). Understanding the arrhythmogenic mechanisms induced by electrical, structural and metabolic remodeling of failing hearts is a key factor in the treatment of this pathology.

1.4.3 Computer Models

From a computational point of view, the first simulation study focusing on HF electrical alterations (at the cellular level) was carried out by Priebe and Beuckelman in 1998 [173]. Selected ion currents, based on experimental data, were remodeled leading to HF phenotype, characterized by a longer action potential duration (APD) and altered Ca^{2+} transient. They also showed that EADs could develop following the block of the rapid delayed K^+ current (I_{Kr}). Later, Winslow et al. [237] defined the minimum model of end-stage heart failure focusing on the protein levels of SR Ca^{2+} ATPase and I_{NCX} in canine cardiac ventricular failing myocytes, to simulate failing Ca^{2+} transients. A more detailed description of Ca^{2+} dynamics and the main role of the ryanodine receptors (RyR) was developed by Shannon et al [199, 200]. Thus, several studies focused on describing the failing phenotype (see chapter 5) in order to understand the arrhythmogenic consequences that may arise during the development of this pathology. However, a more complete model gathering the whole set of electrophysiological and structural alterations ocurring in HF is yet to be adressed.

1.5 Aim and Objectives

In the last decades molecular and cellular observation techniques have improved significantly. However, there are still plenty of situations where the experimental approach is limited, and computer simulations can overcome these limitations. Computer modeling and simulation can reproduce with fidelity experimental observations, shed light on cardiac biophysical phenomena, and bring new understanding on arrhythmogenic mechanisms. Thus, the main objective of the present Thesis is to perform multiscale computer simulations of the cardiac electrical activity at different levels (cellular, wedge, tissue) to understand, analyze, and predict the human cardiac behavior under heart failure conditions. This aim has been splitted into the following specific objectives:

- To develop and validate an AP cellular model of human heart failure, including the role of the late sodium current on account of its relevance in failing phenotype, in order to study the electrical activity of failing cells and possible proarrhythmic effects.
- To evaluate the role of electrophysiological and structural heart failure remodeling on the modulation of key elements of the arrhythmogenic substrate, such as electrophysiological gradients and abnormal impulse propagation.
- To assess vulnerability to reentry under heart failure conditions by incorporating established electrophysiological and anatomical remodeling.
- To summarize and evaluate the advances made in the computational field focusing on simulation approaches to reproduce heart failure phenotype and its implications to arrhythmogenesis, ranging from the cellular level to whole-heart simulations.

1.6 Overview

In this Thesis, we investigate in silico the heart failure phenothype. In this first chapter we introduce the basis of cardiac electrical activity and how computer modeling can be used as a powerful tool to describe electrical dynamics at the cellular level and at the tissue and organ level. The core contents of this Thesis are structured in the following four chapters.

Chapter 2 aims at providing a model for cellular human heart failure using a modified version of Grandi et al. model [79] for the human ventricular action potential, incorporating the formulation of the late sodium current, key factor in the failing phenotype. A sensitivity analysis was performed to take into account experimental variability and simulations of the pathological electrical activity of the cell were conducted in order to validate the heart failure model.

Chapter 3 focuses on the role of electrophysiological and structural heart failure remodeling in setting the stage for malignant life-threatening arrhythmias in a transmural ventricular strand. The presence of controversial M cells is evaluated and the influence of heterogeneous remodeling is tested as well. The heart failure model is adapted to the O'Hara et al. human ventricular AP model [157] in order to assess model dependencies. The influence of heart failure remodeling and fibrotic content within the strand is evaluated.

Chapter 4 aims at characterizing several configurations of human transmural ventricular tissues with diffuse fibrosis embedded. Fibrotic content and intercellular uncoupling are altered in order to investigate vulnerability to reentry under conditions of heart failure electrical and structural remodeling.

In Chapter 5 we summarize published computational studies that focused on the description of either heart failure phenotype or electrophysiological and structural alterations that can be related to this pathology. The main advances and achieved objectives made in heart failure modeling and simulation including the work of the present Thesis and other published studies are discussed. Remaining improvements in this field are suggested and highlighted.

Finally, the results and implications of this Thesis are discussed and summarized in the Conclusions chapter.

CHAPTER 2

Simulation and Mechanistic Investigation of the Arrhythmogenic Role of the Late Sodium Current in Human Heart Failure

The content of this chapter is based on the publication:
Trenor, B., Cardona, K.,**Gomez, JF.**, Rajamani, S., Ferrero, JM., Belardinelli, L., Saiz, J. Simulation and mechanistic investigation of the arrhythmogenic role of the late sodium current in human heart failure. *PloS One*, 7(3):e32659, 2012.

2.1 Abstract

Heart failure constitutes a major public health problem worldwide. The electrophysiological (EP) remodeling of failing hearts sets the stage for malignant arrhythmias, in which the role of the late Na^+ current (I_{NaL}) is relevant and is currently under investigation. In this study we examined the role of I_{NaL} in the electrophysiological phenotype of ventricular myocytes, and its proarrhythmic effects in the failing heart. A model for cellular heart failure was proposed using a modified version of Grandi et al. model for human ventricular action potential that incorporates the formulation of I_{NaL}. A sensitivity analysis of the model was performed and simulations of the pathological electrical activity of the cell were conducted. The proposed model for the human I_{NaL} and the electrophysiological remodeling of myocytes from failing hearts accurately reproduce experimental observations. The sensitivity analysis of the modulation of electrophysiological parameters of myocytes from failing hearts due to ion channels remodeling, revealed a role for I_{NaL} in the prolongation of action potential duration (APD), triangulation of the shape of the AP, and changes in Ca^{2+} transient. A mechanistic investigation of intracellular Na^+ accumulation and APD shortening with increasing frequency of stimulation of failing myocytes revealed a role for the Na^+/K^+ pump, the Na^+/Ca^{2+} exchanger and I_{NaL}. The results of the simulations also showed that in failing myocytes, the enhancement of I_{NaL} increased the reverse rate-dependent APD prolongation and the probability of initiating early afterdepolarizations. The electrophysiological remodeling of failing hearts and especially the enhancement of the I_{NaL} prolong APD and alter Ca^{2+} transient facilitating the development of early afterdepolarizations. An enhanced I_{NaL} appears to be an important contributor to the electrophysiological phenotype and to the dysregulation of $[Ca^{2+}]_i$ homeostasis of failing myocytes.

2.2 Introduction

Over 5 million persons in the United States suffer from heart failure (HF) and more than 250,000 die annually [188]. Patients with congestive HF are prone to develop complex ventricular tachyarrhythmias and some die suddenly [105]. Experimental studies conducted using animal models of HF have shown that ventricular arrhythmias are mainly due to non-reentrant mechanisms, most likely triggered activity based on afterdepolarizations [105].

Much attention has been paid to the understanding of the arrhythmogenic mechanisms induced by the structural, electrical, and metabolic remodeling of the failing heart. The electrophysiological remodeling of the failing heart has been well described (see [213, 214] for review). Action potential (AP) prolongation, altered Ca^{2+} handling, as well as intracellular Na^+ ($[Na^+]_i$) accumulation have been established as the hallmark characteristics of myocytes and tissues isolated from failing human and canine hearts [118–120, 173]. These alterations are closely related to arrhythmogenic mechanisms, such as early (EADs) and delayed (DADs) afterdepolarizations, observed in HF [18]. Functional remodeling of ion channels and pumps is the underlying cause for AP duration (APD) prolongation and altered intracellular Ca^{2+} ($[Ca^{2+}]_i$) homeostasis. Downregulation of outward K^+ currents is the most consistent change in animal models and human HF [20, 119, 120, 213, 214]. Major changes in intracellular and sarcoplasmic reticulum (SR) Ca^{2+} homeostasis are also associated with HF in several animal species, included human [9, 18, 163, 237]. In myocytes from failing hearts $[Na^+]_i$ concentration and Ca^{2+} handling are closely linked; $[Na^+]_i$ is increased in failing ventricular myocytes from human and other animal species[18, 26, 213, 214] and a prominent increase of the human late Na^+ current (I_{NaL}) has also been documented [135, 224], and has been proposed as a therapeutic target [220, 222, 250]. Experimental studies have shown that the I_{NaL} is involved in the generation of EADs in myocytes [220, 250] and life-threatening arrhythmias, such as torsade de pointes (TdP) [140], especially under conditions of reduced repolarization reserve in several animal species [241–243]. Other changes in biomarkers for arrhythmic risk such as the increase in the reverse rate-dependent APD prolongation [140, 242, 244] have been attributed to an increase in I_{NaL} concomitant with inhibition of outward K^+ currents.

Thus, the goal of our study was to analyze, using computer simulations, the role of the I_{NaL} in the setting of human HF. A mathematical model of human HF is proposed at cellular level using a modified version of the Grandi et al. model (from herein referred to as the GPB model) [79] of endocardial AP, in which a new formulation of the I_{NaL} is

included. The sensitivity analysis performed for the HF model, as well as the simulations of the rate-dependence of APD and EAD generation revealed that the mechanisms underlying the arrhythmogenic processes taking place in HF conditions, from a theoretical point of view, include an enhanced I_{NaL}.

2.3 Methods

2.3.1 Model of the human ventricular I_{NaL}

To simulate the electrical activity of human ventricular myocytes, the AP model formulated by Grandi et al. [79] for endocardial cells was used. This model is one of the latest and most detailed mathematical model for ionic currents and Ca^{2+} handling of the human ventricular AP. A particular strength of the GPB model is its ability to reproduce the rate-dependence of APD upon outward K^+ currents block and their individual role in repolarization. Thus, this model provides a powerful tool to explore repolarization abnormalities under conditions of disease, such as HF. However, in order to realistically simulate HF, an important issue remains unresolved in this model, namely the role of I_{NaL}.

We included in the GPB model a new formulation for human I_{NaL} that is described in equations (2.1) to (2.4) and is based on the formulation we included previously [29] in the AP model formulated by ten Tusscher et al. [217].

$$I_{NaL} = g_{NaL} {m_L}^3 h_L (V - E_{NaL}) \tag{2.1}$$

$$\frac{dh_L}{dt} = \frac{h_{L,\infty} - h_L}{\tau_{hL}} \tag{2.2}$$

$$h_{L,\infty} = \frac{1}{1 + e^{((V_m + 91)/6.1)}} \tag{2.3}$$

$$\tau_{hL} = 233ms \tag{2.4}$$

We adopted these equations following Hodgkin Huxley formalism, where the activation gate (m_L) and the Nernst potential for Na^+ (E_{NaL}) were unchanged with respect to I_{NaT} formulation in the GPB model. The steady-state inactivation gate ($h_{L,\infty}$) was taken from Maltsev et al. [132], as did Hund et al. in their model for canine ventricular myocytes [95]. The maximum conductance (g_{NaL}) and the time constant of inactivation (τ_{hL}) were

fitted to reproduce I_{NaL} data taken from human mid-myocardial myocytes [133]. In their experiments, Maltsev et al. [133] measured an I_{NaL}/I_{NaT} ratio of approximately 0.1% using a voltage clamp protocol at room temperature. In our model g_{NaL} was fitted accordingly using voltage clamp simulations, yielding 0.015 mS/mF. No correction factor for temperature was applied, as we assumed that I_{NaL}/I_{NaT} ratio does not change with temperature in myocytes, as reported in transfected HEK-293 cells [149]. However, because experimental data indicate that ion channel dynamics are altered by temperature, the time constant of inactivation (τ_{hL}) of I_{NaL} reported by Maltsev et al. [134] for human ventricular midmyocardial myocytes was multiplied by a Q10 factor of 2.2 [149],yielding 233 ms at 37°C.

2.3.2 Heart failure cellular model for human

The remodeling of myocyte electrophysiology in HF is well described [213] and can explain for the most, the hallmark characteristics of failing cardiac tissues and myocytes, such as AP prolongation and alteration of Ca^{2+} and Na^{+} handling [19, 105, 119]. On the basis of experimental observations [9, 18, 26, 120, 135, 163, 213, 214, 219] and previous simulation studies [173, 200, 237, 251], we hereby propose various changes in the formulation of several ionic currents of the GPB model to reproduce the reported experimental changes in AP and intracellular Ca^{2+} and Na^{+} handling in ventricular myocytes from failing human hearts [19, 118, 232]. Our model will be referred to as the basic HF model.Table 2.1 summarizes the changes we made in the different ionic properties with respect to the GPB model. The ionic remodeling is mainly based on experimental data observed in human hearts.

A prominent increase in I_{NaL} and slowing of current decay has been described in ventricular mid-myocardial myocytes isolated from failing hearts of dogs and humans [135, 219]. Accordingly, the current density and the time constant of inactivation were increased two-fold compared to non-failing cells. Although Maltsev et al. [135] reported a smaller increase in both values in failing myocytes, their experiments were performed at room temperature and stated that the changes are expected to increase at physiological temperature. Furthermore, the values of the time constant of inactivation could be measured for human myocytes, but the current density was only given for dog myocytes, as the authors state the difficulty to measure it in human myocytes where the variability was very high. Also, in a previous study by Valdivia et al. [224], I_{NaL} was increased 5-fold in human failing myocytes with respect to normal myocytes. Downregulation of K^{+} currents is the most consistent ionic current change observed in myocytes isolated from failing hearts from animal models and

Parameter	% Change vs. GPB	References	Experimental conditions
I_{NaL}	↑200	Maltsev et al.,2007 [135]	Isolated cardiomyocytes from LV mid-myocardium of failing dog hearts. Whole cell voltage clamp (room temperature)
		Valdivia et al., 2005 [224]	Isolated cardiomyocytes from LV of failing human hearts. Whole cell voltage clamp(room temperature)
τ_{hL}	↑200	Maltsev et al.,2007 [135]	Isolated cardiomyocytes from LV mid-myocardium of failing human hearts. Whole cell voltage clamp (room temperature)
I_{to}	↓60	Wettwer et al,1994 [233]	Isolated cardiomyocytes from LV endocardium of failing human hearts. Whole cell voltage clamp (room temperature)
		Beuckelmann et al., 1993 [20]	Isolated cardiomyocytes from LV mid-myocardium of failing human hearts. Whole cell voltage clamp (room temperature)
		Nabauer et al., 1996 [147]	Isolated cardiomyocytes from LV endocardium of failing human hearts. Whole cell voltage clamp (room temperature)
I_{K1}	↓32	Tomaselli et al.,1999 [213]	Review article. Several species.
		Beuckelmann et al., 1993 [20]	Isolated cardiomyocytes from LV mid-myocardium of failing human hearts. Whole cell voltage clamp (35°C)
		Li et al., 2004 [120]	Isolated cardiomyocytes from RV epicardium of failing human hearts. Whole cell voltage clamp (room temperature)
I_{NaK}	↓10	Bundgaard et al.,1996 [26]	Measurements of human myocardial. Na,K-ATPase concentration in failing hearts
		Tomaselli et al.,1999 [213]	Review article.
		Tomaselli et al.,2004 [214]	Review article.
I_{Nab}	=0	Priebe and Beuckelmann, 1998 [173]	Simulation of human HF.
I_{Cab}	↑153	Priebe and Beuckelmann, 1998 [173]	Simulation of human HF.
I_{NCX}	↑175	Priebe and Beuckelmann, 1998 [173]	Simulation of human HF.
		Reinecke et al.,1996 [178]	The functional activity of the Na^+-Ca^{2+} exchanger was determined by measuring the Na^+-dependent Ca^{2+} uptake into membrane vesicles prepared from human left ventricular samples.
I_{SERCA}	↓50	Piacentino et al., 2003 [163]	Isolated cardiomyocytes from LV of failing human hearts. Measurements of Ca^{2+} uptake rates by the SR (37°C).
		Hasenfuss et al.,1994 [85]	Endocardial strip preparations from human failing hearts. Measurements of Ca^{2+} uptake in myocardial homogenates (37°C).
		Schwinger et al.,1995 [197]	LV from human failing hearts. Measurements of Ca^{2+} uptake
I_{leak}	↑500	Bers et al.,2006 [18]	Review article.
EC_{50SR}	↓11	Curran et al.,2010 [47]	Isolated cardiomyocytes from LV of failing rabbit hearts. Measurements of RyR sensitivity to SR Ca^{2+}
		Antoons et al.,2007 [9]	Review article.
		Bers et al.,2006 [18]	Review article.

Table 2.1: *Electrophisiological heart failure remodeling. Changes in ion channel, transporters, and pumps activities, and constants used in the basic heart failure (HF) model. The changes are indicated in percentage of increase (↑) or decrease (↓) with respect to the Grandi et al. model (the GPB model) [79].*

humans [20, 119, 120]. Mainly, I_{to} is downregulated without a significant change in the voltage dependence or kinetics [20]. We reduced the transient outward K^+ current (I_{to}) to 40% of its normal value. Reported changes in I_{K1} functional expression are more variable than I_{to} [20, 213] and have a strong dependence on the etiology. The conductance of this ion channel was multiplied by 0.68 as in [237], a value within the experimental range. In regards to $[Na^+]_i$ handling, which is also altered in HF, we reduced I_{NaK} activity by 10%, as the preponderance of experimental data reveal that the expression and function of the Na^+/K^+-ATPase are reduced in HF [26, 213, 214]. Similar to that of Priebe and Beuckelmann simulation study [173], the background Na^+ current (I_{Nab}) was not included in our HF model. Finally, the changes in intracellular and SR Ca^{2+} homeostasis were achieved by an increase of 75% of I_{NCX} [173, 178, 237], and a decrease of 50% of I_{SERCA} [163]. To reproduce the experimentally observed changes in Ca^{2+} sensitivity of the ryanodine receptor (RyR) [9, 47], I_{leak} was increased 3-fold and the parameter $EC50_{SR}$ for SR $[Ca^{2+}]_i$-dependent activation of SR release (see Grandi [79] supplementary data) was reduced to 0.4 mM. The background Ca^{2+} current was changed as in the study of Priebe and Beuckelmann [173].

2.3.3 Sensitivity analysis of the HF model

A sensitivity analysis was performed to investigate how the reported variability in HF remodeling data might modulate the main EP characteristics in HF. These characteristics 'c' include APD at 90% and 50% of repolarization (APD_{90} and APD_{50}), triangulation, peak systolic and diastolic $[Ca^{2+}]_i$ transient, τ_{Ca}decay, peak systolic and diastolic $[Ca^{2+}]_{SR}$, $[Na^+]_i$, and t_{NCXRP}.These characteristics were calculated at steady-state HF conditions (HF basic model) and after varying one parameter 'p' at a time. The parameters included each of the ionic current properties modified in the HF basic model, and were varied to its normal value, as in the GPB model, and to a value representing twice that observed in the HF basic remodeling. Although an important change has been implemented (double change) to be considered as a high variability, only the sensitivity, i.e. the relative effect was analyzed. The sensitivity analysis performed similar to that of Romero et al. [185], where in the indexes percentage of change ($D_{c,p,x}$) and sensitivities ($S_{c,p}$) were calculated as follows:

$$D_{c,p,x} = \frac{C_{p,x} - C_{HFbasic}}{C_{HFbasic}} x100 \tag{2.5}$$

$$S_{c,p} = \frac{D_{c,p,2} - D_{c,p,1}}{\Delta_a} \tag{2.6}$$

with $C_{p,x}$ and $C_{HFbasic}$ being the magnitude of the characteristic c when parameter p undergoes a double change (x = 2) with respect to the HF basic change, or no change at all (x = 1); Δ_a is the total interval of change of parameter p.

2.3.4 Stimulation protocols

Voltage clamp was used to simulate I_{NaL} behavior. A voltage pulse to -20 mV was applied from a holding potential of -120 mV as depicted in the inset of Figure 2.1A. To calculate I_{NaL}/I_{NaT} ratios (see Figure 2.1C) I_{NaL} was measured at 40 ms after the application of the depolarizing pulse and was divided by peak I_{NaT}. Cellular simulations were conducted at a stimulation rate of 1 Hz. Measurements were taken after achieving steady-state conditions. Changes in $[Na^+]_i$ and $[Ca^{2+}]_i$ levels at various stimulation rates were measured using a staircase protocol as previously described [165, 185]. Cardiomyocytes were stimulated at increasing fast frequencies (0.5, 1, 1.5, 2 and 2.5 Hz) for 10 minutes, and $[Ca^{2+}]_i$ and $[Na^+]_i$ levels were recorded for each of the frequencies.To analyze the APD rate-dependence, simulations were performed at different frequencies of stimulation (0.5, 1, 1.25 and 1.6 Hz). Measurements of APD_{90} were taken after achieving the steady-state; likewise for APs, $[Na^+]_i$ and several ionic currents. The rate-dependence was measured as the difference between the maximum APD_{90} for a stimulation rate of 0.5 Hz and the minimum APD_{90} corresponding to the highest stimulation frequency.

2.4 Results

2.4.1 Effects of I_{NaL} on human AP

Figure 2.1A shows the generation of I_{NaL} trace using a voltage clamp protocol similar to that of Maltsev et al [134] in ventricular mid-myocardial myocytes at room temperature. The simulated I_{NaL} had similar time evolution and amplitude to the experimental findings. Panels B and C show the effects of this current on AP and APD at 90% of repolarization (APD_{90}), respectively. The inclusion of I_{NaL} in the GPB model slightly prolongs steady-state APD at 1 Hz (see Figure 2.1B). APD remains within the physiological range for human endocardial myocytes [56, 73, 118]. By increasing the magnitude of I_{NaL} by a factor of two-, five- or ten-fold, we obtained APD_{90} prolongations of 11%, 44% and 78%, respectively. Experimental recordings of monophasic APs (MAPs) under the effects of veratridine, an enhancer of I_{NaL}, show similar effects on APD prolongation in rabbit myocytes [204]. We determined the sensitivity of APD_{90} to I_{NaL} amplitude at different stimulation rates. As shown in Figure 2.1C, I_{NaL}/I_{NaT} ratios, where I_{NaT} is the transient peak I_{Na}, were varied from 0.0298% to 1.26% and APD_{90} significantly increased according to the magnitude of I_{NaL}. Furthermore, the sensitivity of APD_{90} increased with the slowing of the stimulation rate (compare 1 Hz and 0.5 Hz). Similar simulations were carried out in a rabbit model of AP [80]. As shown in Figure 2.1D, the difference in sensitivity of APD_{90} to changes in frequency of stimulation (0.5 and 1 Hz) was also observed. Note that the morphology of the curves in Figure 2.1D is different to our results, as different models for I_{NaL} and different AP models were used. The ratio chosen in our model of 0.12% yields an APD_{90} that is within the physiological range for 1 Hz indicated by the discontinuous lines.

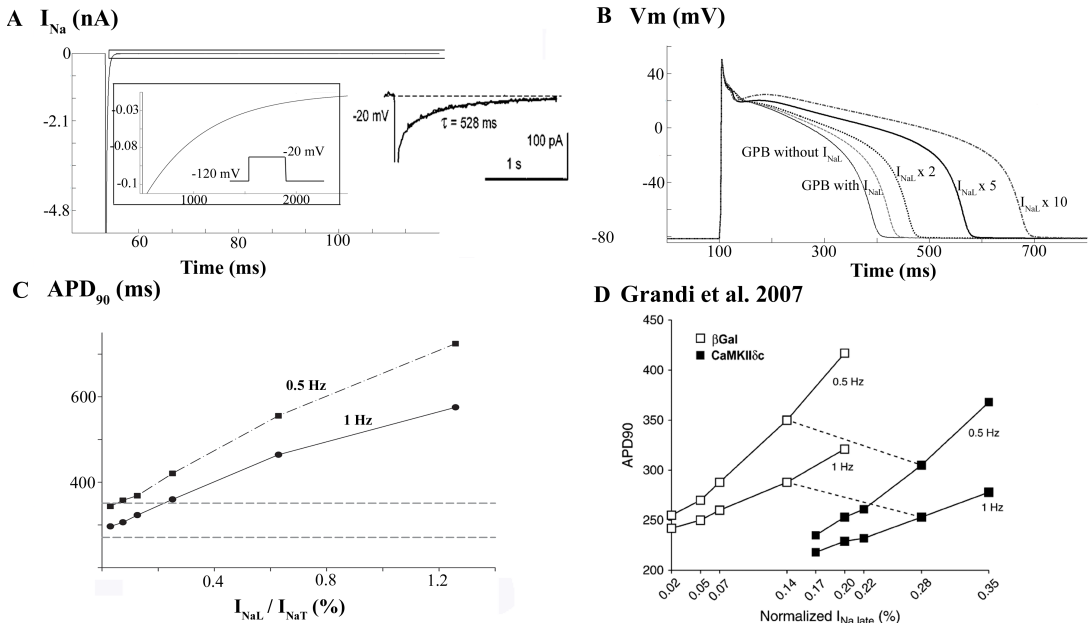

Figure 2.1: *Time course of late Na^+ current and its effects on AP. A: Simulation of late Na^+ current (I_{NaL}) using a voltage clamp protocol similar to that of the experimental measurements obtained by Maltsev et al. [134] (shown in the right inset) in ventricular myocytes at room temperature. The left inset shows an expanded view of the current between 480 ms and 2500 ms. B: Simulated action potentials (APs) at 1-Hz pacing rate using the GPB model, the GPB model modified with control I_{NaL}, and I_{NaL} enhanced 2-fold, 5-fold and 10-fold. C: APD_{90} sensitivity to the I_{NaL} amplitude. APs were simulated at 0.5-Hz (square symbols) and 1-Hz (circle symbols) pacing rate by varying I_{NaL}/I_{NaT} ratio from 0.0298% to 1.26%. The range of experimental APD at 90% repolarization (APD_{90}) for human is represented by the two discontinuous lines. D: APD_{90} sensitivity to the I_{NaL} amplitude (open symbols) taken from Grandi et al. [80] who used a rabbit model.*

2.4.2 Heart Failure model and sensitivity analysis

APs and $[Ca^{2+}]_i$ transients were simulated under conditions of HF. Figure 2.2 shows APs (panel A), $[Ca^{2+}]_i$ transients (panel B) and Na^+/Ca^{2+} exchanger (NCX) function (I_{NCX}) (panel C) of failing (light line) and nonfailing (dark line) ventricular myocytes after achieving steady-state conditions for a stimulation rate of 1 Hz. Our results showed an APD_{90} prolongation of 24% in failing myocytes versus normal ones, as well as a 18% prolongation in APD_{50}, so that triangulation (APD_{90} - APD_{50}) increased by 43% under HF conditions. The experimental observations shown in the inset of Figure 2.2 (panel A) taken from reference [173], show the variability of the APD in failing myocytes from human hearts, which falls within the simulated values of APD observed.

Figure 2.2B depicts an altered $[Ca^{2+}]_i$ transient under HF conditions, as has been documented experimentally and is shown in the inset [232]. Indeed, diastolic $[Ca^{2+}]_i$ is slightly increased, whereas peak systolic $[Ca^{2+}]_i$ is reduced to 41% of the one observed during normal conditions. An additional reported feature of the $[Ca^{2+}]_i$ transient of a failing myocyte is its slow decay. In our simulations Ca^{2+} transient decay, quantified as the time needed from the peak value to reach 10% of the transient amplitude (τ_{Ca} decay), yielded 630 ms and 380 ms in the failing and nonfailing myocytes, respectively. Finally, Figure 2.2C illustrates the changes in I_{NCX} during HF, mainly a shift in the time of the reversal potential for the NCX (t_{NCXRP}) of 20 ms. Similar shifts in t_{NCXRP} have been reported in experimental studies [232].

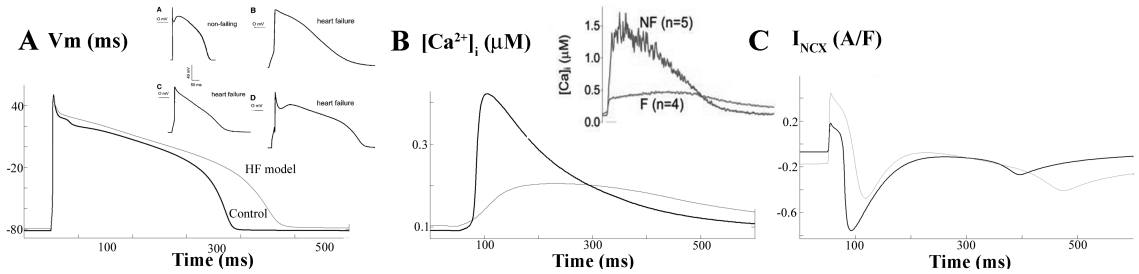

Figure 2.2: *Electrophysiological changes in heart failure. Simulated APs (panel A), $[Ca^{2+}]_i$ transients (panel B), and Na^+/Ca^{2+} exchanger (NCX) activity (panel C) at 1-Hz pacing rate in control (dark line) and in heart failure (HF) conditions (light line). The insets show experimental recordings of Priebe and Beuckelmann et al. [173] (panel A) and Weber et al. [232] (panel B).*

Changes in $[Na^+]_i$ and $[Ca^{2+}]_i$ levels under HF conditions at various stimulation rates were also investigated using a staircase protocol described in the methods section and described previously [31, 165, 185]. Figure 2.3A shows that diastolic $[Ca^{2+}]_i$ level is higher in HF than in normal conditions and systolic level is always higher in normal conditions than in HF, as reported experimentally[15, 53, 173]. The impact of the variability of ion channel remodeling on these results are presented in Figures 2.12, 2.13, 2.14, 2.15.

Another feature of myocytes from failing hearts is the high concentration of $[Na^+]_i$ regardless of the stimulation rate, as observed in Figure 2.3B and experimentally reported by Pieske et al. [165] in failing human myocardial cells. However, as acknowledged by Pieske et al. [165], it should be noted that the absolute $[Na^+]_i$ values in their experimental work were overestimated in normal and failing hearts. The impact of the variability of ion channel remodeling on these results are presented in Figures 2.16 and 2.17.

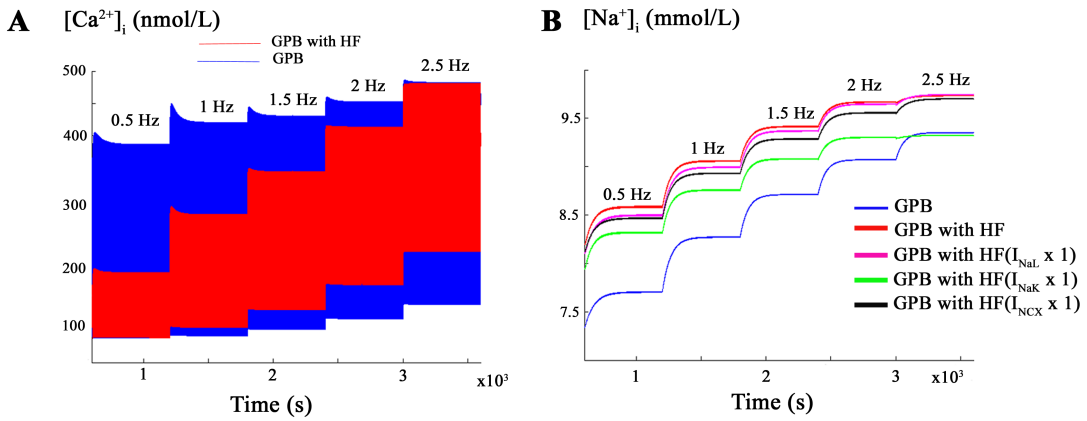

Figure 2.3: *$[Ca^{2+}]_i$ and $[Na^+]_i$ changes with increasing frequency in HF. Influence of the stimulation rate on $[Ca^{2+}]_i$ (panel A) and $[Na^+]_i$ in nmol/L (panel B) determined using the staircase protocol. The simulations were performed using the modified GPB model with I_{NaL} incorporated in normal conditions (blue) and the modified GPB model incorporating HF conditions (red). In panel B, conditions of HF without I_{NaL}, I_{NaL} or I_{NaK} remodeling are also shown.*

To analyze the mechanisms responsible for $[Na^+]_i$ accumulation with frequency in failing myocytes, the above pacing protocol was applied for a) normal conditions (blue), b) HF conditions (red), c) HF with no I_{NaL} upregulation (purple), d) HF with no Na^+/K^+ pump current (I_{NaK}) downregulation (green) and e) HF with no I_{NCX} upregulation (black). From the results obtained in Figure 2.3B,it can be deduced that $[Na^+]_i$ accumulation is mainly driven in HF by alterations in I_{NaK}, and much less by the I_{NCX} and I_{NaL}.

Our basic HF model, as described in Figure 2.2 and 2.3, reproduced the main changes in the electrophysiological characteristics of myocytes from failing hearts. However, the experimentally reported ranges for EP changes, as well as the magnitude of ion channels, transporters and respective current remodeling, vary substantially for different experimental settings and HF stages. Hence, we performed a sensitivity analysis to assess the impact of the main ionic parameters remodeled in HF on the described EP characteristics. Figure 2.4A highlights the role of I_{NaL} and I_{NaK} in APD_{90} under conditions of HF. When I_{NaL} undergoes a 2-fold increase (i.e. doubling) with respect to the basic HF increase, APD is prolonged 22% and no change at all in this current leads to a shortening of the APD_{90} by 10% with respect to basic HF conditions.This result is in agreement with experimental recordings in failing human myocytes, where I_{NaL} has a crucial role in APD [222]. Similarly, the downregulation of Na^+/K^+ pump in HF has a relevant effect on APD_{90} shortening, and further reduction of the current leads to a decrease of 22% with respect to HF APD_{90} value, which is in agreement with experimental observations [117]. Figure 2.4B reveals the importance of I_{NaK}, I_{NCX}, the background Ca^{+2} current (I_{Cab}), the leak Ca^{+2} current (I_{leak}), and I_{NaL} in determining the value of peak systolic $[Ca^{2+}]_i$ during HF. Regarding the regulation of $[Na^+]_i$ value in failing myocytes, Figure 2.4C shows the important role of I_{NaK}, I_{Cab}, the inward rectifier K^+ current (I_{K1}), I_{NCX} and I_{NaL}.

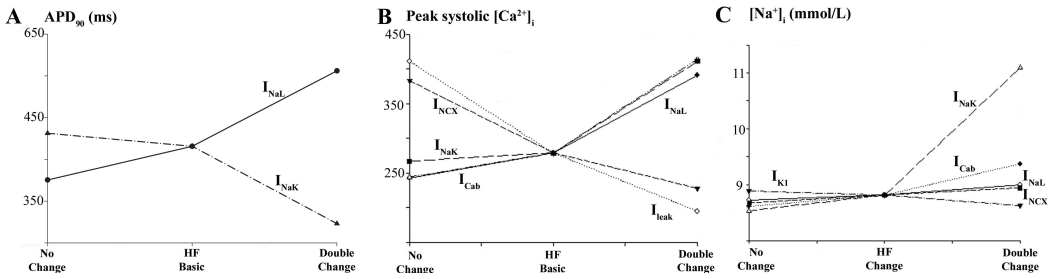

Figure 2.4: *Sensitivity of electrophysiological parameters to changes in ionic current properties. Changes in APD_{90} (panel A), peak systolic $[Ca^{2+}]_i$ (panel B), and $[Na^+]_i$ (panel C) with changes in I_{NaL}, I_{NaK}, I_{leak} , I_{NCX},I_{K1} and I_{Cab}, as labeled next to each curve. Axis x represents the simulation conditions; for 'HF basics' the remodeling of the basic HF model is considered, for 'No Change' the labeled current is unchanged as it is in the GPB model, for 'Double Change' the labeled current undergoes a double change with respect to the change exerted in 'HF basic'.*

To summarize the sensitivity of some of the EP characteristics (1st column) during HF to the altered ionic parameters (1st row), Figure 2.5 shows the relative sensitivity normalized to the maximum sensitivity for that particular characteristic, as described in the methods section. The positive and negative signs indicate whether the change of the ionic current and the HF EP characteristic follow the same or inverse tendency, respectively. Percentages in each box indicate the maximum absolute sensitivity of the EP parameter correspondent to that row for all ionic properties. From this sensitivity analysis it could be deduced that APD was particularly sensitive to I_{NaL} and to I_{NaK} (green and burgundy colors in rows 1 and 2). Furthermore, I_{K1}, I_{NCX} and I_{NaK} have an important effect on AP triangulation. The main features of Ca^{2+} transient in HF (3 medium rows) were mainly influenced in this order by I_{NaK}, SERCA function, I_{NCX}, I_{leak},I_{Cab}, and I_{NaL}. The SR Ca^{2+} concentration ($[Ca^{2+}]_{SR}$) is also influenced by other currents but in this case I_{leak} becomes more important than I_{NCX}. $[Na^+]_i$ is mainly regulated by I_{NaK}, I_{Cab}, I_{K1}, I_{NCX} and I_{NaL}. Finally, t_{NCXRP} is mainly modulated by the SR Ca^{2+} -ATPase activity (I_{SERCA}). The absolute effects of small changes ($\pm$ 15%) in the ionic remodeling of the basic HF model on the main results of our simulations are shown in Figures 2.9, 2.10, 2.11, 2.12, 2.13, 2.14, 2.15, 2.16, 2.17, 2.18, and 2.19. These absolute effects are in agreement with the relative role of the ionic parameters described above. We have especially focused on the sensitivity of APD_{90} in failing myocytes to I_{NaL}/I_{NaT} ratio, as shown in Figure 2.9. In this figure, the values of I_{NaL}/I_{NaT} ratios for 1 Hz in the modified the GPB model and in our basic HF model are indicated by arrows and are within experimental ranges (indicated by blue dotted lines in normal myocytes and by red discontinuous lines in failing myocytes, respectively). Changes in the selected ratios

affect the APD_{90} values of failing and normal myocytes, which stay within experimental ranges provided that the changes of these ratios are not very large.

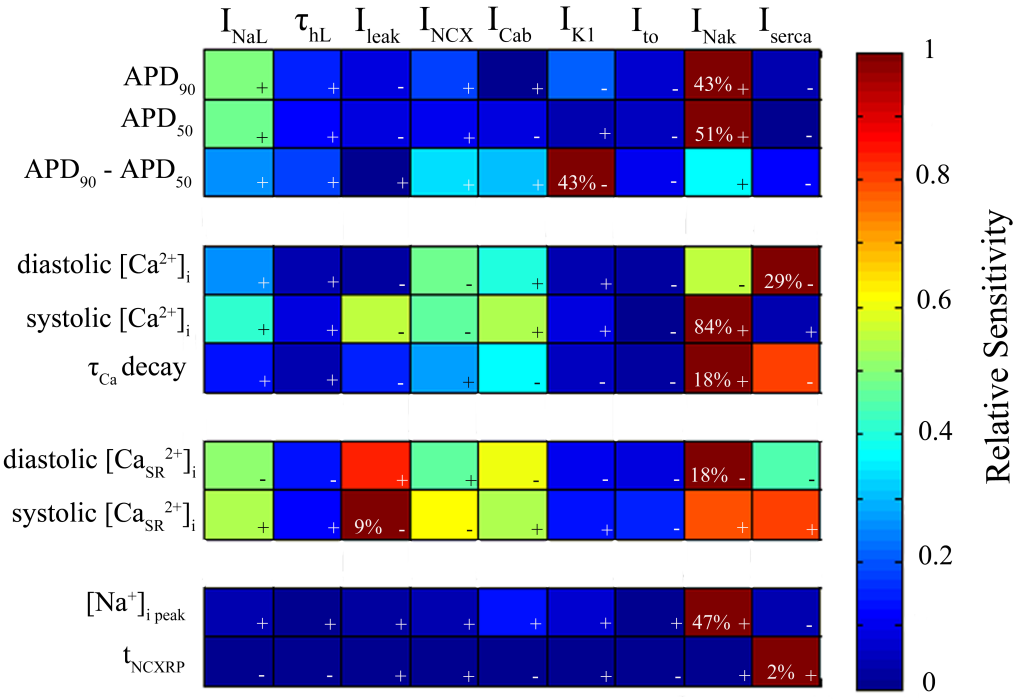

Figure 2.5: *Relative sensitivities of the electrophysiological parameters to changes in ionic current properties.Dark blue color indicates lack of dependency between the ionic property (1st row) and the EP parameter (1st column), and dark red color indicates strong direct (+) dependency or inverse dependency (-). Percents in each box indicate the maximum absolute sensitivity of the EP parameter correspondent to that row for all ionic properties.*

2.4.3 APD rate-dependence and the role of I_{NaL} in HF

The role of I_{NaL} in steady-state APD_{90} rate-dependence during HF was analyzed. An enhanced reverse frequency-dependence of APD_{90} is considered to be a major proarrhythmic risk (see [55] for review). We performed simulations and measured APD_{90} under normal and HF conditions for different magnitudes of I_{NaL} activation (see Figure 2.6A). Also 40% and 60% inhibition of the rapid component of the delayed rectifier K^+ current (I_{Kr}) in failing myocytes were simulated with different degrees of I_{NaL} enhancement (see Figure 2.6B). Indeed, the concomitant alteration of I_{NaL} and I_{Kr} has been reported to have important effects on arrhythmogenicity [140, 241, 243, 244]. An important result obtained in our simulations, as shown in Figure 2.6A, is the reverse rate-dependence effect on APD_{90} exerted by I_{NaL} enhancement for normal conditions (compare circles with stars). The rate-dependence yielded 110 and 190 ms maximal APD_{90} prolongation in normal conditions versus I_{NaL} increased by 4-fold, respectively. Similar observations were reported by others [140, 241–244] in rabbit ventricular myocytes under the effects of I_{NaL} activators, as well as in isolated perfused rabbit heart [243]. When considering HF conditions (squares), the rate-dependence is also increased with respect to normal conditions. The ΔAPD value is very similar to the value obtained with I_{NaL} enhanced (stars). This implies that I_{NaL} might be the main driver of the increased reverse rate-dependent prolongation of APD. Additionally, greater magnitudes of I_{NaL} (black triangles) are associated with greater increase in the reverse rate-dependency of APD of failing myocytes. Experimental studies [120] have also documented the increase of APD rate-dependence in human failing epicardial myocytes, as depicted in the inset. Simulations of APD rate-dependence in HF caused by small changes ($\pm$15%) in the ionic remodeling of the basic HF model (see Figures 2.10, 2.11, 2.12, 2.13, 2.14, 2.15, 2.16, 2.17, 2.18, and 2.19) to take into account the experimental variability on electrical remodeling during HF were also performed. The results do not change significantly with respect to the basic HF model, except for I_{NaK} and I_{NaL}, which have an important effect on APD_{90}, as predicted by the sensitivity analysis shown in Figure 2.5.

Figure 2.6B summarizes the concomitant contribution of I_{NaL} enhancement and I_{Kr} inhibition in the reverse rate-dependency of APD, shown in various experimental studies [140, 241, 243, 244], in failing myocytes.

To analyze the ionic mechanisms responsible for steady-state APD rate-dependence in failing myocytes, we determined the behavior of several ionic currents (I_{NaL}, I_{NCX} and I_{NaK}) and $[Na^+]_i$ at different frequencies of stimulation, as depicted in Figure 2.7. Our re-

sults show that the shortening of the APD with increased frequency in HF is explained on the one hand by the decrease in I_{NaL}, indeed faster rates lead to an incomplete recovery from inactivation of this current [148, 177, 254], and on the other hand by $[Na^+]_i$ accumulation leading to an increase of I_{NaK}. The role of I_{NCX} on APD is not evident as both outward and inward modes are enhanced. Although several experimental studies suggest the direct involvement of this current on APD shortening with frequency, as will be discussed later, its implication in our simulations is not evidenced. Indeed, when we stimulated the cell at high frequency (1.6 Hz) but clamped $[Na^+]_i$ value to the lower $[Na^+]_i$ value corresponding to the low frequency (0.5 Hz), we observed a decrease in APD_{90} with respect to APD_{90} at low frequency, concomitant with a decrease and increase of the outward and inward modes of NCX activity, respectively (results not shown). These changes in I_{NCX} should lead to a longer APD_{90}, instead of shorter, suggesting that I_{NCX} is not determinant in APD rate-dependence in the present model.

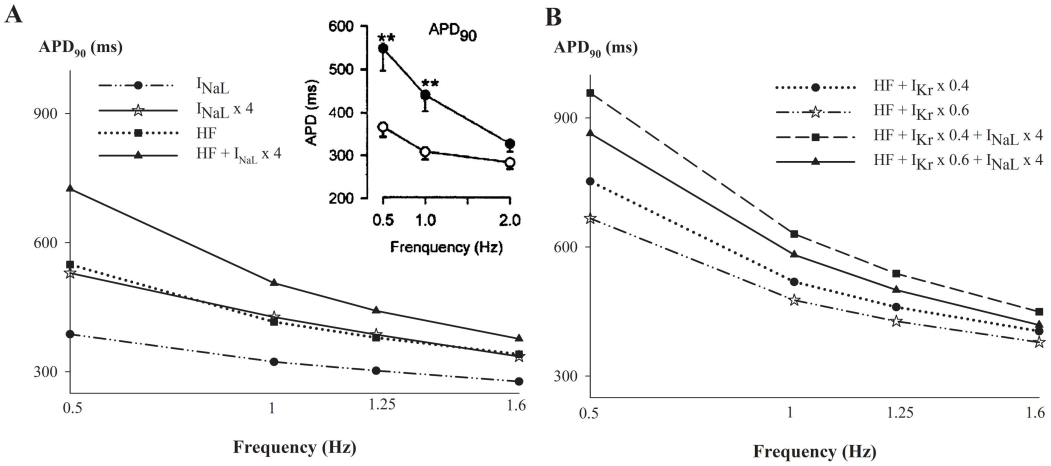

Figure 2.6: *Role of I_{NaL} in APD rate-dependence in HF and reduced repolarization reserve. Simulated APD dependence on stimulation frequency for normal (circles in panel A) and HF (squares in panel A) conditions and in the presence of enhanced I_{NaL} in normal (stars in panel A) and HF (triangles in panel A) conditions. The inset shows experimental results of Li et al. [120]. Panel B, depicts the APD rate-dependence for HF combined with different degrees of I_{Kr} inhibition and I_{NaL} enhancement.*

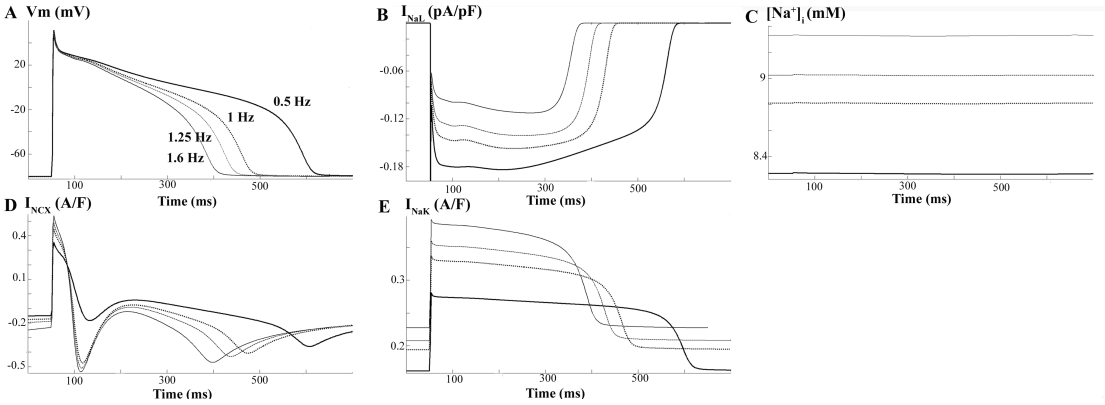

Figure 2.7: *Mechanisms for APD rate-dependence in HF. Simulated APs and ionic currents at different stimulating frequencies (0.5, 1, 1.25 and 1.6 Hz) under HF conditions.*

2.4.4 Arrhythmogenic effects of I_{NaL}

Under basic HF conditions, APD prolongation favors the occurrence of EADs. We were therefore interested in determining the role of I_{NaL} in the repolarization abnormalities of human failing hearts. We stimulated the myocyte at 1 Hz and simulated conditions of low repolarization reserve prone to EADs generation.

Under HF conditions using the basic HF model, I_{Kr} was reduced by 50% and the Ca^{2+} current (I_{CaL}) was increased by 30%. Figure 2.8A shows EADs (dark line) when I_{NaL} was doubled, whereas APs displayed no EADs when I_{NaL} was normal (light line). The impact of the variability in ion channel remodeling on EADs generation can be observed in Figures 2.18 and 2.19. The mechanisms by which EADs arise are dictated by a very delicate balance of ionic currents during AP plateau. Slight changes in this balance can suppress EADs, as occurs in the case when all ionic parameters are reduced in 15% with respect to the basic HF model (see Figure 2.19).

Figure 2.8 depicts APs and ionic currents to provide insight into the mechanisms by which enhancement of I_{NaL} indirectly triggers EADs [250]. The APD prolongation (panel A) caused by enhancement of I_{NaL} (panel B) leads to the reactivation of the activation gate d (panel F) of the I_{CaL}, which triggers the EAD, as was suggested by January et al. [106]. However, the important contribution of the altered Ca^{2+} transient should also be taken into consideration. Indeed, the APD prolongation caused by I_{NaL} enhancement alters Ca^{2+} han-

dling. As observed in panel C, $[Ca^{2+}]_{SR}$ remains elevated and provokes the trigger of a small spontaneous release (panel D, arrow) just before the EAD arises (panel A, arrow). NCX (panel E) extrudes Ca^{2+} operating in the inward mode, which contributes to membrane potential increase. This would contribute to I_{CaL} reactivation which triggers the EAD. The involvement of these currents is also shown in Figures 2.20, 2.21, 2.22, and 2.23, as a partial block of SR Ca^{2+} release (I_{rel}) or I_{NCX} suppresses the EADs.

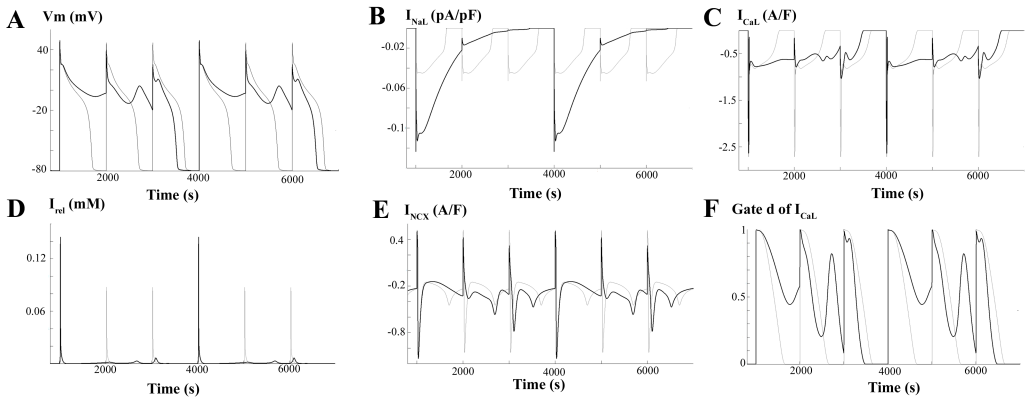

Figure 2.8: *Mechanisms for early afterdepolarizations with enhanced I_{NaL}. Simulated APs and ionic currents at a stimulating rate of 1 Hz for HF conditions, 50% inhibition of I_{Kr} and 30% increase of I_{CaL}. Panel A shows early afterdepolarizations (EADs; dark line) when I_{NaL} was doubled and APs with no EADs when I_{NaL} was normal (light line). The temporal evolutions of I_{NaL} (panel B), I_{rel} (panel D), I_{CaL} (panel C), NCX activity (panel E), and activation gate of I_{CaL} are also depicted when I_{NaL} was doubled (dark line) and when I_{NaL} was normal (light line).*

2.5 Discussion

2.5.1 Major Findings

In this chapter, one of the most recent and detailed AP model for human ventricular myocytes, the GPB model, was modified to simulate HF functional remodeling. The I_{NaL} was formulated and introduced in the model on the basis of human ventricular voltage clamp data. An important novelty of the study is the sensitivity analysis of the modulation of the main EP characteristics due to ion channel and transporters remodeling, highlighting the role of I_{NaL} in the changes of APD, triangulation and Ca^{2+} transient under HF conditions. A mechanistic investigation of $[Na^+]_i$ accumulation and APD shortening with increasing stimulation frequency in failing myocytes, revealed the roles of I_{NaK}, I_{NCX} and I_{NaL}. Finally, the arrhythmogenic effects of increased I_{NaL} were investigated. Our results showed the important role of I_{NaL} in APD reverse rate-dependence and EAD generation in failing myocytes, representing the first realistic simulation study on this issue, which complements experimental studies and sheds light into the ionic mechanisms responsible for HF phenotype.

2.5.2 Simulation of heart failure

Recently, O'Hara et al. [157] published a new AP model for human ventricular myocytes; however, in the present study the GPB model was chosen because its behavior was adequate to analyze the changes exerted in HF in APD, Ca^{2+} transient, the APD rate-dependence and EADs generation. Nevertheless future studies comparing the behavior of both models in pathological situations should be conducted. The GPB model was developed using human voltage-clamp data, and validated against recent experimental results [79]. In the present study, we demonstrate for the first time that the GPB model, subject to ion channel and transporter remodeling, is also appropriate to reproduce the electrical behavior of failing myocytes.

A large body of experimental research has focused on the functional remodeling of failing hearts [20, 26, 119, 120, 163, 213, 214]. However, little has been done in this field from a theoretical perspective. One of the first human ventricular AP models, including HF remodeling, was formulated by Priebe and Beuckelmann in 1998 [173]. However, I_{NaL} was not considered, and the formulation of Ca^{2+} handling was not as realistic as it is in

the GPB model. This represents an important limitation for HF, when Ca^{2+} transient undergoes critical changes. Later, in 2005, Zhang et al. [251] modified the human ten Tusscher model [217] to simulate HF. In the latter model, I_{NaL} was considered, but with experimental data derived using dog ventricular myocytes [95], and remodeling was derived using experimental data from multiple species. However, controversy about the changes introduced in their model for I_{NaT}, the slow component of the delayed rectifier K^+ current (I_{Ks}) or I_{CaL} exists for human failing myocytes [105, 213, 214]. Other authors have simulated ion remodeling of myocytes from canine and rabbit failing hearts [200, 237] that reproduce the APD and Ca^{2+} transient changes associated with HF. Our model of basic HF not only reproduces experimental observations on APD prolongation and Ca^{2+} transients alterations [120, 163, 173, 232], but also the APD, $[Ca^{2+}]_i$ and $[Na^+]_i$ ratedependence reported in failing myocyte[15, 53, 165].The ionic model of ventricular HF presented in this study is not only based on recent human experimental data, but also takes into account the variability documented in EP studies using sensitivity analysis. Sensitivity analysis also elucidates the ionic mechanisms responsible for the main changes in the EP characteristics of HF. Previous sensitivity analysis have been performed using the human ten Tusscher et al. [211] AP model [185], a modified version of the GPB model [31] and O'Hara et al. model [157], as well as rabbit [211] AP model. In these studies, the authors analyzed the effects of the physiological variability of the main ionic properties on several electrophysiological characteristics and biomarkers for arrhythmic risk, under normal physiological conditions. The main similarities of our results in HF with their studies on normal myocytes, are the importance of I_{NaK} [31, 185] and I_{NaL} [157] in regulating APD_{90}, and I_{K1} [31, 185] and I_{NaK} in regulating AP triangulation. The variability of I_{CaL} and I_{Kr} has also an important effect in their studies but was not considered in HF, as these currents are not remodeled. Also the impact of I_{NaK} and I_{NCX} was important on Ca^{2+} transients under normal conditions [31, 185].

Regarding the variability of functional remodeling in HF, it is worth noting that experimental measurements reported in literature have been conducted in different stages of HF (see[213, 214] for review). In the present study, ionic currents are within experimental ranges, but do not take into account differences in various stages of HF. Different combinations of changes were tested in the sensitivity analysis in order to determine the relative effects on the EP characteristics in HF (Figure 2.5) and the absolute effects of small changes ($\pm$15%) in ionic parameters on APD-ratedependence (Figures 2.10 and 2.11), $[Ca^{2+}]_i$ transients (Figures 2.12, 2.13,2.14, and 2.15), $[Na^+]_i$ values (Figures 2.16 and 2.17) and EADs generation (Figures 2.18 and 2.19). It should be noted that the results of the present sensitivity analysis are dependent on the values chosen for the ionic parameters in the basic HF model, as the percents of change also depend on these chosen values. The results suggest

that the downregulation of the Na^+/K^+ pump has an important role in the electrophysiological and Ca^{2+} transient changes in HF, highlighting the need for new experimental data. Electrophysiological studies [227] conducted in failing human hearts revealed increased Ca^{2+} transients under the effects of strophanthidin, a Na^+/K^+ pump blocker, which is in agreement with our results. However, little is known about the effects of Na^+/K^+ pump activity on APD in HF. Experiments carried out on hypertrophic rat hearts by Levi et al. [117] showed that the application of ouabain, a Na^+/K^+ pump blocker, resulted in APD shortening, which was caused by $[Na^+]_i$ accumulation and the subsequent increase in the reverse mode of the NCX. Similar studies should be performed using human failing hearts to determine the role of the effects of Na^+/K^+ pump on APD. Also the $[Na^+]_i$ accumulation with increasing frequency during HF appears to be mainly due to the downregulation of this pump, and a small contribution of I_{NaL} and I_{NCX} upregulation (see Figure 2.3B). Experimental studies reporting $[Na^+]_i$ accumulation in human HF [165] or animal species [15, 169] suggest that I_{NaK} downregulation, I_{NaL} and I_{NCX} upregulation, and altered activity of the Na^+/H^+ exchanger (not included in the GPB model), might be involved. However, no experiments have been performed to in human failing myocytes to clarify the responsible mechanisms. Other simulation studies [80, 230] using the Shannon et al. rabbit AP model [199] have also reported the small and important influence of I_{NaL} and I_{NaK}, respectively, on $[Na^+]_i$ accumulation with frequency under pathological situations other than HF.

Our results also reveal the role of I_{NaK} in APD rate- dependence as stated by Carmeliet [30] and by Eisner et al.[58] in their review on AP rate adaptation as well as shown in the theoretical and experimental findings by Pueyo et al. [174]. Additional simulation studies using different human AP models have also demonstrated this fact in normal conditions [157, 185]. Although O'Hara et al. [157] and Carro et al. [31] human AP models exhibit an improved behavior in the fast phase of APD rate adaptation than the GBP model, our study focused on the steady-state APD rate-dependence, where the GPB model is valid except for low frequencies [157]. Also Faber and Rudy [61] showed that APD shortening at high rates in a guinea pig AP model was due to the increase of the outward NCX activity. This observation is also consistent with experiments conducted on myocytes from human failing hearts [227], where increases in $[Na^+]_i$ led to APD shortening provoked by an increase of the reverse mode of I_{NCX}. However, the GPB model exhibits a much shorter outward mode of NCX than the Faber and Rudy model. Thus its contribution to AP repolarization is not evident in the present study. Furthermore, in failing human myocytes, Ca^{2+} influx via NCX is prominent during most of the plateau phase [232]. Thus changes in I_{NCX} formulation of the GPB model should be addressed to better understand the role of this current in HF APD rate-dependence. Also new experiments in failing human myocytes demonstrating the role

of I_{NaK} and I_{NCX} in APD rate-dependence would be of great interest. This finding also suggests that the functional increase of these outward currents caused by $[Na^+]_i$ accumulation may limit AP prolongation in HF, counterbalancing the increase of I_{NaL}.

Our results also highlight the pivotal role of I_{NaL} in the changes of EP characteristics in HF, which will be discussed in the following section. Finally, another mechanistic effect of relative importance in HF, revealed by the simulations of the present study is the increase of AP triangulation associated with I_{K1} downregulation. Similar observations have been reported in ventricular myocytes from normal dogs when I_{K1} was reduced with barium [22] and in the sensitivity analysis performed by Romero et al. [185] and Carro et al. [31] in normal physiological conditions.

2.5.3 Important role of I_{NaL} during heart failure and clinical implications

The pivotal role of I_{NaL} in the changes of EP characteristics and in arrhythmogenesis in HF has been uncovered in the present work. The formulation of the I_{NaL} model and its introduction in the GPB model was essential to draw our conclusions. Previous formulations have been proposed to model the behavior of I_{NaL} for different animal species using the Hodgkin-Huxley or Markov formalism [80, 95, 133, 140, 155, 222]. Noble and colleagues [155] in 1998 formulated the I_{NaL} for guinea pig by adding to their AP model a Na^+ current with reduced conductance and slow inactivation. Similarly, other Hodgkin-Huxley formulations have been proposed for rabbit [140] and dog [95, 222]. To avoid the complexity of Markov models for I_{NaL} [80], we adapted the Hodgkin-Huxley mathematical description of Hund et al. [95] to human data, as we did in a previous work using ten Tusscher et al. AP model [217]. Our model has been validated against experimental recordings of human APD in normal conditions [56, 73, 118], APD prolongation under the effect of drugs [204] and voltage clamp experiments [133]. Recently, a new AP model for human ventricular myocytes has been published by O'Hara et al. [157] including a formulation for I_{NaL} as in the present work. However, as their AP model includes CaMK regulation, their formulation of I_{NaL} also includes the effect of CaMK regulation.

In agreement with previous experimental observations, the upregulation of I_{NaL} during HF [135] or its enhancement in situations of reduced repolarization reserve [241] prolongs APD, causes AP triangulation and increase the reverse rate-dependent prolongation of APD, which are important harbingers for cardiac arrhythmias. The contribution of I_{NaL} in the reverse APD ratedependence was also previously simulated by our group [29] us-

ing a different human AP model [217] and conditions of reduced repolarization reserve. In regard to HF conditions, there is background of decreased outward currents, and even a small increase of I_{NaL} becomes more efficient in prolonging APD and favoring the trigger of EADs. The high probability of formation of EAD, leading to TdP, during HF has been experimentally demonstrated [120] but few studies have addressed the role of I_{NaL} in such situations [134, 220, 221]. Our results are in keeping with experimental findings, in which the I_{NaL} blocker ranolazine, effectively suppresses EADs from ventricular myocytes from failing hearts [220, 242]. Furthermore, during conditions of reduced repolarization reserve, in which outward K^+ currents are inhibited by drugs or by diseases, results of experimental studies [8, 241–243] have unmasked the role of endogenous or enhanced I_{NaL} in exerting proarrhythmic effects. This is in agreement with the results of our simulations, and provides evidence of this effect in HF. Our findings support the hypothesis that I_{NaL} represents an important target for triggered-arrhythmias treatment [9]. Similarly, inhibition of CaMKII, which is known to be responsible for I_{CaL} and ryanodine receptor phosphorylation as well as I_{NaL} regulation, appears to be an important therapeutic target for suppressing arrhythmias in HF [9, 94, 250].

2.5.4 Limitations of the study

Several limitations need to be considered, when drawing conclusions from the present study. The model for I_{NaL} was formulated on the basis of voltage-clamp human data for midmyocardial cells [133], as no measurements were available for endocardial or epicardial cells. Indeed, I_{NaL} is difficult to record due to the very low magnitude ($\sim$ 30-60pA) of this current under normal conditions [133]. Maltsev and Undrovinas reported a double exponential decay of I_{NaL} [133]. However, we chose a single-exponential decay formulation as proposed in previous studies [95, 132], and also in the new AP model by O'Hara et al. [157], as this model was able to reproduce its main effects on the AP. To build the model of HF used in the present study, the ionic remodeling was mainly based on experimental data observed in human hearts. Data from a large number of experimental studies have been taken into account, thus resulting in a high variability not only in the ionic remodeling but also in the stage of HF. In addition to the difficulties associated with gaining access to human hearts, explanted diseased hearts are usually in the end stage of HF. Moreover, there are controversies regarding specific ion channel currents remodeling during HF, such as I_{NaT}, I_{CaL} I_{Kr}, and I_{Ks}, and changes in these currents were not included in our HF model. Their effects on the EP characteristics would be significant contributors to the phenotype. We did

however simulate changes in I_{NaL} concomitant with inhibition of I_{Kr} and increase in I_{CaL} (Figures 2.6 and 2.8). Finally, our basic HF model has the inherited limitations described for the GPB model. In this sense, improvements related to the rapid phase of APD rate adaptation have been accomplished in later human AP models [31, 157]. The response of failing myocytes to abrupt changes of the stimulation rate was however out of the scope of the present study because of the lack of availability of experimental data in HF. With regard to steady-state APD rate-dependence, the GPB model is accurate except for very low frequencies [157]. Thus the results obtained for APD_{90} at low frequencies should be taken with caution.

2.5.5 Conclusion

This study aimed to investigate in silico the role of I_{NaL} in the electrophysiological and Ca^{2+} homeostasis phenotype of myocytes from failing hearts. Our results showed that the enhancement of this current during HF can lead to important prolongation of APD and triangulation, increases in reverse rate-dependent prolongation of APD, significantly contributes to Ca^{2+} handling changes and has an indirect but pivotal role in the genesis of EADs.

2.6 Supplemental Information

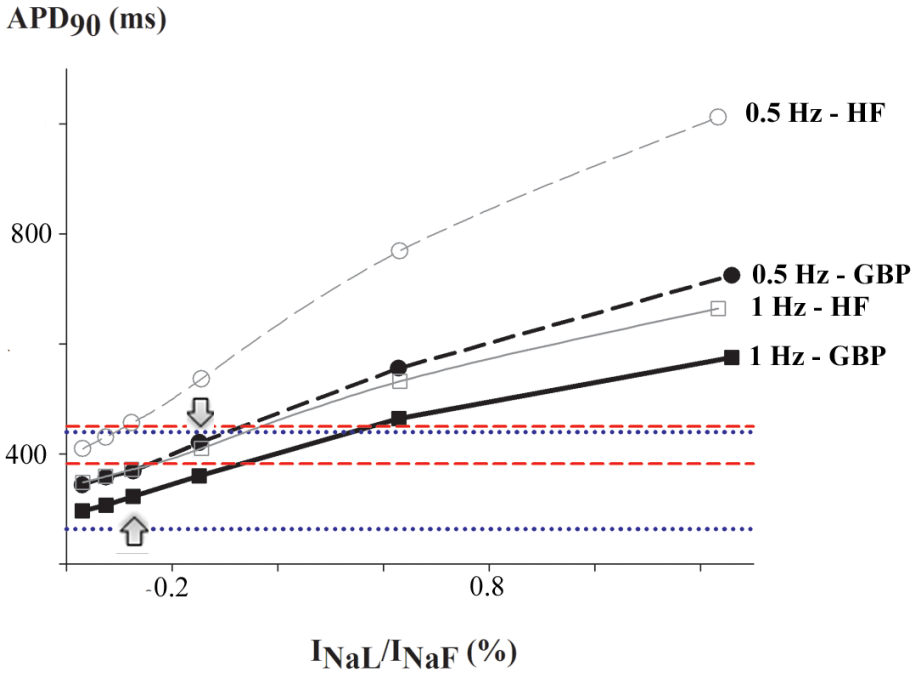

Figure 2.9: *Sensitivity of APD_{90} to the I_{NaL} amplitude in HF. Steady-state APs at 1 Hz (square symbols and solid lines) and 0.5 Hz (circle symbols and dashed lines) pacing rates with varying I_{NaL}/I_{NaT} for normal conditions using the GPB model (thick lines) and under basic HF conditions (thin lines) where I_{NaL} is doubled with respect to normal conditions. The range of experimental APD_{90} for human for normal conditions is represented by the two dotted blue lines. The range of experimental APD_{90} for human for HF conditions is represented by the two discontinuous red lines.*

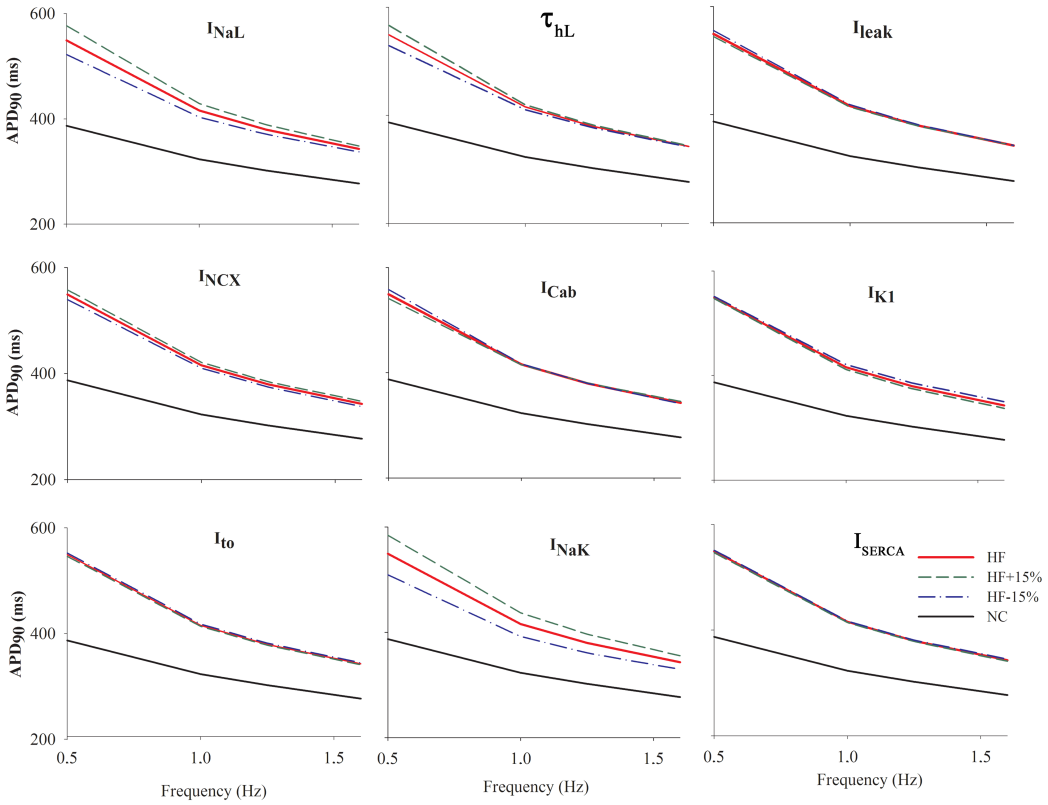

Figure 2.10: *Sensitivity of APD rate-dependence to variations in individual ionic parameters in HF. The steady-state APD_{90} for different stimulation frequencies is shown for normal conditions using the GPB model (thick line), for basic HF conditions (solid line), and for a 15% increase (long dashed line) and a 15% reduction (short dashed line) of one ionic parameter with respect to its value in the basic HF model.*

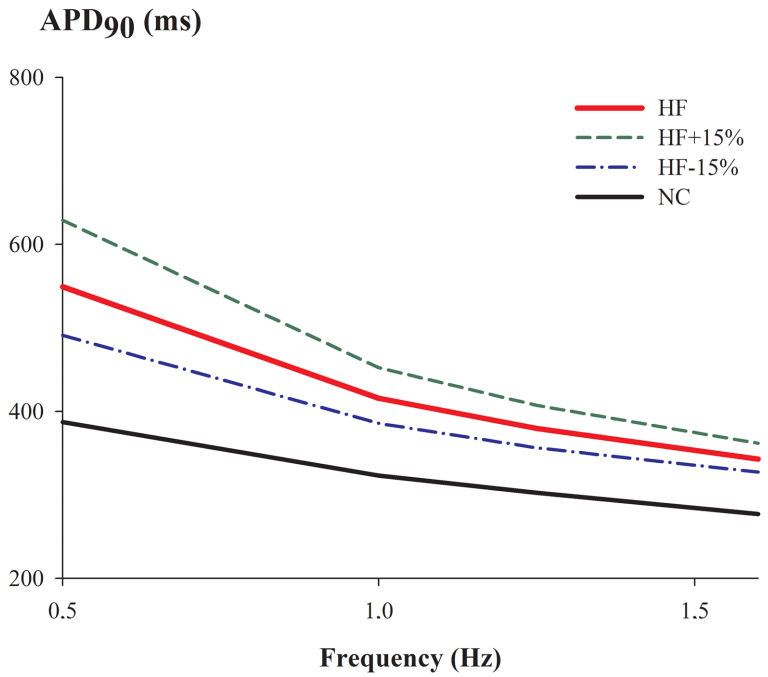

Figure 2.11: *Sensitivity of APD rate-dependence to variations in all ionic parameters in HF. The steady-state APD_{90} for different stimulation frequencies is shown for normal conditions using the GPB model (thick line), for basic HF conditions (solid line), and for a 15% increase (long dashed line) and a 15% reduction (short dashed line) of all the ionic parameters simultaneously with respect to their value in the basic HF model.*

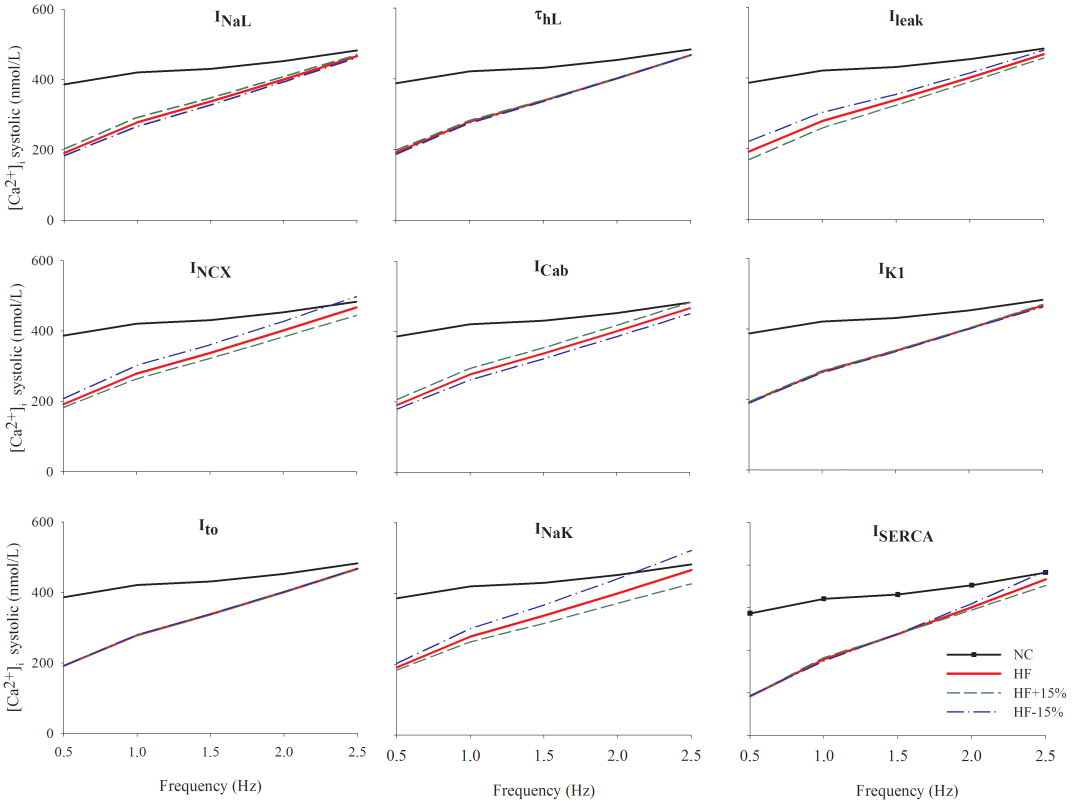

Figure 2.12: *Sensitivity of rate-dependent changes in systolic $[Ca^{2+}]_i$ to variations in individual ionic parameters in HF. Systolic $[Ca^{2+}]_i$ after 10 minutes of stimulation at increasing rates is shown for normal conditions using the GPB model (thick line), for basic HF conditions (solid line), and for a 15% increase (long dashed line) and a 15% reduction (short dashed line) of one ionic parameter with respect to its value in the basic HF model.*

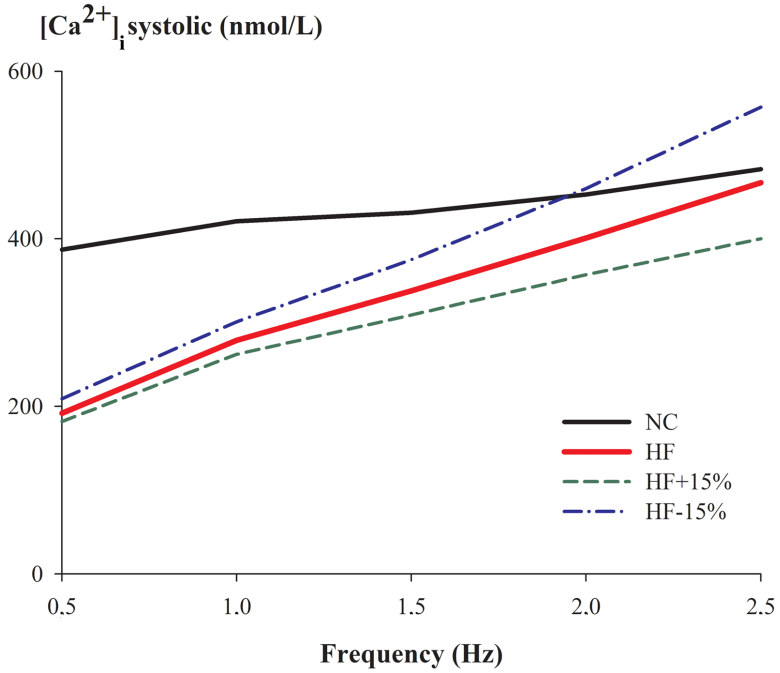

Figure 2.13: *Sensitivity of rate-dependent changes in systolic $[Ca^{2+}]_i$ to variations in all ionic parameters in HF. Systolic $[Ca^{2+}]_i$ after 10 minutes of stimulation at increasing rates is shown for normal conditions using the GPB model (thick line), for basic HF conditions (solid line), and for a 15% increase (long dashed line) and a 15% reduction (short dashed line) of all the ionic parameters simultaneously with respect to their value in the basic HF model.*

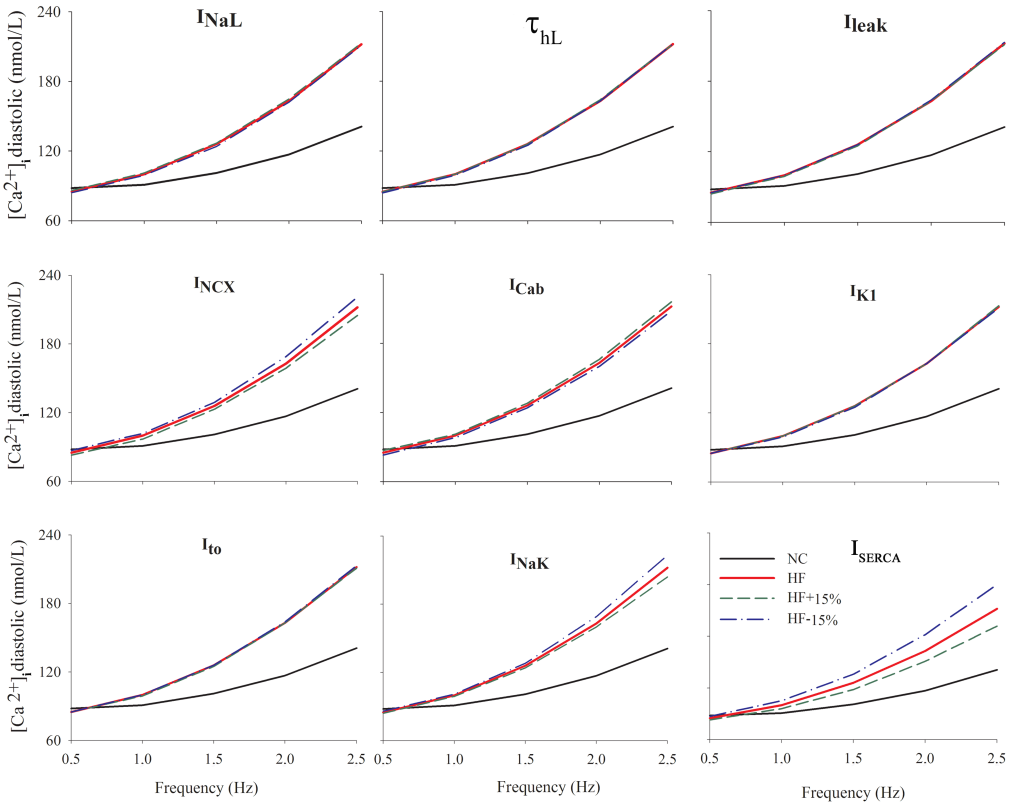

Figure 2.14: *Sensitivity of rate-dependent changes in diastolic $[Ca^{2+}]_i$ to variations in individual ionic parameters in HF. Diastolic $[Ca^{2+}]_i$ after 10 minutes of stimulation at increasing rates is shown for normal conditions using the GPB model (thick line), for basic HF conditions (solid line), and for a 15% increase (long dashed line) and a 15% reduction (short dashed line) of one ionic parameter with respect to its value in the basic HF model.*

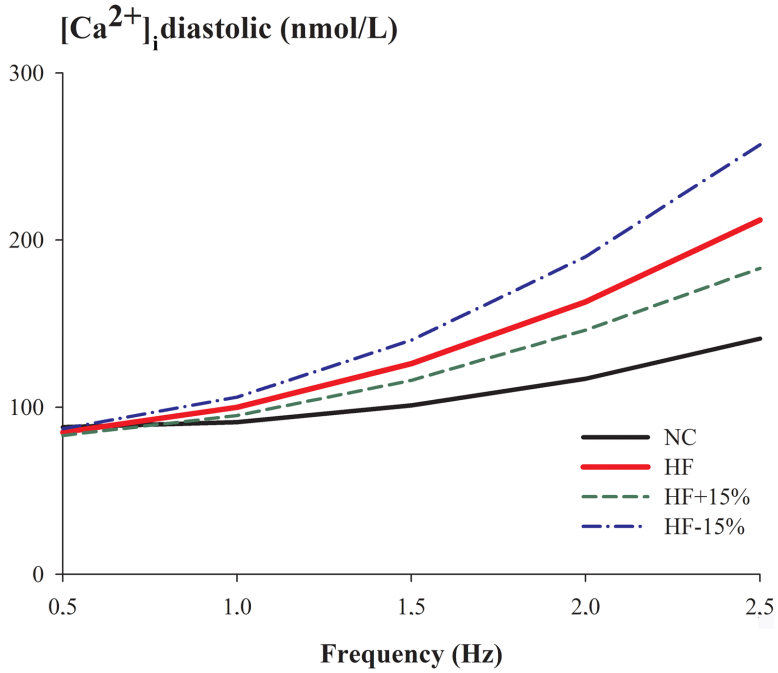

Figure 2.15: *Sensitivity of rate-dependent changes in diastolic $[Ca^{2+}]_i$ to variations in individual ionic parameters in HF. Diastolic $[Ca^{2+}]_i$ after 10 minutes of stimulation at increasing rates is shown for normal conditions using the GPB model (thick line), for basic HF conditions (solid line), and for a 15% increase (long dashed line) and a 15% reduction (short dashed line) of all the ionic parameters simultaneously with respect to their value in the basic HF model.*

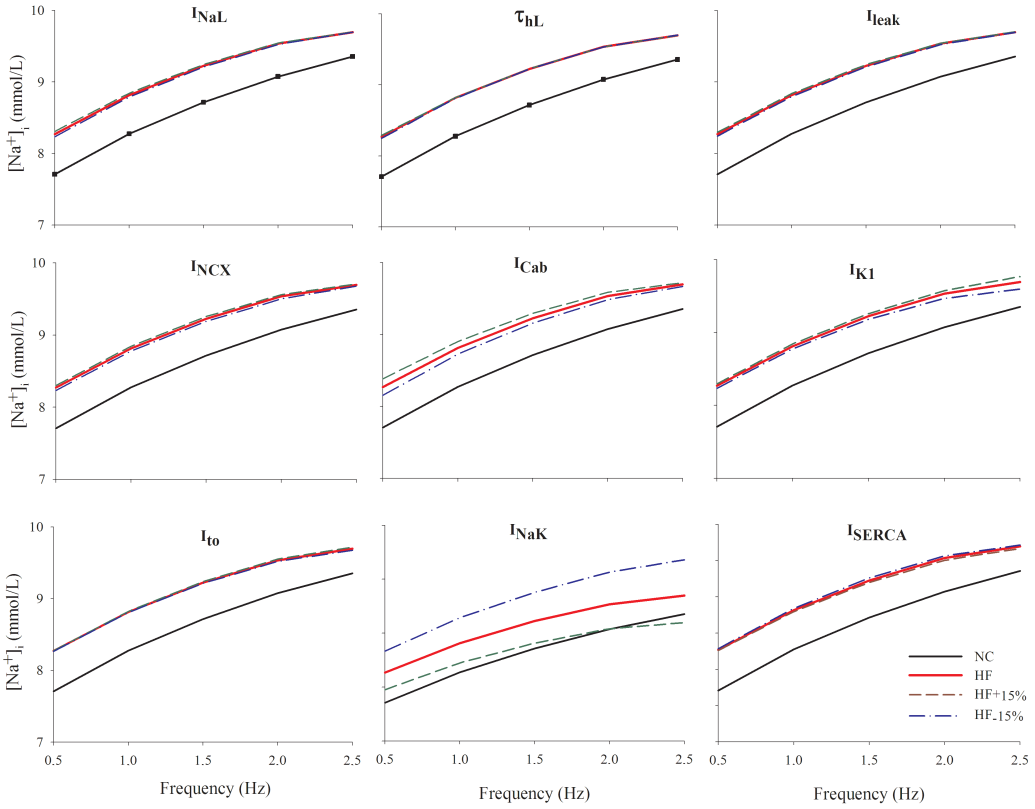

Figure 2.16: *Sensitivity of rate-dependent changes in $[Na^+]_i$ to variations in individual ionic parameters in HF.$[Na^+]_i$ after 10 minutes of stimulation at increasing rates is shown for normal conditions using the GPB model (thick line), for basic HF conditions (solid line), and for a 15% increase (long dashed line) and a 15% reduction (short dashed line) of one ionic parameter with respect to its value in the basic HF model.*

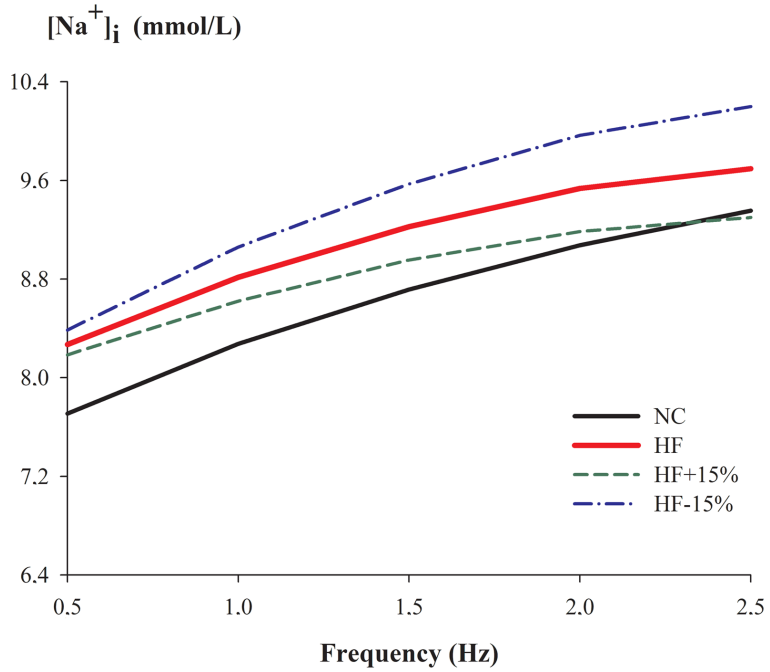

Figure 2.17: *Sensitivity of rate-dependent changes in $[Na^+]_i$ to variations in individual ionic parameters in HF. $[Na^+]_i$ after 10 minutes of stimulation at increasing rates is shown for normal conditions using the GPB model (thick line), for basic HF conditions (solid line), and for a 15% increase (long dashed line) and a 15% reduction (short dashed line) of all the ionic parameters simultaneously with respect to their value in the basic HF model.*

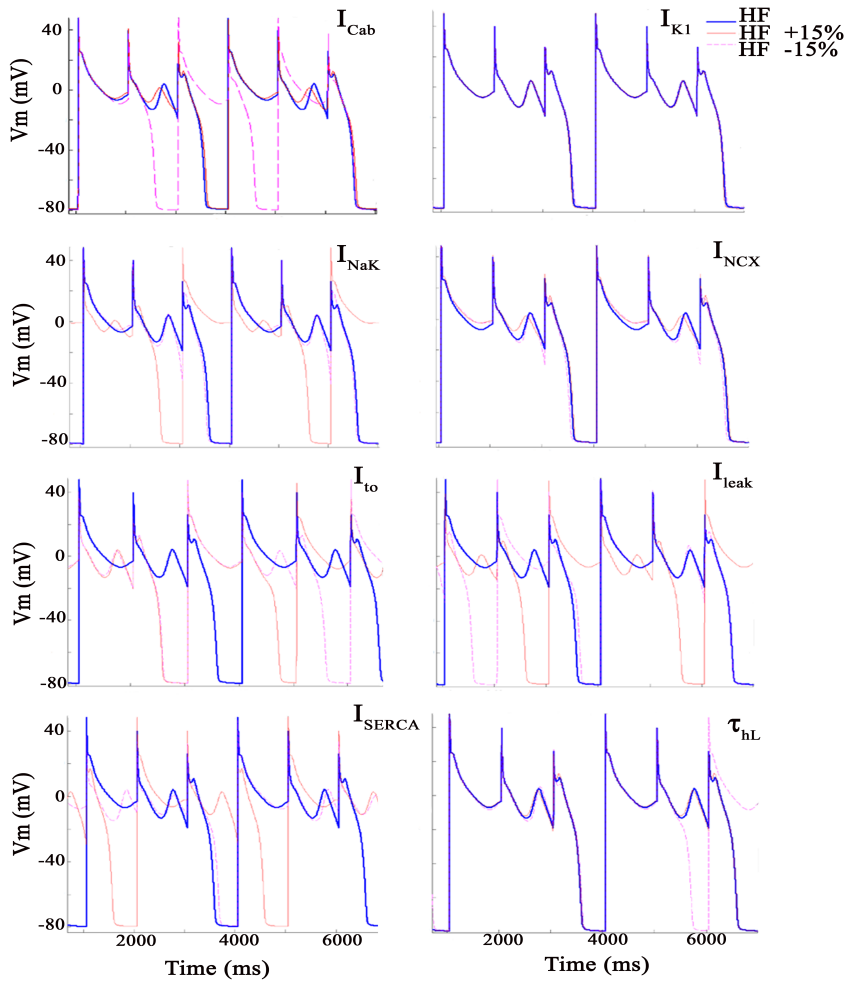

Figure 2.18: *Sensitivity of EAD generation to variations in individual ionic parameters in HF. Steady-state APs at 1-Hz pacing rate with 50% inhibition of I_{Kr}, 30% increase of I_{CaL}.The simulated results using the basic HF model are shown with a thick line, the solid and dashed lines show the results obtained for a 15% increase and a 15% reduction, respectively, of one ionic parameter with respect to its value in the basic HF model.*

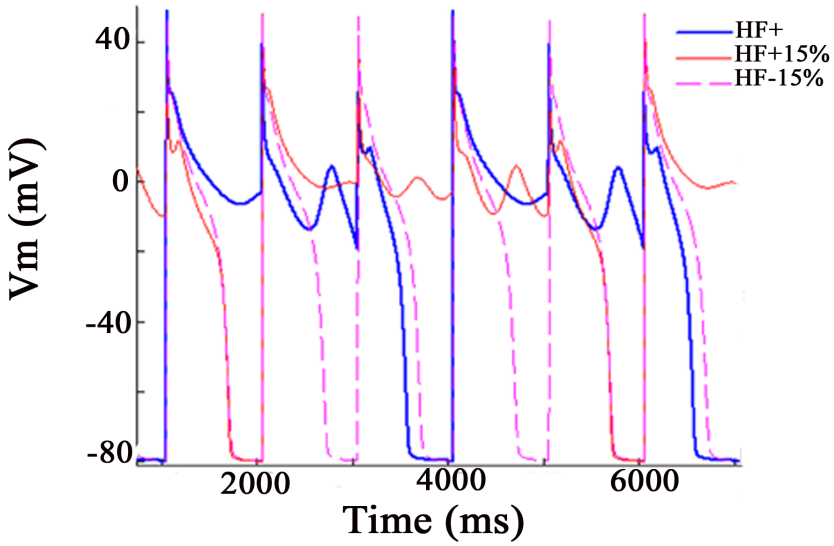

Figure 2.19: *Sensitivity of EAD generation to variations in all ionic parameters in HF. Steady-state APs at 1-Hz pacing rate with 50% inhibition of I_{Kr}, 30% increase of I_{CaL}.The simulated results using the basic HF model are shown with a thick line, the solid and dashed lines show the results obtained for a 15% increase and a 15% reduction, respectively, of one ionic parameter with respect to its value in the basic HF model.*

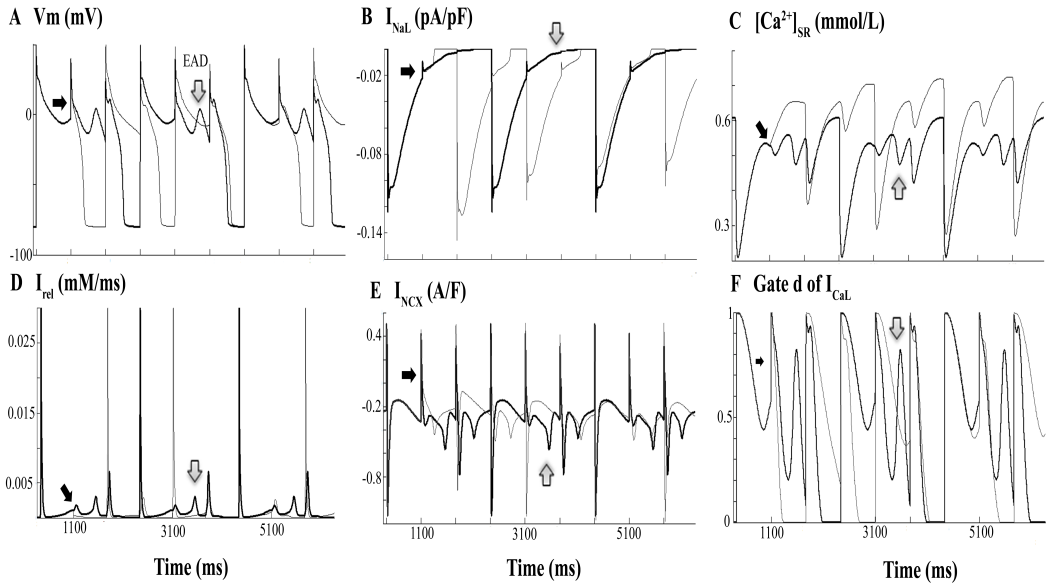

Figure 2.20: *Mechanisms for early afterdepolarizations with a 50% continuous block of I_{rel}.Simulated APs and ionic currents at 1-Hz pacing rate under HF conditions, 50% inhibition of I_{Kr}, 30% increase of I_{CaL}. Panel A shows EADs (dark line) with the basic HF value of I_{rel} and APs with no EADs when I_{rel} was 50% blocked (light line). The temporal evolutions of I_{NaL} (panel B), $[Ca^{2+}]_{SR}$ (panel C), I_{rel} (panel D), NCX activity (panel E), and activation gate of I_{CaL} (panel F) are also depicted with the basic HF value of I_{rel} (dark line) and when I_{rel} was 50% blocked (light line).*

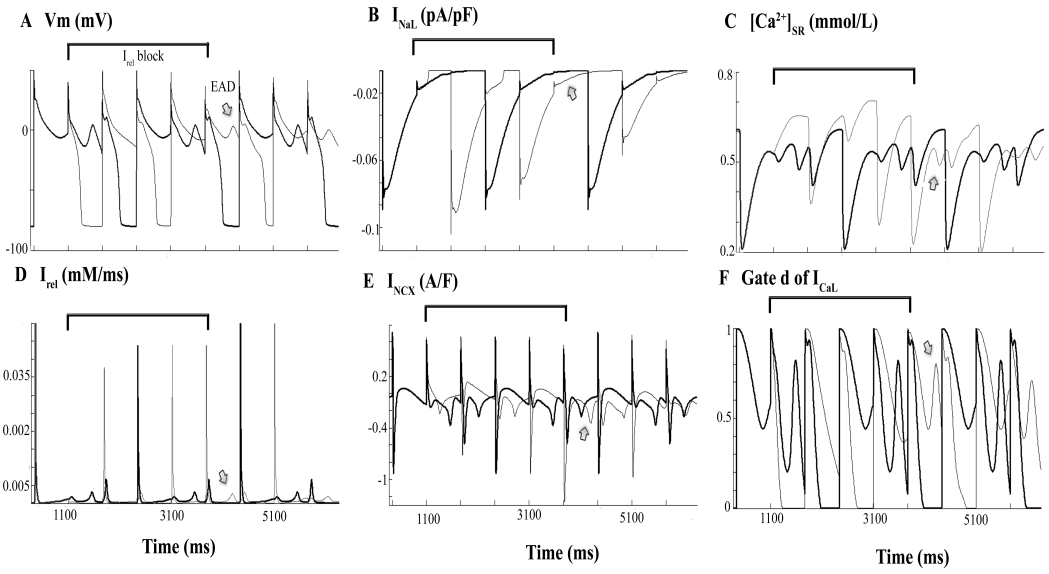

Figure 2.21: *Mechanisms for early afterdepolarizations with a 50% transitory block of I_{rel}.Simulated APs and ionic currents at 1-Hz pacing rate under HF conditions, 50% inhibition of I_{Kr}, 30% increase of I_{CaL}. Panel A shows EADs (dark line) with the basic HF value of I_{rel} and APs with no EADs when I_{rel} was 50% blocked (light line) during the 5 stimulations indicated by a horizontal line. The temporal evolutions of I_{NaL} (panel B), $[Ca^{2+}]_{SR}$ (panel C), I_{rel} (panel D), NCX activity (panel E), and activation gate of I_{CaL} (panel F) are also depicted with the basic HF value of I_{rel} (dark line) and when I_{rel} was 50% blocked (light line) during the 5 stimulations indicated by a horizontal line.*

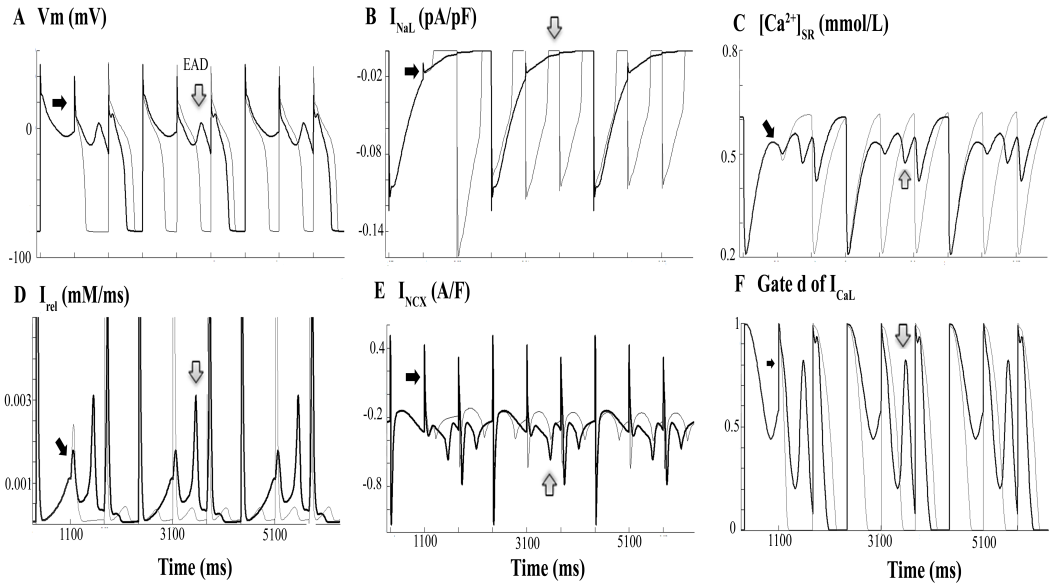

Figure 2.22: *Mechanisms for early afterdepolarizations with a 50% continuous block of I_{NCX}. Simulated APs and ionic currents at 1-Hz pacing rate under HF conditions, 50% inhibition of I_{Kr}, 30% increase of I_{CaL}. Panel A shows EADs (dark line) with the basic HF value of I_{NCX} and APs with no EADs when I_{NCX} was 50% blocked (light line). The temporal evolutions of I_{NaL} (panel B), $[Ca^{2+}]_{SR}$ (panel C), I_{rel} (panel D), NCX activity (panel E), and activation gate of I_{CaL} (panel F) are also depicted with the basic HF value of INCX (dark line) and when I_{NCX} was 50% blocked (light line).*

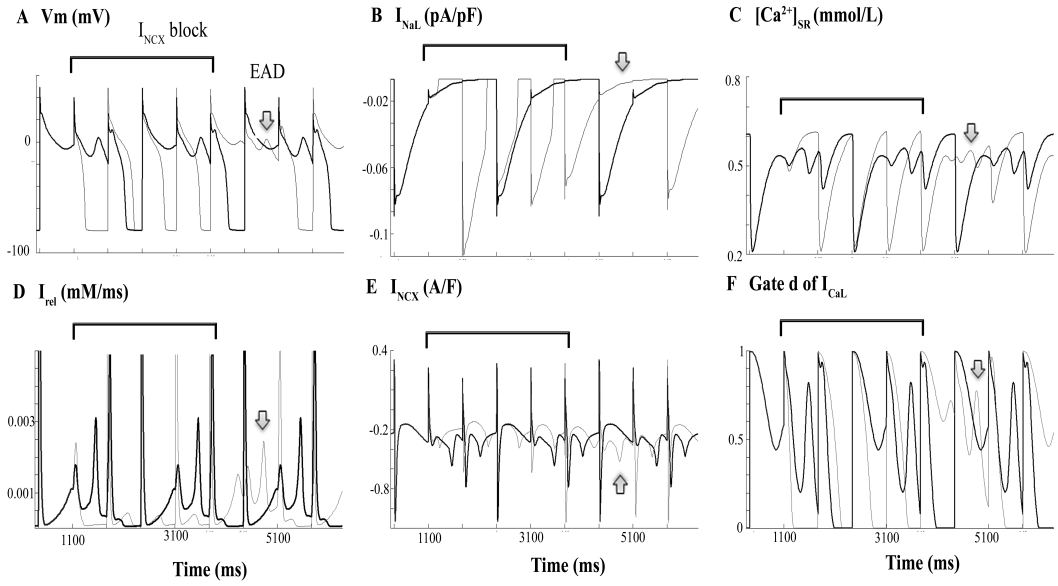

Figure 2.23: *Mechanisms for early afterdepolarizations with a 50% transitory block of I_{NCX}.Simulated APs and ionic currents at 1-Hz pacing rate under HF conditions, 50% inhibition of I_{Kr}, 30% increase of I_{CaL}. Panel A shows EADs (dark line) with the basic HF value of I_{NCX} and APs with no EADs when I_{NCX} was 50% blocked (light line during the 5 stimulations indicated by a horizontal line. The temporal evolutions of I_{NaL} (panel B), $[Ca^{2+}]_{SR}$ (panel C), I_{rel} (panel D), NCX activity (panel E), and activation gate of I_{CaL} (panel F) are also depicted with the basic HF value of I_{NCX} (dark line) and when I_{NCX} was 50% blocked (light line) during the 5 stimulations indicated by a horizontal line.*

CHAPTER 3

Electrophysiological and Structural Remodeling in Heart Failure Modulate Arrhythmogenesis. 1D Simulation Study

The content of this chapter is based on the publication:
Gomez, JF., Cardona, K., Romero, L., Ferrero, JM., Trenor, B. Electrophysiological and structural remodeling in heart failure modulate arrhythmogenesis. 1D simulation study. *PLoS One*, 9(9): e106602, 2014.

3.1 Abstract

Heart failure is a final common pathway or descriptor for various cardiac pathologies. It is associated with sudden cardiac death, which is frequently caused by ventricular arrhythmias. Electrophysiological remodeling, intercellular uncoupling, fibrosis and autonomic imbalance have been identified as major arrhythmogenic factors in heart failure etiology and progression.

In this study we investigate in silico the role of electrophysiological and structural heart failure remodeling on the modulation of key elements of the arrhythmogenic substrate, i.e., electrophysiological gradients and abnormal impulse propagation. Two different mathematical models of the human ventricular action potential were used to formulate models of the failing ventricular myocyte. This provided the basis for simulations of the electrical activity within a transmural ventricular strand. Our main goal was to elucidate the roles of electrophysiological and structural remodeling in setting the stage for malignant life-threatening arrhythmias.

Simulation results illustrate how the presence of M cells and heterogeneous electrophysiological remodeling in the human failing ventricle modulate the dispersion of action potential duration and repolarization time. Specifically, selective heterogeneous remodeling of expression levels for the Na^+/Ca^{2+} exchanger and SERCA pump decrease these heterogeneities. In contrast, fibroblast proliferation and cellular uncoupling both strongly increase repolarization heterogeneities. Conduction velocity and the safety factor for conduction are also reduced by the progressive structural remodeling during heart failure.

An extensive literature now establishes that in human ventricle, as heart failure progresses, gradients for repolarization are changed significantly by protein specific electrophysiological remodeling (either homogeneous or heterogeneous). Our simulations illustrate and provide new insights into this. Furthermore, enhanced fibrosis in failing hearts, as well as reduced intercellular coupling, combine to increase electrophysiological gradients and reduce electrical propagation. In combination these changes set the stage for arrhythmias.

3.2 Introduction

Heart failure (HF) is a clinical syndrome characterized by the marked and progressive inability of the ventricles to fill and generate adequate cardiac output to meet the demands of cellular metabolism that may have significant variability in its etiology [44]. HF is a final common pathway of a multitude of cardiac pathologies. Congenital cardiac abnormalities, valve disease, hypertension, dilated cardiomyopathy, hypertrophic cardiomyopathy, arrhythmogenic right ventricular cardiomyopathy, and ischemic damage can all result eventually in HF. The primary electrophysiological changes and the mechanisms for arrhythmogenesis associated with HF depend on its etiology [45]. Thus, HF is not characterized by a single set of electrophysiological changes. However, there are a number of consistent findings thought to be important for arrhythmogenesis. These include: ion channel remodeling, enhanced cellular uncoupling, altered calcium homeostasis, extracellular matrix changes, and increased sympathetic nerve activity [45].

Marked ion channel remodeling in failing human hearts has been described in several experimental studies [9, 18, 20, 26, 135, 163, 207, 213, 214]. However detailed studies focusing heterogeneous remodeling within the ventricular free wall are lacking [7, 172, 206, 231]. This study was undertaken to evaluate how transmural heterogeneous remodeling of selected ion channels in failing hearts modulates electrophysiological dispersion in the ventricular myocardium, which is known to set the stage for malignant arrhythmias [3, 5, 239]. Furthermore, structural remodeling and cellular uncoupling [40, 73, 79, 123, 226] in failing hearts have long been known to contribute to arrhythmogenesis [72, 92, 208]. However, proliferation of fibroblasts and their possible electrical interaction with cardiac myocytes [67, 100, 111, 141, 143, 225, 253] has only recently emerged as a plausible pro-arrhythmic factor. These factors are known to alter electrical patterns of propagation and dispersion. Enhanced dispersion of repolarization in the failing heart, due to a heterogeneous distribution of action potential duration (APD) through the myocardial wall, is thought to be an important contributor to arrhythmia [3, 5, 123, 239]. However, a recent experimental study by Glukhov et al. [73] reported that transmural APD gradients were decreased in the failing ventricle compared with non-failing hearts. Computational and theoretical analyses may provide useful insights into the mechanisms responsible for this controversy. Mathematical models of disease-specific AP in human heart are powerful tools for improvement of basic understanding of the ionic mechanism(s) of dysfunction in disease, such as arrhythmias and HF. Furthermore, anatomically detailed multiscale models (from cell to organ dimensions) often can provide complementary approach to clinical and physiological measurements with

the common goal of helping to optimize medical devices and pharmacological treatments (see [40, 226] for review).

In the present study, the electrophysiological activity of a transmural one dimensional wedge was simulated using well justified modifications on recent mathematical models of human ventricular AP [79, 157] in an attempt to replicate the experimentally reported human HF phenotypes. The influence of electrophysiological and structural remodeling on transmural dispersion of repolarization (TDR), Ca^{2+} transients, and electrical conduction properties were the foci of this work. New insights include: the effects of (i) transmural heterogeneous remodeling of SERCA pump and Na^{+}/Ca^{2+}, (ii) the presence of M cells, and (iii) the presence of fibrosis and cellular uncoupling, on repolarization and Ca^{2+} transient gradients.

3.3 Methods

3.3.1 Cellular models

Simulations of the electrophysiological activity of endocardial and epicardial human ventricular myocytes were carried out using one of the latest human ventricular AP models, developed by Grandi et al. (GPB model) [79], and characterized by a thorough description of intracellular calcium handling. The O'Hara et al. ventricular AP model (ORd) [157] was also employed to simulate the electrical activity of epicardial, endocardial, and M cells, defined as midmyocardial cells with prolonged APD [10]. Indeed, GPB model does not include a formulation for M cells. ORd model is based on experimental data taken from 140 non-diseased human hearts. It can reproduce the electrophysiological behavior of all three types of human ventricular myocytes, in accordance with experimental observations.

3.3.2 Model of ventricular fibroblast

To simulate the electrical activity of fibroblasts, the formulation of MacCannell et al. [129] was used, which is based on experimental data from adult rat ventricles [35]. Specifically, the active fibroblast model includes a time and voltage- dependent potassium current (I_K), a voltage-dependent inward-rectifying K^+ current (I_{K1}), as well as a Na^+/K^+ pump (I_{NaK}), and a background sodium current ($I_{b,Na}$), with a membrane capacitance of 6.3 pF. The uncoupled resting membrane potential of the active ventricular fibroblast is -49.6 mV.

3.3.3 Homogeneous electrophysiological remodeling in heart failure

To simulate the electrical activity of human ventricular failing myocytes, GPB and ORd models were modified. Quite extensive parameters were changed (based on experimental data from human when it was possible) to describe the hallmark characteristics of failing cardiac tissues and cells, such as AP prolongation and alteration of Ca^{2+} handling [19, 105]. A detailed description of these HF models was previously published by our group [76, 215]. The entire set of currents and parameter modifications (applied homogeneously in all types of cells) are summarized in Table 3.1. As mentioned, ORd model includes an

electrical description for M cells so that heterogeneous HF remodeling in endocardial, M, and epicardial cells was possible to be defined.

3.3.4 Heterogeneous electrophysiological remodeling in heart failure

Experimental studies describing the functional features and changes in expression levels of ion channels across the ventricular free wall in the failing human heart are scarce [7, 172, 206, 231, 247]. Furthermore, extrapolating protein expression levels to channel functional activity is not trivial. Thus, on the basis of the limited literature, we proposed a heterogeneous model of HF based on our previous work [77], where specific parameters were differently altered in epicardial, endocardial, and M cells. Specifically, the activity of the Na^+/Ca^{2+} exchanger (I_{NCX}), which shows a significant upregulation in failing myocytes, was increased 2-fold in epicardial cells and 1.6-fold in M and endocardial cells [77, 247], as shown in Table 3.2. Heterogeneous downregulation of the SERCA pump (I_{SERCA}) has also been described experimentally [172], and was applied in our simulations as follows: a 55% reduction in endocardial cells, a 25% reduction in epicardial cells and a 40% reduction in M cells (see Table 3.2). These changes which strongly modulate Ca^{2+} transient, were considered as a starting point for heterogeneous remodeling. Transmural heterogeneous remodeling of K^+ currents has also been reported in the human failing ventricular wall, mainly the transient outward K^+ current (I_{to}) [92]. Heterogeneous remodeling of I_{to} would surely have an impact on early repolarization; however this is out of the scope of the present work.

3.3.5 Computational methods

To carry out these simulations in strand models of human ventricle we used ELVIRA software[88]. This is based on a pseudo-adaptive finite element method in space and time to solve anisotropic reaction-diffusion equations with highly nonlinear reactive terms. The reaction-diffusion equation 3.1 governs AP propagation through the multicellular strand. The strand was spatially discretized into linear elements (Δx= 0.01 cm) delimited by two nodes, one in each of the element ends, where the ionic model is solved. The temporal resolution was fixed to t = 0.002 ms to ensure convergence. The scheme accounts for the anisotropy of the media and incorporates an adaptive time step algorithm to integrate the stiff reactive term associated with the ionic currents. The resolution of the monodomain equation (3.1) is based on the technique of operator splitting.

Ionic Parameter modified	% of change in the HF model compared to the normal model		Experimental conditions
	GPB model	ORd model	
I_{NaL}	↑200	↑180	Isolated cardiomyocytes from LV mid-myocardium of failing dog hearts. Whole cell voltage clamp (room temperature)[135]
τ_{hL}	↑200	↑180	Isolated cardiomyocytes from LV mid-myocardium of failing human hearts. Whole cell voltage clamp (room temperature)[135]
I_{to}	↓60	↓60	Isolated cardiomyocytes from LV endocardium of failing human hearts. Whole cell voltage clamp (room temperature)[20]
I_{K1}	↓32	↓32	Review article. Several species[213].
I_{NaK}	↓10	↓30	Measurements of human myocardial[26]. Na,K-ATPase concentration in failing hearts. Review articles. Several species [213, 214]
I_{Nab}	= 0	=	Simulation of human HF[173].
I_{Cab}	↑153		Simulation of human HF.[173]
I_{NCX}	↑175	↑175	Simulation of human HF.[178, 237]
I_{SERCA}	↓50	↓50	Isolated cardiomyocytes from LV of failing human hearts. Measurements of Ca^{2+} uptake rates by the SR (37°C)[163].
I_{leak}	↑500	↑130	Review article[18].
EC_{50SR}	↓11		Isolated cardiomyocytes from LV of failing rabbit hearts. Measurements of RyR sensitivity to SR Ca^{2+}[47].Review articles[9, 18]
CaMKa		↑150	Review articles[9].Transgenic mice [207]
$J_{rel,NP,\infty}$		↑80	Review article.[69]

Table 3.1: *Electrophisiological heart failure remodeling.Changes in original Grandi et al. (GPB) [79] and O'Hara et al. (ORd) [157] models to simulate heart failure (HF) phenotype. The changes are indicated in percentage of increase (↑) or decrease (↓) with respect to the original model. The modified parameters are: the late Na^+current (I_{NaL}), the time constant of inactivation of the I_{NaL} (τ_{hL}), the transient outward K^+ current (I_{to}), the inward rectifier K^+ current (I_{K1}), the Na^+/K^+ pump current (I_{NaK}), the background Ca^{2+} current (I_{Cab}), the Na^+/Ca^{2+} exchanger (I_{NCX}), the sarcoplasmic reticulum (SR) Ca^{2+} pump (I_{SERCA}), the SR Ca^{2+} leak current (I_{leak}), the Ca^{2+} sensitivity of SR Ca^{2+} fluxes (EC_{50SR}), the Ca^{2+} calmodulin-dependent protein kinase II, and the non-phosphorylated Ca^{2+} release, via ryanodine receptors ($J_{rel,NP,\infty}$).*

Remodeled Current	% in the HF model compared to GPB/ORd models			Experimental conditions
	Epi	M	Endo	
I_{NCX}	↑200	↑160	↑160	[97, 173, 178, 247]
I_{SERCA}	↓25	↓40	↓55	[85, 163, 172, 197]

Table 3.2: *Electrophisiological heterogeneous heart failure remodeling. Changes in original Grandi et al. (GPB) [79] and O'Hara et al. (ORd) [157] models to simulate heart failure (HF) heterogeneous remodeling. The heterogeneously modified parameters are: the Na^+/Ca^{2+} exchanger (I_{NCX}), the sarcoplasmic reticulum (SR) Ca^{2+} pump (I_{SERCA}). Different percentages of these currents with respect to the control value were used in epicardium, endocardium and M-cells (in the case of the ORd model).*

$$\nabla(D\nabla V_m) = \frac{dV_m}{dt} + \frac{I_{ion}}{C_m} + \frac{I_{stm}}{C_m} \tag{3.1}$$

$$\overrightarrow{n} \cdot \nabla(D\nabla V_m) = 0 \tag{3.2}$$

$$D = \frac{\sigma}{S_V C_m} \tag{3.3}$$

Where V_m is the membrane potential in [V], D is the diffusion conductivity tensor in [m^2/s], σ is the conductivity tensor in [S·m], S_V is the surface to volume ratio of the cell in [m^{-1}], C_m in [F] is the membrane capacity, I_{ion} in (A) is the total ionic current, and I_{stm} in (A) is the stimulus current. Equation (3.1) has boundary conditions (3.2). Further information can be found in [88]. The ionic model that is solved in each node of the discretized domain changes depending on the described cell (myocyte [79, 157] or fibroblast [129]). Temporal equations are computed using a semi-implicit numerical method (implicit for the parabolic equation and explicit for ionic models at each node).

3.3.6 Human ventricular transmural strand models

To simulate the electrical activity of a transmural wedge preparation, a heterogeneous one dimensional strand composed of 165 cells was considered as in [71, 144, 157]. This corresponds to a thickness of 1.65 cm, which is within the range of 1 to 2 cm reported for the width of the human left ventricular wall [179]. The strand was divided into 82 endocardial cells and 83 epicardial cells, each myocyte being driven by GPB formulation [79]. The diffusion tensor (D) in normal conditions (NC) for myocyte cells was set to D_M=D_{xx} = 0.0006 cm/ms resulting in a conduction velocity (CV) of 50 cm/s as in experimental measurements of transmural conduction [209]. The intercellular uncoupling observed in failing hearts was modeled by a two-fold decrease in diffusion coefficient, i.e. intercellular conductivity was halved (D_M= 0.0003 cm/ms), in accordance with experimental measurements in the human failing heart reporting a 50% reduction in connexin43 protein levels [57]. To test other degrees of intercellular uncoupling, mild uncoupling (D_M= 0.00045 cm/ms) and severe uncoupling (D_M= 0.00025 cm/ms) were also considered. The effect of fibroblasts within the strand was simulated by (i) randomly distributing fibroblasts (diffuse fibrosis) or

(ii) considering small localized clusters (patchy fibrosis) [108, 210]. Diffuse fibrosis is defined as small deposits of fibrous tissue. Fibroblasts were thus randomly distributed within the strand so that some nodes were assigned to the fibroblast ionic model and the rest of the nodes to the myocyte ionic model. As in [130], a fibrotic content of 10% or 20% corresponds to the percentage of nodes assigned to the fibroblast ionic model. For each fibrotic content 11 random configurations were simulated (see Figures 3.8 and 3.9).

Patchy fibrosis, i.e. larger clusters of fibrous tissue, was simulated with clusters of 25 interconnected fibroblasts, introduced within the ventricular strand. Fibroblasts were electrotonically coupled to surrounding cells (myocytes or other fibrotic cells) by considering a lower conductivity tensor with respect to conductivity tensor between myocytes. The diffusion coefficient in fibroblast elements was decreased three-fold with respect to myocytes, based on experimental data [225]. To test the effects of the heterogeneous electrophysiological remodeling characteristic of HF, multicellular strands containing also M cells were considered. For this purpose, one dimensional simulations were performed using a heterogeneous multicellular strand, which resembles some functional features of a ventricular transmural wedge preparation, as described in O'Hara et al. [157]. This strand was composed by 60 endocardial, 45 M, and 65 epicardial cells governed by ORd formulation. Stimuli were applied at the extreme endocardial end in all configurations with a basic cycle length (BCL) of 1000 ms. Parameters were measured for the last stimulation, after steady state was reached, i.e. after 200 s and 750 s in the cellular strands using GPB and ORd models, respectively.

3.3.7 Parameter definition

APD at 90% of repolarization (APD_{90}) was computed in myocytes of the strand, then APD dispersion was calculated as the difference between the maximum and minimum APD_{90} along the strand. Border effects were avoided by eliminating 15 cells in each end of the strand for the computation of dispersion. Repolarization time (RT) for a cell was measured by adding APD_{90} of this cell to the time needed by the wavefront to reach the cell. Transmural dispersion of repolarization was then computed as the difference between the maximum and minimum RT along the multicellular strand. Ca^{2+} transient duration was measured as the time from the upstroke to 80% of recovery ($CaTD_{80}$) as in [122], and the voltage-calcium delay was defined as the delay between the upstrokes of AP and Ca^{2+} transient (AP-Ca delay) [122]. $CaTD_{80}$ and AP-Ca delay dispersions were computed as the

difference between the maximum and minimum $CaTD_{80}$ and AP-Ca delay, respectively, along the multicellular strand.

The effective refractory period (ERP) was measured as the minimum time between two consecutive stimuli that resulted in propagation of the AP wave across the strand. Conduction velocity (CV) was measured between the 15th and 150th myocytes (to avoid edge effects), as the distance between cells divided by the difference between the times of maximum depolarization upstroke. The safety factor (SF) for conduction is a quantitative parameter based on the source-sink relationship of electric charge between adjacent cardiac cells. The value of the SF indicates the success or failure in AP propagation. Several definitions of the SF have been published [24, 51, 201], and the formulation proposed by Romero and coworkers [186] (SF_m), described in equation (3.4), was chosen because of its computational advantages. This formulation of the SF was proposed by Shaw and Rudy [201], however, Romero et al. [186] changed the definition of the integration domain, optimizing its calculation and saving computational resources.

$$SF_m = \frac{\int_A I_C \cdot dt + \int_A I_{out} \cdot dt}{\int_A I_{in} \cdot dt} A \mid t \in [t_{1\%}, t_{Vmax}] \tag{3.4}$$

where I_c stands for the capacitive current, I_{in} is the axial current that enters the cell, I_{out} is the axial current that leaves the cell, $t_{1\%}$ in the instant when membrane potential reaches 1% of its maximum and t_{Vmax} is the instant of maximal V_m.

3.3.8 Statistical analysis

SPSS Statistics 17.0 software (IBM SPSS Statistics) was used for student t-test. Values are expressed as mean $\pm$ SD. $p<0.05$ was considered significant.

3.4 Results

3.4.1 Effects of electrophysiological remodeling on transmural repolarization gradients

To assess the influence of HF induced electrophysiological remodeling on repolarization gradients, detailed simulations of the action potential conduction and repolarization in human ventricular transmural wedge preparations were carried out using our modified GPB and ORd AP models. Figure 3.1 shows the results obtained in a wedge composed by endocardial and epicardial myocytes using GPB model. As depicted in panel A, APD_{90} is longer in the failing endocardial and epicardial myocytes (red line) than in normal conditions (blue line) at a stimulation rate of 1 Hz. Note also that APD dispersion is increased in HF to 24 ms versus 20 ms in control conditions. In addition, as shown in panel B, repolarization time along the strand is delayed in failing myocytes (red line). Transmural dispersion of repolarization was slightly decreased in HF with respect to control conditions.

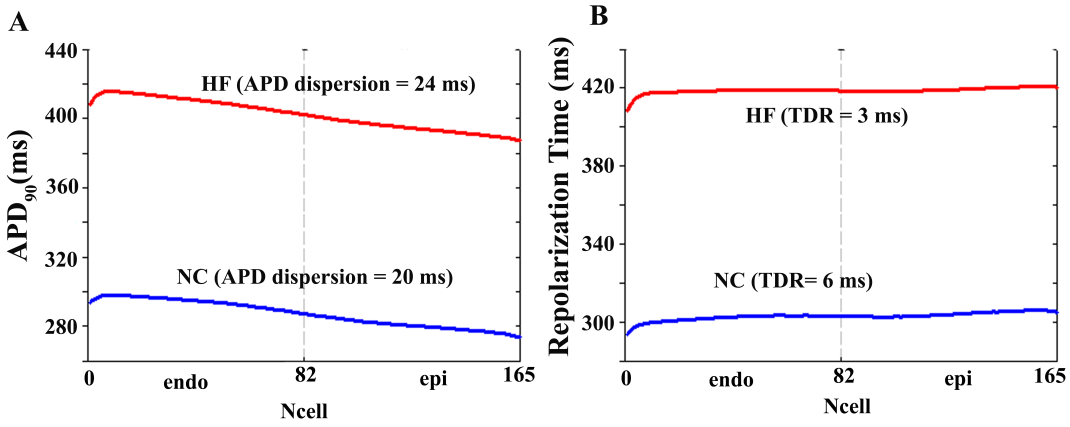

Figure 3.1: *Action potential duration and repolarization time in normal and failing conditions.A. Action potential duration (APD_{90}) measured along a transmural ventricular strand, composed by 82 endocardial and 83 epicardial cells, in normal conditions (NC, blue line) and in heart failure conditions (HF, red line). APD dispersion is indicated in ms for each curve. B. Repolarization time calculated along the ventricular strand in normal (blue line) and failing (red line) conditions. Transmural dispersion of repolarization (TDR) was measured in ms. Simulations were conducted using Grandi et al. (GPB) action potential model [79].*

Similar simulations were conducted using the modified ORd model to assess whether this pattern of results were modeldependent. From Figure 3.2 (panels A and B) it is clear that for ORd model values of APD and repolarization time are also lengthened in HF compared with NC. As expected, some differences with respect to GPB results were observed. The increase in APD dispersion was more pronounced in HF when ORd model was used. TDR increased in HF whereas the opposite result was obtained with the GPB model. Significant differences in the formulation of repolarizing currents of ORd and GPB models, as described with detail in [59] are likely responsible for these differences. Especially, the fact that ORd model considers transmural differences in 11 ionic currents, while GPB model distinguishes only between I_{to} in epicardial and endocardial myocytes, might be responsible for the different behaviors of the models in terms of APD transmural gradients and TDR.

To analyze the influence of M cells on repolarization gradients in the failing tissue, a transmural wedge in which M cells were included was implemented as well. In this analysis only ORd model was used, as GPB model does not include any AP formulation for this type of cells. APD dispersion and TDR along a transmural ventricular strand comprising M cells are shown in Figure 3.2 (panels C and D). The presence of M cells prolongs APD throughout the fiber and increases its dispersion (panel C) in both control and HF. Repolarization time is also increased at each fixed location in the strand and TDR also increased (panel D). However, the relative increase of APD dispersion and TDR in HF with respect to NC, in the presence of M cells is very similar to these changes in their absence. Thus, as expected from their intrinsic properties, M cells increase global repolarization gradients but do not increase the relative changes due to HF electrophysiological remodeling (with respect to control).

3.4.2 Effects of heterogeneous electrophysiological remodeling on transmural repolarization gradients

Several experimental studies [7, 172, 206, 231] have reported differences in the remodeling across the transmural ventricular free wall in failing hearts. To analyze how heterogeneous remodeling can affect APD_{90} and corresponding repolarization time gradients, simulations were performed using HF models with spatially heterogeneous remodeling across the ventricular strand, as described in the Methods section. Figure 3.3 shows the simulation results for GPB model in endocardium and epicardium (blue bars), for ORd model in endocardium and epicardium (red bars), and for ORd model also including M cells

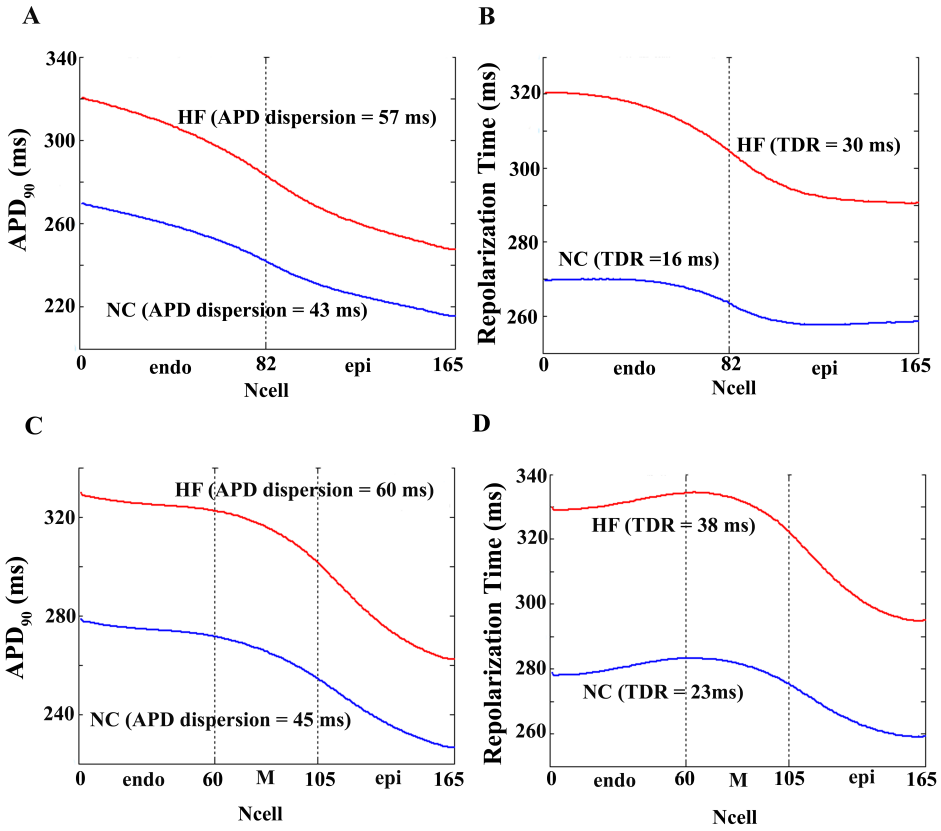

Figure 3.2: *Action potential duration and repolarization time in normal and failing conditions including M cells influence.Panels A and C. Action potential duration (APD_{90}) measured along a transmural ventricular strand, in normal conditions (NC, blue line) and in heart failure conditions (HF, red line). APD dispersion is indicated in ms for each curve. Panels B and D. Repolarization time calculated along the ventricular strand in normal (blue line) and failing (red line) conditions. Transmural dispersion of repolarization (TDR) was measured in ms. The ventricular strands are composed by 82 endocardial and 83 epicardial cells (panels A and B) and by 60 endocardial, 45 M, and 65 epicardial cells (panels C and D). All simulations were conducted using O'Hara et al. (ORd) action potential model [157].*

(green bars). In the case of GPB model, heterogeneous remodeling of I_{NCX} decreased APD dispersion to 19 ms versus 24 ms corresponding to homogeneous HF remodeling and 20 ms corresponding to normal conditions (panel C Figure 3.3). Similarly, using ORd model, heterogeneous remodeling of I_{NCX} and/or I_{SERCA} decreased APD dispersion with respect to homogeneous HF remodeling, regardless of the absence (red bars) or presence (green bars) of M cells. TDR (Figure 3.3 panel D) was also modulated by heterogeneous remodeling and was decreased with respect to homogeneous remodeling when ORd model was used. In general, in the presence of M cells, the values of APD dispersion and TDR are higher, and heterogeneous HF remodeling does not bring these values lower than control values.

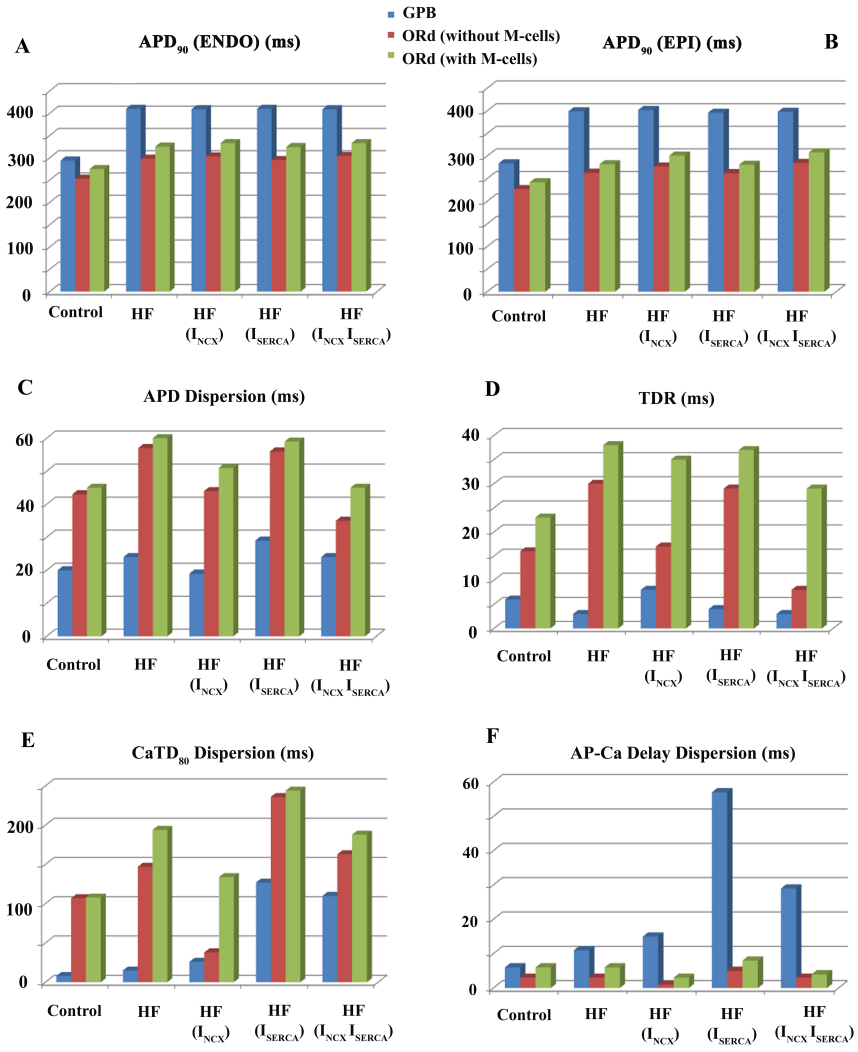

Figure 3.3: *Biomarkers in normal, homogeneous and heterogeneous remodeling failing conditions with GPB, ORd (without M cells), and ORd (with M cells) models.Electrophysiological properties measured in a one dimensional transmural ventricular strand under different pathological conditions. The ventricular strands were composed by 82 endocardial and 83 epicardial cells. All simulations were conducted using Grandi et al. (GPB) action potential model [79](blue bars), O'Hara et al. [157] model (ORd) without M-cells (red bars) and ORd model with M cells (green bars). The cases considered were: normal conditions (Control), electrical homogeneous heart failure remodeling (HF), electrical heterogeneous heart failure remodeling on I_{NCX} (HF I_{NCX}), electrical heterogeneous heart failure remodeling on I_{SERCA}(HF I_{SERCA}), and electrical heterogeneous heart failure remodeling on I_{NCX} and I_{SERCA} simultaneously (HF I_{NCX} I_{SERCA})(see Methods section for details).*

3.4.3 Effects of heterogeneous electrophysiological remodeling on transmural dispersion of Ca^{2+} transients

Because the heterogeneous remodeling that is the focus of the paper is limited to I_{NCX} and I_{SERCA}, which strongly affect Ca^{2+} transients, we also analyzed Ca^{2+} homeostasis. Figure 3.4 depicts Ca^{2+} transients in three different myocytes phenotypes within the transmural strand under normal conditions (blue), and for homogeneous (red) and heterogeneous (pink) HF remodeling. As observed experimentally in HF, the amplitude of Ca^{2+} transients is decreased, and the rise and decay rates are slowed. Figure 3.5 depicts the values of diastolic Ca^{2+} in panel A, systolic Ca^{2+} in panel B, Ca^{2+} duration ($CaTD_{80}$) in panel C, and the delay between AP and Ca^{2+} upstrokes (AP-Ca delay) in panel D, along the transmural strand. Significant differences in these magnitudes are observed along the ventricular strand in normal conditions (blue lines) and also after HF remodeling (red lines for homogeneous HF and pink lines for heterogeneous HF). The dispersion of $CaTD_{80}$ and AP-Ca delay were calculated for the different AP models (panels E and F in Figure 3.3). HF increased $CaTD_{80}$ dispersion in both models, which was strongly modulated by heterogeneous remodeling of I_{NCX} and I_{SERCA}. AP-Ca delay dispersion was increased or unaltered in HF using GPB or ORd models, respectively. Again, heterogeneous remodeling modulated AP-Ca delay, especially when GPB model was used.

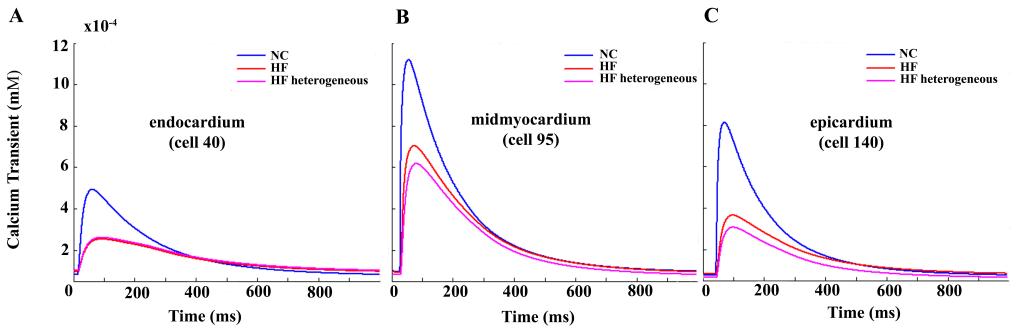

Figure 3.4: *Calcium transient representation under normal and failing conditions.Ca^{2+} transient representation in an endocardial cell (#40) (panel A), in a midmyocardial cell (#95) (panel B), and in an epicardial cell (#140) (panel C) of a heterogeneous ventricular strand for normal conditions (NC blue lines), homogeneous failing conditions (HF red lines), and heterogeneous heart failure (HF) remodeling (magenta lines). Simulations were performed using O'Hara et al. model [157].*

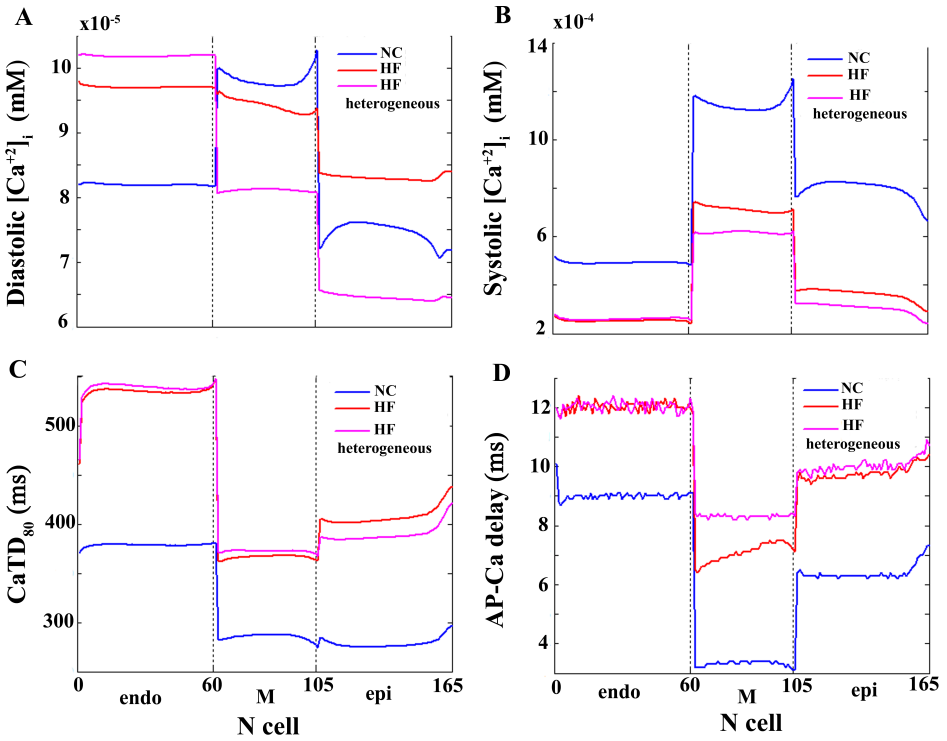

Figure 3.5: *Calcium transient dynamics under normal and failing conditions.Diastolic and systolic $[Ca^{2+}]_i$ levels (panels A and B, respectively), Ca^{2+} transient duration ($CaTD_{80}$) (panel C), and delay between AP and Ca^{2+} transient upstrokes (AP-Ca delay) (panel D) along a transmural ventricular strand under normal conditions (NC blue lines), homogeneous heart failure (HF) remodeling (red lines), and heterogeneous HF remodeling conditions (pink lines). Simulations were performed using O'Hara et al. model [157].*

Heterogeneous remodeling in failing hearts has been considered an important contributor to the HF phenotype and likely a major factor for modulation of transmural repolarization and Ca^{2+} transient gradients, as illustrated in our simulations (see Figure 3.3). The presence of M-cells also contributes to this modulation, by maintaining higher gradients. However, there is limited electrophysiological data from the human heart, and further experimental studies, similar to [201], are needed to fully determine how heterogeneous remodeling modulates APD gradients, TDR and Ca^{2+} transients changes. Specifically, measurements of AP and Ca^{2+} transients transmural gradients and their relation to protein expression levels or activity of the SERCA pump and I_{NCX} in a transmural wedge of the failing heart would be very valuable.

3.4.4 Effects of structural remodeling on repolarization gradients and impulse conduction

The effect of fibrosis within the strand was evaluated in a transmural ventricular wedge composed by endocardial and epicardial cells. GPB model was used because the effects of electrophysiological remodeling in repolarization gradients were less pronounced than in ORd model and we were interested in evaluating whether structural remodeling could significantly increase these gradients and/or alter action potential conduction. When clusters of fibroblasts were inserted randomly in the strand, marked differences in APD and repolarization time resulted, as shown in Figure 3.6. When fibrosis was present in the failing strand (10% of fibrotic content), APD dispersion went up to 70 ms, compared to 24 ms with HF electrophysiological remodeling. When intercellular uncoupling was also introduced, the APD dispersion increased even more to 92 ms.

A similar pattern of change could be observed in TDR . Transmural dispersion of repolarization was also significantly enhanced when the fibrotic content was 10%, as shown in Figure 3.6 panel B and even more when intercellular uncoupling was considered. Thus, inserted fibrosis and intercellular uncoupling increased TDR and APD dispersion. Nevertheless, when the fibrotic content was further enhanced to 20%, APD dispersion and TDR were decreased with respect to 10% fibrosis, showing a biphasic behavior with fibrotic content, as shown in Figure 3.7A and 3.7B. This tendency was maintained for different uncoupling degrees. The values of APD dispersion and TDR shown correspond to one of the random configurations (configuration 1) for each fibrotic content (10% and 20%). Additional random configurations were simulated and the results are shown in the Supplemental Information (see Tables 3.3 and 3.4 for normal intercellular coupling and Tables 3.5, 3.6, 3.7, and 3.8 for the different degrees of intercellular uncoupling and fibrosis). A statistical analysis was also performed and APD dispersion and TDR mean values were lower in the case of 20% of fibrotic content with respect to 10% fibrosis, regardless of the degree of cellular uncoupling (see Tables 3.3, 3.4, 3.5, 3.6, 3.7, and 3.8 and Figures 3.10, 3.11, 3.12, 3.13, 3.14, 3.15, 3.16, and 3.17 in Supplemental information), however only in the case of APD dispersion this difference was statistically different ($p<0.05$).

The excitability and conduction properties were also analyzed in the presence of HF electrophysiological remodeling, fibrosis and/or intercellular uncoupling. Figure 3.6 panel C shows the colorcoded resting membrane potential (V_{rest}) in each cell of the unidimensional strand in HF without fibrosis, in HF with 10% fibrosis, and in HF with 20% fibrosis

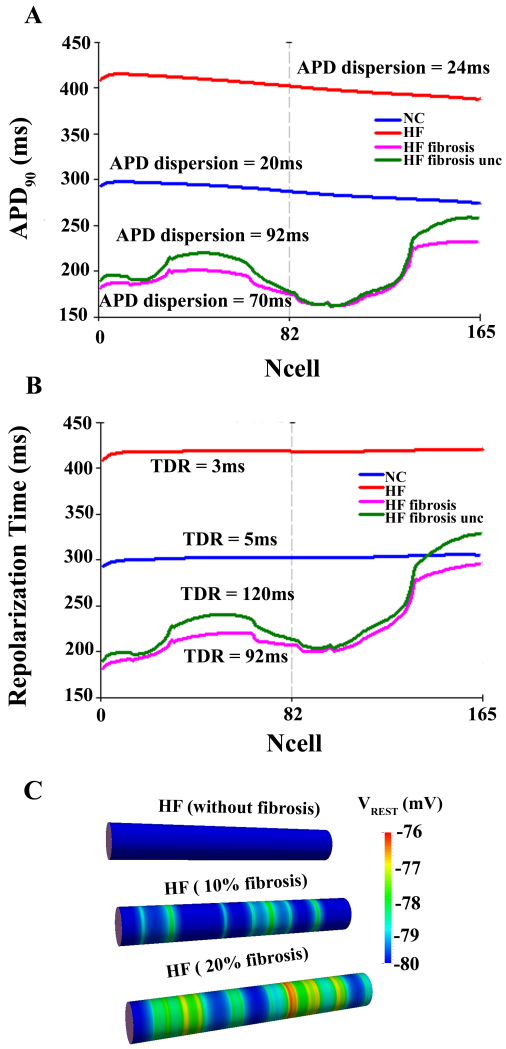

Figure 3.6: *Action potential duration and repolarization time in normal and failing conditions with structural remodeling.Action potential duration (APD_{90}) (panel A) and repolarization time (panel B) measured along transmural ventricular strands, in normal conditions (NC, blue lines), in heart failure electrophysiological remodeling conditions (HF, red lines), in heart failure electrophysiological remodeling conditions with fibrosis 10% (HF fibrosis, pink lines), and in heart failure electrophysiological remodeling conditions with fibrosis10% and intercellular uncoupling (HF fibrosis unc, green lines). APD dispersion and transmural dispersion of repolarization (TDR) were measured in ms for each curve. The ventricular strands were composed by 82 endocardial and 83 epicardial cells. All simulations were conducted using Grandi et al. (GPB) action potential model [79]. Panel C shows in a color code the resting potential (Vrest) along the failing ventricular strand after achieving steady state conditions in the absence of fibrosis, 10% fibrosis, and 20% fibrosis.*

after a period of stabilization. As expected, V_{rest} increases with the fibrotic content. Figure 3.7 panel C shows that HF alone (filled circle with 0% of fibrosis) did not alter significantly CV with respect to control (white circle) but did increase the effective refractory period with respect to control (444 ms vs. 320 ms; results not shown). However, when fibrosis and intercellular uncoupling were considered, separately or concomitantly, the decrease of CV was more pronounced and synergistic. With regard to ERP, uncoupling alone had no significant effect, whereas fibrosis reduced it significantly (results not shown).

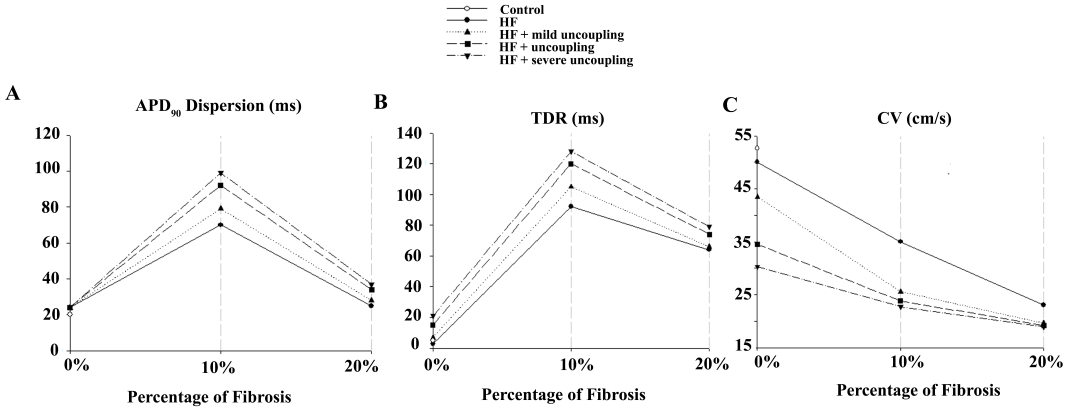

Figure 3.7: *Biomarkers in normal and failing conditions adding structural remodeling with GPB.Electrophysiological properties measured in a one dimensional transmural ventricular strand under different pathological conditions. The ventricular strands were composed by 82 endocardial and 83 epicardial cells. All simulations were conducted using Grandi et al. (GPB) action potential model [79]. The cases considered were: normal conditions (NC) (white circle), electrical heart failure remodeling (HF) (solid line), electrical heart failure remodeling and mild uncoupling (dotted line), normal uncoupling (dashed line) and severe uncoupling (dotted-dashed line). Different degrees of fibrosis were considered: 10% and 20%. Action potential duration (APD) dispersion (panel A), transmural dispersion of repolarization (TDR) (panel B), and conduction velocity (CV) (panel C) along the whole strand were measured (see Methods section for details).*

3.5 Discussion

3.5.1 Major Findings

This computational work, made possible by using two recent, comprehensive, and complimentary mathematical models of the human ventricular AP, provides important new insights into the role of HF-induced electrophysiological and structural remodeling in the modulation of transmural gradients for late repolarization, intracellular Ca^{2+} transient, and action potential conduction. The principal findings and insights from our work are (i) the demonstration that HF heterogeneous remodeling of I_{NCX} and I_{SERCA} modulates Ca^{2+} transient duration and the dispersion of AP-Ca^{2+} transient upstrokes delay. In addition, (ii) simulated homogeneous electrophysiological remodeling during HF increases APD dispersion (more significantly in ORd model than in GPB model), and (iii) HF structural remodeling enhances repolarization gradients and decreases CV and ERP. (iv) We suggest also that although M cells are known to contribute to the increase of APD and repolarization dispersion, they do not to alter the relative change from normal tissue to failing tissue; and (v) confirmation for the first time of the hypothesis that heterogeneous HF remodeling modulates repolarization gradients and can bring them below the values corresponding to normal conditions.

3.5.2 Electrophysiological gradients in heart failure

Transmural heterogeneities of repolarization play a critical role in the genesis of polymorphic ventricular tachycardia (PVT) in HF [5]. Several experimental studies [5, 73, 122, 123] have addressed the impact of the dispersion of repolarization time in the transmural ventricular wall on the generation of reentrant activity in different animal species. In their study on dog ventricle, Akar et al. [5] demonstrated that spatial gradients of repolarization were significantly increased in HF because of the marked prolongation of APD in M cells and concluded that this was directly responsible for PVT generation. In the human right ventricle Lou et al. [123] also observed an increase in APD gradients in HF and related it to increased arrhythmogenesis. In contrast, Coronel et al. [46] observed that in the pig ventricle it is not only the repolarization gradient but also the restitution characteristics in combination with the time of arrival of the premature wavefront, which determines the occurrence of reentry.

Recent experiments have shown that TDR and APD gradient are reduced as a result of heart failure [73, 122]. These studies examined APD prolongation and dispersion of repolarization in coronary artery-perfused left ventricular wedge preparations from the human heart using optical mapping [73]. In these preparations APs were prolonged in HF in a transmurally heterogeneous manner, with the greatest prolongation occurring in the subepicardial layer, so that APD gradients from subendocardium to subepicardium were significantly decreased in failing compared with non-failing hearts. No significant M cell contribution could be identified in these HF wedges. Their identification of M cells was based on the local APD gradient between the areas of delayed repolarization (M cells) and the neighboring myocardium, taking into account intrinsic cellular properties and extrinsic coupling properties of the tissue. M cell islands were found in non-diseased hearts but this was not the case for the failing ones. Although M cells are present in the canine myocardium [5, 220], there is no evidence of the existence of this type of cells under failing conditions in human myocardium [73, 122, 123]. In the present study we analyzed the role of M cells and heterogeneous ionic remodeling in the modulation of repolarization gradients. Our results revealed increased APD dispersion under HF conditions assuming homogeneous remodeling with respect to control conditions. The presence of M cells increased general repolarization gradients but did not alter the relative change in HF with respect to control observed in the absence of M cells.

Assessing the importance of heterogeneous remodeling on the modulation of repolarization gradients was a major highlight in our simulations. Although changes in mRNA and protein expression across the transmural wall have been reported in failing human hearts [7, 92, 172, 206, 231, 247], much more experimental work is required to demonstrate how heterogeneous functional ionic remodeling can alter APD dispersion. Our theoretical results suggest that transmural heterogeneous remodeling of I_{NCX} and/or I_{SERCA} decreased APD dispersion with respect to homogeneous HF remodeling, regardless of the absence (Figure 3.3 red bars) or presence (Figure 3.3 green bars) of M cells. Furthermore, in the absence of M cells, dispersion of repolarization in the heterogeneously remodeled failing tissue, could be brought to lower values than in normal conditions. Thus, this is a plausible explanation for decreased APD dispersion and repolarization gradients in the experimental work of Glukhov et al. [72]. TDR was also modulated by heterogeneous remodeling and was decreased with respect to homogeneous remodeling when ORd model was used.

In the presence of M cells TDR values were higher, and heterogeneous HF remodeling did not bring these values lower than in normal conditions as in [73], where M cells were absent. The effects of heterogeneous remodeling on Ca^{2+} gradients were also ana-

lyzed. It is well known that myocytes in the failing heart exhibit abnormal intracellular Ca^{2+} transients, due in part to the decreased functional expression of the SR Ca^{2+} ATPase (SERCA2a), the enhanced sodium (Na^{+}/Ca^{2+}) exchanger function [12, 90, 159], and the aberrant SR Ca^{2+} leak, due to altered ryanodine receptor (RyR) function [137, 248]. Transmural differences in regulation of these Ca^{2+}-cycling proteins were found in the failing ventricle [172, 247]. Our results accurately reproduce some of these features: the amplitude of Ca^{2+} transients decreases, and the rise and decay rates are slowed down, in accordance with experimental results [163, 164]. Furthermore, homogeneous HF remodeling increases $CaTD_{80}$ dispersion, which is strongly modulated by heterogeneous remodeling of I_{NCX} and I_{SERCA}. Experimentally, Lou et al. [122] found that the gradient of $CaTD_{80}$ was lower in failing conditions. Our results can account for this only if heterogeneous remodeling (I_{NCX}) and no M cells were considered in the analysis using ORd model. In our simulations AP-Ca delay dispersion was slightly increased (GPB) or unaltered (ORd), and heterogeneous remodeling lowered it below the values corresponding to the normal heart (ORd). Lou et al. [122] obtained a slightly lower gradient of AP-Ca delay in failing conditions than in normal conditions. Thus, heterogeneous remodeling could be a possible explanation for these results. Furthermore, heterogeneous remodeling of I_{to} [158], which was not considered in the present work, could also have a role in the modulation of Ca^{2+}transient waveform through changes in early repolarization [193].

3.5.3 The role of structural remodeling in heart failure

In HF significant microanatomical remodeling related to arrhythmogenesis has been observed [48, 78]. The proliferation of fibroblasts and intercellular uncoupling during HF has been the focus of experimental [4, 57, 64, 113, 139, 206, 212] and simulation [100, 138, 245] studies. Experimental work has provided some insights into how gap junctions between myocytes are modified in the failing heart. Specifically, the proteins connexin 43 and 45 (Cx43, Cx45), are reduced and reorganized [57, 72, 113, 167, 225]. Furthermore, it has been hypothesized that cardiac fibroblasts and myocytes could be coupled to each other through gap junctions and modify electrical signal propagation actively, not only as passive insulators. Several experimental studies in vitro [67, 141, 143, 225, 253] corroborate this active interaction between both kinds of cells; However, experimental results in vivo with human cardiac tissue have not been reported. In a variety of species the degree of coupling between myocytes and fibroblasts has been analyzed [99, 101, 111, 129, 138, 187, 191, 210], and a wide range of values were found. In the absence of definitive data, modeling provides

a powerful tool to explore repolarization abnormalities under such hypothetical conditions. Our simulation results showed that the presence of fibrosis significantly modified APD dispersion, TDR and other biomarkers (Figure 3.7). Inserted fibrosis and intercellular uncoupling increased TDR and APD dispersion, and a biphasic behavior was detected depending on the quantity of fibrotic content.

This result might be related to the previous simulation studies reporting that intermediate fibrosis increases the vulnerability to reentry in a virtual infarcted rabbit heart [138] and in a virtual guinea pig fibrotic heart [245]. This is also illustrated in our accompanying paper [74] in the setting of simulated human heart failure. Excitability was also altered in the presence of fibroblasts through the elevation of the resting potential as reported before [99, 129, 151]. Thus, structural remodeling modified the electrical properties of the cardiac tissue generating a substrate for arrhythmogenesis [138, 234, 245, 253], as we illustrated in our accompanying paper [74]. A local decrease in CV when fibrosis was inserted concomitant with intercellular uncoupling was found in our simulations and is in agreement with experimental results [62, 67, 72, 141, 182, 234]. In addition, the ERP was enhanced by ionic remodeling present in HF in agreement with experimental results [72] but was decreased as the fibrotic content increased. This effect may favor the vulnerability to reentry [176], as was reported in other simulation studies [138, 245]. In this study we also demonstrated for the first time that the safety factor for conduction was reduced in the presence of fibrotic clusters, as stated in Glukhov et al. [72], and propagation block could be elicited.

3.5.4 Limitations of the study

Several limitations need to be considered, when drawing inference from mathematical modeling. Our myocyte model for HF based on changes in the ion channel parameters has the inherited limitations described in [215]. Mainly, data from a large number of experimental studies were taken into account, thus resulting in a high variability not only in the ionic remodeling but also in the stage and etiology of HF and its phenotype. For this reason, a sensitivity analysis was performed in our previous work [76], where the experimental variability in ionic remodeling was taken into account and yielded values of APD_{90} and other HF biomarkers within experimental observations. In addition, our HF model was implemented employing two different human AP models: GPB and ORd. These two models were built and validated on the basis of extensive human data. However, there are important discrepancies in their formulations of K^+ currents and Ca^{2+} handling, leading to differences

in the simulation results regarding repolarization and Ca^{2+} transient behavior. Thus, caution should be exercised when comparing simulation results. With regard to heterogeneous remodeling, only the changes in I_{NCX} and I_{SERCA} were applied heterogeneously within the ventricular wall, on the basis of the limited human data available. Experimental results carried out in human hearts have also reported a transmural heterogeneous remodeling in K^+ currents [92, 158]. Although transmural differences in the remodeling of transient outward K^+ current would have affect mainly early repolarization, which was out of the scope of the present analysis, they might also have an impact on Ca^{2+} transient waveform and its dispersion within the ventricular wall [193]. Further combinations of heterogeneous remodeling will be considered in our future work. Finally, to simulate the interaction between human ventricular myocytes and fibroblasts we used an ionic fibroblast model [129] based on experimental data from adult rat fibroblasts, as no voltage clamp data or ionic models of human ventricular fibroblasts have been published so far. Possible inter-species differences might affect the results of our simulations.

3.5.5 Clinical implications and conclusions

This study aimed to investigate in silico the effects of microanatomical and electrophysiological remodeling on the functional properties (phenotype) of the human failing ventricle. Two of the most recent and detailed human AP models (GPB and ORd) were modified to mimic HF phenotype.

Transmurally heterogeneous HF induced ionic remodeling modulated repolarization and Ca^{2+} transient gradients, which could be driven to values lower than the gradients corresponding to normal tissue. In contrast, homogeneous HF ionic remodeling, intercellular uncoupling, and fibrosis increased these gradients. Structural remodeling also altered conduction properties setting the substrate for arrhythmogenesis. Our findings may have important consequences for the treatment and prevention of human HF-induced arrhythmias and its potential contribution to mortality. Pharmacological modulation of intercellular coupling with rotigaptide, an antiarrhythmic substance increasing gap junctional conductance, may have beneficial effects in patients with heart failure. The concomitant reduction of the amount of fibrosis might be successful in these patients but requires further investigation.

3.6 Supplemental Information

The electrical activity of multicellular strands of 165 nodes was simulated containing coupled myocytes and fibroblasts. Fibroblasts distribution was organized randomly, by assigning a probabilistic function. Fibrotic contents of 10% and 20% were chosen corresponding to the percentage of nodes assigned to the fibroblast ionic model. For each fibrotic content 11 random configurations were simulated and are shown in Figure 3.8 (fibrotic content of 10%) and Figure 3.9 (fibrotic content of 20%). These gave rise to different levels of fibrosis (represented in light blue in the figures) quantified as the percentage of nodes executing the fibroblast model (Pf) comprised between 9.03% and 10.84% (15 and 18 nodes, respectively), for a fibrotic content of 10% and Pf comprised between 19.87% and 22.89% (33 and 38 nodes, respectively) for a fibrotic content of 20%.

The dispersion of action potential duration and transmural dispersion of repolarization were calculated (as described in the methods section of the main text) in all the configurations. Tables 3.3 and 3.4 show the results for a fibrotic content of 10% and 20%, respectively, and a normal intercellular coupling (D_M=0.0006 cm/ms). The results of configuration 1 are shown in this chapter.

A statistical analysis was performed to evaluate the mean and the standard deviation. Values are expressed as mean$\pm$SD in the last line of Tables 3.3 and 3.4.

To evaluate the effects of the different degrees of fibrosis (10% and 20%) on APD dispersion and TDR, boxplots diagrams for AP dispersion (Figure 3.10) and TDR (Figure 3.11) for a fibrotic content of 10% and 20% were performed with SPSS Statistics 17.0 software (IBM SPSS Statistics). The difference of means using student t-test was also evaluated and $p<0.05$ was considered significant. In the case of APD dispersion, the difference between 10% and 20% fibrosis was considered significative. For TDR, although the mean for 10% of fibrosis was higher than for 20%, the difference was not significative.

The same analyses were performed for different intercellular coupling degrees and the results are shown in tables 3.5, 3.6, 3.7 and 3.8. The corresponding boxplots are depicted in Figures 3.12, 3.13, 3.14, 3.15, 3.16 and 3.17. For the different intercellular coupling degrees 10% fibrosis presents always bigger APD dispersion and TDR than for 20%.

Configurations	APD dispersion (ms)	TDR (ms)
Config. 1	70	97
Config. 2	88	59
Config. 3	38	53
Config. 4	57	50
Config. 5	71	106
Config. 6	92	71
Config. 7	60	38
Config. 8	112	88
Config. 9	59	48
Config. 10	44	33
Config. 11	46	76
Mean±SD	67±23	97±60

Table 3.3: *APD dispersion and TDR for 10% fibrosis. Action potential duration (APD) dispersion and transmural dispersion (TDR) for the random configurations corresponding to a fibrotic content of 10% and normal intercellular coupling (D_M=0.0006 cm/ms).*

Configurations	APD dispersion (ms)	TDR (ms)
Config. 1	24	64
Config. 2	30	37
Config. 3	28	37
Config. 4	28	75
Config. 5	80	65
Config. 6	31	45
Config. 7	35	40
Config. 8	25	78
Config. 9	48	44
Config. 10	44	88
Config. 11	24	48
Mean±SD	36±16	56±18

Table 3.4: *APD dispersion and TDR for 20% fibrosis. Action potential duration (APD) dispersion and transmural dispersion (TDR) for the random configurations corresponding to a fibrotic content of 20% and normal intercellular coupling (D_M=0.0006 cm/ms).*

Configurations (HF 10% Fib)	D_M**=0.00025**	D_M**=0.0003**	D_M**=0.00045**
	APD dispersion (ms)		
Config. 1	99	92	79
Config. 2	109	104	94
Config. 3	67	61	47
Config. 4	74	70	62
Config. 5	94	89	78
Config. 6	120	113	100
Config. 7	84	77	66
Config. 8	141	135	121
Config. 9	92	84	67
Config. 10	52	49	46
Config. 11	65	61	52
Mean±SD	90±26	85±25	73±23

Table 3.5: *APD dispersion for 10% fibrosis and intercellular uncoupling. Action potential duration (APD) dispersion for the random configurations corresponding to a fibrotic content of 10% and several degrees of intercellular uncoupling (D_M in cm/ms).*

Configurations (HF 10% Fib)	D_M**=0.00025**	D_M**=0.0003**	D_M**=0.00045**
	TDR (ms)		
Config. 1	128	120	106
Config. 2	80	73	65
Config. 3	83	76	61
Config. 4	72	66	54
Config. 5	136	129	115
Config. 6	97	91	78
Config. 7	56	52	43
Config. 8	114	108	96
Config. 9	82	74	58
Config. 10	49	45	38
Config. 11	103	97	83
Mean±SD	90±27	84±26	72±25

Table 3.6: *TDR for 10% fibrosis and intercellular uncoupling. Transmural dispersion of repolarization (TDR) for the random configurations corresponding to a fibrotic content of 10% and several degrees of intercellular uncoupling (D_M in cm/ms).*

Configurations (HF 20% Fib)	D_M**=0.00025**	D_M**=0.0003**	D_M**=0.00045**
	APD dispersion (ms)		
Config. 1	37	34	28
Config. 2	38	36	32
Config. 3	33	32	29
Config. 4	35	33	30
Config. 5	102	97	86
Config. 6	43	40	34
Config. 7	45	42	38
Config. 8	36	33	28
Config. 9	70	64	54
Config. 10	54	52	47
Config. 11	32	30	26
Mean±SD	47±21	44±20	39±17

Table 3.7: *APD dispersion for 20% fibrosis and intercellular uncoupling. Action potential duration (APD) dispersion for the random configurations corresponding to a fibrotic content of 20% and several degrees of intercellular uncoupling (D_M in cm/ms).*

Configurations (HF 20% Fib)	D_M**=0.00025**	D_M**=0.0003**	D_M**=0.00045**
	TDR (ms)		
Config. 1	37	34	28
Config. 2	45	42	38
Config. 3	44	42	39
Config. 4	79	79	73
Config. 5	88	82	71
Config. 6	53	51	47
Config. 7	44	42	42
Config. 8	93	90	83
Config. 9	51	48	44
Config. 10	95	93	89
Config. 11	46	45	42
Mean±SD	61±22	58±22	54±20

Table 3.8: *TDR for 20% fibrosis and intercellular uncoupling. Transmural dispersion of repolarization (TDR) for the random configurations corresponding to a fibrotic content of 20% and several degrees of intercellular uncoupling (D_M in cm/ms).*

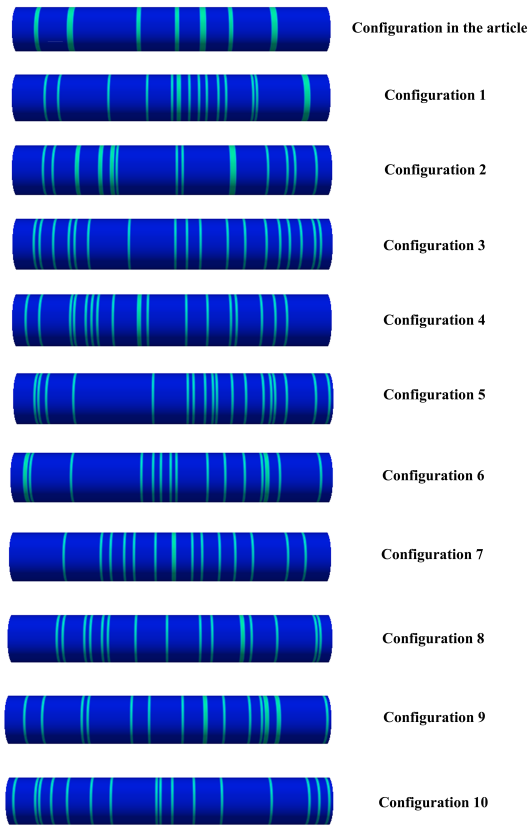

Figure 3.8: *Random configurations for 10% fibrosis in the multicellular strand. The multicellular strand is composed by 165 nodes, where the fibroblast model is solved in 10% of the nodes (light color) and the myocyte AP model is solved in the rest of the nodes (blue). See Methods for details.*

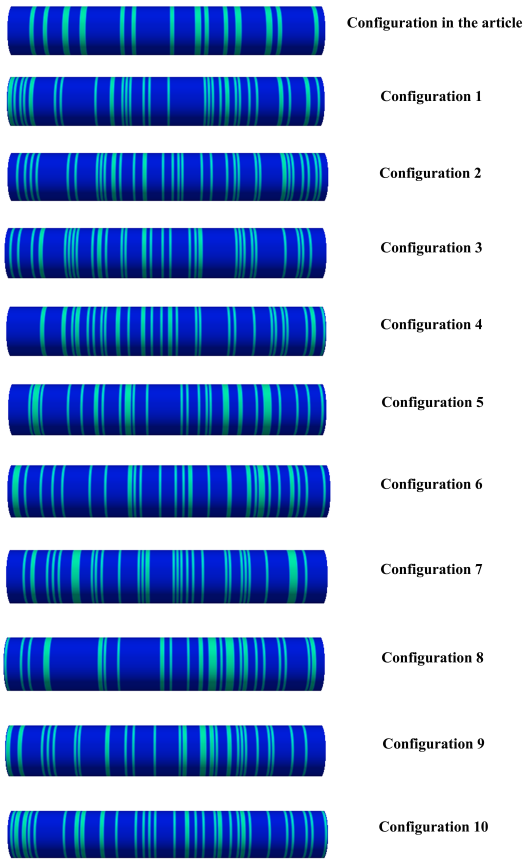

Figure 3.9: *Random configurations for 20% fibrosis in the multicellular strand. The multicellular strand is composed by 165 nodes, where the fibroblast model is solved in 20% of the nodes (light color) and the myocyte AP model is solved in the rest of the nodes (blue). See Methods for details.*

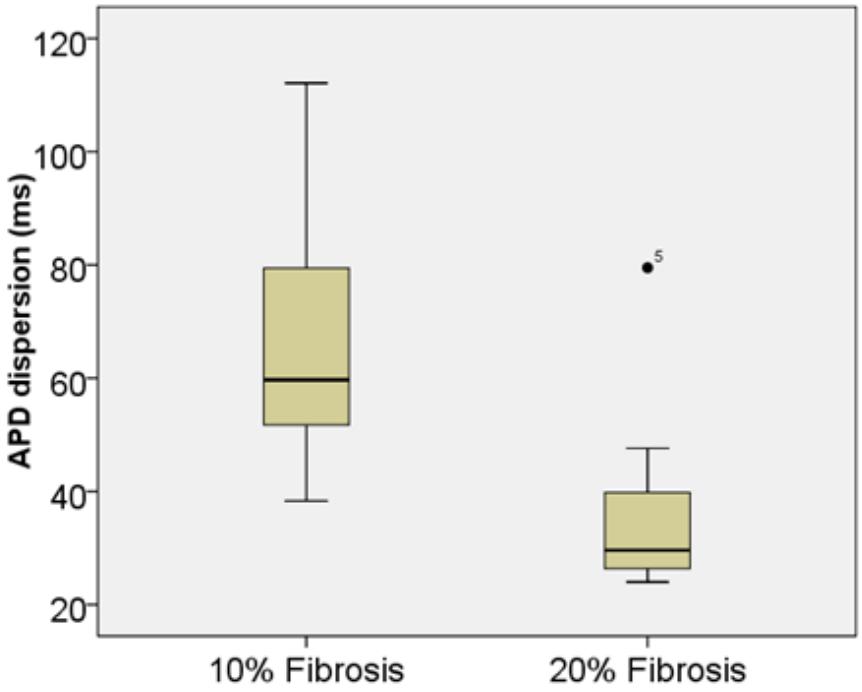

Figure 3.10: *APD dispersion for normal coupling. Boxplots showing action potential duration (ADP) dispersion for low fibrosis (10%) and high fibrosis (20%), and D_M=0.0006 cm/ms.*

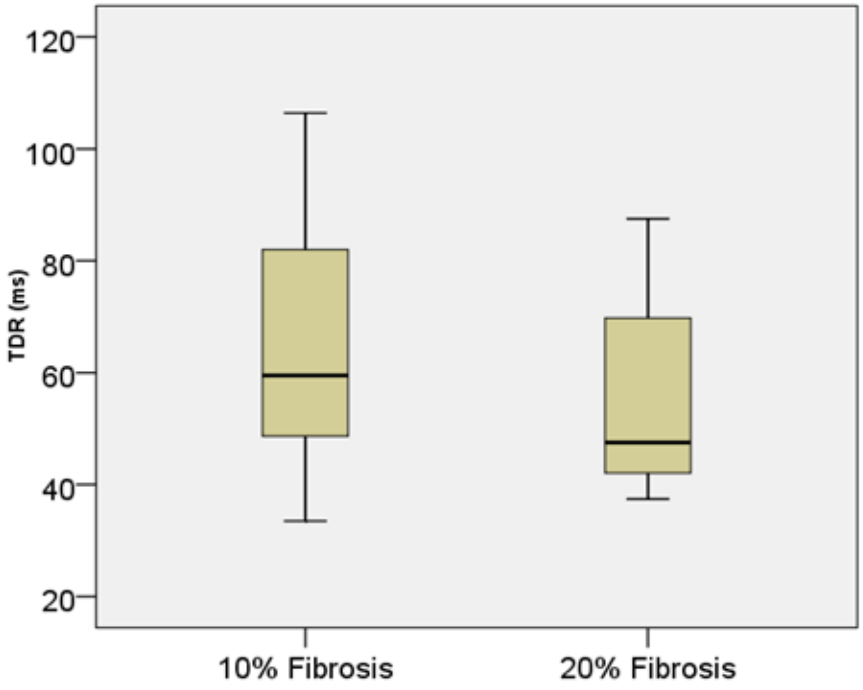

Figure 3.11: *TDR for normal coupling. Boxplots showing transmural dispersion (TDR) for low fibrosis (10%) and high fibrosis (20%), and D_M=0.0006 cm/ms.*

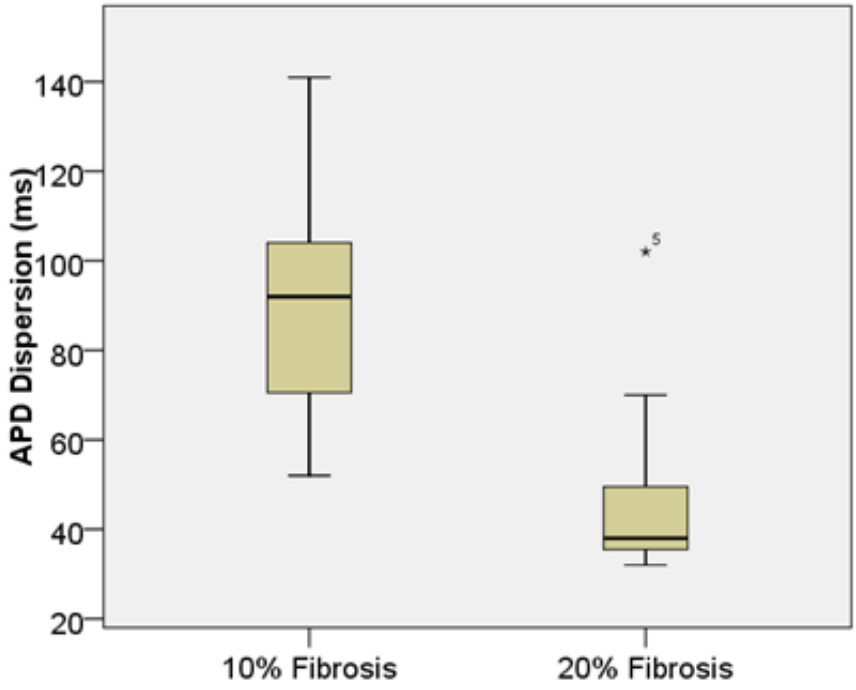

Figure 3.12: *APD dispersion for severe uncoupling. Boxplots showing action potential duration (ADP) dispersion for low fibrosis (10%) and high fibrosis (20%), and D_M=0.00025 cm/ms.*

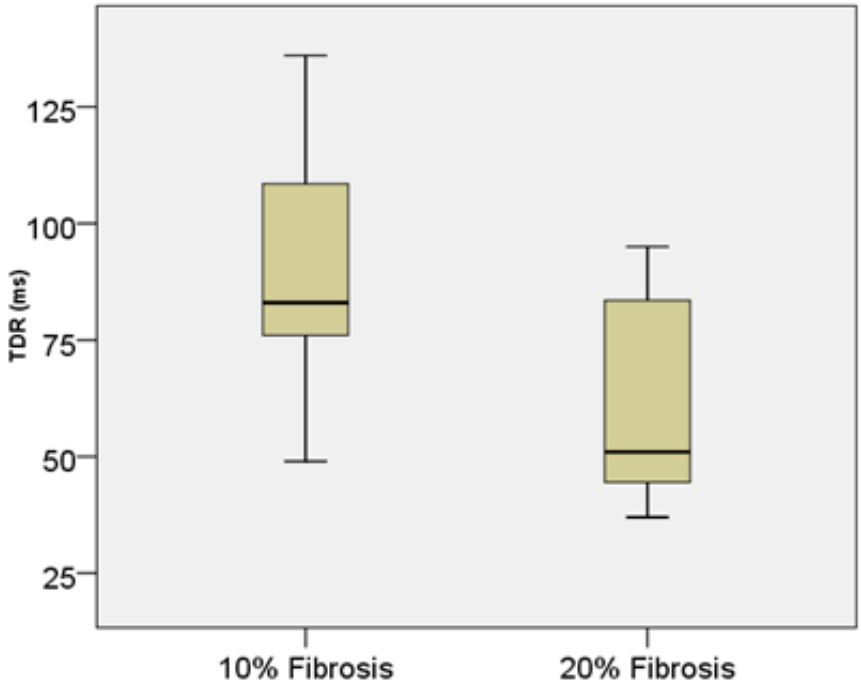

Figure 3.13: *TDR for severe uncoupling. Boxplots showing transmural dispersion (TDR) for low fibrosis (10%) and high fibrosis (20%), and D_M=0.00025 cm/ms.*

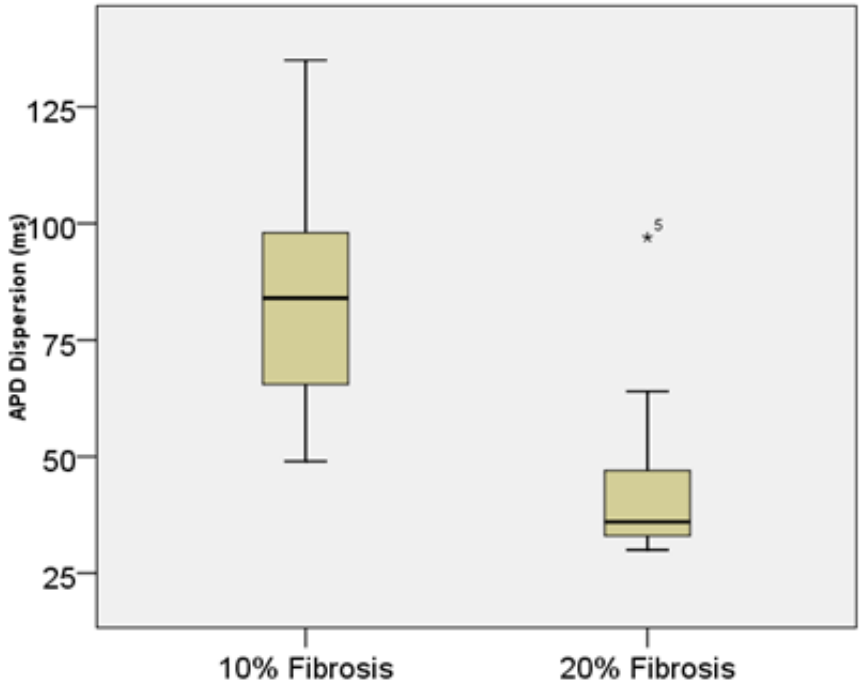

Figure 3.14: *APD dispersion for intermediate uncoupling. Boxplots showing action potential duration (ADP) dispersion for low fibrosis (10%) and high fibrosis (20%), and D_M=0.0003 cm/ms.*

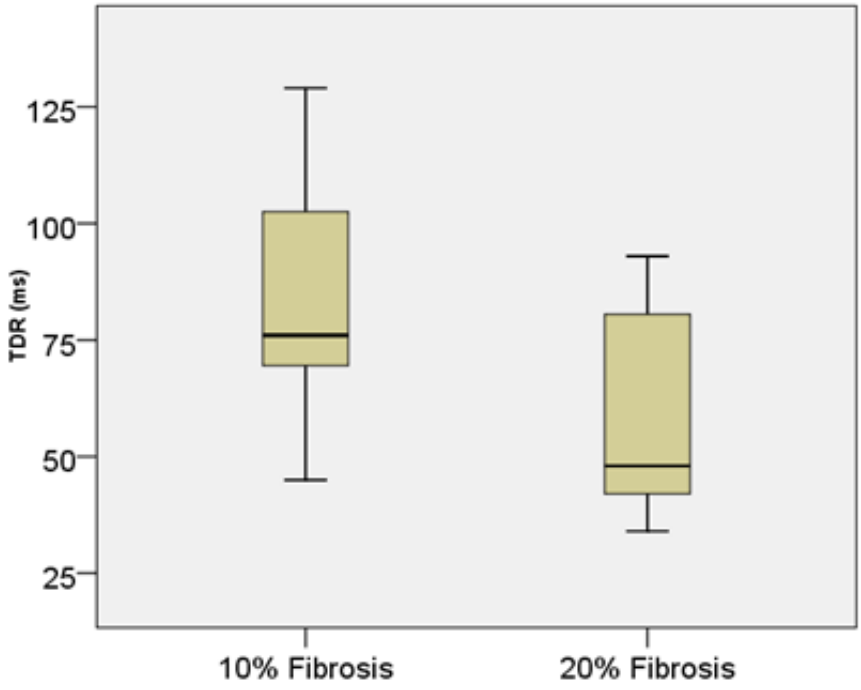

Figure 3.15: *TDR for intermediate uncoupling. Boxplots showing transmural dispersion (TDR) for low fibrosis (10%) and high fibrosis (20%), and D_M=0.0003 cm/ms.*

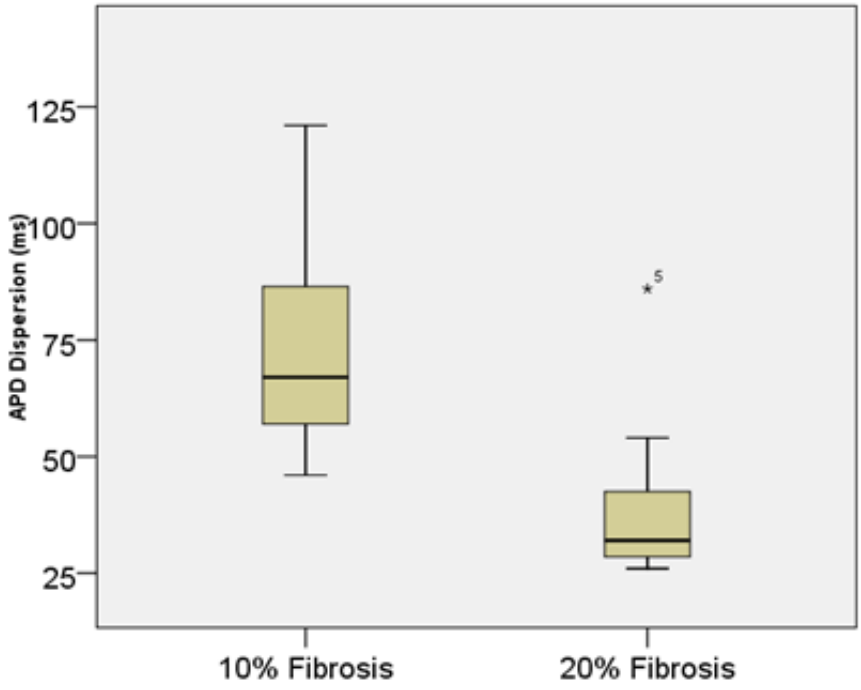

Figure 3.16: *APD dispersion for mild uncoupling. Boxplots showing action potential duration (ADP) dispersion for low fibrosis (10%) and high fibrosis (20%), and D_M=0.00045 cm/ms.*

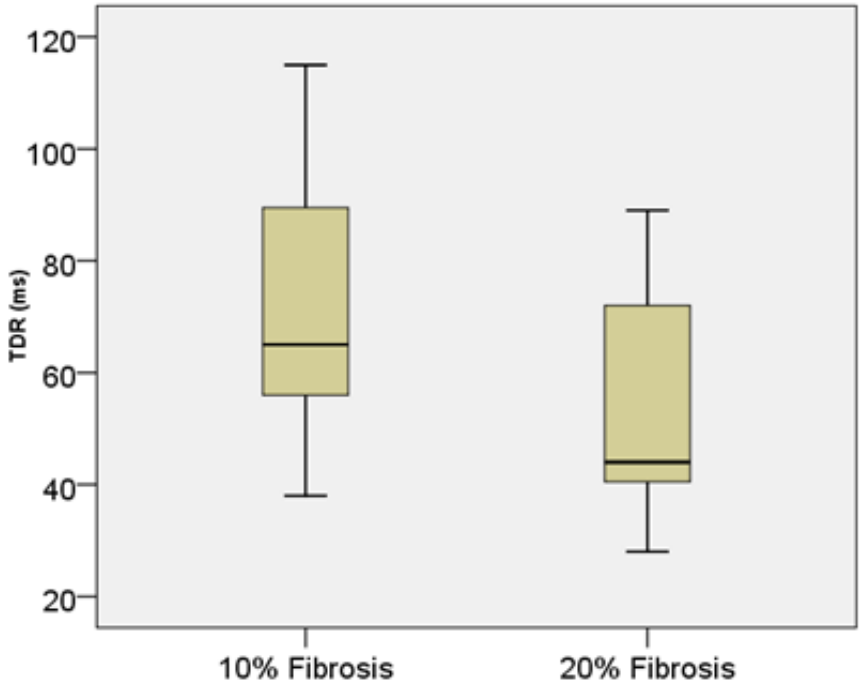

Figure 3.17: *TDR for mild uncoupling. Boxplots showing transmural dispersion (TDR) for low fibrosis (10%) and high fibrosis (20%), and D_M=0.00045 cm/ms.*

CHAPTER 4

Electrophysiological and Structural Remodeling in Heart Failure Modulate Arrhythmogenesis. 2D Simulation Study

The content of this chapter is based on the publication:
Gomez, JF., Cardona, K., Martinez, L., Saiz, J., Trenor, B. Electrophysiological and structural remodeling in heart failure modulate arrhythmogenesis. 2D simulation study. *PLoS One*, 9(7): e103273.

4.1 Abstract

Heart failure is operationally defined as the inability of the heart to maintain blood flow to meet the needs of the body and it is the final common pathway of various cardiac pathologies. Electrophysiological remodeling, intercellular uncoupling and a pro-fibrotic response have been identified as major arrhythmogenic factors in heart failure.

In this study we investigate vulnerability to reentry under heart failure conditions by incorporating established electrophysiological and anatomical remodeling using computer simulations.

The electrical activity of human transmural ventricular tissue (5 cm $\times$ 5 cm) was simulated using the human ventricular action potential model Grandi et al. under control and heart failure conditions. The MacCannell et al. model was used to model fibroblast electrical activity, and their electrotonic interactions with myocytes. Selected degrees of diffuse fibrosis and variations in intercellular coupling were considered and the vulnerable window (VW) for reentry was evaluated following cross-field stimulation.

No reentry was observed in normal conditions or in the presence of HF ionic remodeling. However, defined amount of fibrosis and/or cellular uncoupling were sufficient to elicit reentrant activity. Under conditions where reentry was generated, HF electrophysiological remodeling did not alter the width of the VW. However, intermediate fibrosis and cellular uncoupling significantly widened the VW. In addition, biphasic behavior was observed, as very high fibrotic content or very low tissue conductivity hampered the development of reentry. Detailed phase analysis of reentry dynamics revealed an increase of phase singularities with progressive fibrotic components.

Structural remodeling is a key factor in the genesis of vulnerability to reentry. A range of intermediate levels of fibrosis and intercellular uncoupling can combine to favor reentrant activity.

4.2 Introduction

Ventricular arrhythmias in patients with congestive heart failure (HF), contribute to the high incidence of sudden cardiac death associated with HF [105, 214]. The mechanisms of the arrhythmias occurring in the setting of HF are not fully understood. Afterdepolarization-induced trigger activity has a high tendency to develop in the failing myocardium. However, conditions favoring reentrant arrhythmias have also been described in failing hearts [105]. Reentrant activity is generated by wave interaction with anatomical or functional obstacles combined with specific excitability conditions [239]. In diseased hearts, preexisting electro anatomic tissue heterogeneity is amplified considerably, increasing vulnerability to reentrant arrhythmias [239, 245].

In the case of HF, electrical and structural changes significantly increase the occurrence of reentry. The failing heart phenotype is characterized by distinct alterations in selected ion channels, changes in intracellular calcium cycling, alterations in cell-cell coupling proteins, enhanced interstitial fibrosis, and cellular hypertrophy [45, 122, 213]. Experimental studies in animal models provide evidence for enhanced repolarization gradients in the setting of the failing heart [5, 202] and these can promote reentrant arrhythmias. However, recent studies performed using explanted failing human hearts [72, 73, 122] provide little evidence for these enhanced repolarization gradients. These controversial results were theoretically approached in our accompanying paper [75], showing that heterogeneous ionic remodeling modulates repolarization gradients. These repolarization gradients can also be enhanced by structural remodeling, for example fibrosis and/or cellular uncoupling [77], which simultaneously alter conduction properties [72, 234, 236], increasing the likelihood of reentry. The lack of detailed functional and structural information limits the utility of experimental studies for identifying the precise role of HF remodeling on propagation disorders of the cardiac electrical activity. Computational approach can provide a powerful tool for the analysis of the contributions of different components of a disease. Simulations of reentrant rhythms in the human heart with emphasis on electrophysiological remodeling in HF have been published by Moreno et al. [145] focussing on the effect of drugs. Zlochiver et al. [252] evaluated the current density threshold for cardiac resynchronization treatment, and Turner et al. [216] analyzed electrogram fractionation. Recent studies have simulated the effects of fibrosis on reentry in ventricle [60, 130, 138, 151, 162, 245, 252] and atrium [13, 210]. However, no simulation studies combining electrophysiological HF remodeling, fibrosis and intercellular uncoupling to analyze the vulnerability to reentry in the failing human heart have been performed (see Figure 4.9, Figure 4.10, Figure 4.11, and Figure 4.12 in

Supplemental Information). Furthermore, the analysis of the reentry dynamics under these pathological conditions has not been addressed. We have evaluated whether phase analysis could reveal how heterogeneities caused by electrophysiological and structural remodeling may lead to reentrant waves. Indeed, phase analysis provides a useful tool to follow the electrical propagation activity of the spiral wave and to analyze the arrhythmogenic substrate under such pathophysiological settings. Several studies have used phase maps to follow the trajectory of reentrant activity experimentally [124, 218] and theoretically [25, 42] but none of these have focused on considered conditions of heart failure remodeling in conjunction with fibrosis.

In the present study the electrical activity of a transmural twodimensional human ventricular tissue was simulated using a human action potential (AP) model [79, 215] modified to replicate a HF phenotype. The influence of HF-induced electrophysiological and structural remodeling on vulnerability for reentrant arrhythmia occurrence was studied, and the dynamics of reentrant circuits under such pathological conditions were analyzed.

4.3 Methods

4.3.1 Tansmural failing tissue

The electrical activity of a two dimensional (2D) cardiac tissue of 5cm $\times$ 5cm was simulated. Anisotropy was modeled by considering that transverse conductivity was lower than longitudinal conductivity (anisotropy conductance ratio (σ_x/σ_y=4),and the longitudinal direction of cellular fibers was horizontal. Half of the tissue corresponded to endocardial cells and the other half to epicardial cells. This domain was discretized with 250000 square elements (Δx= 0.01 cm) which resulted in a total of 251001 nodes within the tissue. Temporal resolution (Δt) was fixed to 0.002 ms to ensure numerical convergence ($\Delta t < \Delta x^2/2D$). Human myocyte electrical activity was simulated using a modified version of Grandi et al. model (GPB) [79], in which a late sodium current (I_{NaL}) was added [215]. In order to assess the influence of HF-induced electrophysiological remodeling, our HF model [215] was implemented, as described in the accompanying paper [75]. Thereafter, structural remodeling was also considered by adding 'fibrosis' and/or intercellular uncoupling within this tissue. The electrical activity of fibroblasts was simulated using the 'active' formulation of MacCannell et al. [129].

The diffusion coefficient (D) in normal conditions (NC) for myocytes was set to D_M= 0.0013 cm^2/ms resulting in a conduction conduction velocity (CV) of 50 cm/s which agreed with experimental measurements of transmural conduction [209]. To simulate cell-to-cell uncoupling in heart failure, D was reduced in accordance with experimental data [57]. A 50% reduction was applied between failing myocytes (D_{LOW}) and a three-fold reduction was used between fibroblasts [187, 225] and for the myocyte-fibroblast interaction (D_{Fib}). A wide range of fibroblast-myocyte gap junctional conductance has been reported in experimental [35, 109, 187] and simulation studies [100, 129, 192, 225, 245]. Selected values within these ranges were used.

Fibroblast distribution was organized randomly, by assigning a probabilistic function. Random arrays were generated with different probabilities of assigning the fibroblast ionic model to the nodes. Four configurations of the same random condition were made. These gave rise to different levels of fibrosis quantified as the percentage of nodes executing the fibroblast model (P_f). Tissue configurations were denoted as 'minimal fibrosis' (P_f = 4%), 'mild fibrosis 1' (P_f= 14.5%), 'mild fibrosis 2' (P_f=28%), and 'high fibrosis' (P_f= 40%).

These values of P_f are similar to the ones considered in [130] and would correspond to fibrotic areas within experimental ranges [108].

As stated above, the mesh was discretized in square elements of 100 μm $\times$100 μm. One element was composed of four nodes (separated in 100 μm), as shown in Figure 4.1. Each node executed either the fibroblast ionic model or the myocyte AP model. The value of the diffusion coefficient of a myocyte (D_M) was assigned to an element composed of 4 nodes executing the myocyte AP model. If one or more nodes of an element executed the fibroblast ionic model, then the diffusion coefficient of a fibroblast (D_{Fib}), was assigned to this element.

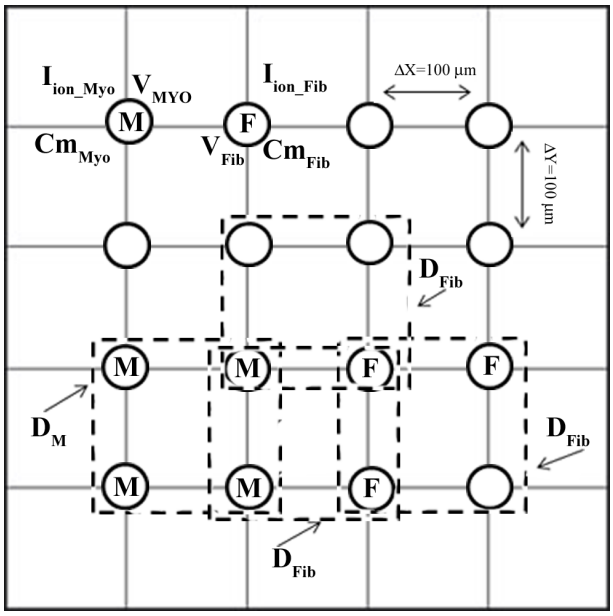

Figure 4.1: *Illustration of the configuration of our virtual human ventricular mesh of interconnected myocytes and fibroblasts. V is the membrane voltage computed for each node, i.e. V_{MYO} for myocytes and V_{Fib} for fibroblasts. C_m is the cell capacitance, i.e. C_{mMyo} for myocytes and C_{mFib} for fibroblasts. D is the diffusion coefficient, i.e. D_M between myocytes in normal conditions (D_M= 0.0013 cm^2/ms), and D_{Fib} between a myocyte and a fibroblast, assigned to each element in the discretized domain. I_{ion} is the total transmembrane ionic current, i.e. I_{MYO} for myocytes and I_{Fib} for fibroblasts. 'M' and 'F' correspond to the 'myocyte' and 'fibroblast' model respectively that are computed in each node.*

4.3.2 Stimulation protocol

After achieving steady-state conditions, five stimuli adjusted to 2 times the excitation threshold in amplitude and 2 ms in duration were applied at the endocardial end of the tissue with a basic cycle length (BCL) of 1000 ms. Electrophysiological properties were measured for the last AP.

To generate spiral wave in 2D simulations, we applied the crossfield stimulation protocol [82]. Once the tissue was stabilized, five stimuli were applied at the endocardial end of the tissue to get an entire wavefront throughout the tissue. After allowing the excitation wave-tail corresponding to the last stimulus to reach the middle part of the tissue, a second S2 stimulation was applied at the endocardial left bottom corner of the tissue (2.5 cm high$\times$1.25 cm wide). This triggered a meandering activation wave (due to wavefront/wave-tail interaction) leading to the formation of a spiral wave. The vulnerable window (VW), an indicator for vulnerability to reentry, was defined as the value of the coupling intervals (CIs) for S2 that led to reentry (at least two spiral wave rotations).

4.3.3 Spiral wave dynamics

To analyze the dynamics of the spiral waves, the dominant spiral wave period was calculated and phase analyses were performed. Using the information of the AP upstroke in all points of the sheet, histograms of cycle lengths values measured to the nearest 1 ms were developed during the simulation and were used to calculate the dominant spiral wave period as in [59].

Phase analysis of the membrane potential signal (V_m) represents a useful method to identify and quantify spatiotemporal organization of reentry dynamics. The phase tracks the progression of a defined region of the myocardium through the action potential and has been demonstrated to be an effective parameter in analyzing spatiotemporal changes. Points around which the phase progresses through a complete cycle from -π to π are of special interest. At these points, the phase becomes indeterminate and the activation wave fronts hinge on these points and rotate around them in an organized fashion. These points in the phase map are called phase singularity points (PS). PSs share location with anatomic heterogeneities, and their spatial meandering is modulated by these heterogeneities. PS also correlate with the location of wave breaks [121] in myopathic human hearts. At a phase

singularity point the following condition is met:

$$\oint \nabla\theta \cdot dr = \pm 2\pi \tag{4.1}$$

where θ is the instantaneous phase. The integral is computed along the closed curve surrounding the anatomical or functional defect.

To obtain phase maps an algorithm in MATLAB calculated the Hilbert Transform (HT) of the membrane potential (Vm) signal in every node of the discretized domain to avoid the results dependence with the chosen time delay [218], and the 'instantaneous phase' was calculated in each node as follows:

$$\theta = tan^{-1}\frac{HT(V_m)}{V_m} \tag{4.2}$$

Phase maps were codified between [-π,π] as in [181]. In our discretized mesh domain PS was defined as a singular point around which the condition of equation 4.3 was met.

$$||\Delta\theta_1 + \Delta\theta_2 + \Delta\theta_3 + \Delta\theta_4| - 2\pi| < 0.001 \tag{4.3}$$

where $\Delta\theta_1$ is the phase difference between nodes B and A, $\Delta\theta_2$ is the phase difference between nodes C and B, $\Delta\theta_3$ is the phase difference between nodes D and C, $\Delta\theta_4$ is the phase difference between nodes A and D [181], as depicted in Figure 4.2.

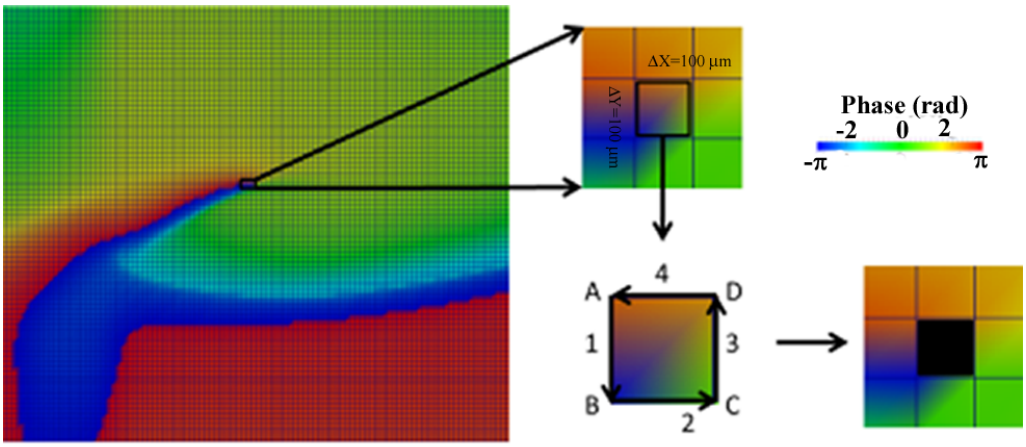

Figure 4.2: *Illustration of phase map analysis. Instantaneous phase of the membrane potential (V_m) signal at the different nodes of the tissue is computed. A phase singularity in an element is operationally defined as all phases being detected within the element (see Methods section for details).*

4.3.4 Computational methods

ELVIRA software was used in our simulations, which is based on a pseudo-adaptive finite element method in space and time to solve reaction-diffusion equations with highly nonlinear reactive terms [88]. The scheme accounts for the anisotropy of the media and incorporates an adaptive time step algorithm to integrate the stiff reactive term associated with the ionic currents. The solution of the monodomain equation 4.4 is computed using the technique of operator splitting.

$$\nabla(D\nabla V_m) = \frac{dV_m}{dt} + \frac{I_{ion}}{C_m} + \frac{I_{stm}}{C_m} \tag{4.4}$$

$$\overrightarrow{n} \cdot \nabla(D\nabla V_m) = 0 \tag{4.5}$$

$$D = \frac{\sigma}{S_V C_m} \tag{4.6}$$

Where V_m is the membrane potential in [V], D is the diffusion conductivity tensor

in [m^2/s], σ is the conductivity tensor in [S·m], S_V is the surface to volume ratio of the cell in [m^{-1}], C_m in [F] is the membrane capacity, I_{ion} in (A) is the total ionic current, and I_{stm} in (A) is the stimulus current. Equation (4.4) has boundary conditions (4.5). Further information can be found in [88]. Tissue mesh representation is shown in Figure 4.1.

4.4 Results

4.4.1 Effects of heart failure remodeling on reentry generation

To simulate reentrant activity, cross-field stimulation was applied to the transmural tissue composed of endocardial and epicardial cells, as described in the Methods section. Reentrant activity or unidirectional block was not observed, either in normal conditions or under HF ionic remodeling conditions. In both situations repolarization time was too large to enable propagation and the wave front was blocked after premature stimulation. If the premature stimulus S2 was applied with a longer coupling interval (S1-S2), complete propagation of S2 was achieved. It is to be noted that the size of the tissue, 5 cm$\times$5 cm in the present simulations, is an important factor for the generation of spiral waves [41], and bigger tissues might lead to the generation of reentry for the above conditions. However, because of the high computational cost of a larger tissue, simulations were performed for the described size.

Fibrosis (14.5%) was then added to NC configuration and reentrant activity was observed (see Figure 4.3, panel A). A set of simulations varying the coupling interval was performed to determine the vulnerable window for reentry (VW). This was approximately 20 ms. When the HF model was studied with the same amount of fibrosis, reentrant activity was also observed (see Figure 4.3, panel B). The VW was as wide as that in NC, but the limits of the VW were delayed (corresponding to bigger coupling intervals).

These results suggest that HF electrical remodeling does not alter the width of the VW, and for this reason the likelihood of reentrant activity is unchanged. However, fibrosis seems to be an important determining factor for reentry generation.

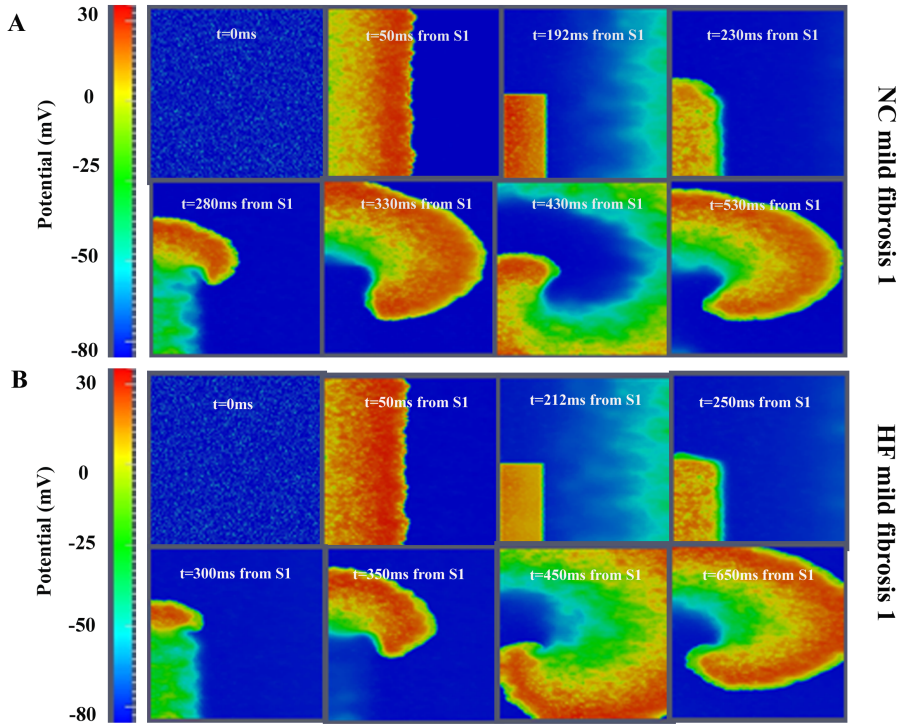

Figure 4.3: *Reentrant activity intransmural fibrotic human ventricular tissue. A. Voltage snapshots in the transmural tissue under normal conditions (NC) and following introduction of 14.5% random fibrosis (mildfibrosis1). B. Voltage snapshots in the transmural tissue assuming heart failure (HF) induced electrophysiological remodeling together with 14.5% random fibrosis (mildfibrosis1). In both panels a cross-field protocol S1-S2 was applied to initiate conduction(see Methods section for details).*

4.4.2 Effects of fibrosis on reentry generation

In order to understand the role of fibrosis in reentry generation several degrees of fibrosis were considered. Figure 4.4 panel A shows the initial membrane potential for different densities of fibroblasts in the failing tissue. Due to the depolarized resting potential of fibroblasts, spontaneous activity appeared in different zones of the ventricular tissue even when the percentage of fibrosis was relatively small ('mild fibrosis 2'), as shown in Figure 4.4 panel B. After cross-field stimulation, as described above, the presence of intermediate fibrosis ('mild fibrosis 1', 14.5% of fibrotic content) led to reentrant activity in both normal and HF conditions. A more detailed analysis of how fibrosis density can affect the probabil-

ity of reentry was carried out in HF conditions, (when fibrosis is known to develop). Indeed, the quantity of fibrosis significantly alters the electrical properties of the tissue, as we have shown in the accompanying paper [75]. When 'low fibrosis' (4%) configuration was considered, we could not induce reentrant activity, regardless of the CI. Thus, there was no VW. As described in the previous section, with an intermediate level of fibrosis (14.5%) a VW of around 20 ms was obtained (see Table 4.1). Indeed, when enough fibrosis is present, the APD and effective refractory period of the myocardial cells are shortened [75], so that when the premature stimulation was applied, part of the ventricular tissue had recovered enough to be excited and a spiral reentry was generated (see Figure 4.3 panel B). Similar results were obtained using 'mild-fibrosis 2' (28%) configuration, and an example of reentry is shown in Figure 4.4 panel C. Under these conditions, the VW was even longer, around 33 ms. When the 'high fibrosis' (40%) configuration was evaluated (see Figure 4.4 panel D), a spiral wave front could be observed. However, in this case, the depolarizing wave front reached very low potentials, leading to electrotonic voltage changes, and could not be considered as reentrant activity, as will be demonstrated later in the phase maps analysis. Thus, intermediate fibrosis increases the VW and very high fibrosis avoids reentry generation, as summarized in Table 4.1. Several random realizations were simulated for each degree of fibrosis (see Table 4.2 in Supplemental Information) and similar results were obtained for the widths of the vulnerable windows corresponding to the same amount of fibrosis.

Simulation	Vulnerable window for reentry (ms)	Limits of the VW (ms)	Rotation Period (ms)
HF 4% fibrosis	0	-	0
HF 14.5% fibrosis	20	[204;224]	240
HF 28% fibrosis	33	[170;203]	250
HF 40% fibrosis	0	-	0

Table 4.1: *Vulnerable window analysis. Vulnerable window for reentry under conditions of heart failure (HF) induced ionic remodeling with different amounts of diffuse fibrosis. The first column shows the width of the vulnerable window, the second column shows the limits of the vulnerable windows, i.e. the first and last instants of time at which S2 is applied to generate reentry, the third column shows the rotation period of the spiral waves taken from Figure 4.5.*

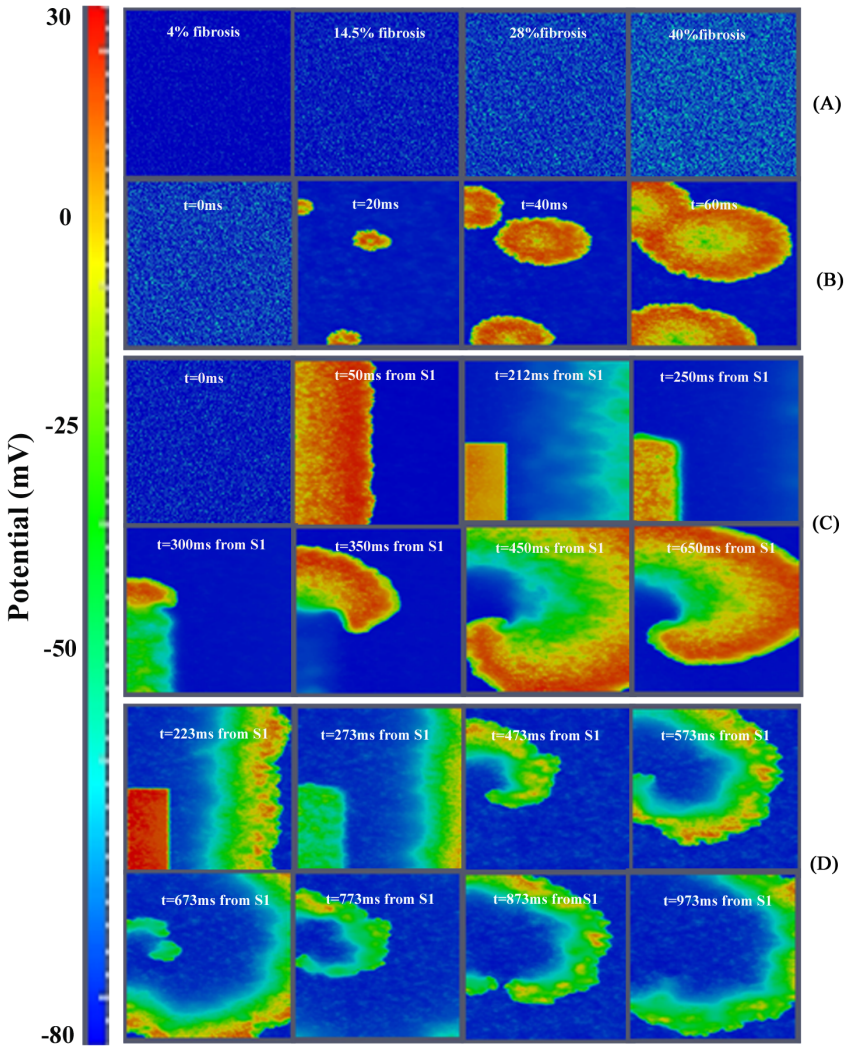

Figure 4.4: *Illustration of the effect of fibrosis in human ventricular tissue. A. Voltage snapshots corresponding to initial conditions, different fibrotic tissue configurations. B. Spontaneous electrical activity in 'mildfibrosis 2'. C. Voltage snapshots of transmural tissue assuming heart failure conditions together with 28% of random fibrosis ('mildfibrosis 1'). In the first two frames, propagation of the action potential due to the S1 stimulus is observed and note also that propagation of the action potential elucidated by the S2 stimulus is observed after the third frame. D. Voltage snapshots of transmural tissue assuming heart failure conditions together with 40% of random fibrosis ('high fibrosis'). S1-S2 cross-field protocol was also used to stimulate the tissue, but in this case only the propagation of stimulus S2 is shown.*

In the cases where spiral waves were obtained the dominant period was measured, as shown in Figure 4.5 and indicated in Table 4.1. For a reentrant wave generated after an S2 stimulus applied at an instant of time within the vulnerable window (S2 applied at t= 210 ms for 'mild fibrosis 1' and t =170 ms for 'mild fibrosis 2') the dominant spiral wave periods were 240 ms and 250 ms for 'mild fibrosis 1' and 'mild fibrosis 2', respectively. Thus, the rotation frequency of the spiral wave slightly decreased with increased fibrosis.

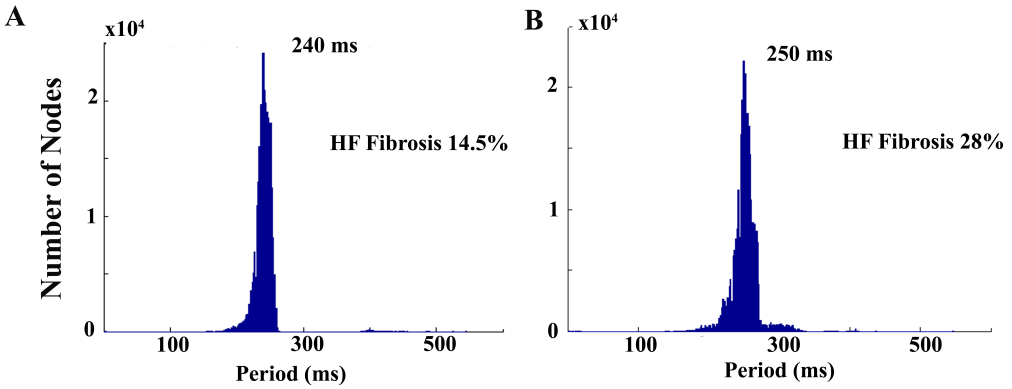

Figure 4.5: *Spiral waves periods. Using the information of the AP upstroke in all points of the sheet, histograms of cycle lengths values measured to the nearest 1 ms were developed during the simulation as in [59]. The reentrant waves generated after an S2 stimulus applied at an instant of time situated in the center of the vulnerable window (S2 applied at t = 210 ms for 'mild fibrosis 1' and t = 170 ms for 'mild fibrosis 2') were considered to build the histograms. The dominant spiral wave periods were 240 ms and 250 ms for 'mild fibrosis 1' and 'mild fibrosis 2', respectively.*

4.4.3 Intercellular uncoupling effects on reentry generation

The structural remodeling of HF includes not only fibrosis but also intercellular uncoupling. To understand the role of this uncoupling in the generation of reentry, simulations were performed using NC tissue with reduced electrical conductivity (D_{LOW}). Under normal coupling conditions, reentry was not obtained (see Figure 4.6 panel A) for the selected size of the tissue. Thus, the conductivity was gradually reduced until reentrant activity developed (see Figure 4.6 panel B), which would be formally equivalent to increase the size of the tissue. This required a tenfold reduction of the diffusion coefficient . Normal CV was

50 cm/s [209], and was reduced down to 18 cm/s, for the low conductivity conditions. This could also be estimated by the proportionality between CV and $\sqrt{D}$.

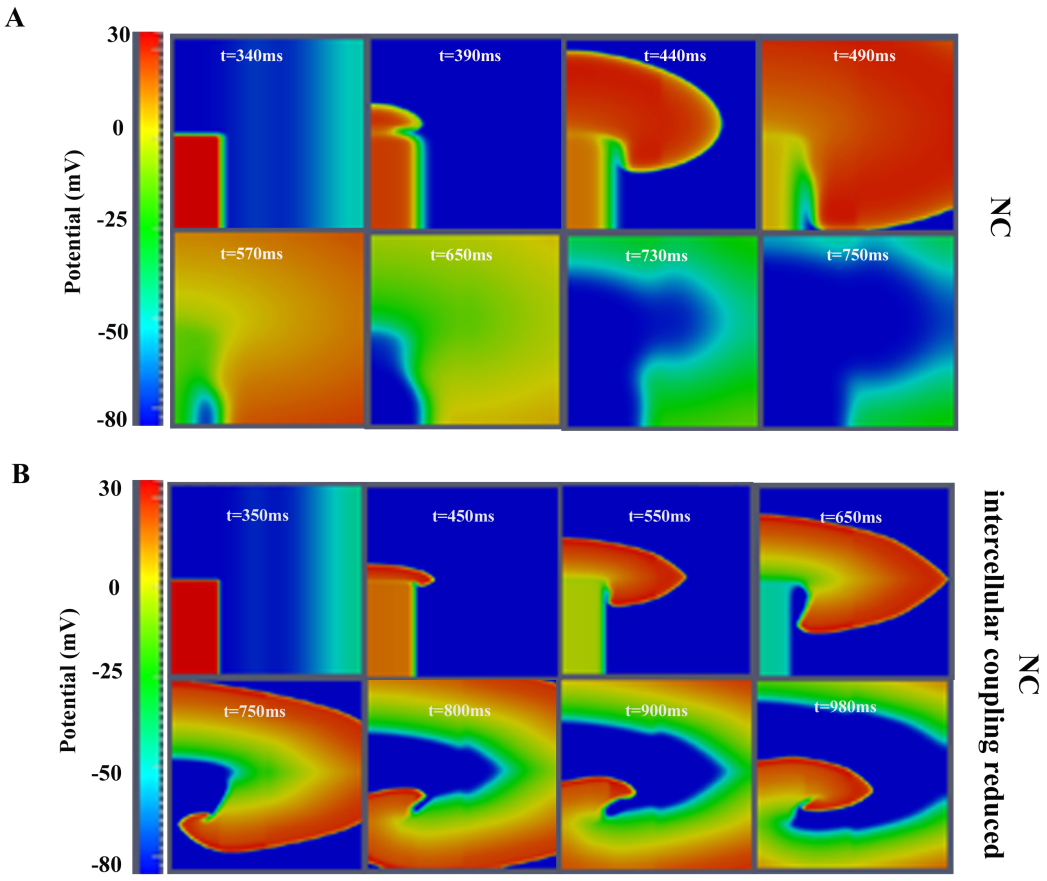

Figure 4.6: *Effects of cell-to-cell uncoupling on reentry generation. A. Voltage snapshots in the transmural human ventricular tissue under normal conditions (NC). B. Voltage snapshots in the transmural tissue NC with a marked decrease in intercellular coupling (conductivity was reduced ten-fold). S1-S2 cross-field protocol was used to stimulate the tissue. Only the response to S2 stimulus is shown.*

Although intercellular uncoupling led to reentry in normal conditions, we also inves-

tigated this effect in failing tissues with defined levels of fibrosis. To determine how the VW was modified by intercellular uncoupling, 'mild-fibrosis 2' configuration was adopted and different levels of uncoupling were employed in the simulations. Under such conditions with normal cellular coupling, the VW was 30 ms (see Table 4.1). When intercellular uncoupling was increased (two-fold decrease of the diffusion coefficient), VW was increased to 42 ms. A ten-fold reduction of conductivity yielded a VW of 112 ms. For very low diffusion coefficients (one hundred-fold reduction), cellular uncoupling was high enough to block the electrical propagation. Thus, as shown in Figure 4.7, an intermediate level of cellular uncoupling favors reentry generation.

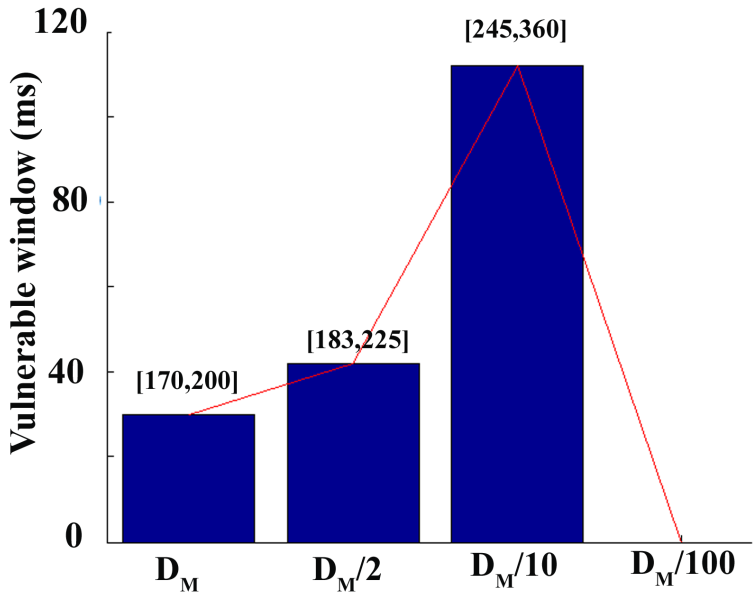

Figure 4.7: *Summary of the computed vulnerable window corresponding to selected reductions inintercellular coupling. Vulnerable window for reentry in ms versus diffusion coefficient in 'mild fibrosis 2' configuration (HF ionic remodeling and 28% of fibrosis).*

4.4.4 Analysis of reentry generation in HF with fibrosis using phase maps

To more completely understand the dynamics of reentry in the presence of fibrosis, we employed phase maps, to illustrate and analyze the spatiotemporal organization of reentry dynamics. Figure 4.8 depicts the evolution of the spiral wave for the selected fibrotic conditions with electrical HF-induced ionic remodeling. When no fibroblasts were present ('without fibrosis' configuration), concentrated phase singularities were detected, revealing clearly the trajectory of the rotor tip. This trajectory can be observed in red color in the last snapshot of panel A. In this setting, reentry developed when intercellular uncoupling was increased. As the fibrotic content of the tissue increased ('mild fibrosis 2'), under HF electrophysiological remodeling conditions and normal intercellular coupling, the phase singularities were transient and sparse throughout the ventricular tissue. The trajectory of the rotor tip could also be identified (red color in the last snapshot of panel B), although it was less concentrated than in the absence of fibrosis, due to the fibroblast-induced electrical heterogeneities. In this last snapshot all transient phase singularities throughout the simulation time are also shown in black.When a high level of fibrosis was introduced ('high fibrosis' configuration), with HF electrophysiological remodeling and normal intercellular coupling, multiple phase singularities appeared during the entire simulation. However, PSs did not follow a specific trajectory. In this case, a rotor tip could not be defined. The phase maps show (in red and blue colors) the phases of the small depolarization, showing only electrotonic interactions, as opposed to AP propagation.

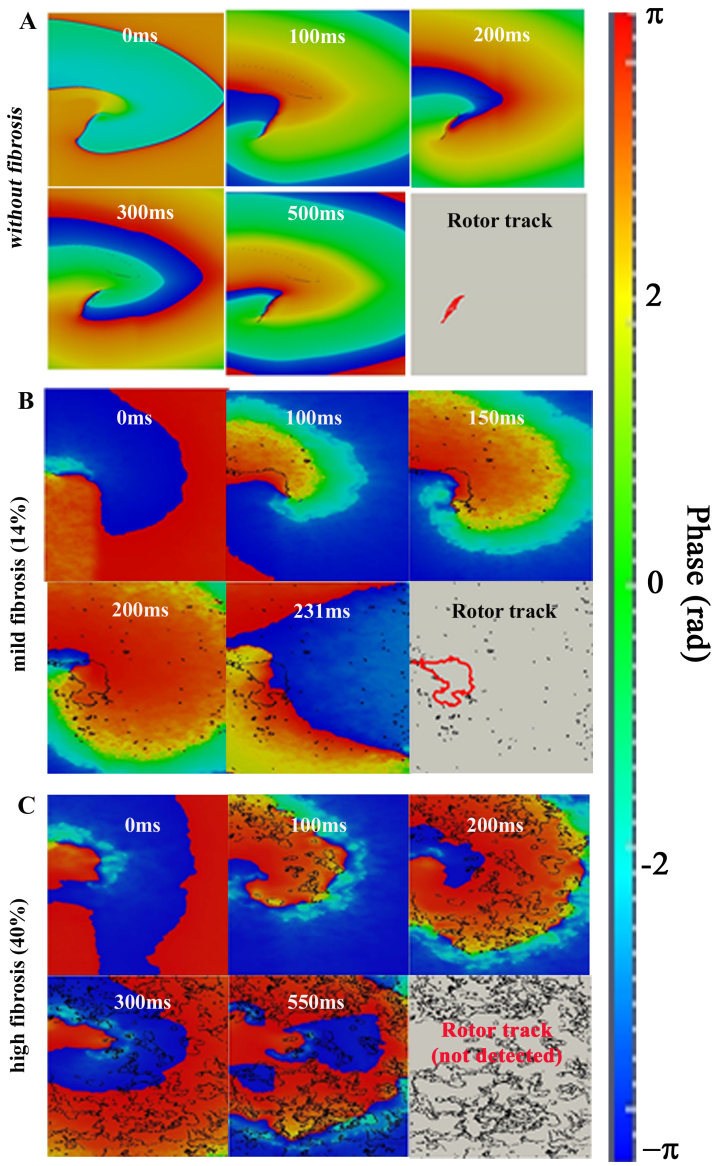

Figure 4.8: *Phase map analysis of evoked rhythm disturbances on the failing human ventricular tissue. Phase maps in electrically remodeled failing tissues assuming selected levels of fibrotic content. In the first case (panel A), 'without fibrosis', the intercellular coupling is increased ten-fold. The 'mild fibrosis' (panel B) and 'high fibrosis' (panel C) cases assume normal intercellular coupling conditions. All transient phase singularities are indicated in black, and the tip of the trajectory is indicated in red in the last snapshot of each panel.*

4.5 Discussion

This computational study focussed on the vulnerability to reentry and the dynamics of spiral waves in a virtual failing human ventricular tissue, with transmural heterogeneity, electrophysiological remodeling, cellular uncoupling and fibrosis. It was designed to assess the contributions of each component of heart failure, i.e. ionic remodeling, intercellular uncoupling and fibrosis, to arrhythmogenesis. The principal findings and insights from our work are (i) demonstration that HF electrophysiological remodeling delays the limits of the vulnerable window for reentry but does not alter the width of the VW, so that the likelihood of reentrant activity is not enhanced; (ii) confirmation that fibrosis is determinant for reentry generation; intermediate fibrotic levels increase the VW and favor reentry generation, while high levels hamper it; (iii) evidence that intermediate intercellular uncoupling enhances the VW; (iv) understanding how the active interaction between fibroblasts and failing myocytes increases the presence of phase singularities in ventricular tissues and alters the spiral wave dynamics in reentrant circuits.

4.5.1 Contribution of electrical remodeling on reentry generation

Patients with severe heart failure are at high risk of sudden cardiac death. In the majority of these patients, sudden cardiac death is due to ventricular tachyarrhythmias (VT). Alterations of the electric properties of single myocytes in heart failure may favor the occurrence of VT in these patients by inducing early or delayed afterdepolarizations (EADs or DADs) [45]. In failing hearts with a healed infarct, VT is caused by reentrant excitation within the network of surviving myocardial fibers in the infarct. In nonischemic cardiomyopathies, both in humans and in animal models, VT is predominantly due to non-reentrant mechanisms, most likely triggered activity caused by DADs [105, 168]. The generation of EADs and DADs in failing human hearts has also been simulated in computational studies [144, 215] using Grandi et al. AP model [79]. Electrophysiological remodeling in failing hearts not only facilitates triggered activity but it also results in an arrhytmogenic substrate, as shown in the accompanying paper [75]. Both effects are necessary to reentry generation. One of the aims of the present study was to evaluate how HF electrophysiological remodeling affects the probability of reentry generation. Our results suggest that HF electrical remodeling (alone) does not alter the width of the VW with respect to normal conditions, although the limits of the VW are delayed. Indeed, repolarization is delayed in HF and premature stimulation can lead to reentry if applied at later instants of time Moreno et al. [145]

evaluated the effects of drugs on reentry generation in a virtual human ventricular tissue with HF-induced electrophysiological remodeling and observed also that conduction block occurred at slower frequencies with HF remodeling, thus delaying the limits of the vulnerable window for reentry generation. This was due to the alteration of cell excitability caused by prolongation of APD in HF. Other computational studies introducing HF electrophysiological remodeling in 2D tissues [216, 252] have been performed but none of these studies focused on the effect of electrical remodeling on vulnerability to reentry, as illustrated in the present study.

4.5.2 Contribution of structural remodeling on reentry generation

Structural remodeling in the failing heart, i.e. fibrosis and intercellular uncoupling, is an important factor favoring the formation of reentrant waves. Fibrosis is thought to contribute to the deterioration of LV function (impairing the mechanical properties of the left ventricle during diastole) and electrical activity (facilitating arrhythmogenesis) [78, 104]. As shown in the accompanying paper [75], fibrosis decreased conduction velocity in accordance with other studies [72, 245].Figures 4.3 and 4.4 show a discontinuous wavefront in the presence of fibrosis as in [130]. Experimentally, Glukhov et al. [72] optically mapped the coronary perfused left ventricular wedge preparations from human hearts with end-stage nonischemic cardiomyopathy and reported nonuniform propagation discontinuities and wave breaks conditioned by strands of increased interstitial fibrosis. It is also known that the excitability of the tissue is altered in the presence of fibroblasts and spontaneous depolarizations were observed in our simulations (see Figure 4.4). As shown experimentally by Miragoli et al. [143] in tissue cultures, myocytes coupled to fibroblasts might exhibit spontaneous depolarizations, depending on the density of fibrosis and heterocellular coupling conductance (see [183] for review). Similarly, in their simulation study, Greisas and Zlochiver [82] obtained spontaneous excitations. These spontaneous excitations are the result of the myocyte membrane depolarization up to the threshold imposed by the coupled fibroblasts, which exhibit a less negative resting potential. Dispersion of repolarization is also enhanced by structural remodeling [75], setting the substrate for reentry. The alteration of the electrical properties of the tissue in the presence of fibrosis might lead to a higher probability of reentry generation. Indeed, our results suggest that intermediate fibrosis increases the VW and that very high fibrosis hampers reentry generation.

A similar biphasic behavior was observed in the computational work of McDowell

et al. [138] who simulated reentry in a virtual infarcted rabbit heart for different degrees of fibrosis. Xie et al. [245] also demonstrated that functional fibroblast-myocyte coupling facilitates induction of reentry in a virtual heterogeneous cardiac tissue. Majumder et al. [130] added several levels of diffuse fibrosis with passive interaction with myocytes, in a two dimensional transmural tissue. They reported a variety of non-equilibrium states which led to conduction block and spiral waves; they did not consider the possibility of active interaction between both kind of cells as we did in the present study.

Our results also highlighted the fact that an intermediate level of cellular uncoupling favors reentry generation. This was also reported by Ramirez et al. in the setting of myocardial ischemia (phase 1b) with different intercellular uncouling degrees. Wiegerinck et al. [234] also related the increase of intercellular coupling to arrhtyhmia inducibility in a rabbit experimental model of HF.

Thus, structural remodeling strongly modulates the substrate for arrhythmogenesis, as was demonstrated in the accompanying paper [75], and seems to be a determinant factor in reentry generation according to our present results. Although the relationship between the type of reentry and tissue architecture has not been identified, it is likely that in hearts with diffuse fibrosis one or more rotors may maintain the arrhythmia [194] whereby the tissue discontinuities may function as (temporary) anchoring points for the mother rotor [49]. The analysis of the reentrant waves dynamics with structural remodeling deserves in fact special attention.

4.5.3 Reentrant wave dynamics in the failing heart

During reentry, electrical activity propagates within a defined closed path, thus forming a spiral wave of activation in two dimensions and a scroll wave in three dimensions (3D) [41]. Spiral and scroll waves are active sources of excitation, which organize the spatiotemporal pattern of excitation of the myocardium during arrhythmia. 2D spiral waves are characterized by a wave break at the core of the spiral (spiral wave tip). Gray et al. [81] developed the technique we used in the present study based on phase plane analysis to investigate the dynamics of spiral rotors. They identified phase singularities, and their characterization allowed the tracking of the spiral and its tip dynamics in space, over time [160] and the systematic study of initiation, maintenance and termination of rotors. Wave break and formation of a PS is an essential condition for a rotor to exist. The formation of PS is necessary, although not sufficient, for sustained rotation. In addition, a new excitation

wave must be generated. Furthermore, a PS must last over time (at least one rotation period) to form a rotor.

In the present work phase maps analysis was used to assess for the first time the influence of fibrotic content under failing conditions on reentry generation. Our simulation results showed that in the absence of fibrosis the induced reentrant waves presented concentrated and regular rotors; when intermediate levels of fibrosis were considered, the tip of the reentry meandered within a larger area and the vulnerable window was wider. The compactness of the tip trajectory prevents a single spiral from splitting into multiple spirals [151]. Thus, the extent of the fibrosis is a key factor in determining the dynamics of reentrant waves under failing conditions. In the case of a high level of fibrosis only electrotonic cell-cell communication was found, the density of PSs was very high but no tip trajectory could be identified. The amount of PSs in this case gave evidence of the heterogeneous nature of the tissue. The ability to correlate PSs with anatomy provides the potential to investigate the relationship between PSs and structural heterogeneities.

Others have employed phase map analysis to follow the trajectory of the spiral tip and the rotor dynamics during tachycardia or fibrillation [124, 218]. However, little research has been done on the relationship between fibrosis, phase singularities and spiral wave dynamics. Recently Majumder et al. [130] and Nayak et al. [151] performed a dynamical analysis of simulated spiral waves in the presence of fibrosis. However, their study was focussed on the tip trajectory and the non-equilibrium states. A phase analysis was not performed. To our knowledge, the only study analyzing the relationship between simulated fibrosis and phase maps was done by Zlochiver et al. [253]. They demonstrated also that the amount of PSs increased with fibrotic content. However, in their work fibroblasts were considered as passive elements and no heart failure ionic remodeling was considered. In this way, our simulation work complements the above mentioned studies and brings new insights into the effects of heart failure induced electrophysiological and structural remodeling on spiral wave dynamics.

To further characterize the dynamics of spiral waves the spiral wave rotation period was calculated under different conditions of fibrosis (see Figure 4.5 and table 4.1) and the rotation frequency slightly decreased with the increase of fibrosis. Zlochiver et al. [253] also observed a decrease in the rotor frequency when the amount of fibrosis was increased. Tanaka et al. [210] reported as well a decrease in the dominant frequency in atrial fibrillation in failing sheep atria and related it to the presence of fibrosis. In a recent study, Greisas et al. [82] calculated the rotation period of the spiral wave, however they used the information

of the AP in only one site of the tissue to calculate the period of the rotation wave and found a biphasic behavior: the rotation frequency increased and then decreased when fibrosis was increased.

4.5.4 Conclusions and clinical implications

In summary, this study shows that electrophysiological and structural remodeling in failing hearts exert an essential influence on reentry generation and dynamics. Electrical coupling of cardiomyocytes with fibroblasts cells alters the anisotropic action potential propagation in the human failing heart in a fashion that significantly depends on the density of fibrotic content and on the degree of intercellular coupling. This raises the possibility that pharmaceutical treatment with eg. rotigaptide, (which increases intercellular coupling), might affect reentrant activity. Phase maps analysis provides a powerful tool to explore abnormal conduction patterns in the setting of ventricular fibrosis. Identifying and studying the different organizational manifestations of phase distribution during arrhythmias in the presence of fibrosis provides one means for objective characterization of arrhythmias. Our findings also may be relevant to ablative procedures, which might have improved success when the targets for ablation enclose the boundaries of tip meandering, as revealed by the phase analysis. Indeed, understanding the relationship between VT organizing centers and fibrosis has important implications for VT ablation since it could provide guidance in determining the optimal targets of VT ablation, as demonstrated by Ashikaga et al. 2013 [14] in their simulation study. They accurately identified optimal targets of ablation in patient-specific heart models and carried out effectively non-invasive ablation. This computational method prior to the clinical procedure supposes a potential translational effort in developing simulation predictions for the optimal targets of VT ablation. Similarly, ablation in zones of complex fractionated electrograms, which are related to the presence of fibrosis [101], and surrounded by phase singularities, has been shown to be effective in simulation studies [249]. Thus, phase maps analysis related to fibrosis seems to be a potent tool prior to the clinical ablation procedures.

4.5.5 Limitations of the study

This study provides novel mechanistic insights into reentry generation in the human failing human heart. We acknowledge, however, that our work has some significant limitations. Firstly, our anatomical description of the cardiac tissue does not include accurate fiber orientation or electrophysiological heterogeneities, as more detailed 3D ventricular models can provide. However, anisotropic conduction was considered in our 2D tissue simulations. Secondly, only the active model of fibroblasts (including ionic currents) was considered as in [99, 129, 138, 192], while others have considered a passive interaction between myocytes and fibroblasts [130, 151, 245, 253]. Although functional coupling between myocytes and fibroblasts has been identified in cultured preparations [36] and ionic currents have been identified in fibroblasts [35], no experiments have reported the presence of active fibroblasts in human. Furthermore, due to the irregular shape of coupled fibroblasts, these are difficult to identify [111]. Thus, modeling and simulation work provides a helpful tool to reproduce this hypothetical scenario. It is also to be noted that a smaller spatial discretization as in [245], would allow a more realistic definition of the size of fibroblasts, taking into account that a fibroblast is more than four times smaller than a myocyte. However, this would increase significantly the computational cost. In any case, in our simulations the ionic models consider the difference of capacity between a fibroblast and a myocyte, scaling accordingly the ionic currents. Finally, with regard to the random introduction of fibroblasts in the tissue, an increase in the number of random configurations for each level of fibrosis would allow to perform a statistical analysis of the effects of fibrosis. Because of the high computational cost this would suppose, we only simulated four different configurations for each case, and it can be stated that the results were very similar.

4.6 Supplemental Information

4.6.1 Random fibrosis configurations

The electrical activity of a two dimensional (2D) human cardiac tissue of 5cm $\times$ 5cm was simulated containing coupled myocytes and fibroblasts. Heart failure ionic remodeling was applied to myocytes. Fibroblasts distribution was organized randomly, by assigning a probabilistic function. Fibrotic contents of 4%, 14.5%, 28% and 40% were chosen corresponding to the percentage of nodes assigned to the fibroblast ionic model. For each fibrotic content 4 random configurations were simulated and are shown in Figure 4.9 (fibrotic content of 4%), Figure 4.10 (fibrotic content of 14.5%), Figure 4.11 (fibrotic content of 28%) and in Figure 4.12 (fibrotic content of 40%). Myocytes are represented in dark blue and fibroblasts are represented in light blue.

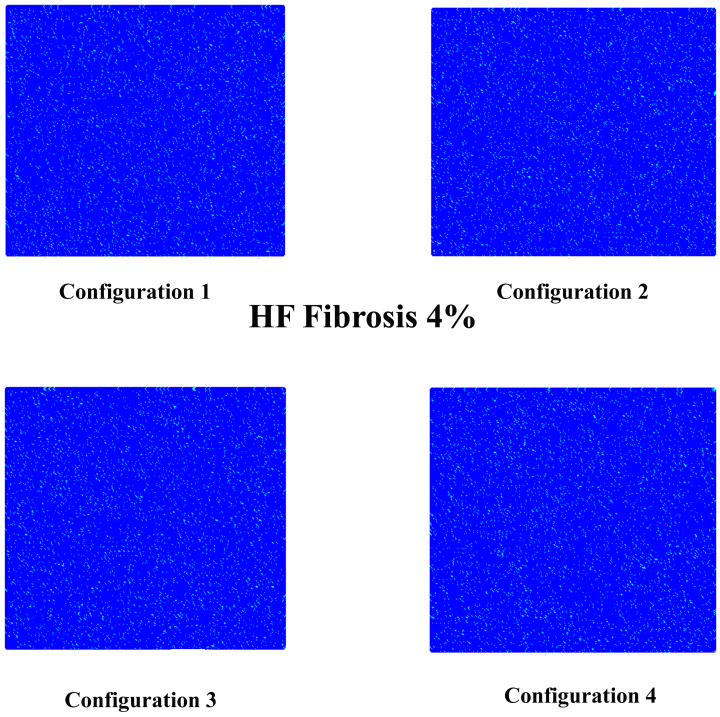

Figure 4.9: *Random configurations for 4% fibrosis in the human failing ventricular tissue.*

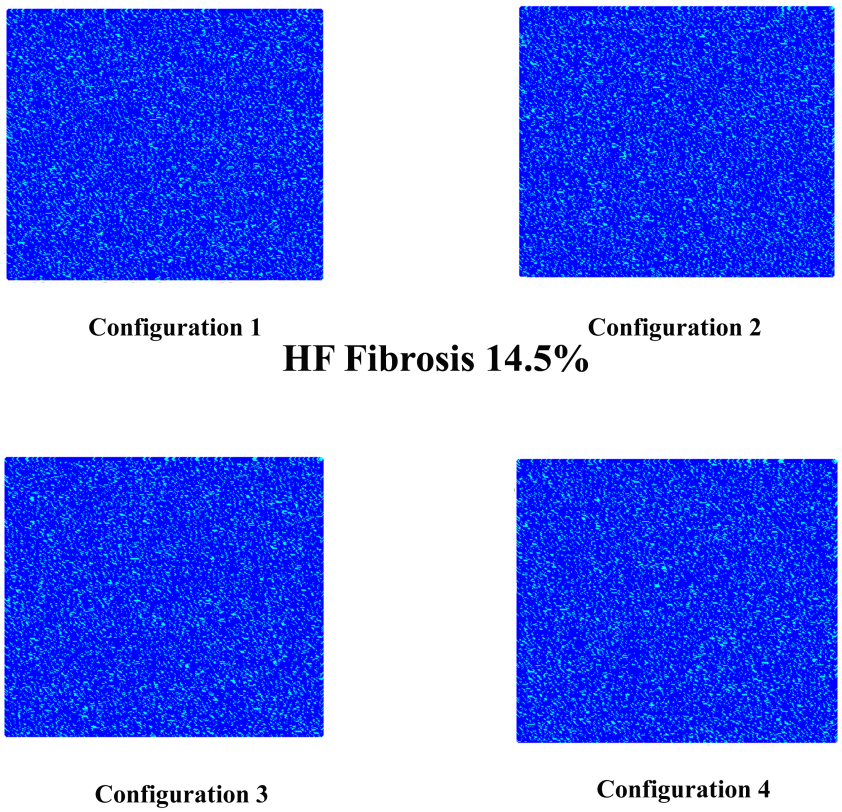

Figure 4.10: *Random configurations for 14.5% fibrosis in the human failing ventricular tissue.*

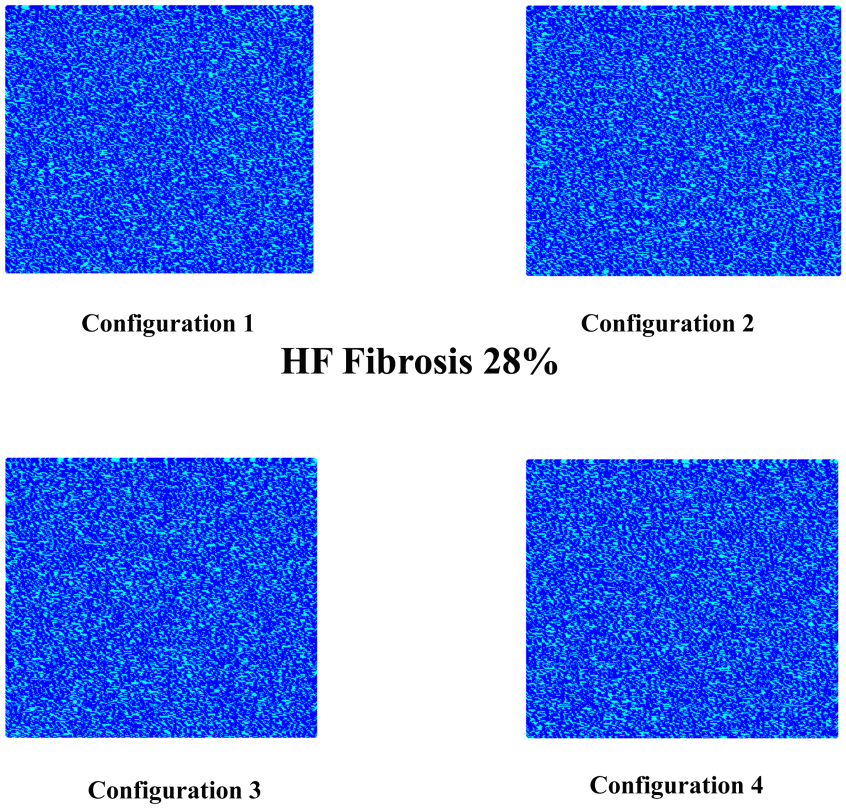

Figure 4.11: *Random configurations for 28% fibrosis in the human failing ventricular tissue.*

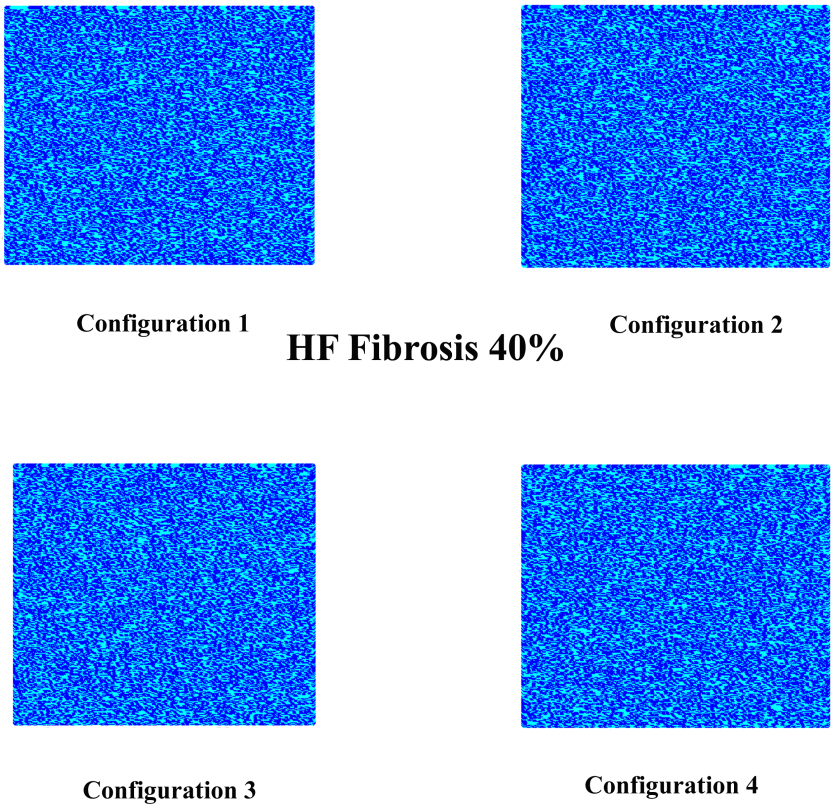

Figure 4.12: *Random configurations for 40% fibrosis in the human failing ventricular tissue.*

4.6.2 Vulnerable window

The vulnerable window for reentry was evaluated (as described in the Methods section of the main text) in all the configurations. Table 4.2 shows the limits and the width of the vulnerable window (VW) in each case. The results of configurations 1 are shown in the text and Figures of the chapter. For all the configurations of low fibrosis and high fibrosis no reentry was observed. In the case of 'mild fibrosis 1', the width of the VW ranged from 20 to 24 ms, and the limits were very similar. When fibrosis increased to 'mild fibrosis 2', the width of the VW was larger, ranging from 33 to 39 ms.

Fibrotic content	Random Configuration	Limits of the VW (ms)	Width of the VW (ms)
Low fibrosis (4%)	1	-	0
	2	-	0
	3	-	0
	4	-	0
Mild fibrosis 1 (14.5%)	1	[204;224]	20
	2	[203;223]	20
	3	[203;225]	22
	4	[203;227]	24
Mild fibrosis 2 (28%)	1	[170;203]	33
	2	[178;212]	34
	3	[178;212]	34
	4	[175;214]	39
High fibrosis (40%)	1	-	0
	2	-	0
	3	-	0
	4	-	0

Table 4.2: *Vulnerable window (VW) analysis for different random configurations of fibrosis.*

CHAPTER 5

Lessons Learned from Multiscale Modeling of the Failing Heart

The content of this chapter is based on the publication (to be submitted):
Gomez, JF., Cardona, K., Martinez, L., Saiz, J., Trenor, B. Lessons Learned from Multiscale Modeling of the Failing Heart *Journal of Molecular and Cellular Cardiology*, (to be submitted)

5.1 Abstract

Heart failure constitutes a major public health problem worldwide. Affected patients experience a number of changes in the electrical function of the heart that predispose to potentially lethal cardiac arrhythmias. Due to the complexity of the electrophysiological changes that may occur during heart failure, the scientific literature is complex and sometimes ambiguous, perhaps because these findings are highly dependent on the etiology, the stage of heart failure, and the model used to study these changes. Nevertheless, a number of common features of failing hearts have been documented. Prolongation of the action potential (AP) involving ion channel remodeling and alterations in calcium handling have been established as the hallmark characteristics of myocytes isolated from failing hearts. Intercellular uncoupling and fibrosis are identified as major arrhythmogenic factors.

Multiscale computational simulations are now a powerful tool to complement experimental and clinical research. The rapid development of biophysically detailed computer models of single myocytes and cardiac tissues have contributed greatly to our understanding of processes underlying excitation and repolarization in the heart. The electrical, structural, and metabolic remodeling that arises in cardiac tissues during heart failure has been addressed from different computational perspectives to further understand the arrhythmogenic substrate.

This review summarizes and evaluates the advances made in the computational field focusing on simulation approaches to reproduce heart failure phenotype and its implications for arrhythmogenesis, ranging from the cellular level to whole-heart simulations. The main aspects of heart failure are presented in several related sections. An overview of the main electrophysiological and structural changes that have been observed experimentally in failing hearts is followed by the description and discussion of the simulation work in this field at the cellular level, and then in 2D and 3D cardiac structures. The implications for arrhythmogenesis in heart failure will also be evaluated including usual therapeutical measures, such as drug effects and cardiac resynchronization therapy. Finally, the future challenges in heart failure modeling and simulation will be discussed.

5.2 Introduction

5.2.1 Experimental Heart Failure

The definition of heart failure (HF) is still changing and evolving. Indeed, definitions of heart failure depend on the contexts in which this term is used, but it is generally considered a syndrome in which the pumping action of the heart fails to provide sufficient amount of blood and oxygen to the organs, including the heart itself [44]. HF is the final common pathway of various cardiac pathologies such as myocardial infarction, hypertrophy, congenital cardiac abnormalities, valve disease, hypertension, dilated cardiomyopathy, and tachycardia dependent cardiomyopathy. The primary electrophysiological changes and the mechanisms of arrhythmogenesis associated with HF depend on the etiology [45]. However, there are some common features, which are described in this section.

At the cellular level, prolongation of the action potential involving ion channel remodeling results from a reduction of some of the repolarizing currents [213], in combination with an increase in the late sodium current (I_{NaL}) [135, 224]. Increased I_{NaL} and elevated cytosolic Na^+ ($[Na^+]_i$) in HF is linked to the cellular Ca^{2+} overload via the reverse mode of the Na^+-Ca^{2+} exchanger (NCX) [53]. Alterations in calcium handling, as well as intracellular sodium accumulation have been established as the hallmark characteristics of myocytes and tissues isolated from failing hearts, especially in terminal HF [118–120]. Detubulation and changes in the beta adrenergic system have also been observed in failing hearts and have been related to the alterations of Ca^{2+} transient [128, 229].

Animal studies [4, 6] have shown that the gap junctional protein connexin43 (Cx43) is redistributed from the intercalated disk to the lateral ventricular myocyte borders and that the amount of hypophosphorylated Cx43 is increased, leading to intercellular uncoupling and reduced conduction velocity in heart failure [57, 234]. In addition, remodeling of the extracellular matrix including the presence of cardiac myofibroblasts [67, 110, 141, 143] and their interactions with cardiomyocytes is determinant in HF arrhythmogenesis.

During HF, non-reentrant mechanisms are initiated by either early after depolarizations (EADs) or delayed after depolarizations (DADs) [45]. In addition, reentrant rhythms have been observed in failing hearts and an improved understanding of the responsible mechanisms is much needed. New therapies including both the use of drugs and instrumentation (cardiac resynchronization therapy) continues to be advanced and assessed with

a computational approach saving resources and time.

5.3 Modeling Heart Failure at the Cellular Level

5.3.1 Electrophysiological Remodeling

Multiple electrophysiological changes have been experimentally observed in failing cardiac cells. Computational models have helped to analyze the cellular electrophysiological consequences of these changes observed in heart failure. The first simulation study that focused on these electrical alterations (at the cellular level) was carried out by Priebe and Beuckelman in 1998 [173]. In this work, the AP of a human ventricular myocyte was modeled and modified to simulate HF. Selected ion currents, based on experimental data, were remodeled leading to HF phenotype, characterized by a longer action potential duration (APD) and a corresponding altered Ca^{2+} transient. Ever since, several computational works have focused on describing HF phenotype on the basis of new emerging experimental data. Table 5.1 summarizes and describes HF computational models and its variability. These models were able to reproduce the hallmark characteristics for HF, i.e. AP prolongation and altered Ca^{2+} transient, as depicted in Figure 5.1.

These computational models for HF have contributed significantly to the understanding of the mechanisms underlying arrhythmogenic processes at the cellular level. Indeed, in the first HF simulation study by Priebe and Beuckelman [173] it was shown that EADs could develop in HF conditions following the block of the rapid delayed K^+ current (I_{Kr}), and how HF promoted spontaneous calcium release. To gain more insight on the effects of an altered Ca^{2+} transient in HF, improved models describing with detail the behavior of intracellular calcium pathways have been developed. For this purpose, Winslow et al. [237] defined the minimum model of 'end-stage heart failure' focusing on the protein levels of SR Ca^{2+} ATPase and NCX in canine cardiac ventricular failing myocytes. Using a somewhat similar approach, Puglisi et al. [175] developed a computational model allowing the analysis of the electrophysiological and Ca^{2+} transport properties of failing rabbit ventricular myocytes. A more detailed description of Ca^{2+} dynamics and the main role of the ryanodine receptors (RyR) was developed by Shannon et al. [200]. The improvement in Ca^{2+} dynamics modeling has meant a significant advance in the understanding of arrhythmogenesis driven by Ca^{2+} disorders in the setting of HF. Calcium calmodulin kinase

II (CaMKII) pathway, another important factor for Ca^{2+} dynamics especially in HF, was recently introduced in AP models. CaMKII-induced alterations of sodium current (I_{Na}), Ca^{2+} current (I_{Ca}), and transient outward K^+ current (I_{to}) were modeled by Grandi et al. [80] complicating CaMKII-dependent AP changes. Also, the development of an advanced coupled model integrating the spatiotemporal Ca^{2+} reaction-diffusion system into the cellular electrophysiological model by Lu et al. [126] revealed that in the presence of rogue RyRs (non-clustered RyRs), Ca^{2+} dynamics is unstable and Ca^{2+} waves are prone to be initiated spontaneously. This might induce delayed afterdepolarizations or triggered action potentials in HF. A further step in the simulation of HF was taken by Moreno et al. [144] by including the β-adrenergic signaling pathway in a computational work. They previously assessed the effects of the antiarrhythmic drugs flecainide and lidocaine in HF forecasting the clinically relevant concentrations at which flecainide and lidocaine exacerbate, rather than ameliorate, arrhythmia [145].

Computer models of HF have also helped to understand how HF alters tissue excitability. In this respect, Zlochiver et al. [252] employed ten Tusscher et al. [217] model to demonstrate that higher stimulation current magnitudes were needed for excitation of the failing tissue, as well as larger liminal areas. Such observations contribute to our understanding of the generation of ectopic foci-originated arrhythmias and to the efficient design of cardiac stimulating electrodes.

The experimentally reported ranges for electrophysiological (EP) changes, as well as the extent of the changes of ion channels, transporters and respective current remodeling, vary substantially for different experimental settings and HF stages. Therefore, taking into account the available literature, a sensitivity analysis aimed at assessing the impact of the main ionic parameters remodeled in HF was performed in Trenor et al. [215]. Also the study by Walmsley et al. [231] takes into account this variability by defining a population of models for HF.

Although considerable research has been devoted to the effect of altered channel function in the failing heart, less attention has been paid to mRNA expression channel levels [7]. Functional ion channel activity is not always directly related with protein expression levels in the cell membrane, but may be influenced. In this respect, the work of Walmsley et al. [231] focused on the role that mRNA expression levels may play in the electrophysiological changes in human HF. As mentioned above, these authors defined a population of disease models, taking into account the variability in altered ion channels activity.

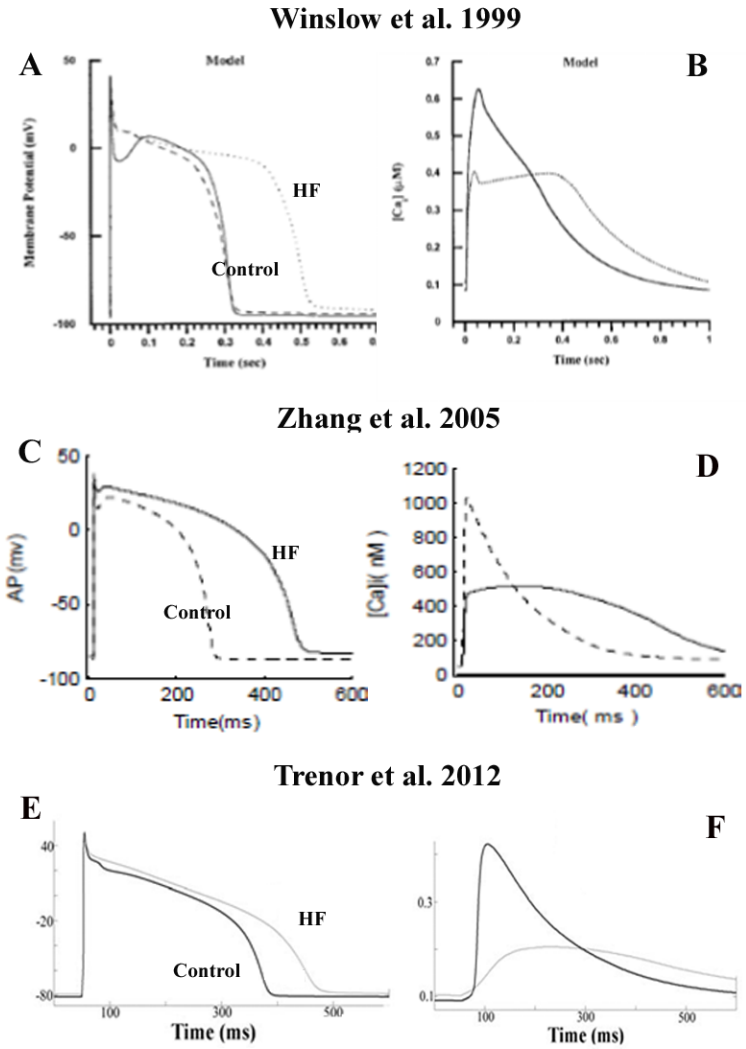

Figure 5.1: *Electrophysiological changes in heart failure. Simulated action potentials (APs) (left panels) and Ca^{2+} transients (right panels) obtained in normal conditions and after heart failure electrophysiological remodeling. Panels A and B, C and D, and E and F illustrate the simulations carried out by Winslow et al. [237], Zhang et al. [251], and Trenor et al. [215], respectively. Reproduced with permission from [237].*

HF Simulation Models	Species	I_{Na}	I_{NaL}	τ_{NaL}	I_{CaL}	I_{to}	I_{Kr}	I_{Ks}	I_{NCX}	I_{K1}	I_{NaK}	I_{up}/J_{SERCA}	I_{leak}	I_{Nab}	I_{Cab}
Winslow et al,1999 [237]	dog								↑104%			↓28%			
Winslow et al,2000 [238]	dog					↓66%			↑75%	↓33%		↓68%			
Puglisi et al,2001 [175]	rabbit/guinea pig					↓36%			↑100%	↓49%		↓24%			
Shannon et al,2005 [200]	rabbit								↑100%			↓50%			
Morita et al,2009 [146]	rabbit				↑200%				↑200%			↓20%			
P & B,1998 [173]	human/guinea pig								↑65%	↓25%	↓42%	↓66%	↓65%		
Zhang et al,2008 [251]	human/guinea pig	↓57%	↑1200%		↑200%	↓36%		↓?	↑65%	↓25%	↓42%	↓?%			
Narayan et al,2008 [150]	human			↓25-200%								↓25-200%			
Zlochiver et al,2010 [252]	human			↓34%		↓36%		↓50%	↑36%	↓43%					
Moreno et al,2011 [145]	human				↑250%	↓36%			↑65%	↓25%		↓36%	↓31%		
Lu et al,2012 [126]	human	↓40%				↓64%		↓50%	↑65%	↓20%	↓42%	↓45%	=		↑53%
Trenor et al,2012 [215]	human		↑200%	↑200%		↓40%			↑75%	↓32%	↓10%	↓50%	↑500%	=0	↑53%
Moreno et al,2013 [144]	human/rabbit		↑1000%			↓36%				↓25%	↓10-42%	↓36%	↑350%	↑1600%	
Walmsley et al,2013 [231]	human				↓(0-60)%	↓(0-60)%	↓(0-60)%	=	↑(0-60)%	=		↓(0-60)%			

Table 5.1: *The percentage of increase (↑) or decrease (↓) of ion currents are indicated with respect to the original and physiological normal corresponding action potential model. The modified parameters are: the fast sodium current (I_{Na}), the late Na^+ current (I_{NaL}), the time constant of inactivation gate of the I_{NaL} (τ_{NaL}), the L-Type calcium channel current (I_{CaL}), the transient outward K^+ current (I_{to}), the rapid delayed rectifier potassium current (I_{Kr}), the slow delayed rectifier potassium current (I_{Ks}), the Na^+/Ca^{2+} exchanger (I_{NCX}), the inward rectifier K^+ current (I_{K1}), the Na^+/K^+ pump current (I_{NaK}), the sarcoplasmic reticulum (SR) Ca^{2+} pump (I_{up}/J_{SERCA}), the SR Ca^{2+} leak current (I_{leak}), the background Na^+ current (I_{Nab}), and the background Ca^{2+} current (I_{Cab}).*

5.3.2 Calcium Handling in HF

Failing mammalian ventricular myocytes are characterized by significant alterations of Ca^{2+} handling [18, 232], i.e. elevation of diastolic $[Ca^{2+}]_i$ levels, a significant reduction of peak systolic $[Ca^{2+}]_i$ and a slow delay of Ca^{2+} transient (see Figure 5.1). Abnormal Ca^{2+} uptake into the sarcoplasmic reticulum, and a high risk of triggered activity in failing hearts has been documented [18].

Computer modeling has been helpful in illustrating and improving the understanding of the arrhythmogenic processes related to altered Ca^{2+} dynamics that arise as heart failure develops. In 1998 Jafri et al. [103] explored the effects of RyR activity and SR load on the cardiac AP and on the cardiac Ca^{2+} transient, setting the basis for an accurate description of the Ca^{2+} dynamics in the failing heart [237], further analyzed by other groups [125]. The increasing importance of protein Kinases, such as CaMKII was also investigated in several extensive simulations [80, 86, 156]. Indeed, CaMKII is upregulated in HF and strongly affects Ca^{2+} handling. These simulation studies suggest potential pathways by which CaMKII may contribute to arrhythmogenesis. Additionally, Ca^{2+} dynamics is closely related to Na^+ fluxes, thus increased intracellular Na^+ [52] and increased late sodium current (I_{NaL}) in the failing myocardium contribute to the alteration of Ca^{2+} load. In this way, simulation studies have been very helpful as described below.

5.3.3 Late Sodium Current (I_{NaL}) Role in HF

Experimental approaches and computational modeling are complementary methods of assessing how abnormalities in sodium behavior at the cellular level can lead to arrhythmias in the whole heart. The I_{NaL} has been recognized as one of the major factors contributing to abnormal repolarization in HF [11, 214, 220, 250]. Also mutations in SCN5A causing LQT3-related arrhythmias were shown to increase I_{NaL}, demonstrating its arrhythmogenic potential [11, 16]. A computational model analysis was used to predict the magnitude and rate dependence of I_{NaL} expected from ensemble currents in heterogeneously expressed single Nav1.5 channels [38].

The enhancement of I_{NaL} in failing human hearts as compared to normal hearts has been measured by several experimental groups [135, 224]. However, I_{NaL} was rarely included in the basic formulation of AP models developed to reproduce control conditions. In

the last decade, substantial improvements in AP models have been made and this current has been modeled using both Markov models and Hodgking Huxley formulations. I_{NaL} has been added to the existing AP models for different animal species [21, 37, 80, 95, 140, 144, 215]. Hund et al. [95] included a formulation for the I_{NaL} in a canine cardiac ventricular AP model. Trenor et al. [215] adapted this formulation with the experimental human available data to reproduce the failing phenotype and introduced it into Grandi et al. human AP model [79]. The most recent AP human model includes this formulation under control conditions [157].The consideration of this current is crucial in simulating the activity of failing ventricular cells because of its important role in repolarization abnormalities, such as EAD generation [75, 144, 145, 215, 251, 252]. Indeed, many of these HF simulation studies considering I_{NaL} enhancement have suggested I_{NaL} as a novel therapeutical target in HF.

5.3.4 Changes in T-tubules and Cellular Size in HF

It is now well-known that loss and disruptions of T-tubules occur in failing ventricular myocytes [87, 128], contributing to dyssynchronous calcium release and impaired contraction. T-tubules disruption removes the L-type Ca channels from the associated Ca^{2+} release units and results in 'orphaned' RyR clusters. In addition, loss of T-tubules leads to a redistribution of β2-adrenergic receptors (β2AR) from T-tubules to detubulated membrane areas changing compartmentation of cAMP and contributing to the failing myocardial phenotype [153], especially affecting Ca^{2+} transients. It is also important to highlight the T-tubule localization of the inward rectifier K^+ channels [39]. Indeed, detubulation has been shown to decrease I_{K1} activity [33], which might have important consequences for membrane resting potential. The mechanisms by which detubulation disrupts the electrical activity in the failing heart are poorly understood and is an area in which computer simulations can definitely help.

Few simulation studies exist on modeling detubulation in the failing heart. Gaur et al. [68] developed a model of Ca^{2+} cycling which takes into account local dyadic Ca^{2+} release activities and interactions between dyads via Ca^{2+} diffusion. Under failing conditions, SR Ca^{2+} release becomes dyssynchronous and interdyad coupling serves as a compensatory mechanism that improves synchrony. A reduced number of Ca^{2+} channels due to detubulation was tested in the dyad model of Louch et al. [125], leading to the experimentally observed dyssychronous Ca^{2+} release in HF. Alternans were also observed in a HF cellular model were detubulation was considered [154]. Similarly, Wrigth et al. [240] simulated

detubulation and highlighted the role of altered β2AR and cAMP signaling in failing cardiomyocytes. Including detubulation in cellular models of HF is thus important in order to fully represent Ca^{2+} transient alterations.

Another important change observed in failing hearts is an increase of the cellular size. The loss of contractile function is compensated by cardiac hypertrophy [45]. Patients with HF have an increased QRS duration, which cannot only be attributed to decreased conduction velocity, but also to an increase of myocytes size. Wiegerinck and coworkers carried out a set of simulations focused on the effect of hypertrophied myocytes [235] and found that although conduction velocity was increased the larger cellular size led to QRS prolongation. Thus, larger myocytes should be considered in HF models.

5.3.5 β-adrenergic Stimulation in HF

The β-adrenergic signaling pathway regulates cardiac myocyte contractility, which is impaired in the failing heart. Increased β-adrenergic sympathetic activity is a hallmark of HF and β-blockers appear to reduce mortality in these patients [228], although the responsible mechanisms are not completely understood. Detailed electrophysiological models have become helpful in understanding this complex cell signaling pathway and its effects after HF changes.

β-adrenergic signaling and stimulation is considered in several models of the electrical activity of the cardiac cell (see table in pages 9 through 11 in the Supporting Material of Heijman et al. [89]). The modeling approaches include either parameter-shift, i.e. selected conductances of ion channels or the voltage dependence of several ion channel gates are modified by β-adrenergic stimulation, or population-based, i.e. a portion of selected ion channels population is altered by β-adrenergic stimulation. Saucerman et al. [195] developed a detailed parameter-shift model of the β-adrenergic signaling pathway for rat ventricular myocytes considering that altered β-adrenergic signaling may also play an important role in the progression of HF. They improved this model adding interactions of the protein Kinase A (PKA) with other ion channels [196, 205] and adapted it to a mathematical model of the rabbit ventricular myocyte. Recently, the population-based model developed by Heijman et al. [89] incorporated the effect of CaMKII and β-adrenergic signaling systems in a multi-compartmental description of protein signaling networks for canine ventricular myocytes. O'Hara et al. [156] used this model and adapted it for human ventricular AP to analyze the effect of β-adrenergic stimulation in LQT syndrome. Also Wright et al. [240]

used Heijman et al. [89] model to simulate detubulation in HF and thus relocation of β2-adrenergic receptors, which alters the protective effect of β2-adrenergic stimulation. An important finding of their study is that caveolin-3 (Cav3) overexpression can partially restore the disrupted localization of these receptors. It is important to distinguish between β1AR and β2AR activity in simulating HF, because they could have different effects on arrhythmogenesis, as shown by clinical trials and a number of studies [50, 116, 190]. In this way, the model developed by Bondarenko for mouse myocytes [23] focused on the effects of β1-adrenergic receptor (β1AR) stimulation and represents an initial framework for future developments of cellular models for heart failure.

5.4 Structural Remodeling in Virtual Failing Cardiac Tissues

In addition to electrophysiological remodeling, microanatomical changes, such as intercellular uncoupling and fibrosis, have been identified as major arrhythmogenic factors in HF etiology and progression. This section describes the main findings derived from computational studies related to structural remodeling.

5.4.1 Consequences of Fibrosis Derived from Computational Studies

Fibroblasts are cells of mesenchymal origin that produce interstitial collagen and are responsible for the synthesis and maintenance of the extra-cellular matrix (ECM), which surrounds and supports cardiomyocytes. A detailed description of these cells and the role they play in cardiac tissue is described in the work of Camelliti and coworkers [27]. The proliferation of fibroblasts in the failing heart alters substantially the electrical activity of the heart [45, 214]. Despite the fact that fibroblasts form a majority cell population in the normal adult heart, they are electrically inexcitable, but the electrical interaction with myocytes through gap junctions proteins was early observed by Kohl et al. [109] and corroborated later in several species [28, 67, 111] in vitro. However, the presence and extent of fibroblast-myocyte electrotonic coupling in native myocardium (in vivo) remain controversial [112]. Myocyte-fibroblast interaction is a key factor to a better comprehension of the electrical cardiac propagation in cardiac failing hearts. Detailed findings concerning the electrophysiological behavior of fibroblast membrane is scarce. In that sense, only potassium ionic channels were found by Chilton et al. [35] providing data to develop the electrophysiological membrane model for mammalian ventricular fibroblasts by MacCannell and coworkers [129] and another contemporary model developed by Sachse et al. [192] including a markovian description of the outward potassium current. Later, Maleckar et al. [131] adapted MacCannell's model to simulate the behavior of atrial fibroblasts. These models have enabled the simulation of the electrical activity of 2D and 3D cardiac tissues with fibrosis and the analysis of the consequences of fibrosis in cardiac electrical activity. The first computational study simulating electrical coupling between fibroblasts and myocytes (from sino-atrial node) was performed by Kohl et al. [109]. The fibroblast was modeled as an electrically passive cell, the most common description until MacCannell's model formulation was published [129]. Later, Turner and colleagues [216] simulated fibrotic content in the ventricle as lines of insulating, unexcitable elements in the longitudinal and transverse direction. They highlighted the role of fibrosis on electrogram fractionation. Computer sim-

ulations have also helped to interpret how location and distribution of fibrosis alters cardiac conduction and favors arrhythmias. Xie et al [245] developed several configurations of two dimensional sheets with fibroblasts and myocytes, showing an increased vulnerability to reentry when fibroblasts were electrotonically coupled to myocytes with respect to tissues where fibroblasts were uncoupled, acting as pure insultors. The same model was used later to study the formation of EADs during oxidative stress [146]. EADs generation was favored by intermediate degrees of fibrosis content. In the same line, Petrov et al. [162] showed the influence of fibrosis on restitution properties and spiral wave stability in a three-domain model approach, while Engelman et al. [60] used a computer model containing non-uniformly distributed barriers of excitation resembling patchy fibrosis to demonstrate that structural heterogeneity alone is sufficient to give rise to discordant alternans at rapid stimulus rates.

Cardiac fibroblasts may act as a 'current sink' for connected myocytes changing cardiomyocyte excitability [152]. Zlochiver et al. [252] used a numerical model of human cardiac tissue to quantify the current threshold for atrial and ventricular tissues under diffuse fibrosis conditions. Later, the same group showed how spiral wave dynamics is altered by the presence of fibroblasts [82].

Very few simulation studies have focused on the effects of fibrosis in the setting of HF. Our group used computational models to describe various ways by which fibrotic content and structural remodeling modulates the arrhythmogenic susbtrate of the failing heart, increasing repolarization gradients and leading to abnormal impulse propagation [75]. The vulnerability to reentry under HF conditions and several degrees of diffuse fibrosis was also assessed considering active fibroblasts interaction. Our results showed that intermediate degrees of fibrosis increased the probability of reentrant arrhythmias [74]. Similarly, Nayak et al. [151] focused on the influence of fibroblasts features on spiral-wave control in a 2D model, and then the work of Majumder et al. [130] classified a variety of spiral wave non-equilibrium states depending on the percentage of fibroblasts. None of these two last studies considered HF conditions in their simulations.

Finally, other computational studies utilized 3D ventricular models to simulate the effects of fibrosis at the organ level [130, 138]. Similarly to our results, they found that intermediate fibrosis increased vulnerability to arrhythmias.

5.4.2 Simulation of Intercellular Uncoupling

As stated above, the structural remodeling of the failing heart includes not only proliferation of fibroblasts but also cellular uncoupling. The total amount of connexin 43 is reduced in the failing heart and is redistributed from an end-to-end to a lateral location in the myocyte [107, 161, 234]. This reduction and reorganization gives rise to decreased conduction velocities in the failing heart [72]. Gima and Rudy have addressed the effects of cellular uncoupling on AP propagation and conduction velocity in the normal cardiac tissue [71]. However, very few works have simulated cellular uncoupling in the setting of heart failure [145, 252]. In our previous works, we showed that an intermediate degree of cellular uncoupling increased the vulnerability to reentry of the failing heart and how the degree of coupling could ensure conduction [74, 76].

5.5 In Silico Analysis of Arrhythmias in the Failing Heart

It is well known that cardiac arrhythmias need a trigger and an electrophysiologically and structurally altered heterogeneous substrate to be initiated and maintained. Both conditions are fulfilled in HF and this section describes how computational models have contributed to the understanding of arrhythmogenesis in the failing heart.

5.5.1 Triggered Activity in HF

It is well known that APD prolongation favors the occurrence of EADs, triggered during the plateau phase of an AP, and caused mainly by reactivation of the L-type Ca channels. Ca^{2+} handling alterations in HF favor also the occurrence of DADs, which is related with the up-regulation of the NCX in combination with intracellular Ca^{2+} overload [45]. But what are the specific mechanisms underlying EAD and DAD formation in the failing heart? Computational models have significantly contributed to the understanding of triggered activity in the setting of HF.

Priebe and Beuckelman [173] obtained EADs and DADs utilizing their HF cellular model but not the normal physiological model. Remodeling of selected ion currents was the responsible mechanism. The influence of RyR and CaMKII on EAD generation has also been analyzed in a computational work, which showed that hyperphosphorilated L-type calcium channels were responsible for triggered activity [86]. Our group also showed the important role of an enhanced I_{NaL} on EAD generation in simulated failing cells [215], as suggested experimentally by Maltsev et al [136]. Similarly, Morita and coworkers [146] simulated the electrical activity of ageing hearts and showed that these hearts are prone to develop EAD-mediated arrhythmias due to oxidative stress, when I_{NaL} is enhanced.

Although DADs have been measured experimentally in the setting of HF [15], very little computational work has addressed this issue. DADs are not likely to trigger a premature beat in the intact heart because the strong electrotonic coupling between myocytes acts as a sink for local depolarizing currents. Mathematical models have shown that to overcome the source-sink mismatch, DADs must occur simultaneously in a large number of cells. These numbers are significantly decreased by reduced gap junction conductance, simulated fibrosis, reduced repolarization reserve, and heart failure electrical remodeling [246]. The beneficial effects of drugs, such as ranolazine, in reversing the formation of DADs have

also been suggested in a computational study [144] of HF. Computer simulations add value to experimental studies by showing how HF-induced alterations favor the occurrence of triggered activity and also provide the substrate for arrhythmia maintenance.

5.5.2 Altered Substrate in HF

Arrhythmogenic processes develop in pathological cardiac tissues having altered biomarkers, such as repolarization gradients, restitution curves or conduction velocity. An important feature of diseased tissues is the presence of increased electrophysiological gradients, which favor the maintenance of reentrant rhythms. An increase of transmural dispersion of repolarization (TDR) has been identified in the failing canine heart [5]. This can lead to the generation of polymorphic ventricular tachycardia. In the human right ventricle, Lou et al. [123] also observed an increase in APD gradients in HF and related it to increased arrhythmogenesis. In contrast, Coronel et al. [46] observed that in the pig ventricle it is not only the repolarization gradient but also the restitution characteristics in combination with the time of arrival of the premature wavefront, which determines the occurrence of reentry. Recent experiments have shown that TDR and APD gradient are reduced in human HF [73, 122]. Mathematical models of disease-specific AP in the human heart may provide useful insights into the mechanisms responsible for this controversy. In this way, our simulation study revealed increased APD dispersion under HF conditions assuming homogeneous remodeling with respect to control, but decreased gradients when heterogeneous remodeling was considered [75]. Then, the presence of fibrosis and cellular uncoupling increased repolarization gradients [75].

APD restitution gives information about APD adaptation to selected pacing rhythms. Glukhov et al. [73] obtained a smaller slope of the restitution curve in the failing human heart than in normal donor hearts. Different results were obtained by the computational study of Elshrif et al. [59] where restitution curves were steeper in virtual failing cells than in normal cells using O'Hara et al. human AP model [157]. Further simulation studies would be very valuable to enrich our understanding of the relationship between this biomarker and arrhythmias in the setting of HF.

Computational simulation studies also aimed at providing insights into ionic mechanisms underlying the occurrence of alternans. Much emphasis has been placed on the restitution curve slope as a major factor in the onset of arrhythmias following the development of discordant alternans where flattening the APD restitution curve is postulated to inhibit

alternans development and subsequent conduction block [66]. Walmsley et al. [231] suggested that alternans are due to different causes in the failing population versus non-failing population cellular models. Their results showed that alternans are primarily favored by low values of I_{Kr} conductance in failing human cardiomyocytes and by reduced SERCA pump and enhanced I_{CaL} conductance in non-failing human cardiomyocytes. Although these results should be taken with caution, this is a first step towards clinical translation from disease modeling.

A reduction in conduction velocity (CV) has been measured experimentally in the failing human heart [72]. Loss of gap junctions proteins in the intercalated disk and interaction with fibroblast give rise to alterations in conduction velocity. In this regard, several works studied how the percentage of fibrotic content alters normal wave propagation [75, 101, 102, 130, 245] and how increased or reduced coupling resistance modulates wave propagation velocity [71] and vulnerability to reentry in the failing heart [74].

5.5.3 Reentrant Arrhythmias in HF

Changes in myocardial structure, including microanatomy, in combination with the electrophysiological remodeling in the failing heart underlies arrhythmogenesis mechanisms. Generation of triggered activity helps to initiate arrhythmias and an altered substrate contributes to maintenance. Reduced excitability at the cellular level emerges in coupled tissue as a slowing of conduction velocity of the propagating depolarizing wave. Furthermore, repolarization gradients and electrophysiological heterogeneity favor unidirectional block and reentry. To generate reentrant circuits an excitable gap or a vulnerable window (VW) is required [45], and slow conduction and heterogeneities widen the VW.

Several simulation studies have modeled some of the structural alterations observed in HF to reproduce reentrant activity. The importance of fibrosis in determining the dynamics and stability of reentry has been highlighted in several computational studies [130, 151]. In this way, phase map analysis is a valuable tool which helps to identify and quantify spatiotemporal organization of reentry dynamics [81]. The phase tracks the progression of a defined region of the myocardium through the action potential. Points around which the phase progresses through a complete cycle from -π to π are of special interest. At these points, the phase becomes indeterminate and the activation wave fronts hinge on these points and rotate around them in an organized fashion. These points in the phase map are called phase singularity points (PS). PS share location with anatomic heterogeneities, and their spatial

meandering is modulated by these heterogeneities. Phase analysis was employed in our work (see Figure 5.2) [74] and other [124, 218] studies. We showed that the presence of structural heterogeneities, such as fibrosis, increased the number of phase singularities, and thus the risk of wave break [74, 253]. Furthermore, when intermediate levels of fibrosis are considered, the tip of the reentry meanders within a larger area and the vulnerable window was wider [74] as illustrated in Figure 5.2. Finally, fibrosis seems to have an important role in the reduction of the rotation frequency of spiral waves [74, 82, 210, 253].

Further computational research combining structural and electrical remodeling [74, 75] would be useful to improve our understanding of reentry mechanisms.

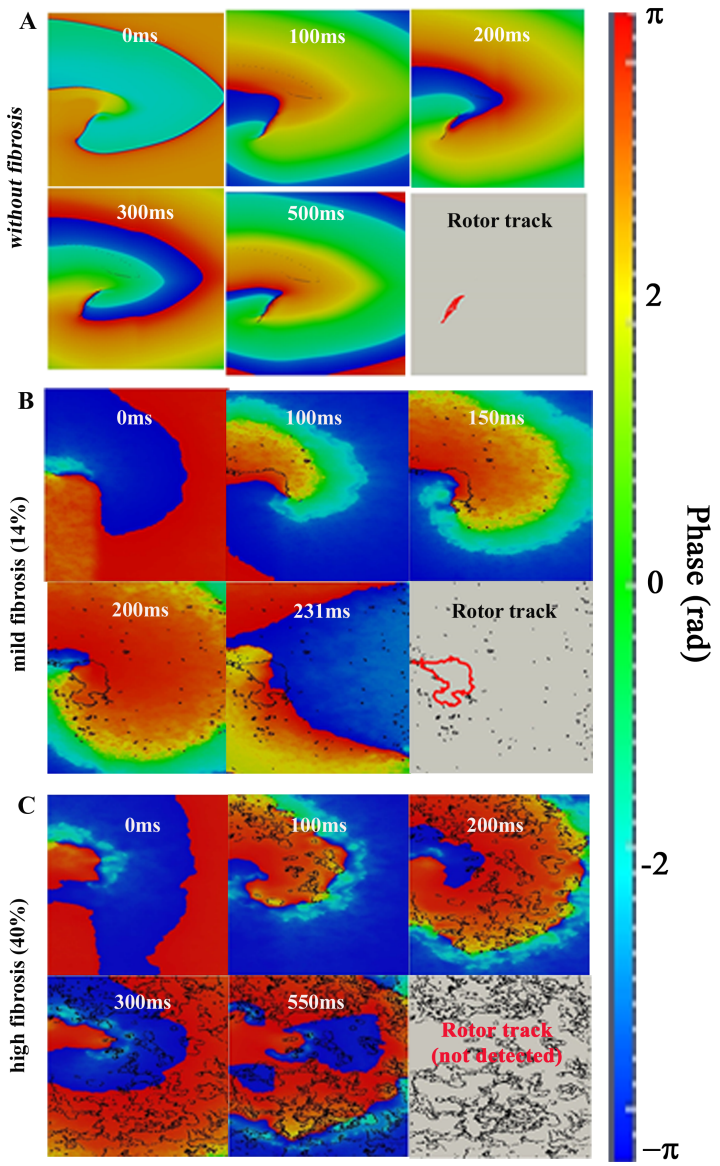

Figure 5.2: *Phase map analysis of evoked rhythm disturbances on the failing human ventricular tissue. Phase maps in electrically remodeled failing tissues assuming selected levels of fibrotic content. The rotor tip trajectory altered by structural heterogeneities. All transient phase singularities are indicated in black, and the tip of the trajectory is indicated in red in the last snapshot of each panel. Reproduced with permission from [74].*

5.6 Heart Failure Treatment. Modeling of Drug Effects and CRT

5.6.1 Simulation of Drug Effects in Heart Failure

Integrative computational simulation has become a powerful tool to complement experimental and clinical research in multidisciplinary efforts that can elucidate the basic mechanisms of drug effects on ion channel-mediated phenomena. Pharmaceutical companies have already suggested the implementation of new testing protocols including the effects of drugs on multiple cardiac ion channels and integration of this information using computational modeling and simulation approaches [34]. Here we describe some insights given in this direction in the setting of HF. Moreno and coworkers developed a computational model to simulate the interaction of the anti-arrhythmic drugs flecainide and lidocaine with cardiac sodium channels [145] in the failing human heart. Their results suggested that lidocaine was more efficient than flecainide in the reduction of reentrant rhythms in the failing heart. In another work, the effects of Ranolazine were assessed and the results pointed out this drug as an effective therapeutic strategy against HF due to I_{NaL} preferential targeting [144]. Further simulation works focusing the effects of other drugs, such as β-blockers, utilizing a detailed model of HF would be very useful.

5.6.2 Cardiac Resynchronization Therapy (CRT). Electromechanical Approach.

Cardiac resynchronization therapy (CRT) is an established therapy for selected heart failure (DHF) patients. CRT typically employs bi-ventricular pacing, with an endocardial right ventricular (RV) pacing lead and an epicardial left ventricular (LV) pacing lead. It aims to capture RV and LV and thus recoordinate contraction. Simulation approaches can be used to optimize CRT therapies. For example, seeking for the optimal pacing timing and location to induce the electrical shock in order to obtain most beneficial regional energy consumption [43]. These studies can also provide new tools to better discriminate CRT patients. Galeotti and coworkers increased the specificity of left bundle branch block (LBBB) diagnosis in the presence of LV dilation and hypertrophy [65], while Potse et al. focused on the effects of uncoupling due to this pathology [171]. Aiba et al. showed that CRT reduces the frequency of EADs through I_{NaL} decrement [2], while others studied how geometry and anatomical structures such as the conduction system affects pacing in failing hearts [180, 184]. In this concern, patient-specific models of hearts with contractile dyssynchrony have been recently

developed providing a new clinical tool in the treatment of dyssynchronous heart failure [1, 115, 198]

An important step in computational modeling of the heart is the link of the electrical activity of the myocardium with the mechanical contraction. Several simulation studies have been undertaken to evaluate the electromechanical behavior of the heart in selected animal species [83, 84, 223] but literature is scarce in the setting of human HF [93, 114]. Electromechanical simulations based on computational models could guide and improve CRT, as in Constantino et al., who suggested that an adequate pacing location would be the site of longest electromechanical delay [43].

5.7 Concluding Remarks and Future Challenges

This chapter reviews the main computational studies on HF from cell to organ. These studies illustrate how modeling and computer simulations may reveal the mechanisms of arrhythmogenic processes and therapies in the setting of HF (Figure 5.3). In this last section, the main advances, as well as limitations and future challenges of the computational approach of HF are presented. Indeed, in addition to the generic limitations of cardiac models [166], several improvements in the pathological models of HF have to be highlighted to guide research to future challenges.

As summarized in Figure 5.3, simulations at the cellular level have contributed to elucidate the role of ion channels remodeling in AP and Ca^{2+} handling HF-induced changes. However, the effect of changes in the T-tubule system [142] and β-adrenergic pathways in the failing cell need further analysis. Simulations of AP prolongation and altered Ca^{2+} transient have also furthered our understanding of the mechanisms of triggered activity: EADs and DADs in failing cells. 1D, 2D, and 3D models of the failing tissue have allowed to simulate the effects of structural remodeling in the failing heart. The increase of cellular uncoupling and fibrosis in heart failure may have a significant role in setting an arrhythmogenic substrate, leading to cardiac arrhythmias. Although fibroblasts interaction with cardiomyocytes has been addressed in several multiscale computational studies in normal physiological conditions, the literature is scarce in the setting of HF. In addition, only the work of Chilton and coworkers [35] provides experimental data to build an electrical model of ventricular fibroblasts. In this sense, further experiments are needed to improve these models, such as the work of Chatelier et al. [32] that reported the expression of voltage gated sodium channels in human atrial fibroblasts. Recently, much effort is made to improve electromechanic models of the heart, which allow the link between the electrical activity and especially Ca^{2+} transient and cellular and organ contraction (see Figure 5.3). In terms of HF, electromechanical simulation works are scarce and further studies are needed. These computational models can help to evaluate mechanical heart dysfunction and improve CRT.

With regard to drug therapy in HF, besides several studies focusing on late sodium channel blockers, computational work is lacking. The analysis of the effects of β-blockers in the failing heart through computer simulations would help to understand why these drugs are effective in these patients. It is important to mention that the efforts recently made in the development of patient-specific models, based on high resolution images, will be of

great help if they are extended to different stages of HF and different etiologies. Finally, a crucial challenge is the integration of computer pathological models and simulations into the clinical practice.

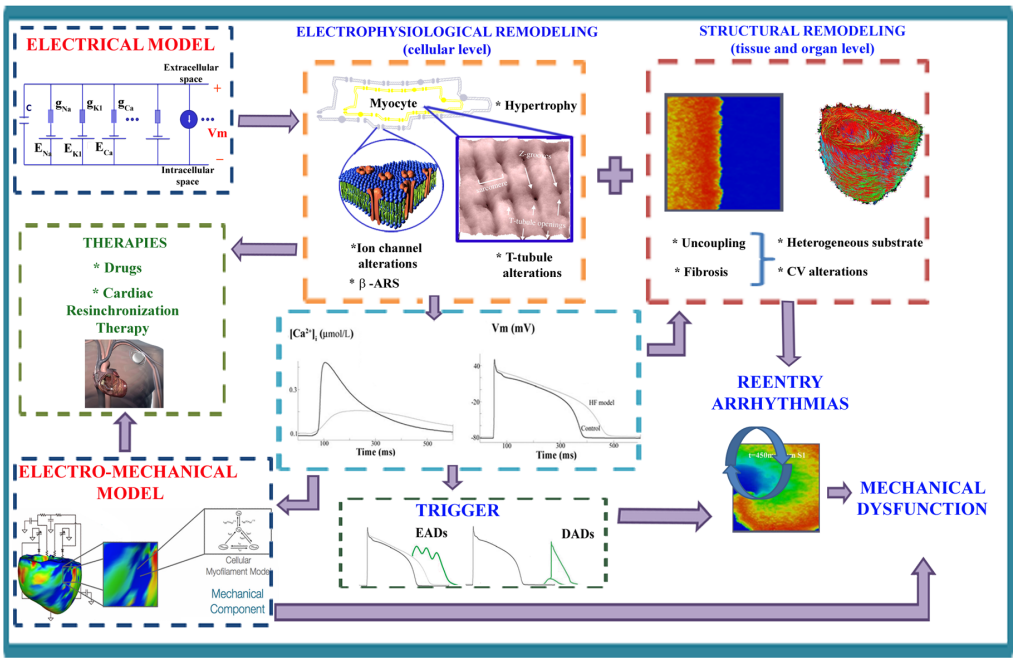

Figure 5.3: *What can be learnt from computer simulations in heart failure. Multiscale electromechanical models of heart failure (HF) help to understand arrhythmogenic mechanisms. At the cellular level, electrophysiological remodeling can be modeled by alterations in ion channels, in β-adrenergic system, and in T-tubules (image taken from [142]) and is responsible for significant changes in action potential and Ca^{2+} transient waveforms, which might lead to EADs and DADs generation. At the tissue and organ level, structural remodeling (intercellular uncoupling and fibrosis) lead to discontinuous and decreased conduction velocity and electrophysiological heterogeneities. Triggered events and heterogenous substrate set the stage for ventricular arrhythmias in the failing heart. Incorporating the mechanical response (electro-mechanical model reproduced with permission from [43]) in a HF model will improve the understanding of the mechanical dysfunction of the failing heart and the design of cardiac resynchronization therapy.*

CHAPTER 6

Conclusions and Outlook

6.1 Overview

The aim of this Thesis was to investigate the mechanisms of HF-induced arrhythmias with a computational approach, where multiscale simulations can shed light into the arrhythmogenic processes that may arise during this pathology. It is important to highlight that HF is a dynamic process during which many parameters are subject to continuous change, however, our model was validated against the experimental data available so far. On the basis of our simulation results, we can conclude that patients in moderate stages of heart failure are more prone to arrhythmias than patients in the end-stage of heart failure, due to intermediate levels of fibrotic content and intercellular uncoupling. The pivotal role of I_{NaL} in the changes of electrophysiological characteristics and in arrhythmogenesis in HF suggests that this current should be a therapeutical target in the treatment of HF. Here below a summary of our main findings is provided for each of the specific aims of this Thesis.

To develop and validate an AP cellular model under heart failure conditions, including the role of the late sodium current on account of its relevance in failing phenotype, in order to study the electrical activity of failing cells and possible proarrhythmic effects.

The proposed model for human I_{NaL} and the electrophysiological remodeling of myocytes from failing hearts accurately reproduce experimental observations. The sensitivity analysis of the modulation of the electrophysiological parameters due to ion channels remodeling, revealed a significant role of I_{NaL} increase in the prolongation of action potential duration (APD), triangulation of AP, and changes in Ca^{2+} transient. A mechanistic investigation of intracellular Na^+ accumulation and APD shortening with increasing frequency of stimulation of failing myocytes revealed the underlying responsability of the Na^+/K^+ pump, the Na^+/Ca^{2+} exchanger and I_{NaL}. The results of the simulations also showed that in human failing myocytes, the enhancement of I_{NaL} increases the reverse rate-dependent APD prolongation and the probability of initiating early afterdepolarizations. The electrophysiological remodeling of failing hearts and especially the enhancement of I_{NaL} prolongs APD and alters Ca^{2+} transient facilitating the development of early afterdepolarizations. An enhanced I_{NaL} appears to be an important contributor to the electrophysiological phenotype and to the dysregulation of $[Ca^{2+}]_i$ homeostasis of human failing myocytes.

To evaluate the role of electrophysiological and structural heart failure remodeling on the modulation of key elements of the arrhythmogenic substrate, such as electrophysiological gradients and abnormal impulse propagation.

The current controversy found in the literature about the increase or decrease of electrophysiological gradients in the failing heart has been approached in the present thesis through computer modeling. We showed that HF heterogeneous remodeling of I_{NCX} and I_{SERCA} modulates Ca^{2+} transient duration and the dispersion of AP-Ca^{2+} transient upstrokes delay. Heterogeneous remodeling can also bring repolarization gradients below the normal values. Our simulations illustrate and provide new insights into this. We suggest also that although M cells are known to contribute to the increase of APD and repolarization dispersion, they do not to alter the relative change from normal tissue to failing tissue. Furthermore, we showed how safety factor for conduction was reduced in the presence of fibrotic clusters, and how enhanced fibrosis in failing hearts, as well as reduced intercellular coupling, increase electrophysiological gradients and reduce electrical propagation. In combination, these changes set the stage for arrhythmias.

To assess vulnerability to reentry under heart failure conditions by incorporating established electrophysiological and anatomical remodeling.

Our simulations showed that structural remodeling is a key factor in the genesis of vulnerability to reentry. The electrical coupling of cardiomyocytes with fibroblasts cells alters the anisotropic action potential propagation in the human failing heart in a fashion that significantly depends on the density of fibrotic content and on the degree of intercellular coupling. A range of intermediate levels of fibrosis and intercellular uncoupling can combine to favor reentrant activity. Phase maps analysis provides a powerful tool to explore abnormal conduction patterns in the setting of ventricular fibrosis, where phase singularities increase due to structural heterogeneities. This tool may be relevant to inspire and guide ablative procedures.

To summarize and evaluate the advances made in the computational field focusing on simulation approaches to reproduce heart failure phenotype and its implications to arrhythmogenesis, ranging from the cellular level to whole-heart simulations.

After reviewing the literature, including the work of the present Thesis, we can affirm that simulations at the cellular level have contributed to elucidate the role of ion channels remodeling in AP and Ca^{2+} handling HF-induced changes. However, the effect of changes in the T-tubule system and β-adrenergic pathways in the failing cell need further analysis.

Multiscale simulations have furthered our understanding of the mechanisms of triggered activity (EADs and DADs) in failing cells. Several models of the failing tissue have allowed us to simulate the effects of structural remodeling in the failing heart and their arrhythmogenic substrate. Although fibroblasts interaction with cardiomyocytes has been addressed in several multiscale computational studies in normal physiological conditions, the literature is scarce in the setting of HF . Furthermore, computer simulations would also help to evaluate the effect of drug therapies in HF patients. The development of patient-specific models, based on high resolution images, will be of great help into the clinical practice if they are extended to different stages of HF and different etiologies.

In addition , the improvement of electromechanic models of the heart, which allow the link between the electrical activity and cellular and organ contraction, is necessary to a better undertanding of the real processes during a heart beat,to help in evaluation of mechanical heart dysfunction and to guide and improve cardiac resyncronization therapies. In terms of HF, electromechanical simulation works are scarce and further studies are needed.

6.2 Outlook and future work

The ultimate aim of the present computational research on HF is to extend our model to 3D anatomical realistic simulations, in order to explore depolarization and repolarization mechanisms in control versus failing conditions (including several HF stages). This is an on going work,in which we will personalize our already implemented 3D ventricular model to the HF pathology. In our ventricular 3D model the geometry has been segmented from a DTMRI data set acquired at John Hopkins University (Helm 2005). The DTMRI volume stack had a resolution of 0.4297 x 0.4297 x 1.0 mm^3 (256 x 256 x 144 voxels). The heart volume has been extracted directly from myocardial segmentation, using a simple threshold and allowed reconstruction of whole ventricular geometry and fiber structure. Although realistic geometry of the heart has been already reconstructed, there still remain several unresolved issues to improve the model and personalize it to the failing heart.

Realistic and validated Cardiac Conduction Cystem (CCS). The distal regions of the CCS and in particular the Purkinje network structure are fundamental to ensure a normal sequence of cardiac activation and subsequent contraction. Nevertheless, during HF many cardiac disorders might result from abnormalities in one of the sections of the CCS. One important example is the Left Bundle Branch Block (LBBB), a cardiac conduction abnormality seen on the ECG. In this condition, activation of the left ventricle (LV) is delayed, which results in the LV contracting after the right ventricle (RV) and a decreased cardiac ejection fraction, a common symptom of failing hearts. In order to better understand the underlying mechanisms that lead to certain types of arrhythmia, it is crucial to look for new tools that allow studying in detail the electrical coupling of the CCS and the myocardium under normal and pathological conditions.

Estimation of fibrotic content and distribution. In order to study fibrotic interactions with failing or non-failing cells at the organ level from a computational point of view it is necessary to delimitate infarcted regions and border zones. Therefore, segmentation procedures of MRI images are necessary to accurate reproduce infarcted areas.

Bidomain approach. In this thesis we solved propagation equation based on monodomain approximation. Currently we are working on a defibrillator model to study cardiac resynchronization therapies, so it is necessary to use a bidomain formulation to take into account defibrillator shocks in our simulations.

Adaptation of the model to different HF stages. In collaboration with Dr. Efimov's group, we will apply different values of remodeling of the ionic currents depending on the stage of HF. This group has access to human failing hearts at different stages of the pathology and can make measurements, which can be used to adapt our model. Structural remodeling can also be defined for different degrees of fibrosis and uncoupling to test the arrythmogenic consequences of the different stages of HF.

Publications

6.3 Contributions derived from the Thesis

International Journal

5. **Gomez, JF.**, Cardona, K., Martinez, L., Saiz, J., Trenor, B. Multiscale Modeling can Summarize and Illustrate the Electrophysiological Changes in the Failing. Heart *Journal of Molecular and Cellular Cardiology*, (to be submitted)

   IF: 5.218

4. Holzem, K., **Gomez, JF.**, Glukhov, A., Madden,E.J., Koppel,A., Ewald,G., Trenor, B.,Efimov,I., Reduced Response to I_{Kr} Blockade and Altered hERG1a/1b Stoichiometry in Human Heart Failure. *Journal of Molecular and Cellular Cardiology* , (in press)

   IF: 5.218

3. **Gomez, JF.**, Cardona, K., Martinez, L., Saiz, J., Trenor, B. Electrophysiological and structural remodeling in heart failure modulate arrhythmogenesis. 2D simulation study. *PLoS One*, 9(7): e103273. doi:10.1371/journal.pone.0103273.

   IF: 3.534

2. **Gomez, JF.**, Cardona, K., Romero, L., Ferrero, JM., Trenor, B. Electrophysiological and structural remodeling in heart failure modulate arrhythmogenesis. 1D simulation study. *PLoS One*, 9(9): e106602, 2014. doi:10.1371/journal.pone.0106602.

   IF: 3.534

1. Trenor, B., Cardona, K.,**Gomez, JF.**, Rajamani, S., Ferrero, JM., Belardinelli, L., Saiz, J. Simulation and mechanistic investigation of the arrhythmogenic role of the late sodium current in human heart failure. *PloS One*, 7(3):e32659, 2012. doi:10.1371/journal.pone.0032659.

   IF: 3.73

Peer-reviewed conference papers

9. **Gomez, JF.**, Holzem, K., Glukhov, A., Efimov,I., Trenor, B. Experimental and Simulation Study of the Effects of I_{Kr} Downregulation in Human Heart Failure. *2015 Gordon Research Conference (GRC) on Cardiac Arrhythmia Mechanisms*, Renaissance Tuscany Il Ciocco Lucca (Barga), Italy.
8. Cardona, K., **Gomez, JF.**, Saiz, J., Giles, W., Trenor, B. The Effect of Low Potassium in Brugrada Syndrome: A Simulation Study. *XXXXI Computing in Cardiology Conference (CinC 2014)*, Cambridge, USA.
7. **Gomez, JF.**, Cardona, K., Romero, L., Saiz, J.,Trenor, B. Heterogeneous Electrical Remodeling of the Failing Heart Modulates the Arrythmogenic Substrate. *XXXX Computing in Cardiology Conference (CinC 2013)*, Zaragoza, Spain.
6. **Gomez, JF.**, Cardona, K., Romero, L., Saiz, J.,Trenor, B. Effects of Electrical and Structural Remodeling on the Electrical Properties of The Failing Heart. *2013 Gordon Research Conference (GRC) on Cardiac Arrhythmia Mechanisms*,Ventura, California,USA.
5. **Gomez, JF.**, Cardona, K., Romero, L., Saiz, J.,Trenor, B. Simulació n de los Efectos de la Insuficiencia Cardíaca en la Repolarización y Conducción del Potencial de Acción. *XXX Congreso Anual de la Sociedad Española de Ingeniería Biomédica (CASEIB 2012)*, San Sebastián, Spain. ISBN / ISSN:978-84-616-2147-7.
4. **Gomez, JF.**, Cardona, K., Romero, L., Saiz, J.,Trenor, B. Increase in Late Sodium Current and Cellular Uncoupling Exacerbates Transmural Dispersion of Repolarization in Heart Failure. *XXXIX Computing in Cardiology 2012*, Krakow, Poland. ISBN / ISSN:978-1-4673-2074-0.233:237.
3. **Gomez, JF.**,Cardona, K., Saiz, J., Ferrero, JM., Trenor, B. Estudio de Simulación de los Mecanismos Electrofisiológicos del Fenotipo de Insuficiencia Cardíaca. *XXIX Congreso Anual de la Sociedad Española de Ingeniería Biomédica (CASEIB 2011)*, Cáceres, Spain. ISBN / ISSN:84-614-2693-4.
2. Cardona, K.,**Gomez, JF.**, Ferrero, JM., Saiz, J.,Trenor, B. Simulation Study of the Electrophysiological Mechanisms for Heart Failure Phenotype. *XXXVIII Computing in Cardiology 2011*, Hangzhou, China. ISBN / ISSN:0276-6574.610-614.
1. Trenor, B.,Cardona, K.,**Gomez, JF.**, Ferrero, JM., Saiz, J. Understanding Human Heart Failure Remodeling through Computer Simulations. *4th Cardiac Physiome Workshop*, Merton College, Oxford, 2011.

Bibliography

[1] Aguado-Sierra J, Krishnamurthy A, Villongco C, Chuang J, Howard E, Gonzales MJ, Omens J, Krummen DE, Narayan S, Kerckhoffs RCP, and McCulloch AD. Patient-specific modeling of dyssynchronous heart failure: A case study. *Progress in Biophysics and Molecular Biology*, 107(1):147–155, 2011. 155

[2] Aiba T, Barth AS, Hesketh GG, Hashambhoy YL, Chakir K, Tunin RS, Greenstein JL, Winslow RL, Kass DA, and Tomaselli GF. Cardiac resynchronization therapy improves altered Na channel gating in canine model of dyssynchronous heart failure. *Circulation. Arrhythmia and electrophysiology*, 6(3):546–54, June 2013. 154

[3] Akar FG. Unique Topographical Distribution of M Cells Underlies Reentrant Mechanism of Torsade de Pointes in the Long-QT Syndrome. *Circulation*, 105(10):1247–1253, February 2002. 63

[4] Akar FG, Nass RD, Hahn S, Cingolani E, Shah M, Hesketh GG, DiSilvestre D, Tunin RS, Kass Da, and Tomaselli GF. Dynamic changes in conduction velocity and gap junction properties during development of pacing-induced heart failure. *American journal of physiology. Heart and circulatory physiology*, 293(2):H1223–H1230, August 2007. 84, 137

[5] Akar FG and Rosenbaum DS. Transmural electrophysiological heterogeneities underlying arrhythmogenesis in heart failure. *Circulation research*, 93(7):638–45, October 2003. 63, 82, 83, 107, 150

[6] Akar FG, Wu RC, Juang GJ, Tian Y, Burysek M, Disilvestre D, Xiong W, Armoundas Aa, and Tomaselli GF. Molecular mechanisms underlying K+ current downregulation in canine tachycardia-induced heart failure. *American journal of physiology. Heart and circulatory physiology*, 288(6):H2887–96, June 2005. 15, 137

[7] Ambrosi CM, Yamada Ka, Nerbonne JM, and Efimov IR. Gender differences in electrophysiological gene expression in failing and non-failing human hearts. *PloS one*, 8(1):e54635, January 2013. 63, 66, 73, 83, 139

[8] Antoons G and Oros A. Late Na+ current inhibition by ranolazine reduces torsades de pointes in the chronic atrioventricular block dog model. *Journal of the . . .* , 55(8):801–809, February 2010. 43

[9] Antoons G, Oros A, Bito V, Sipido KR, and Vos Ma. Cellular basis for triggered ventricular arrhythmias that occur in the setting of compensated hypertrophy and heart failure: considerations for diagnosis and treatment. *Journal of Electrocardiology*, 40(6 SUPPL. 1):S8–14, 2007. 21, 24, 25, 26, 43, 63, 67

[10] Antzelevitch C. M cells in the human heart. *Circulation research*, 106(5):815–7, March 2010. 65

[11] Antzelevitch C, Nesterenko V, Shryock JC, Rajamani S, Song Y, and Belardinelli L. The role of late I Na in development of cardiac arrhythmias., 2014. 142

[12] Armoundas AA, Hobai IA, Tomaselli GF, Winslow RL, and O'Rourke B. Role of sodium-calcium exchanger in modulating the action potential of ventricular myocytes from normal and failing hearts. *Circulation research*, 93(1):46–53, July 2003. 84

[13] Ashihara T, Haraguchi R, Nakazawa K, Namba T, Ikeda T, Nakazawa Y, Ozawa T, Ito M, Horie M, and Trayanova Na. The role of fibroblasts in complex fractionated electrograms during persistent/permanent atrial fibrillation: implications for electrogram-based catheter ablation. *Circulation research*, 110(2):275–84, January 2012. 107

[14] Ashikaga H, Arevalo H, Vadakkumpadan F, Blake RC, Bayer JD, Nazarian S, Muz Zviman M, Tandri H, Berger RD, Calkins H, Herzka Da, Trayanova Na, and Halperin HR. Feasibility of image-based simulation to estimate ablation target in human ventricular arrhythmia. *Heart rhythm : the official journal of the Heart Rhythm Society*, 10(8):1109–16, August 2013. 128

[15] Baartscheer A, Schumacher CA, Belterman CNW, Coronel R, and Fiolet JWT. [Na+]i and the driving force of the Na+/Ca2+-exchanger in heart failure. *Cardiovascular research*, 57(4):986–95, March 2003. 31, 40, 41, 149

[16] Bennett PB, Yazawa K, Makita N, and George AL. Molecular mechanism for an inherited cardiac arrhythmia. *Nature*, 376(6542):683–5, August 1995. 142

[17] Bernus O, Wilders R, Zemlin CW, Verschelde H, and Panfilov aV. A computationally efficient electrophysiological model of human ventricular cells. *American journal of physiology. Heart and circulatory physiology*, 282(6):H2296–308, June 2002. 8

[18] Bers DM, Despa S, and Bossuyt J. Regulation of Ca2+ and Na+ in normal and failing cardiac myocytes. In *Annals of the New York Academy of Sciences*, volume 1080, pages 165–177, October 2006. 21, 24, 25, 63, 67, 142

[19] Beuckelmann DJ, Näbauer M, and Erdmann E. Intracellular calcium handling in isolated ventricular myocytes from patients with terminal heart failure. *Circulation*, 85:1046–1055, 1992. 24, 65

[20] Beuckelmann DJ, Nabauer M, and Erdmann E. Alterations of K+ currents in isolated human ventricular myocytes from patients with terminal heart failure, August 1993. 21, 25, 26, 39, 63, 67

[21] Biktasheva IV, Simitev RD, Suckley R, and Biktashev VN. Asymptotic properties of mathematical models of excitability. *Philosophical transactions. Series A, Mathematical, physical, and engineering sciences*, 364(1842):1283–98, May 2006. 143

[22] Biliczki P, Virág L, Iost N, Papp JG, and Varró A. Interaction of different potassium channels in cardiac repolarization in dog ventricular preparations: role of repolarization reserve. *British journal of pharmacology*, 137(3):361–368, October 2002. 42

[23] Bondarenko VE. A compartmentalized mathematical model of the β1-adrenergic signaling system in mouse ventricular myocytes. *PloS one*, 9(2):e89113, January 2014. 145

[24] Boyle PM and Vigmond EJ. An intuitive safety factor for cardiac propagation. *Biophysical Journal*, 98, 2010. 71

[25] Bray MA, Lin SF, Aliev RR, Roth BJ, and Wikswo JP. Experimental and Theoretical Analysis of Phase Singularity Dynamics in Cardiac Tissue. *Journal of Cardiovascular Electrophysiology*, 12(6):716–722, June 2001. 108

[26] Bundgaard H and Kjeldsen K. Human myocardial Na,K-ATPase concentration in heart failure. *Molecular and cellular biochemistry*, 163-164:277–283, 1996. 21, 24, 25, 26, 39, 63, 67

[27] Camelliti P, Borg TK, and Kohl P. Structural and functional characterisation of cardiac fibroblasts. *Cardiovascular research*, 65(1):40–51, January 2005. 146

[28] Camelliti P, Devlin GP, Matthews KG, Kohl P, and Green CR. Spatially and temporally distinct expression of fibroblast connexins after sheep ventricular infarction. *Cardiovascular research*, 62(2):415–25, May 2004. 146

[29] Cardona K, Trenor B, Rajamani S, Romero L, Ferrero JM, and Saiz J. Effects of late sodium current enhancement during LQT-related arrhythmias. A simulation study. In *2010 Annual International Conference of the IEEE Engineering in Medicine and Biology Society, EMBC'10*, pages 3237–3240, 2010. 23, 42

[30] Carmeliet E. Intracellular Ca2+ concentration and rate adaptation of the cardiac action potential, 2004. 41

[31] Carro J, Rodriguez JF, Laguna P, and Pueyo E. A human ventricular cell model for investigation of cardiac arrhythmias under hyperkalaemic conditions, November 2011. 31, 40, 41, 42, 44

[32] Chatelier A, Mercier A, Tremblier B, Thériault O, Moubarak M, Benamer N, Corbi P, Bois P, Chahine M, and Faivre JF. A distinct de novo expression of Nav1.5 sodium channels in human atrial fibroblasts differentiated into myofibroblasts. *The Journal of physiology*, 590:4307–19, 2012. 156

[33] Cheng LF, Wang F, and Lopatin aN. Metabolic stress in isolated mouse ventricular myocytes leads to remodeling of t tubules. *AJP: Heart and Circulatory Physiology*, 301:H1984–H1995, 2011. 143

[34] Chi KR. NEWS & ANALYSIS Revolution dawning in cardiotoxicity testing. *Nature Reviews in Drug Discovery*, 12(August):565–567, 2013. 154

[35] Chilton L, Ohya S, Freed D, George E, Drobic V, Shibukawa Y, Maccannell Ka, Imaizumi Y, Clark RB, Dixon IMC, and Giles WR. K+ currents regulate the resting membrane potential, proliferation, and contractile responses in ventricular fibroblasts and myofibroblasts. *American journal of physiology. Heart and circulatory physiology*, 288(6):H2931–9, June 2005. 65, 109, 129, 146, 156

[36] Chilton L, Giles WR, and Smith GL. Evidence of intercellular coupling between co-cultured adult rabbit ventricular myocytes and myofibroblasts. *The Journal of physiology*, 583(Pt 1):225–36, August 2007. 129

[37] Clancy CE. Na+ Channel Mutation That Causes Both Brugada and Long-QT Syndrome Phenotypes: A Simulation Study of Mechanism. *Circulation*, 105(10):1208–1213, February 2002. 143

[38] Clancy CE, Tateyama M, Liu H, Wehrens XHT, and Kass RS. Non-equilibrium gating in cardiac Na+ channels: an original mechanism of arrhythmia. *Circulation*, 107(17):2233–7, May 2003. 142

[39] Clark RB, Tremblay a, Melnyk P, Allen BG, Giles WR, and Fiset C. T-tubule localization of the inward-rectifier K+ channel in mouse ventricular myocytes: a role in K+ accumulation. *The Journal of Physiology*, 537(3):979–992, December 2001. 143

[40] Clayton RH, Bernus O, Cherry EM, Dierckx H, Fenton FH, Mirabella L, Panfilov aV, Sachse FB, Seemann G, and Zhang H. Models of cardiac tissue electrophysiology: progress, challenges and open questions. *Progress in biophysics and molecular biology*, 104(1-3):22–48, January 2011. 63, 64

[41] Clayton RH, Zhuchkova Ea, and Panfilov aV. Phase singularities and filaments: simplifying complexity in computational models of ventricular fibrillation. *Progress in biophysics and molecular biology*, 90(1-3):378–98, 2006. 115, 126

[42] Clayton RH and Taggart P. Regional differences in APD restitution can initiate wavebreak and re-entry in cardiac tissue: a computational study. *Biomedical engineering online*, 4:54, January 2005. 108

[43] Constantino J, Hu Y, and Trayanova NA. A computational approach to understanding the cardiac electromechanical activation sequence in the normal and failing heart, with translation to the clinical practice of CRT. *Progress in biophysics and molecular biology*, 110(2-3):372–9, 2012. 154, 155, 157

[44] Coronel R, de Groot JR, and van Lieshout JJ. Defining heart failure. *Cardiovascular research*, 50(3):419–22, June 2001. 63, 137

[45] Coronel R, Wilders R, Verkerk AO, Wiegerinck RF, Benoist D, and Bernus O. Electrophysiological changes in heart failure and their implications for arrhythmogenesis. *Biochimica et biophysica acta*, 1832(12):2432–41, December 2013. 63, 107, 124, 137, 144, 146, 149, 151

[46] Coronel R, Wilms-Schopman FJG, Opthof T, and Janse MJ. Dispersion of repolarization and arrhythmogenesis. *Heart rhythm : the official journal of the Heart Rhythm Society*, 6(4):537–43, April 2009. 82, 150

[47] Curran J, Brown KH, Santiago DJ, Pogwizd S, Bers DM, and Shannon TR. Spontaneous Ca waves in ventricular myocytes from failing hearts depend on Ca2+-calmodulin-dependent protein kinase II. *Journal of Molecular and Cellular Cardiology*, 49(1):25–32, July 2010. 25, 26, 67

[48] Cutler MJ, Rosenbaum DS, and Dunlap ME. Structural and electrical remodeling as therapeutic targets in heart failure. *Journal of electrocardiology*, 40(6 Suppl):S1–7, 2007. 84

[49] Davidenko JM, Pertsov AV, Salomonsz R, Baxter W, and Jalife J. Stationary and drifting spiral waves of excitation in isolated cardiac muscle. *Nature*, 355:349–351, 1992. 126

[50] de Peuter OR, Lussana F, Peters RJG, Büller HR, and Kamphuisen PW. A systematic review of selective and non-selective beta blockers for prevention of vascular events in patients with acute coronary syndrome or heart failure. *The Netherlands journal of medicine*, 67(9):284–94, October 2009. 145

[51] Delgado C, Steinhaus B, Delmar M, Chialvo DR, and Jalife J. Directional differences in excitability and margin of safety for propagation in sheep ventricular epicardial muscle. *Circulation Research*, 67(1):97–110, July 1990. 71

[52] Despa S and Bers DM. Na+ transport in the normal and failing heart - remember the balance. *Journal of molecular and cellular cardiology*, 61:2–10, August 2013. 142

[53] Despa S, Islam Ma, Weber CR, Pogwizd SM, and Bers DM. Intracellular Na+ concentration is elevated in heart failure but Na/K pump function is unchanged. *Circulation*, 105(21):2543–2548, May 2002. 31, 40, 137

[54] DiFrancesco D and Noble D. A model of cardiac electrical activity incorporating ionic pumps and concentration changes. *Philosophical transactions of the Royal Society of London. Series B, Biological sciences*, 307(1133):353–398, 1985. 8

[55] Dorian P and Newman D. Rate dependence of the effect of antiarrhythmic drugs delaying cardiac repolarization: An overview. *Europace*, 2(4):277–285, October 2000. 35

[56] Drouin E, Charpentier F, Gauthier C, Laurent K, and Le Marec H. Electrophysiologic characteristics of cells spanning the left ventricular wall of human heart: Evidence for presence of M cells. *Journal of the American College of Cardiology*, 26(1):185–192, 1995. 28, 42

[57] Dupont E, Matsushita T, Kaba Ra, Vozzi C, Coppen SR, Khan N, Kaprielian R, Yacoub MH, and Severs NJ. Altered connexin expression in human congestive heart failure. *Journal of molecular and cellular cardiology*, 33(2):359–71, February 2001. 15, 69, 84, 109, 137

[58] Eisner Da, Dibb KM, and Trafford aW. The mechanism and significance of the slow changes of ventricular action potential duration following a change of heart rate. *Experimental physiology*, 94(5):520–528, May 2009. 41

[59] Elshrif MM and Cherry EM. A quantitative comparison of the behavior of human ventricular cardiac electrophysiology models in tissue. *PloS one*, 9(1):e84401, January 2014. 73, 111, 119, 150

[60] Engelman ZJ, Trew ML, and Smaill BH. Structural heterogeneity alone is a sufficient substrate for dynamic instability and altered restitution. *Circulation. Arrhythmia and electrophysiology*, 3(2):195–203, May 2010. 107, 147

[61] Faber GM and Rudy Y. Action potential and contractility changes in [Na +] i overloaded cardiac myocytes: A simulation study . . *Biophysical Journal*, 78(5):2392–2404, 2000. 41

[62] Fast VG, Darrow BJ, Saffitz JE, and Kléber AG. Anisotropic activation spread in heart cell monolayers assessed by high-resolution optical mapping. Role of tissue discontinuities. *Circulation research*, 79:115–127, 1996. 85

[63] Fink M and Noble D. Markov models for ion channels: versatility versus identifiability and speed. *Philosophical transactions. Series A, Mathematical, physical, and engineering sciences*, 367:2161–2179, 2009. 8

[64] Fontes MSC, van Veen TaB, de Bakker JMT, and van Rijen HVM. Functional consequences of abnormal Cx43 expression in the heart. *Biochimica et biophysica acta*, 1818(8):2020–9, August 2012. 84

[65] Galeotti L, van Dam PM, Loring Z, Chan D, and Strauss DG. Evaluating strict and conventional left bundle branch block criteria using electrocardiographic simulations. *Europace : European pacing, arrhythmias, and cardiac electrophysiology : journal of the working groups on cardiac pacing, arrhythmias, and cardiac cellular electrophysiology of the European Society of Cardiology*, 15(12):1816–21, December 2013. 154

[66] Garfinkel A, Kim YH, Voroshilovsky O, Qu Z, Kil JR, Lee MH, Karagueuzian HS, Weiss JN, and Chen PS. Preventing ventricular fibrillation by flattening cardiac restitution. *Proceedings of the National Academy of Sciences of the United States of America*, 97(11):6061–6066, 2000. 151

[67] Gaudesius G, Miragoli M, Thomas SP, and Rohr S. Coupling of cardiac electrical activity over extended distances by fibroblasts of cardiac origin. *Circulation research*, 93(5):421–8, September 2003. 63, 84, 85, 137, 146

[68] Gaur N and Rudy Y. Multiscale modeling of calcium cycling in cardiac ventricular myocyte: macroscopic consequences of microscopic dyadic function. *Biophysical journal*, 100(12):2904–12, June 2011. 143

[69] George CH. Sarcoplasmic reticulum Ca2+ leak in heart failure: mere observation or functional relevance? *Cardiovascular research*, 77(2):302–14, January 2008. 67

[70] Geselowitz DB and Miller WT. A bidomain model for anisotropic cardiac muscle. *Annals of Biomedical Engineering*, 11:191–206, 1983. 10

[71] Gima K. Ionic Current Basis of Electrocardiographic Waveforms: A Model Study. *Circulation Research*, 90(8):889–896, March 2002. 69, 148, 151

[72] Glukhov AV, Fedorov VV, Kalish PW, Ravikumar VK, Lou Q, Janks D, Schuessler RB, Moazami N, and Efimov IR. Conduction remodeling in human end-stage nonischemic left ventricular cardiomyopathy. *Circulation*, 125(15):1835–47, April 2012. 63, 83, 84, 85, 107, 125, 148, 151

[73] Glukhov AV, Fedorov VV, Lou Q, Ravikumar VK, Kalish PW, Schuessler RB, Moazami N, and Efimov IR. Transmural dispersion of repolarization in failing and nonfailing human ventricle. *Circulation Research*, 106(5):981–991, March 2010. 28, 42, 63, 82, 83, 107, 150

[74] Gomez JF, Cardona K, Martinez L, Saiz J, and Trenor B. Electrophysiological and structural remodeling in heart failure modulate arrhythmogenesis. 2D simulation study. *PloS one*, 9(7):e103273, January 2014. 85, 147, 148, 151, 152, 153

[75] Gomez JF, Cardona K, Romero L, Ferrero JM, and Trenor B. Electrophysiological and structural remodeling in heart failure modulate arrhythmogenesis. 1D simulation study. *PloS one*, 9(9):e106602, January 2014. 107, 109, 117, 124, 125, 126, 143, 147, 150, 151, 152

[76] Gomez JF, Cardona K, Romero L, Saiz J, Belardinelli L, Rajamani S, Trenor B, València UPD, and Science G. Increase in Late Sodium Current and Cellular Uncoupling Exacerbates Transmural Dispersion of Repolarization in Heart Failure. In *Computing in Cardiology*, pages 39:233–236, 2012. 65, 85, 148

[77] Gomez JF, Cardona K, Romero L, Saiz J, Trenor B, and València UPD. Heterogeneous Electrical Remodeling of the Failing Heart Modulates the Arrhythmogenic Substrate. *Computing in Cardiology*, pages 49–52, 2013. 66, 107

[78] González A, Ravassa S, Beaumont J, López Bn, and Díez J. New targets to treat the structural remodeling of the myocardium. *Journal of the American College of Cardiology*, 58(18):1833–43, October 2011. 84, 125

[79] Grandi E, Pasqualini FS, and Bers DM. A novel computational model of the human ventricular action potential and Ca transient. *Journal of molecular and cellular cardiology*, 48(1):112–21, January 2010. 8, 17, 21, 23, 25, 26, 39, 63, 64, 65, 67, 68, 69, 72, 76, 80, 81, 108, 109, 124, 143

[80] Grandi E, Puglisi J, Wagner S, and Maier L. Simulation of Ca-calmodulin-dependent protein kinase II on rabbit ventricular myocyte ion currents and action potentials. *Biophysical journal*, 93(11):3835–3847, December 2007. 28, 29, 41, 42, 139, 142, 143

[81] Gray RA, Pertsov AM, and Jalife J. Spatial and temporal organization during cardiac fibrillation. *Nature*, 392(May):75–78, 1998. 126, 151

[82] Greisas A and Zlochiver S. Modulation of spiral-wave dynamics and spontaneous activity in a fibroblast/myocyte heterocellular tissue–a computational study. *IEEE transactions on bio-medical engineering*, 59(5):1398–407, May 2012. 111, 125, 127, 147, 152

[83] Gurev V, Constantino J, Rice JJ, and Trayanova NA. Distribution of electromechanical delay in the heart: insights from a three-dimensional electromechanical model. *Biophysical journal*, 99(3):745–54, August 2010. 155

[84] Gurev V, Lee T, Constantino J, Arevalo H, and Trayanova NA. Models of cardiac electromechanics based on individual hearts imaging data: image-based electromechanical models of the heart. *Biomechanics and modeling in mechanobiology*, 10(3):295–306, June 2011. 155

[85] Hasenfuss G, Reinecke H, Studer R, Meyer M, Pieske B, Holtz J, Holubarsch C, Posival H, Just H, and Drexler H. Relation between myocardial function and expression of sarcoplasmic reticulum Ca(2+)-ATPase in failing and nonfailing human myocardium. *Circulation research*, 75(3):434–442, 1994. 25, 68

[86] Hashambhoy YL, Greenstein JL, and Winslow RL. Role of CaMKII in RyR leak, EC coupling and action potential duration: a computational model. *Journal of molecular and cellular cardiology*, 49(4):617–24, October 2010. 142, 149

[87] He JQ, Conklin MW, Foell JD, Wolff MR, Haworth RA, Coronado R, and Kamp TJ. Reduction in density of transverse tubules and L-type Ca2+ channels in canine tachycardia-induced heart failure. *Cardiovascular Research*, 49:298–307, 2001. 143

[88] Heidenreich Ea, Ferrero JM, Doblaré M, and Rodríguez JF. Adaptive macro finite elements for the numerical solution of monodomain equations in cardiac electrophysiology. *Annals of biomedical engineering*, 38(7):2331–45, July 2010. 10, 13, 66, 69, 113, 114

[89] Heijman J, Volders PGA, Westra RL, and Rudy Y. Local control of β-adrenergic stimulation: Effects on ventricular myocyte electrophysiology and Ca(2+)-transient. *Journal of molecular and cellular cardiology*, 50(5):863–71, May 2011. 144, 145

[90] Hobai Ia and O'Rourke B. Decreased Sarcoplasmic Reticulum Calcium Content Is Responsible for Defective Excitation-Contraction Coupling in Canine Heart Failure. *Circulation*, 103(11):1577–1584, March 2001. 84

[91] HODGKIN AL and HUXLEY AF. Currents carried by sodium and potassium ions through the membrane of the giant axon of Loligo. *The Journal of physiology*, 116:449–472, 1952. 6, 8

[92] Holzem KM and Efimov IR. Arrhythmogenic remodelling of activation and repolarization in the failing human heart. *Europace : European pacing, arrhythmias, and cardiac electrophysiology : journal of the working groups on cardiac pacing, arrhythmias, and cardiac cellular electrophysiology of the European Society of Cardiology*, 14 Suppl 5:v50–v57, November 2012. 63, 66, 83, 86

[93] Huang R, Zhang Y, and Xia L. Cellular level electromechanical modeling and simulation of heart failure. *Conference proceedings : ... Annual International Conference of the IEEE Engineering in Medicine and Biology Society. IEEE Engineering in Medicine and Biology Society. Annual Conference*, 7:7301–4, January 2005. 155

[94] Hund TJ, Koval OM, Li J, Wright PJ, Qian L, Snyder JS, Gudmundsson H, Kline CF, Davidson NP, Cardona N, Rasband MN, Anderson ME, and Mohler PJ. A β(IV)-spectrin/CaMKII signaling complex is essential for membrane excitability in mice. *The Journal of clinical investigation*, 120(10):3508–19, October 2010. 43

[95] Hund TJ and Rudy Y. Rate dependence and regulation of action potential and calcium transient in a canine cardiac ventricular cell model. *Circulation*, 110(20):3168–74, November 2004. 8, 23, 40, 42, 43, 143

[96] Hunt SA, Baker DW, Chin MH, Cinquegrani MP, Feldman AM, Francis GS, Ganiats TG, Goldstein S, Gregoratos G, Jessup ML, Noble RJ, Packer M, Silver MA, Stevenson LW, Gibbons RJ, Antman EM, Alpert JS, Faxon DP, Fuster V, Gregoratos G, Jacobs AK, Hiratzka LF, Russell RO, and Smith SC. ACC/AHA Guidelines for the Evaluation and Management of Chronic Heart Failure in the Adult: Executive Summary A Report of the American College of Cardiology/American Heart Association Task Force on Practice Guidelines (Committee to Revise the 1995 Guideli. *Circulation*, 104:2996–3007, 2001. 14

[97] Iyer V, Heller V, and Armoundas Aa. Altered spatial calcium regulation enhances electrical heterogeneity in the failing canine left ventricle: implications for electrical instability. *Journal of applied physiology (Bethesda, Md. : 1985)*, 112(6):944–55, March 2012. 68

[98] Iyer V, Mazhari R, and Winslow RL. A computational model of the human left-ventricular epicardial myocyte. *Biophysical journal*, 87(3):1507–25, September 2004. 8

[99] Jacquemet V and Henriquez CS. Modelling cardiac fibroblasts: interactions with myocytes and their impact on impulse propagation. *Europace : European pacing, arrhythmias, and cardiac electrophysiology : journal of the working groups on cardiac pacing, arrhythmias, and cardiac cellular electrophysiology of the European Society of Cardiology*, 9 Suppl 6:vi29–37, November 2007. 84, 85, 129

[100] Jacquemet V and Henriquez CS. Loading effect of fibroblast-myocyte coupling on resting potential, impulse propagation, and repolarization: insights from a microstructure model. *American journal of physiology. Heart and circulatory physiology*, 294(5):H2040–52, May 2008. 63, 84, 109

[101] Jacquemet V and Henriquez CS. Genesis of complex fractionated atrial electrograms in zones of slow conduction: A computer model of microfibrosis. *Heart Rhythm*, 6(6):803–810, June 2009. 84, 128, 151

[102] Jacquemet V and Henriquez CS. Modulation of conduction velocity by nonmyocytes in the low coupling regime. *IEEE Transactions on Biomedical Engineering*, 56(3):893–896, 2009. 151

[103] Jafri MS, Rice JJ, and Winslow RL. Cardiac Ca2+ dynamics: the roles of ryanodine receptor adaptation and sarcoplasmic reticulum load. *Biophysical journal*, 74(March):1149–1168, 1998. 142

[104] Janicki JS and Brower GL. The role of myocardial fibrillar collagen in ventricular remodeling and function. *Journal of cardiac failure*, 8(6 Suppl):S319–25, December 2002. 125

[105] Janse M. Electrophysiological changes in heart failure and their relationship to arrhythmogenesis. *Cardiovascular research*, 61(2):208–217, February 2004. 14, 21, 24, 40, 65, 107, 124

[106] January CT, Riddle JM, and Salata JJ. A model for early afterdepolarizations: induction with the Ca2+ channel agonist Bay K 8644. *Circulation research*, 62(3):563–71, March 1988. 37

[107] Jongsma HJ and Wilders R. Gap Junctions in Cardiovascular Disease. *Circulation Research*, 86(12):1193–1197, June 2000. 148

[108] Kawara T, Derksen R, de Groot JR, Coronel R, Tasseron S, Linnenbank aC, Hauer RN, Kirkels H, Janse MJ, and de Bakker JM. Activation Delay After Premature Stimulation in Chronically Diseased Human Myocardium Relates to the Architecture of Interstitial Fibrosis. *Circulation*, 104(25):3069–3075, December 2001. 70, 110

[109] Kohl P, Kamkin AG, Kiseleva IS, and Noble D. Mechanosensitive fibroblasts in the sino-atrial node region of rat heart: interaction with cardiomyocytes and possible role. *Experimental physiology*, 79:943–956, 1994. 109, 146

[110] Kohl P. Heterogeneous cell coupling in the heart: an electrophysiological role for fibroblasts. *Circulation research*, 93(5):381–3, September 2003. 137

[111] Kohl P, Camelliti P, Burton FL, and Smith GL. Electrical coupling of fibroblasts and myocytes: relevance for cardiac propagation. *Journal of electrocardiology*, 38(4 Suppl):45–50, October 2005. 63, 84, 129, 146

[112] Kohl P and Gourdie RG. Fibroblast-myocyte electrotonic coupling: Does it occur in native cardiac tissue? *Journal of Molecular and Cellular Cardiology*, 70:37–46, 2014. 146

[113] Kostin S, Rieger M, Dammer S, Hein S, Richter M, Klövekorn Wp, Bauer EP, and Schaper J. Gap junction remodeling and altered connexin43 expression in the failing human heart. *Molecular and cellular biochemistry*, 242(1-2):135–44, January 2003. 84

[114] Krishnamurthy A, Villongco CT, Chuang J, Frank LR, Nigam V, Belezzuoli E, Stark P, Krummen DE, Narayan S, Omens JH, McCulloch AD, and Kerckhoffs RC. Patient-Specific Models of Cardiac Biomechanics. *Journal of computational physics*, 244:4–21, July 2013. 155

[115] Kuijpers NHL, Hermeling E, Bovendeerd PHM, Delhaas T, and Prinzen FW. Modeling cardiac electromechanics and mechanoelectrical coupling in dyssynchronous and failing hearts: insight from adaptive computer models. *Journal of cardiovascular translational research*, 5(2):159–69, April 2012. 155

[116] Lang D, Holzem K, Kang C, Xiao M, Hwang HJ, Ewald GA, Yamada KA, and Efimov IR. Arrhythmogenic Remodeling of 2 versus 1 Adrenergic Signaling in the Human Failing Heart. *Circulation: Arrhythmia and Electrophysiology*, 2015. 145

[117] Levi aJ, Dalton GR, Hancox JC, Mitcheson JS, Issberner J, Bates Ja, Evans SJ, Howarth FC, Hobai Ia, and Jones JV. Role of intracellular sodium overload in the genesis of cardiac arrhythmias. *Journal of cardiovascular electrophysiology*, 8(6):700–721, 1997. 32, 41

[118] Li GR, Feng J, Yue L, and Carrier M. Transmural heterogeneity of action potentials and Ito1 in myocytes isolated from the human right ventricle. *The American journal of physiology*, 275(2 Pt 2):H369–77, August 1998. 21, 24, 28, 42, 137

[119] Li GR, Lau CP, Ducharme A, Tardif JC, and Nattel S. Transmural action potential and ionic current remodeling in ventricles of failing canine hearts. *American journal of physiology. Heart and circulatory physiology*, 283(3):H1031–H1041, September 2002. 21, 24, 26, 39

[120] Li GR, Lau CP, Leung TK, and Nattel S. Ionic current abnormalities associated with prolonged action potentials in cardiomyocytes from diseased human right ventricles. *Heart rhythm : the official journal of the Heart Rhythm Society*, 1(4):460–468, October 2004. 21, 24, 25, 26, 35, 36, 39, 40, 43, 137

[121] Liu YB, Peter A, Lamp ST, Weiss JN, Chen PS, and Lin SF. Spatiotemporal Correlation Between Phase Singularities and Wavebreaks During Ventricular Fibrillation. *Journal of Cardiovascular Electrophysiology*, 14(10):1103–1109, October 2003. 111

[122] Lou Q, Fedorov VV, Glukhov AV, Moazami N, Fast VG, and Efimov IR. Transmural heterogeneity and remodeling of ventricular excitation-contraction coupling in human heart failure. *Circulation*, 123(17):1881–90, May 2011. 70, 82, 83, 84, 107, 150

[123] Lou Q, Janks DL, Holzem K, Lang D, Onal B, Ambrosi CM, Fedorov VV, Wang IW, and Efimov IR. Right Ventricular Arrhythmogenesis in Failing Human Heart: The Role of Conduction and Repolarization Remodeling, December 2012. 63, 82, 83, 150

[124] Lou Q, Ripplinger CM, Bayly PV, and Efimov IR. Quantitative panoramic imaging of epicardial electrical activity. *Annals of Biomedical Engineering*, 36(10):1649–1658, October 2008. 108, 127, 152

[125] Louch WE, Hake J, Jø lle GF, Mø rk HK, Sjaastad I, Lines GT, and Sejersted OM. Control of Ca2+ release by action potential configuration in normal and failing murine cardiomyocytes. *Biophysical journal*, 99(5):1377–86, September 2010. 142, 143

[126] Lu L, Xia L, and Zhu X. Simulation of arrhythmogenic effect of rogue RyRs in failing heart by using a coupled model. *Computational and mathematical methods in medicine*, 2012:183978, January 2012. 139, 141

[127] Luo Ch and Rudy Y. A dynamic model of the cardiac ventricular action potential. I. Simulations of ionic currents and concentration changes. *Circulation research*, 1994. 8

[128] Lyon AR, MacLeod KT, Zhang Y, Garcia E, Kanda GK, Lab MJ, Korchev YE, Harding SE, and Gorelik J. Loss of T-tubules and other changes to surface topography in ventricular myocytes from failing human and rat heart. *Proceedings of the National Academy of Sciences of the United States of America*, 106(16):6854–6859, April 2009. 137, 143

[129] MacCannell KA, Bazzazi H, Chilton L, Shibukawa Y, Clark RB, and Giles WR. A mathematical model of electrotonic interactions between ventricular myocytes and fibroblasts. *Biophysical journal*, 92(11):4121–32, June 2007. 65, 69, 84, 85, 86, 109, 129, 146

[130] Majumder R, Nayak AR, and Pandit R. Nonequilibrium arrhythmic states and transitions in a mathematical model for diffuse fibrosis in human cardiac tissue. *PloS one*, 7(10):e45040, January 2012. 70, 107, 110, 125, 126, 127, 129, 147, 151

[131] Maleckar MM, Greenstein JL, Giles WR, and Trayanova Na. Electrotonic coupling between human atrial myocytes and fibroblasts alters myocyte excitability and repolarization. *Biophysical journal*, 97(8):2179–90, October 2009. 146

[132] Maltsev Va, Sabbah HN, and Undrovinas aI. Late sodium current is a novel target for amiodarone: studies in failing human myocardium. *Journal of molecular and cellular cardiology*, 33(5):923–932, May 2001. 23, 43

[133] Maltsev Va and Undrovinas aI. A multi-modal composition of the late Na+ current in human ventricular cardiomyocytes. *Cardiovascular Research*, 69(1):116–127, January 2006. 24, 42, 43

[134] Maltsev VA, Sabbah HN, Higgins RSD, Silverman N, Lesch M, and Undrovinas AI. Novel, Ultraslow Inactivating Sodium Current in Human Ventricular Cardiomyocytes. *Circulation*, 98(23):2545–2552, December 1998. 24, 28, 29, 43

[135] Maltsev VA, Silverman N, Sabbah HN, and Undrovinas AI. Chronic heart failure slows late sodium current in human and canine ventricular myocytes: implications for repolarization variability. *European journal of heart failure*, 9(3):219–27, March 2007. 21, 24, 25, 42, 63, 67, 137, 142

[136] Maltsev Va and Undrovinas A. Late sodium current in failing heart: friend or foe? *Progress in biophysics and molecular biology*, 96(1-3):421–51, 2008. 149

[137] Marx SO, Gaburjakova J, Gaburjakova M, Henrikson C, Ondrias K, and Marks aR. Coupled Gating Between Cardiac Calcium Release Channels (Ryanodine Receptors). *Circulation Research*, 88(11):1151–1158, May 2001. 84

[138] McDowell KS, Arevalo HJ, Maleckar MM, and Trayanova Na. Susceptibility to arrhythmia in the infarcted heart depends on myofibroblast density. *Biophysical journal*, 101(6):1307–15, September 2011. 84, 85, 107, 126, 129, 147

[139] McSpadden LC, Kirkton RD, and Bursac N. Electrotonic loading of anisotropic cardiac monolayers by unexcitable cells depends on connexin type and expression level. *American journal of physiology. Cell physiology*, 297(2):C339–51, August 2009. 84

[140] Milberg P, Pott C, Fink M, Frommeyer G, Matsuda T, Baba A, Osada N, Breithardt G, Noble D, and Eckardt L. Inhibition of the Na+/Ca2+ exchanger suppresses torsades de pointes in an intact heart model of long QT syndrome-2 and long QT syndrome-3. *Heart rhythm : the official journal of the Heart Rhythm Society*, 5(10):1444–52, October 2008. 21, 35, 42, 143

[141] Miragoli M, Gaudesius G, and Rohr S. Electrotonic modulation of cardiac impulse conduction by myofibroblasts. *Circulation research*, 98(6):801–10, March 2006. 63, 84, 85, 137

[142] Miragoli M, Moshkov A, Novak P, Shevchuk A, Nikolaev VO, El-Hamamsy I, Potter CMF, Wright P, Kadir SHSA, Lyon AR, Mitchell JA, Chester AH, Klenerman D, Lab MJ, Korchev YE, Harding SE, and Gorelik J. Scanning ion conductance microscopy: a convergent high-resolution technology for multiparametric analysis of living cardiovascular cells. *Journal of the Royal Society, Interface / the Royal Society*, 8:913–925, 2011. 156, 157

[143] Miragoli M, Salvarani N, and Rohr S. Myofibroblasts induce ectopic activity in cardiac tissue. *Circulation research*, 101(8):755–8, October 2007. 63, 84, 125, 137

[144] Moreno JD, Yang PC, Bankston JR, Grandi E, Bers DM, Kass RS, and Clancy CE. Ranolazine for congenital and acquired late iNa-linked arrhythmias: In silico pharmacological screening. *Circulation Research*, 113(7):e50–61, September 2013. 69, 124, 139, 141, 143, 150, 154

[145] Moreno JD, Zhu ZI, Yang PC, Bankston JR, Jeng MT, Kang C, Wang L, Bayer JD, Christini DJ, Trayanova NA, Ripplinger CM, Kass RS, and Clancy CE. A computational model to predict the effects of class I anti-arrhythmic drugs on ventricular rhythms. *Science translational medicine*, 3(98):98ra83, August 2011. 107, 124, 139, 141, 143, 148, 154

[146] Morita N, Sovari Aa, Xie Y, Fishbein MC, Mandel WJ, Garfinkel A, Lin SF, Chen PS, Xie LH, Chen F, Qu Z, Weiss JN, and Karagueuzian HS. Increased susceptibility of aged hearts to ventricular fibrillation during oxidative stress. *American journal of physiology. Heart and circulatory physiology*, 297(5):H1594–605, November 2009. 141, 147, 149

[147] Nabauer M, Beuckelmann DJ, Uberfuhr P, and Steinbeck G. Regional Differences in Current Density and Rate-Dependent Properties of the Transient Outward Current in Subepicardial and Subendocardial Myocytes of Human Left Ventricle. *Circulation*, 93(1):168–177, January 1996. 25

[148] Nagatomo T, January CT, and Makielski JC. Preferential block of late sodium current in the LQT3 DeltaKPQ mutant by the class I(C) antiarrhythmic flecainide. *Molecular pharmacology*, 57(1):101–107, 2000. 36

[149] Nagatomo T, Fan Z, Ye B, Tonkovich GS, January CT, Kyle JW, and Makielski JC. Temperature dependence of early and late currents in human cardiac wild-type and long Q-T DeltaKPQ Na+ channels. *The American journal of physiology*, 275(6 Pt 2):H2016–24, December 1998. 24

[150] Narayan SM, Bayer JD, Lalani G, and Trayanova Na. Action potential dynamics explain arrhythmic vulnerability in human heart failure: a clinical and modeling study implicating abnormal calcium handling. *Journal of the American College of Cardiology*, 52(22):1782–92, November 2008. 141

[151] Nayak AR, Shajahan TK, Panfilov aV, and Pandit R. Spiral-wave dynamics in a mathematical model of human ventricular tissue with myocytes and fibroblasts. *PloS one*, 8(9):e72950, January 2013. 85, 107, 127, 129, 147, 151

[152] Nguyen TP, Qu Z, and Weiss JN. Cardiac fibrosis and arrhythmogenesis: The road to repair is paved with perils. *Journal of Molecular and Cellular Cardiology*, 70:83–91, 2014. 147

[153] Nikolaev VO, Moshkov A, Lyon AR, Miragoli M, Novak P, Paur H, Lohse MJ, Korchev YE, Harding SE, and Gorelik J. Beta2-adrenergic receptor redistribution in heart failure changes cAMP compartmentation. *Science (New York, N.Y.)*, 327(5973):1653–7, March 2010. 143

[154] Nivala M, Song Z, Weiss JN, and Qu Z. T-tubule disruption promotes calcium alternans in failing ventricular myocytes: Mechanistic insights from computational modeling. *Journal of molecular and cellular cardiology*, 79:32–41, 2015. 143

[155] Noble D, Varghese A, Kohl P, and Noble P. Improved guinea-pig ventricular cell model incorporating a diadic space, IKr and IKs, and length- and tension-dependent processes. *The Canadian journal of cardiology*, 14:123–134, 1998. 8, 42

[156] O'Hara T and Rudy Y. Arrhythmia formation in subclinical ("silent") long QT syndrome requires multiple insults: quantitative mechanistic study using the KCNQ1 mutation Q357R as example. *Heart rhythm : the official journal of the Heart Rhythm Society*, 9(2):275–82, February 2012. 142, 144

[157] O'Hara T, Virág L, Varró A, and Rudy Y. Simulation of the undiseased human cardiac ventricular action potential: model formulation and experimental validation. *PLoS computational biology*, 7(5):e1002061, May 2011. 8, 9, 17, 39, 40, 41, 42, 43, 44, 64, 65, 67, 68, 69, 70, 74, 76, 77, 78, 143, 150

[158] Ohler A, Amos GJ, Wettwer E, and Ravens U. Frequency-dependent effects of E-4031, almokalant, dofetilide and tedisamil on action potential duration: no evidence for "reverse use dependent" block. *Naunyn-Schmiedeberg's Archives of Pharmacology*, 349:602–610, 1994. 84, 86

[159] O'Rourke B, Kass Da, Tomaselli GF, Kaab S, Tunin R, and Marban E. Mechanisms of Altered Excitation-Contraction Coupling in Canine Tachycardia-Induced Heart Failure, I : Experimental Studies. *Circulation Research*, 84(5):562–570, March 1999. 84

[160] Pandit SV and Jalife J. Rotors and the dynamics of cardiac fibrillation. *Circulation research*, 112(5):849–62, March 2013. 126

[161] Peters NS, Green CR, Poole-Wilson Pa, and Severs NJ. Reduced content of connexin43 gap junctions in ventricular myocardium from hypertrophied and ischemic human hearts. *Circulation*, 88(3):864–875, September 1993. 15, 148

[162] Petrov VS, Osipov GV, and Kurths J. Fibroblasts alter spiral wave stability. *Chaos (Woodbury, N.Y.)*, 20(4):045103, December 2010. 107, 147

[163] Piacentino V, Weber CR, Chen X, Weisser-Thomas J, Margulies KB, Bers DM, and Houser SR. Cellular basis of abnormal calcium transients of failing human ventricular myocytes. *Circulation Research*, 92(6):651–658, April 2003. 21, 24, 25, 26, 39, 40, 63, 67, 68, 84

[164] Pieske B, Maier LS, Bers DM, and Hasenfuss G. Ca2+ Handling and Sarcoplasmic Reticulum Ca2+ Content in Isolated Failing and Nonfailing Human Myocardium. *Circulation Research*, 85(1):38–46, July 1999. 84

[165] Pieske B, Maier LS, Piacentino V, Weisser J, Hasenfuss G, and Houser S. Rate dependence of [Na+]i and contractility in nonfailing and failing human myocardium. *Circulation*, 106(4):447–453, July 2002. 27, 31, 40, 41

[166] Plank G, Zhou L, Greenstein JL, Cortassa S, Winslow RL, O'Rourke B, and Trayanova NA. From mitochondrial ion channels to arrhythmias in the heart: computational techniques to bridge the spatio-temporal scales. *Philosophical transactions. Series A, Mathematical, physical, and engineering sciences*, 366(1879):3381–409, September 2008. 156

[167] Poelzing S and Rosenbaum DS. Altered connexin43 expression produces arrhythmia substrate in heart failure. *American journal of physiology. Heart and circulatory physiology*, 287(4):H1762–70, October 2004. 84

[168] Pogwizd SM, Schlotthauer K, Li L, Yuan W, and Bers DM. Arrhythmogenesis and Contractile Dysfunction in Heart Failure : Roles of Sodium-Calcium Exchange, Inward Rectifier Potassium Current, and Residual Â -Adrenergic Responsiveness. *Circulation Research*, 88(11):1159–1167, May 2001. 124

[169] Pogwizd SM and Bers DM. Cellular basis of triggered arrhythmias in heart failure, 2004. 41

[170] Potse M, Dubé B, Vinet A, and Cardinal R. A comparison of monodomain and bidomain propagation models for the human heart. *Conference proceedings : ... Annual International Conference of the IEEE Engineering in Medicine and Biology Society. IEEE Engineering in Medicine and Biology Society. Annual Conference*, 1:3895–8, January 2006. 10

[171] Potse M, Krause D, Bacharova L, Krause R, Prinzen FW, and Auricchio A. Similarities and differences between electrocardiogram signs of left bundle-branch block and left-ventricular uncoupling. *Europace : European pacing, arrhythmias, and cardiac electrophysiology : journal of the working groups on cardiac pacing, arrhythmias, and cardiac cellular electrophysiology of the European Society of Cardiology*, 14 Suppl 5:v33–v39, November 2012. 154

[172] Prestle J, Dieterich S, Preuss M, Bieligk U, and Hasenfuss G. Heterogeneous transmural gene expression of calcium-handling proteins and natriuretic peptides in the failing human heart. *Cardiovascular research*, 43(2):323–31, August 1999. 63, 66, 68, 73, 83, 84

[173] Priebe L and Beuckelmann DJ. Simulation Study of Cellular Electric Properties in Heart Failure. *Circulation Research*, 82(11):1206–1223, June 1998. 8, 15, 21, 24, 25, 26, 30, 31, 39, 40, 67, 68, 138, 141, 149

[174] Pueyo E, Husti Z, and Hornyik T. Mechanisms of ventricular rate adaptation as a predictor of arrhythmic risk. *American Journal of . . .* , 298(5):H1577–H1587, May 2010. 41

[175] Puglisi JL and Bers DM. LabHEART: an interactive computer model of rabbit ventricular myocyte ion channels and Ca transport. *American journal of physiology. Cell physiology*, 281(6):C2049–60, December 2001. 8, 138, 141

[176] Qu Z, Karagueuzian HS, Garfinkel A, and Weiss JN. Effects of Na(+) channel and cell coupling abnormalities on vulnerability to reentry: a simulation study. *American journal of physiology. Heart and circulatory physiology*, 286(4):H1310–21, April 2004. 85

[177] Rajamani S, El-Bizri N, Shryock JC, Makielski JC, and Belardinelli L. Use-dependent block of cardiac late Na+ current by ranolazine. *Heart Rhythm*, 6(11):1625–1631, November 2009. 36

[178] Reinecke H, Studer R, Vetter R, Holtz J, and Drexler H. Cardiac Na+/Ca2+ exchange activity in patients with end-stage heart failure. *Cardiovasc Res*, 31(1):48–54, 1996. 25, 26, 67, 68

[179] Remy-Jardin M RJ. *Integrated Cardiothoracic Imaging with MDCT*. 2009. 69

[180] Rodríguez B, Li L, Eason JC, Efimov IR, and Trayanova NA. Differences between left and right ventricular chamber geometry affect cardiac vulnerability to electric shocks. *Circulation research*, 97(2):168–75, July 2005. 154

[181] Rogers JM. Combined phase singularity and wavefront analysis for optical maps of ventricular fibrillation. *IEEE transactions on bio-medical engineering*, 51(1):56–65, January 2004. 112

[182] Rohr S. Role of gap junctions in the propagation of the cardiac action potential. *Cardiovascular research*, 62(2):309–22, May 2004. 85

[183] Rohr S. Arrhythmogenic implications of fibroblast-myocyte interactions. *Circulation. Arrhythmia and electrophysiology*, 5(2):442–52, April 2012. 125

[184] Romero D, Sebastian R, Bijnens BH, Zimmerman V, Boyle PM, Vigmond EJ, and Frangi AF. Effects of the purkinje system and cardiac geometry on biventricular pacing: a model study. *Annals of biomedical engineering*, 38(4):1388–98, April 2010. 154

[185] Romero L and Pueyo E. Impact of ionic current variability on human ventricular cellular electrophysiology. *American Journal of . . .*, 297(4):H1436–H1445, October 2009. 26, 27, 31, 40, 41, 42

[186] Romero L, Trénor B, Alonso JM, Tobón C, Saiz J, and Ferrero JM. The relative role of refractoriness and source-sink relationship in reentry generation during simulated acute ischemia. *Annals of biomedical engineering*, 37(8):1560–71, August 2009. 71

[187] Rook MB, van Ginneken AC, de Jonge B, el Aoumari A, Gros D, and Jongsma HJ. Differences in gap junction channels between cardiac myocytes, fibroblasts, and heterologous pairs. *The American journal of physiology*, 263:C959–C977, 1992. 84, 109

[188] Rosamond W, Flegal K, Friday G, Furie K, Go A, Greenlund K, Haase N, Ho M, Howard V, Kissela B, Kittner S, Lloyd-Jones D, McDermott M, Meigs J, Moy C, Nichol G, O'Donnell CJ, Roger V, Rumsfeld J, Sorlie P, Steinberger J, Thom T, Wasserthiel-Smoller S, and Hong Y. Heart disease and stroke statistics - 2007 Update: A report from the American Heart Association Statistics Committee and Stroke Statistics Subcommittee, February 2007. 14, 21

[189] Ruan Y, Liu N, and Priori SG. Sodium channel mutations and arrhythmias. *Nature reviews. Cardiology*, 6:337–348, 2009. 4

[190] Ruwald MH, Ruwald ACH, Jons C, Alexis J, McNitt S, Zareba W, and Moss AJ. Effect of metoprolol versus carvedilol on outcomes in MADIT-CRT (multicenter automatic defibrillator implantation trial with cardiac resynchronization therapy). *Journal of the American College of Cardiology*, 61(14):1518–26, April 2013. 145

[191] Sachse FB, Moreno aP, Seemann G, and Abildskov Ja. A model of electrical conduction in cardiac tissue including fibroblasts. *Annals of biomedical engineering*, 37(5):874–89, May 2009. 84

[192] Sachse FB, Moreno AP, and Abildskov Ja. Electrophysiological modeling of fibroblasts and their interaction with myocytes. *Annals of biomedical engineering*, 36(1):41–56, January 2008. 109, 129, 146

[193] Sah R. Modulation of Ca2+ Release in Cardiac Myocytes by Changes in Repolarization Rate: Role of Phase-1 Action Potential Repolarization in Excitation-Contraction Coupling. *Circulation Research*, 90(2):165–173, December 2001. 84, 86

[194] Samie F. Mechanisms underlying ventricular tachycardia and its transition to ventricular fibrillation in the structurally normal heart. *Cardiovascular Research*, 50(2):242–250, May 2001. 126

[195] Saucerman JJ, Brunton LL, Michailova AP, and McCulloch AD. Modeling beta-adrenergic control of cardiac myocyte contractility in silico. *The Journal of biological chemistry*, 278(48):47997–8003, November 2003. 144

[196] Saucerman JJ, Healy SN, Belik ME, Puglisi JL, and McCulloch AD. Proarrhythmic consequences of a KCNQ1 AKAP-binding domain mutation: computational models of whole cells and heterogeneous tissue. *Circulation research*, 95(12):1216–24, December 2004. 144

[197] Schwinger RH, Böhm M, Schmidt U, Karczewski P, Bavendiek U, Flesch M, Krause EG, and Erdmann E. Unchanged protein levels of SERCA II and phospholamban but reduced Ca2+ uptake and Ca(2+)-ATPase activity of cardiac sarcoplasmic reticulum from dilated cardiomyopathy patients compared with patients with nonfailing hearts. *Circulation*, 92(11):3220–3228, December 1995. 25, 68

[198] Sermesant M, Chabiniok R, Chinchapatnam P, Mansi T, Billet F, Moireau P, Peyrat JM, Wong K, Relan J, Rhode K, Ginks M, Lambiase P, Delingette H, Sorine M, Rinaldi CA, Chapelle D, Razavi R, and Ayache N. Patient-specific electromechanical models of the heart for the prediction of pacing acute effects in CRT: A preliminary clinical validation. *Medical Image Analysis*, 16(1):201–215, 2012. 155

[199] Shannon TR, Wang F, Puglisi J, Weber C, and Bers DM. A mathematical treatment of integrated Ca dynamics within the ventricular myocyte. *Biophysical journal*, 87(5):3351–71, November 2004. 15, 41

[200] Shannon T, Wang F, and Bers D. Regulation of cardiac sarcoplasmic reticulum Ca release by luminal and altered gating assessed with a mathematical model. *Biophysical journal*, 89(6):4096–4110, December 2005. 15, 24, 40, 138, 141

[201] Shaw RM and Rudy Y. Electrophysiologic effects of acute myocardial ischemia: a theoretical study of altered cell excitability and action potential duration. *Cardiovascular research*, 35:256–272, 1997. 71, 78

[202] Shi C, Wang X, Dong F, Wang Y, Hui J, Lin Z, Yang J, and Xu Y. Temporal alterations and cellular mechanisms of transmural repolarization during progression of mouse cardiac hypertrophy and failure. *Acta physiologica (Oxford, England)*, 208(1):95–110, May 2013. 107

[203] Silva J and Rudy Y. Subunit interaction determines IKs participation in cardiac repolarization and repolarization reserve. *Circulation*, 112(10):1384–91, September 2005. 8

[204] So PPS, Backx PH, and Dorian P. Slow delayed rectifier K+ current block by HMR 1556 increases dispersion of repolarization and promotes Torsades de Pointes in rabbit ventricles. *British journal of pharmacology*, 155(8):1185–1194, December 2008. 28, 42

[205] Soltis AR and Saucerman JJ. Synergy between CaMKII substrates and β-adrenergic signaling in regulation of cardiac myocyte Ca(2+) handling. *Biophysical journal*, 99(7):2038–47, October 2010. 144

[206] Soltysinska E, Olesen SrP, Christ T, Wettwer E, Varró A, Grunnet M, and Jespersen T. Transmural expression of ion channels and transporters in human nondiseased and end-stage failing hearts. *Pflügers Archiv : European journal of physiology*, 459(1):11–23, November 2009. 63, 66, 73, 83, 84

[207] Sossalla S, Maurer U, Schotola H, Hartmann N, Didié M, Zimmermann WH, Jacobshagen C, Wagner S, and Maier LS. Diastolic dysfunction and arrhythmias caused by overexpression of CaMKIIδ(C) can be reversed by inhibition of late Na(+) current. *Basic research in cardiology*, 106(2):263–72, March 2011. 63, 67

[208] Spach MS and Boineau JP. Microfibrosis produces electrical load variations due to loss of side-to-side cell connections: a major mechanism of structural heart disease arrhythmias. *Pacing and clinical electrophysiology : PACE*, 20(2 Pt 2):397–413, February 1997. 63

[209] Taggart P, Sutton PM, Opthof T, Coronel R, Trimlett R, Pugsley W, and Kallis P. Inhomogeneous transmural conduction during early ischaemia in patients with coronary artery disease. *Journal of molecular and cellular cardiology*, 32(4):621–30, April 2000. 69, 109, 120

[210] Tanaka K, Zlochiver S, Vikstrom KL, Yamazaki M, Moreno J, Klos M, Zaitsev AV, Vaidyanathan R, Auerbach DS, Landas S, Guiraudon G, Jalife J, Berenfeld O, and Kalifa J. Spatial distribution of fibrosis governs fibrillation wave dynamics in the posterior left atrium during heart failure. *Circulation research*, 101(8):839–47, October 2007. 70, 84, 107, 127, 152

[211] Ten Tusscher KHWJ and Panfilov aV. Cell model for efficient simulation of wave propagation in human ventricular tissue under normal and pathological conditions. *Physics in medicine and biology*, 51(23):6141–56, December 2006. 40

[212] Thompson Sa, Copeland CR, Reich DH, and Tung L. Mechanical coupling between myofibroblasts and cardiomyocytes slows electric conduction in fibrotic cell monolayers. *Circulation*, 123(19):2083–93, May 2011. 84

[213] Tomaselli GF and Marbán E. Electrophysiological remodeling in hypertrophy and heart failure, May 1999. 15, 21, 24, 25, 26, 39, 40, 63, 67, 107, 137

[214] Tomaselli GF and Zipes DP. What causes sudden death in heart failure? *Circulation research*, 95(8):754–63, October 2004. 15, 21, 24, 25, 26, 39, 40, 63, 67, 107, 142, 146

[215] Trenor B, Cardona K, Gomez JF, Rajamani S, Ferrero JM, Belardinelli L, and Saiz J. Simulation and mechanistic investigation of the arrhythmogenic role of the late sodium current in human heart failure. *PloS one*, 7(3):e32659, January 2012. 65, 85, 108, 109, 124, 139, 140, 141, 143, 149

[216] Turner I, L-H Huang C, and Saumarez RC. Numerical simulation of paced electrogram fractionation: relating clinical observations to changes in fibrosis and action potential duration. *Journal of cardiovascular electrophysiology*, 16(2):151–61, February 2005. 107, 125, 146

[217] Tusscher KT and Noble D. A model for human ventricular tissue. *American Journal of ...*, 286(4):H1573–89, April 2004. 8, 23, 40, 42, 43, 139

[218] Umapathy K, Nair K, Masse S, Krishnan S, Rogers J, Nash MP, and Nanthakumar K. Phase mapping of cardiac fibrillation. *Circulation. Arrhythmia and electrophysiology*, 3(1):105–14, February 2010. 108, 112, 127, 152

[219] Undrovinas aI, Maltsev Va, and Sabbah HN. Repolarization abnormalities in cardiomyocytes of dogs with chronic heart failure: Role of sustained inward current. *Cellular and Molecular Life Sciences*, 55(3):494–505, 1999. 24

[220] Undrovinas AI, Belardinelli L, Undrovinas NA, and Sabbah HN. Ranolazine improves abnormal repolarization and contraction in left ventricular myocytes of dogs with heart failure by inhibiting late sodium current. *Journal of cardiovascular electrophysiology*, 17 Suppl 1:S169–S177, May 2006. 21, 43, 83, 142

[221] Undrovinas AI, Maltsev Va, Kyle JW, Silverman N, and Sabbah HN. Gating of the late Na+ channel in normal and failing human myocardium. *Journal of molecular and cellular cardiology*, 34(11):1477–1489, November 2002. 43

[222] Undrovinas NA, Maltsev VA, Belardinelli L, Sabbah HN, and Undrovinas A. Late sodium current contributes to diastolic cell Ca2+ accumulation in chronic heart failure. *The journal of physiological sciences : JPS*, 60(4):245–57, July 2010. 21, 32, 42

[223] Usyk TP and McCulloch AD. Electromechanical Model of Cardiac Resynchronization in the Dilated Failing Heart with Left Bundle Branch Block. In *Journal of Electrocardiology*, volume 36, pages 57–61, January 2003. 155

[224] Valdivia C, Chu W, and Pu J. Increased late sodium current in myocytes from a canine heart failure model and from failing human heart. *Journal of molecular and ...*, 38(3):475–483, March 2005. 21, 24, 25, 137, 142

[225] Vasquez C, Moreno A, and Berbari E. Modeling fibroblast-mediated conduction in the ventricle. *Computers in Cardiology, 2004*, pages 349–352, 2004. 63, 70, 84, 109

[226] Vigmond E, Vadakkumpadan F, Gurev V, Arevalo H, Deo M, Plank G, and Trayanova N. Towards predictive modelling of the electrophysiology of the heart. *Experimental physiology*, 94(5):563–577, May 2009. 63, 64

[227] von Lewinski D, Bisping E, Elgner A, Kockskämper J, and Pieske B. Mechanistic insight into the functional and toxic effects of Strophanthidin in the failing human myocardium. *European journal of heart failure*, 9(11):1086–94, November 2007. 41

[228] Wachter SB and Gilbert EM. Beta-adrenergic receptors, from their discovery and characterization through their manipulation to beneficial clinical application. *Cardiology*, 122(2):104–12, January 2012. 144

[229] Wagner E, Lauterbach Ma, Kohl T, Westphal V, Williams GSB, Steinbrecher JH, Streich JH, Korff B, Tuan HTM, Hagen B, Luther S, Hasenfuss G, Parlitz U, Jafri MS, Hell SW, Lederer WJ, and Lehnart SE. Stimulated emission depletion live-cell super-resolution imaging shows proliferative remodeling of T-tubule membrane structures after myocardial infarction. *Circulation research*, 111(4):402–14, August 2012. 137

[230] Wagner S, Ruff HM, Weber SL, Bellmann S, Sowa T, Schulte T, Anderson ME, Grandi E, Bers DM, Backs J, Belardinelli L, and Maier LS. Reactive oxygen species-activated Ca/calmodulin kinase IIδ is required for late INa augmentation leading to cellular Na and Ca overload. *Circulation Research*, 2011. 41

[231] Walmsley J, Rodriguez JF, Mirams GR, Burrage K, Efimov IR, and Rodriguez B. mRNA expression levels in failing human hearts predict cellular electrophysiological remodeling: a population-based simulation study. *PloS one*, 8(2):e56359, January 2013. 63, 66, 73, 83, 139, 141, 151

[232] Weber C, Piacentino V, Houser S, and Bers D. Dynamic regulation of sodium/calcium exchange function in human heart failure. *Circulation*, 108(18):2224–2229, November 2003. 24, 30, 40, 41, 142

[233] Wettwer E, Amos GJ, Posival H, and Ravens U. Transient outward current in human ventricular myocytes of subepicardial and subendocardial origin. *Circulation research*, 75(3):473–482, 1994. 25

[234] Wiegerinck RF, van Veen TaB, Belterman CN, Schumacher Ca, Noorman M, de Bakker JMT, and Coronel R. Transmural dispersion of refractoriness and conduction velocity is associated with heterogeneously reduced connexin43 in a rabbit model of heart failure. *Heart rhythm : the official journal of the Heart Rhythm Society*, 5(8):1178–85, August 2008. 15, 85, 107, 126, 137, 148

[235] Wiegerinck RF, Verkerk AO, Belterman CN, van Veen TaB, Baartscheer A, Opthof T, Wilders R, de Bakker JMT, and Coronel R. Larger cell size in rabbits with heart failure increases myocardial conduction velocity and QRS duration. *Circulation*, 113(6):806–13, February 2006. 144

[236] Wilson LD, Jeyaraj D, Wan X, Hoeker GS, Said TH, Gittinger M, Laurita KR, and Rosenbaum DS. Heart failure enhances susceptibility to arrhythmogenic cardiac alternans. *Heart rhythm : the official journal of the Heart Rhythm Society*, 6(2):251–9, February 2009. 107

[237] Winslow RL, Rice J, Jafri S, Marbán E, and O'Rourke B. Mechanisms of altered excitation-contraction coupling in canine tachycardia-induced heart failure, II: model studies. *Circulation research*, 84(5):571–586, March 1999. 15, 21, 24, 26, 40, 67, 138, 140, 141, 142

[238] Winslow RL, Scollan DF, Holmes A, Yung CK, Zhang J, and Jafri MS. Electrophysiological modeling of cardiac ventricular function: from cell to organ. *Annual review of biomedical engineering*, 2:119–55, January 2000. 141

[239] Wit AL and Coromilas J. Role of alterations in refractoriness and conduction in the genesis of reentrant arrhythmias. Implications for antiarrhythmic effects of class III drugs. *The American journal of cardiology*, 72:3F–12F, 1993. 63, 107

[240] Wright PT, Nikolaev VO, O'Hara T, Diakonov I, Bhargava A, Tokar S, Schobesberger S, Shevchuk AI, Sikkel MB, Wilkinson R, Trayanova Na, Lyon AR, Harding SE, and Gorelik J. Caveolin-3 regulates

compartmentation of cardiomyocyte beta2-adrenergic receptor-mediated cAMP signaling. *Journal of molecular and cellular cardiology*, 67:38–48, February 2014. 143, 144

[241] Wu L, Guo D, Li H, Hackett J, Yan GX, Jiao Z, Antzelevitch C, Shryock JC, and Belardinelli L. Role of late sodium current in modulating the proarrhythmic and antiarrhythmic effects of quinidine. *Heart rhythm : the official journal of the Heart Rhythm Society*, 5(12):1726–34, December 2008. 21, 35, 42, 43

[242] Wu L, Ma J, Li H, Wang C, Grandi E, Zhang P, Luo A, Bers DM, Shryock JC, and Belardinelli L. Late sodium current contributes to the reverse rate-dependent effect of IKr inhibition on ventricular repolarization. *Circulation*, 123(16):1713–1720, April 2011. 21, 43

[243] Wu L, Rajamani S, Li H, January CT, Shryock JC, and Belardinelli L. Reduction of repolarization reserve unmasks the proarrhythmic role of endogenous late Na(+) current in the heart. *American journal of physiology. Heart and circulatory physiology*, 297(3):H1048–57, September 2009. 21, 35, 43

[244] Wu L, Shryock JC, Song Y, Li Y, Antzelevitch C, and Belardinelli L. Antiarrhythmic effects of ranolazine in a guinea pig in vitro model of long-QT syndrome. *The Journal of pharmacology and experimental therapeutics*, 310(2):599–605, 2004. 21, 35

[245] Xie Y, Garfinkel A, Camelliti P, Kohl P, Weiss J, and Qu Z. Effects of fibroblast-myocyte coupling on cardiac conduction and vulnerability to reentry: a computational study. *Heart Rhythm*, 6(11):1641–9, November 2009. 84, 85, 107, 109, 125, 126, 129, 147, 151

[246] Xie Y, Sato D, Garfinkel A, Qu Z, and Weiss JN. So little source, so much sink: requirements for afterdepolarizations to propagate in tissue. *Biophysical journal*, 99(5):1408–15, September 2010. 149

[247] Xiong W, Tian Y, DiSilvestre D, and Tomaselli GF. Transmural heterogeneity of Na+-Ca2+ exchange: evidence for differential expression in normal and failing hearts. *Circulation research*, 97(3):207–9, August 2005. 66, 68, 83, 84

[248] Yano M, Ono K, Ohkusa T, Suetsugu M, Kohno M, Hisaoka T, Kobayashi S, Hisamatsu Y, Yamamoto T, Noguchi N, Takasawa S, Okamoto H, and Matsuzaki M. Altered Stoichiometry of FKBP12.6 Versus Ryanodine Receptor as a Cause of Abnormal Ca2+ Leak Through Ryanodine Receptor in Heart Failure. *Circulation*, 102(17):2131–2136, October 2000. 84

[249] Yun Y, Hwang M, Park JH, Shin H, Shim EB, and Pak HN. The relationship among complex fractionated electrograms, wavebreak, phase singularity, and local dominant frequency in fibrillation wave-dynamics: a modeling comparison study. *Journal of Korean medical science*, 29(3):370–7, March 2014. 128

[250] Zaza A, Belardinelli L, and Shryock JC. Pathophysiology and pharmacology of the cardiac "late sodium current". *Pharmacology and Therapeutics*, 119(3):326–339, September 2008. 21, 37, 43, 142

[251] Zhang Y, Xia L, Tang M, Sun Q, and Zhang S. Simulation study of transmural cellular electrical properties in failed human heart. *Chinese Journal of Biomedical Engineering*, 27(4):526–532, 2008. 24, 40, 140, 141, 143

[252] Zlochiver S. Subthreshold parameters of cardiac tissue in a bi-layer computer model of heart failure. *Cardiovascular engineering (Dordrecht, Netherlands)*, 10(4):190–200, December 2010. 107, 125, 139, 141, 143, 147, 148

[253] Zlochiver S, Muñoz V, Vikstrom KL, Taffet SM, Berenfeld O, and Jalife J. Electrotonic myofibroblast-to-myocyte coupling increases propensity to reentrant arrhythmias in two-dimensional cardiac monolayers. *Biophysical journal*, 95(9):4469–80, November 2008. 63, 84, 85, 127, 129, 152

[254] Zygmunt aC, Eddlestone GT, Thomas GP, Nesterenko VV, and Antzelevitch C. Larger late sodium conductance in M cells contributes to electrical heterogeneity in canine ventricle. *American journal of physiology. Heart and circulatory physiology*, 281(2):H689–H697, 2001. 36

Acknowledgements

This Thesis marks the fulfillment of my journey to obtain my Ph.D degree at Universitat Politècnica de València. I would like to thank several people who have contributed to the accomplishment of this work.

First and foremost, I would like to thank my supervisor Dr. Beatriz Trenor for giving me the opportunity to obtain the Ph.D. degree and for trusting me and guiding me from the beginning of this trip. I will always remember who gave me the chance to become a researcher. Her continuous commitment to my work and organizational aspects have been fundamental.

I would also like to thank Dr. Javier Saiz and Dr. Chema Ferrero, who introduced me to the biomedical research field. Two very different people, who brought to me different views of the field. Their advice helped me out several times along the way. I would like to thank Dr. Lucía Romero for her support and specially Dr. Karen Cardona for her willingness to listen to me and to help me in every aspect of the work, sincerely thank you. I would like to express my sincere gratitude to Dr. Rafael Sebastian who guided me and helped me out in every technical aspect of the Thesis. The kind of researcher I would like to be. I could not have done it without you.

I am also really grateful to Dr. Jose Félix Rodríguez who helped me countless times from the distance and all my past and current colleagues of the laboratory, Victor Zena, Laura Martinez, Ana Talavera, Ana Ferrer, Eduardo Godoy, Jose V. Visconti, Bea Carbonell, Alejandro López, Pepe Alberola, Javier G. Casado and Gema Prats. Together they have created a very friendly working environment to share constructive discussions.

I would like to thank Dr. Igor Efimov from Washington University in Saint Louis, USA, for letting us visit his laboratory during our research stay in order to learn a different point of view of the biomedical area.

A mis padres, por que me han permitido estudiar lo quería y donde quería. Me han apoyado durante todo el trayecto ante las decisiones que he tomado, y siempre han estado ahí cuando los he necesitado. A mis hermanas, por creer en mí, apoyarme y quererme como soy, a todos ellos, gracias.

A mi pareja, Maria del Mar, por permanecer a mi lado tanto en los ratos buenos como en los malos, por apoyarme y liberarme en mis ratos de frustración, por compartir tu vida conmigo y por hacerme felíz cada día.

Curriculum Vitae

Juan Francisco Gómez obtained his B.Sc degree in Physics from the University of Valencia,Spain, in 2009. Later, he received his M.Sc. degree on Biomedical Engineering from the Polytechnic University of Valencia, Spain, in 2012. Afterwards, he has worked as a research student on the topic of computer cardiac modeling and simulation at Polytechnic University of Valencia, in order to obtain the Ph.D. degree. In 2014, he visited Dr. Igor Efimov's laboratory at the Department of Biomedical Engineering at Washington University in Saint Louis (WUSTL), USA , for a research collaboration.